DISSERTATION

THE PI3K-AKT-MTOR SIGNAL TRANSDUCTION PATHWAY AND PI3K/MTOR INHIBITION IN CANINE OSTEOSARCOMA AND LYMPHOMA

Submitted by Travis Kuder Meuten

Department of Microbiology Immunology and Pathology

In partial fulfillment of the requirements

For the Degree of Doctor of Philosophy

Colorado State University

Fort Collins, Colorado

Spring 2026

Doctoral Committee:

Advisor: Gary L. Mason
Co-Advisor: Douglas H. Thamm

Gregg A. Dean
Dawn L. Duval
Daniel L. Gustafson

ABSTRACT

THE PI3K-AKT-MTOR SIGNAL TRANSDUCTION PATHWAY AND PI3K/MTOR INHIBITION IN CANINE OSTEOSARCOMA AND LYMPHOMA

The research discussed herein presents an important opportunity to better understand and advance the treatment of canine osteosarcoma and lymphoid tumors, which carry a poor prognosis and serve as a valuable resource for the advancement of comparative oncology in the canine and human patient. Canine hematopoietic tumors are among the most common tumors in dogs and advancements in treatment are necessary to improve outcomes. Lymphoma represents one of the most common tumor types, accounting for 7-24% of all canine neoplasms and 80% of canine hematopoietic tumors, with many subtypes and heterogeneous biological behavior. Canine diffuse large B-cell lymphoma, which comprises 50% of all lymphoma cases, is also a valuable spontaneous animal model for non-Hodgkin lymphoma in humans. Canine osteosarcoma presents a significant clinical challenge in veterinary oncology. Due to the similarities in aggressive biologic behavior, mutation status, and gene expression profiles, the canine patient also provides a spontaneous animal model for osteosarcoma in humans. Advancements in the treatment of osteosarcoma and lymphoma have been slow to progress in recent years. In multiple tumor types of both species, including osteosarcoma and lymphoid neoplasms, there is similar dysregulation of signal transduction through phosphatidylinositol 3-kinase (PI3K), AKT serine/threonine kinase (AKT), and mechanistic target of rapamycin (mTOR), collectively known as the PI3K-

AKT-mTOR pathway, which contributes to disease progression and poorer outcomes. In human medicine, there have been many attempts to induce cessation of signal transduction with halting progress due to the complexity of signal transduction feedback and resistance to broad or single-point pathway inhibition. Through these efforts we have come to better comprehend the potential benefits of targeted and multi-nodal PI3K-AKT-mTOR pathway inhibition as a component of cancer treatment. As is often the case in the veterinary field, the research in cellular signaling cascades in health and cancer development is not as completely documented for canine neoplasms as in human tumors.

Presented in Chapter 1 is a review of the current knowledge of PI3K-AKT-mTOR signal transduction activity in health and disease, with a comparative focus on human and canine osteosarcoma and lymphoid tumors. The current body of knowledge regarding the role of PI3K-AKT-mTOR pathway in tumorigenesis serves as a basis for our investigation of the role of signal transduction in canine osteosarcoma and lymphoma and the efficacy of multi-nodal pathway inhibition with a dual PI3K/mTOR inhibitor, VDC597. In order to better understand the role of PI3K-AKT-mTOR signaling in these canine tumors, further investigation into pathway activity and the efficacy of dual-inhibition is warranted. We hypothesized that, in comportment with existing literature in canine and human tumors, there would be increased PI3K-AKT-mTOR activity in the canine osteosarcoma and lymphoid neoplastic samples and cells we examined. We further hypothesized that inhibition of signal transduction with VDC597 would result in antineoplastic effects that would provide a potentially beneficial

additional component of chemotherapeutic protocols in the treatment of canine osteosarcoma and lymphoid tumors.

Chapters 2 and 3 initially report the *in vitro* expression and activation of the pathway in canine osteosarcoma cells and lymphoid tumor cells, respectively. Subsequently, PI3K/mTOR dual-inhibition with VDC597 was examined for antineoplastic activity, as a single-agent treatment and in conjunction with currently used chemotherapy drugs for these tumor cell types. Growth inhibition and cell death assays were used to evaluate the efficacy of VDC597 for reducing cell survival and induction of apoptosis in these tumors. Western blots and immunohistochemistry were used to study the reduction in pathway activation. Scratch assays and Boyden chamber assays were used to investigate the inhibition of chemotactic and non-chemotactic migration and invasion in osteosarcoma cells. ELISA assays were used to examine the anti-angiogenic effects of the compound on vascular endothelial growth factor production by lymphoma, leukemia, and osteosarcoma cells. In all these tumor types, the results of this study demonstrate a dose-dependent: reduced signal transduction; increased cell death; reduced cell proliferation, migration, invasion, and vascular endothelial growth factor production *in vitro*. These effects were additive to mildly synergistic when VDC597 was combined with the chemotherapy drugs tested.

Chapter 2 also presents our evaluation of the efficacy of oral administration of VDC597 for osteosarcoma treatment in a xenograft mouse model. Our results demonstrate reduced tumor growth and increased survival time in mice treated with VDC597 alone and in combination with carboplatin. We also used immunohistochemistry to evaluate pathway activation, and localization of a downstream

target—the forkhead box O1 transcription factor (FOXO1)—in tumor samples from these mice. There was marked reduction in phosphorylation of pathway components and increased intranuclear FOXO1 immunolocalization in mice treated with VDC597, indicating a correlation between reduced tumor growth and inhibition of signal transduction. Based on these findings, we sought to use FOXO1 immunohistochemistry as a proxy for phosphoprotein detection in decalcified formalin fixed paraffin embedded osteosarcoma samples from canine patients, but found that, unlike the xenograft tumors which were treated with a PI3K/mTOR inhibitor, a correlation between tumor biologic behavior and FOXO1 immunoreactivity was not present in the patient derived tumor sections. Chapter 3 also presents findings from immunohistochemical evaluation of formalin-fixed paraffin embedded lymph node samples from patients diagnosed with B-cell lymphoma, in which the expression of phosphorylated components of the PI3K-AKT-mTOR pathway was examined for correlation to outcome data and prognostic indicators. We noted marked variation in the degree of phosphorylation in lymphoma samples between different patients. Major histocompatibility complex class II expression and post-treatment relapse status were correlated to phosphorylated AKT and phosphorylated eukaryotic translation initiation factor 4E-binding protein 1 expression, respectively. There was no correlation, however, between phosphoprotein immunoreactivity and clinical outcome.

Collectively, the results from our *in vitro* and *in vivo* xenograft experiments indicate there is a good basis for the use of dual-inhibition with VDC597 in the treatment of canine osteosarcoma and lymphoid tumors. Our immunohistochemical examination of osteosarcoma expression of FOXO1 and lymphoma expression of phospho-proteins

within the signaling cascade indicate there is need for further investigation to better understand the variability and complexity of signal transduction in the canine patient to help better guide treatment regimens that involve such targeted inhibition. Through future studies to better characterize and correlate pathway expression by these tumors in the canine patient, we can better tailor treatment protocols. Future clinical trials will better demonstrate the potential efficacy of incorporation of VDC597 into cancer treatment in the canine patient and serve as a useful model for comparative oncology and similar inhibition in human tumors.

ACKNOWLEDGEMENTS

Good research and publication are never done alone. None of this would be possible without all the hard work, innovative contributions, and support of colleagues, advisors, professors, family, and the institutions they form. After all, that's what institutions are: people, and a lot of good ones. Being as grateful as I am to everyone who contributed to finally seeing this project to completion, sometimes hard to avoid feeling unworthy. I'll attempt refrain from maudlin meanderings and *try* to avoid being absurdly loquacious. The collaborative environment at the FACC and CSU allows for young scientists to take advantage of resources that can truly help to shape an investigative career. So many experiments utilizing IHC would not be possible without the assistance provided by Mac Harris and Laura Ashton at the Experimental Pathology Facility, by Todd Bass and all the folks in the Histology Lab, and by Jade Kurihara and the Dow lab in photomicrograph acquisition.

None of this would be possible without the guidance, support, direction, and drive of Dr. Doug Thamm, for whom I truly lack the capacity to express my respect and appreciation. This is someone who manages to coordinate a lab, foster a collaborative and fun environment, allow lab members the free-rein and flexibility to run on tangential investigations, and somehow remains as productive and innovative as he is. How someone manages this is impressive. How someone does this while so consistently remaining easy-going and generous in offering his wisdom, insight, understanding, and time is so utterly baffling to me that I admittedly have occasionally been inclined to think there must be *some* point at which he at least exhibits a break in the professional, friendly, conscientiousness, and collaborative drive. After knowing him for over a

decade—yes, I said *decade*—I have yet to find that point. I am indescribably grateful for his role as advisor, principal investigator, and friend.

My committee members have each given me more than I could rightfully ask. Dawn Duval's insights into various aspects of investigation (both genomic and practical) have not only taught me some valuable lessons in considerations for study design, but also saved me from many long nights in the lab. The understated cutting humor with which she delivers some of these insights is the kind of lagniappe that is capable of bringing forth an appreciative smirk and chuckle over several recollections. Dan Gustafson is an absolutely invaluable member of my committee and I can only hope that there are many graduate students lucky enough to have him or someone like him to offer advice. His ability to analyze study design, stats, and experimental results to find points to strengthen is undoubtedly well known and greatly appreciated. But his scant tolerance for, and ability to cut through, the fallalery sometimes encountered in the academic research setting is greatly appreciated by someone like me, who can get hung up in the minutiae. The no-nonsense delivery is also the kind of thing I value, as I can be a bit dense and *genuinely* value a helpful "Nah, don't waste your time on that" (which is sound advice because it sits on the foundation of his wealth of knowledge). Gregg Dean consistently offers incisive assessments and analytical insight into research reporting and study design, which I'm sure is well known. But his skills of observation and compassion extend into the to the interpersonal realm in a way I suspect to be underappreciated due to his professionalism and friendliness. I can say without doubt that Gregg was the one person who *saw* me when I likely most needed someone to, and helped me to recognize something in myself and turn the corner I

needed to (it's something I reflect on and appreciate probably more than he knows). Gary Mason is the type of professor that every academic institution needs. In fact, every academic institution needs *many* Gary Masons. In the somewhat insular world of academic tertiary care facilities, it's all too easy to see only the trees without recognizing the forest. Dr. Mason has an ability to jolt someone out of the hyper-focused state and look at the context that I wish was more prevalent in our world. If, by some odd chance, any pathology residents are reading this, don't let that "aw shucks" demeanor fool you. This guy is smart as a whip and has a plethora of knowledge and can help you to maintain a perspective that will allow you to evaluate a case better than you ever could by burying yourself in all the specialized publications you can find. As with academia, a Mason is needed on the committee of every graduate student, because a Mason will be able to pull you out of your simultanagnosia with a single simply stated yet perspicacious observation.

My colleagues and friends in the lab have helped in more ways than they could know. From Barb Rose and Jenette Shoeneman, who were there to help me get my feet on the ground, to Rachel Brady, Sam Brill, Kristen Farrell, and Lisa Schlein, who offered not only technical help and insight but also valuable perspective, I think the single thing that was the greatest boon was actually not related to work much at all (though I could enumerate myriad ways in which each of them provided the key to a problem that unlocked a new avenue of investigative thought for me). Each and every one of them provided a moment of enjoyable conversation or witty observation or amusing anecdote that not only made me value their friendship, but helped to pull me out of my shell in a

way that I will likely carry with me and value more than the numerous technical or practical professional insights.

Loved ones are indeed the foundation on which we build our pinnacles and there is no stronger support than I have been fortunate enough to have in my wife, Alice Baker Meuten, and my father, Don Meuten. There are no words. Truly. The sound advice and unconditional support are something I can only wish others are lucky enough to find in their lives. The astute reader who has managed to slog through all my meanderings here may have noticed a theme focusing on the interpersonal and a couple glancing references to some slow progress or difficulties I may have had. To that reader, and to anyone who may need to hear it: your observations are accurate. I've learned to value the interpersonal aspects because those can sometimes be the gifts you didn't know you needed. The people mentioned in this acknowledgement have my thanks not only for their professional help but also for their patience and personal help. To this reader I would also say: if you're having any mental health issues, don't stay silent. People like those mentioned above will surprise you. Statistically speaking, it's impossible that I found *all* the good ones.

DEDICATION

To Alice. I can only hope that, over our remaining years, I can provide some fraction of the love, patience, and extraordinary level of support to you in our lives that you have provided to me. I'm certainly going to try my best to one up you on this front.

TABLE OF CONTENTS

CHAPTER 1: LITERATURE REVIEW[i]

Overview

Tumors in dogs and humans share many similar molecular and genetic features, incentivizing a better understanding of canine neoplasms not only for the purpose of treating companion animals, but also to facilitate research of spontaneously developing tumors with similar biologic behavior and treatment approaches in an immunologically competent animal model. In multiple tumor types of both species, there is similar dysregulation of signal transduction through phosphatidylinositol 3-kinase (PI3K), AKT serine/threonine kinase (AKT), and mechanistic target of rapamycin (mTOR), collectively known as the PI3K-AKT-mTOR pathway, which is involved in many processes promoting tumor growth, survival, metabolism, angiogenesis, extracellular matrix interactions, and neoplastic cell motility and invasion necessary for metastasis. As is often the case in the veterinary field, the basic research in normal cellular signaling cascades for dogs is not as completely documented. As such, this review utilizes the discoveries in PI3K-AKT-mTOR signaling in human literature to build the foundational background information for a better understanding of the criticality of this pathway in cellular homeostatic and regulatory activity, as well as feedback mechanisms. This chapter aims to summarize the development to our current understanding and review the role of PI3K-AKT-mTOR signaling in health, alterations in cancer development and progression, and significance specifically to canine

[i] Portions of this chapter are previously published in:
Meuten TK, Dean GA, Thamm DH. Review: The PI3K-AKT-mTOR signal transduction pathway in canine cancer. *Vet Pathol*. 2023;6(3)(3):339–356. https://doi.org/10.1177/03009858231207021

neoplasms, with a brief discussion of pathway activity in human osteosarcoma and lymphoma for comparative purposes. It will then present a synopsis of current understanding of PI3K-AKT-mTOR signaling in important canine cancers and advancements in targeted inhibitors of this pathway.

Historical perspective of PI3K-AKT-mTOR Pathway Research[ii]

Formerly known as protein kinase-B (PKB), AKT serine/threonine kinase (AKT) research originated in 1977 with the discovery of a murine leukemia virus (MuLV), AKT8, isolated from T-cell lymphoma of thymuses of pre-leukemic and leukemic high ecotropic MuLV AKR/J mice that was capable of producing *in vitro* foci of malignant transformation in the mink lung epithelial cell line, CCL-64.[1] However, investigators found that AKT8 was incapable of producing foci in other cell lines, suggesting the presence of a novel oncogene.[1] Further study demonstrated that this was, in fact, a cell-derived oncogenic sequence, which investigators termed *v-akt.*[2] The AKT8 virus was also found to be capable of inducing thymic lymphoma in AKR/N and NFS mice.[2] A subsequent survey of human neoplasms found amplification of *AKT1*, the human homologue of *v-akt*, in gastric adenocarcinoma, demonstrating that AKT8 contained a highly conserved cellular sequence we now know to be involved in multiple malignancies affecting humans and animals, alike.[3] Later investigation identified a gene encoding a serine/threonine protein kinase related to the A and C kinases, which had *in vitro* kinase activity (the protein was termed Rac, and later PKBα, and then AKT1).[4]

[ii] The genes and proteins currently abbreviated as *AKT*/AKT were previously known as PKB. As such, there are references made to genes identified and reported as *PKB* or *pkb* at that time. For clarity, the corresponding protein is abbreviated herein as AKT instead of the original PKB. Additionally, references to mouse viruses and strains mentioned in this historical context, and not discussed later, use abbreviations standard at that time.

Bellacosa et al. found that the sequence for *v-akt* and its translated protein shared similarity with protein kinase C (PKC) and demonstrated that AKT, the cellular homolog of *v-akt* is a PKC-related serine-threonine kinase with a noncatalytic domain containing Src homology-2 (SH2) region, suggesting that AKT is a functional link between tyrosine and serine-threonine phosphorylation pathways.[5] Concurrent molecular cloning investigation, using human cell lines, identified the *PKB* gene and characterized two isoforms of the translated AKT protein independent of the viral form previously used, thus confirming a cellular origin of the widely expressed phospho-protein kinase corresponding not only to the oncogene but also indicative of normal cellular function.[6,7] Within a few years, the specific structural properties and the role of Pleckstrin homology (PH) domains in recruitment, binding, and activation of AKT—along with upstream members of the phosphatidylinositol 3-kinase (PI3K) to AKT signal transduction pathway—were characterized and are discussed below.[8,9] By 1995, wider examination of the roles of AKT in cellular processes and in other species had greatly accelerated. As more thorough research into the structure of AKT progressed, investigators recognized its role in nucleating the formation of protein complexes in cells to mediate protein interactions.[10] We now know about the activity of 3 widely expressed isoforms of AKT, highly conserved in mammalian species and involved in diverse cellular processes through a web of signaling pathway interactions. During the same time of these discoveries, investigation into other upstream activators of AKT was simultaneously unfolding through the study of cellular metabolic processes and insulin receptor signaling.

Identification and characterization of the PI3K-AKT pathway—and activating receptor tyrosine kinases (RTKs)—dates back to the 1980's, during investigation of metabolic cellular activity in response to hormones and insulin receptor signaling.[11,12] At this time, there was great interest in cellular pathways leading to PKC activation, due to its importance in multiple cellular processes. There was particular focus on signal transduction pathways involving phospholipase C (PLC) hydrolysis of membrane phospholipids, phosphatidylinositol-4,5-bisphosphate (PIP_2; formerly $PtdIns(4,5)P_2$) and phosphatidylcholine for the generation of inositol-1,4,5-trisphosphate (IP_3; $Ins(1,4,5)P_3$), phosphocholine, and diacylglycerol (DAG), which then activated PKC in conjunction with calcium mobilization.[13,14] During this time, there was a gap in understanding of the specific mechanistic links by which this important activation occurred. However, during the same period, investigation leading to the discovery and characterization of PI3K was sparked by Cantley et al. with the observation that transforming viral oncoproteins $pp60^{v\text{-}src}$ (of Rous sarcoma virus) and middle-T antigen (of polyoma virus) interact with phosphatidylinositol (PI) kinase activity and greater PI turnover, indicating that viral transformation may be directly connected to a network of second messengers involved in PI turnover.[15,16] In the subsequent years, researchers more thoroughly classified multiple PI kinases. Initial studies classified Type I PI kinase, associated with activated tyrosine kinases and platelet derived growth factor receptor (PDGFR) and Type II PI kinase, inhibited by greater concentrations of adenosine diphosphate and adenosine monophosphate. The authors concluded that these relationships indicated a role in cell signaling cascades involved in cell growth and transformation (Type I) and cellular metabolism/energy (Type II).[17,18] Further study characterized the specific reactions and

products of these kinases, finding that a Type I PI kinase phosphorylated the D-3 position on the inositol ring to generate phosphatidylinositol-3-phosphate (PI3P), marking the discovery of the PI3K family of kinases involved in this process.[19] The subsequent characterization of additional PDGF-dependent phosphatidylinositol-phosphate (PIP) intermediates in PI3K-dependent signaling, and isolation of PI3K from animal tissue underlined the important role of PI3K in cellular metabolic and mitogenic activity.[20,21] Additionally, around that same time, Stephens et al. demonstrated that PI3K was the mechanism through which PIP_2 was phosphorylated to become phosphatidylinositol-3,4,5-trisphosphate (PIP_3), which would later be emphasized as an important component of many signal transduction cascades, including AKT activation.[22]

Knowledge of the mitogenic activity of RTKs (as shown through RTK oncogene studies) and the expanding understanding of the role of PI3K in cellular functions initiated by growth factor receptors with intrinsic RTKs (including receptors for insulin, CSF1, EGF, FGF2, and PDGF) paved the way for further investigation of intracellular downstream targets for their contribution to mitogenic potentiation.[23] A major step in advancing understanding of target interactions downstream from PI3K was the identification of conserved modular protein domains and the importance of the 100-amino acid residue length PH domain in binding to lipophilic molecules, notably PIP_2, indicating a step of membrane localization for these proteins.[24,25] The conclusion of such findings in the early 1990's was that proteins with PH domains likely had important roles as downstream effectors of PI3K activation.[26] As mentioned above, in 1993, AKT was found to be one of the many signal transduction proteins with the same highly conserved PH domain, indicating a potential relationship to PI3K signaling.[9] This

relationship of AKT activation occurring in a PI3K-dependent manner was then demonstrated by using the PI3K inhibitor, wortmannin, and a dominant-negative mutant of PI3K to block activation of AKT by platelet derived growth factor (PDGF), epidermal growth factor (EGF) and basic fibroblast growth factor (now known as fibroblast growth factor 2; FGF2).[27] However, it was also found that PI3K was not the only regulator of AKT activation when a group demonstrated that the binding of Akt-1 to PIP_3 alone did not produce the kinase activation expected.[28] These findings suggested that there was another component to AKT activation. In 1997, the link between PI3K and AKT was more completely elucidated when researchers demonstrated that AKT activation was dependent not only upon the phosphorylation of PIP_2 to PIP_3, but also upon the activity of phosphoinositide dependent protein kinase 1 (PDPK1; formerly abbreviated PDK1), concluding that the binding to the PH domain of AKT to PIP_3 promotes the phosphorylation of AKT on the threonine 308 amino acid residue (T308) by PDPK1, which was also later shown to be dependent on PH domain binding for its localization in this phosphorylation process both *in vitro* and confirmed *in vivo* through knockout experiments.[29-31] Collectively, these findings make it apparent that AKT activity is promoted in response to growth factor stimulation through PI3K phosphorylation of a second messenger system using PIP_3 that allows for PDPK1 and AKT localization for activating phosphorylation of AKT. This PI3K-dependent PIP3 generation is now generally accepted as the rate-limiting step in AKT activation.[32] However, the above findings do not account for the negative regulation of PI3K-dependent AKT activation that logically must be present as well under normal conditions. That question is largely

answered by concurrent study into the regulatory role of phosphatase and tensin homolog (PTEN) as the primary means of inhibition in this process.

During the same period as the PI3K research discussed above, other groups noted the presence of deletions of large regions of chromosome 10 in multiple tumor types.[33] The identification of the *PTEN* gene (encoded on chromosome 10) by Steck et al., in concert with characterization of the encoded protein by Li et al. during their investigation of the tumor suppressor activity of protein tyrosine phosphatases, highlighted the importance of the role of PTEN in suppressing tumorigenicity.[33,34] PTEN specifically dephosphorylates PIP_3 to PIP_2, not only inhibiting PI3K-AKT signal transduction, but reducing signaling to downstream targets and countering the tumorigenic effects of AKT activation, including an induction of G1 cell cycle arrest, in a manner independent of upstream PI3K or growth factor receptor activity.[35-37] While PTEN phosphatase activity is still regarded as the primary means of limiting PI3K-AKT signaling, additional regulatory proteins were also found to play an inhibitory role in AKT phosphorylation and activation. In 1996, researchers discovered that protein phosphatase 2A (PP2A) dephosphorylates AKT at the T308 position.[38] In later years, Gao et al. found that The PH domain leucine-rich repeat protein phosphatases (PHLPPs) dephosphorylated AKT at its other primary site of activating phosphorylation: the serine 473 amino acid residue (S473), resulting in suppression of some of the tumorigenic effects of AKT signaling.[39] At the same time, investigations into the phosphatase activity of inositol polyphosphate 4-phosphatase-II (INPP4B), inositol polyphosphate-5-phosphatase D (INPP5D; formerly known as SH2 domain-containing inositol 5'-phosphatase 1; SHIP1), and inositol polyphosphate phosphatase like 1

(INPPL1; formerly known as SH2 domain-containing inositol 5'-phosphatase 2; SHIP2) revealed that they also played a role in inhibition of PI3K-AKT signaling. Collectively, the studies showed that: SHIP and INPP4B both play a role in dephosphorylation of PIP_3 to PIP_2 and phosphatidylinositol 3-phosphate (PI3P) in an insulin responsive manner, wherein the initial dephosphorylation of PIP_3 by SHIP-1/2 (INPP5D/INPPL1) results in a specific form of PIP_2 (PI(3,4)-P2), which is still able to recruit AKT and be converted to an active PIP_3 by some class II PI3Ks.[40-48] However, INPP4B is then able to dephosphorylate PI(3,4)-P2 to PI3P, which prevents both recruitment of AKT and ready generation of PIP_3.[40-48] Additionally, INPP4B is now considered likely to inhibit selectively inhibit AKT2 beyond simple generation of PI3P.[42,48] The antitumorigenic effects of this process were supported by the finding that *INPP4B* loss of heterozygosity is associated with high grade carcinomas and poorer prognosis.[43]

The contributions by the many investigations to this point combine to paint a more complete picture of the relationship between AKT and its activation due to PI3K and PDPK1, leading to the numerous downstream effects of PI3K-AKT signal transduction, as well as physiologic inhibition of PI3K-AKT signaling by PTEN, SHIP, INPP4B, PHLPPs, and PP2A.[29-31,38,39,49,50] At the present juncture, this summary of the foundational research of the PI3K-AKT-mTOR pathway has only discussed the initial phases of signal transduction, without discussing the importance of S473 phosphorylation or examining the downstream effects. For that knowledge, we must first turn to the study of another kinase by many researchers that traces its origins to a discovery initially made on Rapa Nui (aka Easter Island) for an understanding of the important signal transduction proteins downstream of AKT.

Investigation of the highly evolutionarily conserved checkpoint protein kinase, mechanistic target of rapamycin (mTOR), dates back to the study of the immunosuppressive and anti-proliferative effects of the antifungal macrocyclic lactone, rapamycin, originally isolated from *Streptomyces hygroscopicus* on Rapa Nui.[51] In 1991, Heitman et al. published their findings that resistance to the antimycotic properties of rapamycin was conferred when there was a mutation in the genes encoding for the Tor protein in *Saccharomyces cerevisiae*.[52] Specifically, they found that the active complex formed between rapamycin and FK506-binding proteins (FKBP; prototypic members of the immunophilin family) induces irreversible cell-cycle arrest in G1 phase, and that the effects of the rapamycin-FKBP complex were negated when there were mutations in the genes FPR1, TOR1, and TOR2.[52,53] Rapamycin and FK506 (now commonly known as tacrolimus) are structurally similar macrolides that were under investigation at that time as potential immunosuppressant drugs for their ability to inhibit T-cell-dependent immune responses by interfering with signal transduction necessary for antigen-induced T-cell activation and proliferation.[54] It was found that, similar to observations in *S. cerevisiae*, rapamycin induced G1 arrest in T-cells in a manner that occurred regardless of IL-2 stimulation, which differentiated it from the mechanism of action of tacrolimus.[55,56] Following on these findings, there was examination of G1 arrest in multiple mammalian cell types, which yielded not only the characterization of a rapamycin-FKBP12 complex in mammalian cells, but also the isolation of a mammalian ortholog of the yeast Tor proteins.[57-63] Upon the discovery of this highly conserved and widely active mammalian TOR—now known as mechanistic target of rapamycin (mTOR)—there began targeted research into the specific role in pathways, including

indicators of mTOR activity and downstream effectors. Subsequent studies elucidated the ability of the intrinsic kinase activity of mTOR to autophosphorylate, as well as its phosphorylation of immediate downstream targets, inhibiting eukaryotic translation initiation factor 4E (EIF4E)-binding protein 1 (4EBP1) and activating ribosomal protein S6 kinase beta-1 (S6K1; RPS6Kβ1), which was blocked with rapamycin administration.[63,64] Additionally, research at this time noted the inhibition of mTOR activity using PI3K inhibitors, including wortmannin, indicating mTOR to be a downstream effector of PI3K pathway activation, responsive to growth factor and insulin activity, among other stimuli.[65] The specific mechanisms by which TOR proteins were responsive to upstream metabolic signals was better elucidated when Tor1 and Tor2 protein complexes were isolated and constituent proteins in the complexes were identified in yeasts.[66] Subsequently, the mammalian orthologs associated with the rapamycin-sensitive mTORC1 and rapamycin-insensitive mTORC2 were identified. Researchers found that, beyond the kinase activity, the protein complexes functioned in specific ways. The mammalian ortholog of lethal with SEC13 protein 8—known as mTOR associated protein mLST8 (mLST8)—is a subunit present in both TOR complexes, and potentiates activity.[67] mTORC2 was found to be primarily involved in cytoskeletal regulation, and rapamycin-insensitive companion of TOR (RICTOR) is a necessary scaffold protein of the complex for functionality.[68] Further study of the function of RICTOR demonstrated that it is needed for mTORC2 to phosphorylate and partially activate AKT on the S473 amino acid residue, which in turn greatly facilitates phosphorylation and full activation of AKT on T308 by PDPK1.[69] Regulatory-associated protein of TOR (RAPTOR) is associated with mTORC1, and research at the time found

that it binds to 4EBP1 and S6K1, indicating a key role for RAPTOR in mTORC1 phosphorylation of these downstream effectors, in response to changes in nutrient inputs.[70-72]

The connection between mTOR activity and PI3K pathway activation in response to insulin, nutrients, and growth factor signals was elucidated through evaluation of AKT expression *in vitro*. Gingras et al. found that overexpression of activated AKT in HEK-293 embryonic kidney cells resulted in wortmannin-resistant, rapamycin-sensitive phosphorylation of 4EBP1 in the absence of growth factors via mTORC1, and that insulin-mediated phosphorylation of 4EBP1 was suppressed in cells expressing a dominant-negative form of *AKT*.[73] There were concurrent studies in *Drosophila* further supporting and clarifying the relationship between mTor and Akt *in vivo*, as well as evaluation of *Akt1/Akt2* double-knockout mice demonstrating that Akt is upstream of mTOR.[74,75] However, there was a disparity in the phosphorylation of S6K1 and 4EBP1 relative to AKT activation that indicated an additional step between AKT and mTORC1, that mediated the effect of AKT activation on S6K1 and 4EBP1 phosphorylation.[76] Studies in *Drosophila* evaluating mutations of the tuberous sclerosis complexes that form a heterodimer (TSC1 and TSC2), demonstrated that alterations in expression of Tsc1 and Tsc2 yielded similar phenotypic changes to inactivation of *PTEN*.[77] These researchers then demonstrated that Tsc1-Tsc2 complex is inhibited through phosphorylation of Tsc2 by Akt, thus showing that Tsc1 and Tsc2 were components of the PI3K-Akt pathway.[78] The phenotypic changes associated with changes in expression of Tsc and Pten were consistent with it acting through Torc1, and this conclusion was supported through *in vitro* experiments in mammalian cells directly

demonstrating that mTORC1 and its downstream targets are negatively regulated by the TSC1/TSC2 heterodimeric complex, unless TSC2 is phosphorylated by AKT.[79,80] The specific mechanism was uncovered by referring to structural and functional studies of TSC1 and TSC2. These studies found that TSC2 possessed a GTPase-activating protein (GAP) at its carboxyl-terminus (C-terminus), which in turn required binding by TSC1 through the leucine zipper on its amino-terminus (N-terminus) for full enzymatic activity.[81,82] The answer to how GAP activity of the TSC1/TSC2 complex was involved in mTORC1 inhibition came about with the characterization of Ras homolog enriched in brain—now known as Ras homolog, mTORC1 binding (RHEB)—through genetic and epistatic experiments in *Drosophila*, as well as biochemical analyses of mammalian cells *in vitro*. Collectively, the research demonstrated that: RHEB acts downstream of TSC1/TSC2 and upstream of mTOR; TSC2 functions as a GAP to RHEB, inhibiting its activity; overexpression of RHEB results in activation of mTORC1, despite upstream PI3K pathway inhibition; dominant-negative RHEB expression blocks mTORC1 activation by PI3K pathway activation; and these results are measurable by downstream phosphorylation of 4EBP1 and S6K1, which can be inhibited by rapamycin.[83-87]

The above findings solidified understanding of the roles of PI3K, AKT, and mTOR—leading to downstream effectors 4EBP1/EIF4E, S6K1, and others—in synthesis of proteins involved in cellular metabolic functions, which are now implicated in cancer development and progression. The pathway interactions described above are shown in Figure 1.01 later in the chapter. The numerous contributions to the body of research leading to the present day were made by examining the mechanisms of PI3K-AKT-mTOR signaling across multiple species and integrating the findings from *in vitro*

and *in vivo* studies in yeasts, insects, rodents, higher mammals including humans, and cell lines of the respective species to build a foundation that we can now use for veterinary and medical oncology. The remainder of the chapter will build on this foundation to reframe the preceding historical perspective in the context of the current understanding of the role of PI3K-AKT-mTOR signal transduction in neoplasia and the current state of targeted pathway inhibition in oncology. The following review aims to delineate the pertinent aspects of the PI3K-AKT-mTOR signaling pathway in health and in tumor development, and examine the results of activity on downstream effectors on tumor growth and survival with a focus on canine cancers. It will then present a synopsis of current understanding of PI3K-AKT-mTOR mutations and dysregulation in important canine cancers and advancements in targeted inhibitors of this pathway for the canine patient and the value of that information for contribution to comparative oncology.

The Canine Patient and Comparative Medicine

Tumors in dogs and humans share many similar molecular and genetic features, incentivizing a better understanding of canine neoplasms not only for the purpose of treating companion animals, but also to facilitate research of spontaneously developing tumors with similar biologic behavior and treatment approaches in an immunologically competent animal model. Comparative oncology is an expanding field that offers unique benefits for better understanding cancer development in humans and companion animals. Neoplasia is one of the leading causes of morbidity and mortality in dogs, with 4.2 million dogs diagnosed with cancer each year in the USA (population rate of

5,300/100,000), as reported in 2015.[88] Dogs provide a valuable spontaneous animal model for cancer with distinct advantages as compared to rodent models, including a genetically diverse population with comparable environmental exposures and complex interactions between the immune system and tumor. Canine neoplasms also have clinical presentations, pathophysiology, chemotherapeutic resistance, and biologic behavior that better recapitulate the natural progression of human cancer than induced cancer animal models. Advancements in genomic and molecular understanding of cancer in dogs and humans is revealing increasing numbers of conserved biochemical pathways shared between the species.[89] For these reasons, there is great value in investigating signal transduction cascades in canine tumor development for comparative oncology, as well as to provide our canine companions with improved cancer treatment.

The PI3K-AKT-mTOR signal transduction pathway is constitutively activated in many cancers and is involved in mediating an array of cellular processes, including proliferation, survival, nutrient uptake, metabolic activity, and anabolic reactions (protein synthesis). This signaling pathway is highly conserved across species. Likewise, there is evidence for similar roles of pathway activation in tumor development across species as well, and the value of canine and human studies to comparative oncology in multiple tumor types has been analyzed and reviewed elsewhere.[90-96] As is often the case in the veterinary field, the basic research in normal cellular signaling cascades for dogs is not as completely documented and an effective summary of PI3K-AKT-mTOR signal transduction must incorporate knowledge from human medicine for comparative purposes.

While not as expansive in physiologic mechanistic descriptions, the veterinary literature does elucidate the value to comparative oncology offered by the similar mutations and PI3K-AKT-mTOR pathway activation between human and canine neoplasms. Often the contributions to the body of knowledge are small and stepwise in veterinary oncology, in part due to limitations on scope of experimentation. Veterinary research does not always examine tumor samples through multiple modalities for more thorough correlation between genes, transcripts, protein expression, and protein phosphorylation (indicating pathway activation). Moreover, consistent antibody validation for canine studies is needed. As such, there are greater limitations on the breadth of definitive statements that can be made regarding the relationship of mutations, expression, and pathway activation in canine tumors. However, it is an expanding field.

Current Understanding of PI3K-AKT-mTOR Signal Transduction

The canonical PI3K-AKT-mTOR signal transduction cascade is complex with multiple points of initiation, regulation, and effector outcomes (**Figure 1.01**). Normal pathway activation occurs when extracellular signals activate growth factor receptor tyrosine kinases (RTKs), such as insulin receptor (IR), insulin-like growth factor 1 receptor (IGF1R), fibroblast growth factor receptor (FGFR), epidermal growth factor receptor (EGFR), platelet-derived growth factor receptor (PDGFR), erb-b2 receptor tyrosine kinase 2 (HER2; ERBB2), and hepatocyte growth factor receptor (HGFR; also known as mesenchymal-epithelial transition factor; c-MET). Activated RTKs phosphorylate adaptor proteins, GRB2-associated-binding protein 1 and 2 (GAB1/2),

insulin receptor substrate 1 and 2 (IRS1/2), and fibroblast growth factor receptor substrate 2 (FRS2), which bind the amino-terminal domain of the p85 regulatory subunit of PI3K, via YXXM motifs.[97,98] This binding relieves p85 inhibition of the p110 catalytic subunit of PI3K and recruits the p85–p110 heterodimer to its substrate, PIP_2, at the plasma membrane to activate class I PI3K.[99] Isoforms of these catalytic and regulatory subunits are pertinent to feedback mechanisms, correspond to genetic mutations altering expression in various neoplasms, and are targets for specific PI3K inhibitors in oncology.

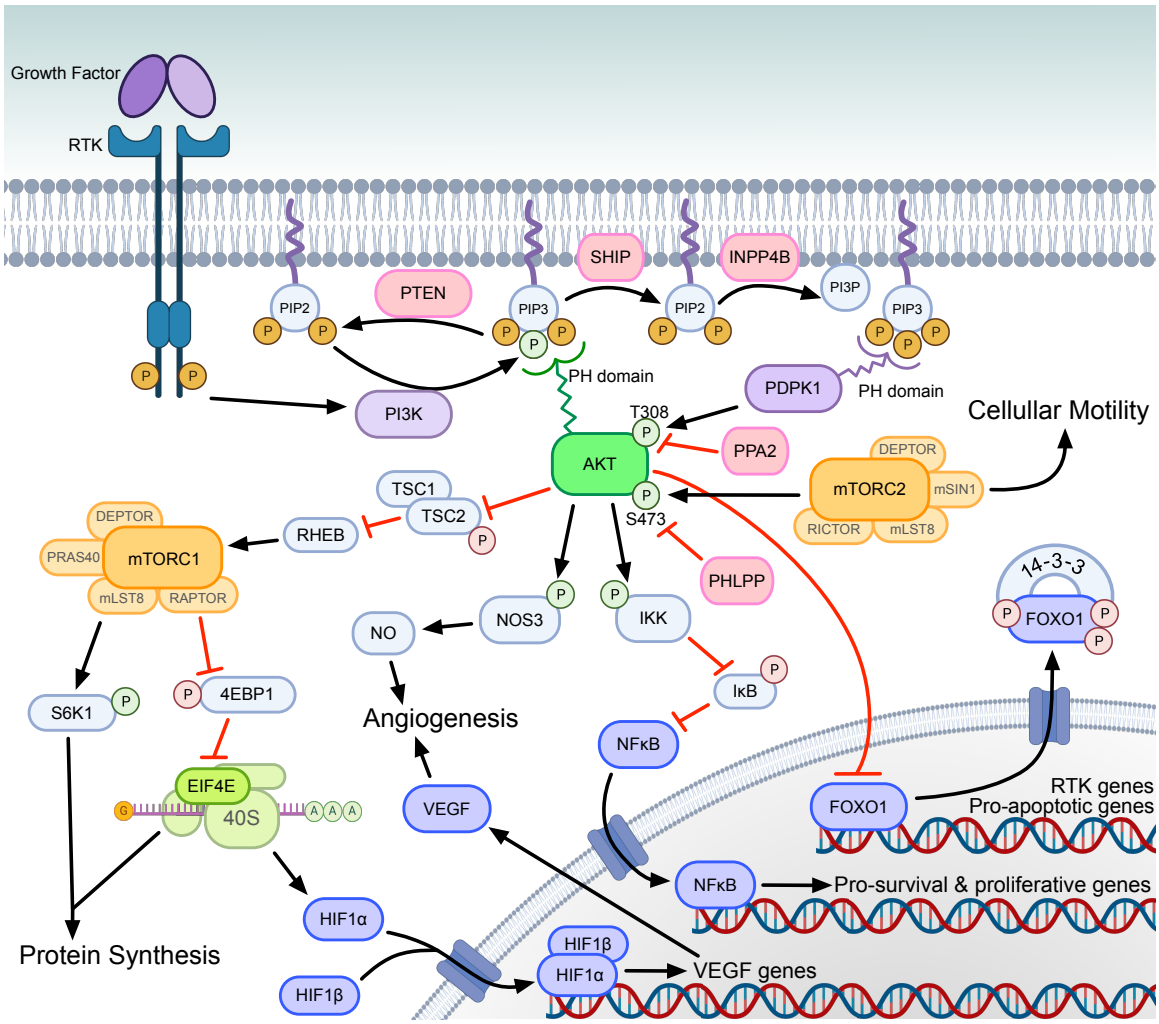

Figure 1.01: PI3K-AKT-mTOR signal transduction cascade.
Activation: Growth factors and signaling proteins activate RTKs at the cell surface, which activate PI3K. PI3K is responsible for phosphorylating PIP_2 to PIP_3. PIP_3 is necessary for recruitment, PH domain binding, and subsequent activation of AKT by PDPK1 and mTORC2. Green and red phosphates in the figure indicate activating and inhibiting phosphorylation events, respectively. Phosphorylated AKT acts on multiple target proteins that promote the survival, growth, and metastasis of cancer cells. AKT alters gene expression through regulation of nuclear translocation of transcription factors (dark blue) both indirectly (e.g. NFκB) and directly (e.g. FOXO1). Phosphorylation of FOXO1 causes extranuclear transport, reducing transcription of pro-apoptotic genes. Phosphorylation of IKK allows NFκB to enter the nucleus and transcribe genes promoting survival. AKT phosphorylates and inhibits the TSC heterodimer, which leads to mTORC1 activation. mTORC1 activates S6K1, which phosphorylates ribosomal protein S6 to promote translation of mRNA to proteins involved in cellular growth, proliferation, and glucose metabolism. mTORC1 also inhibits 4EBP1, which allows for EIF4E to selectively translate oncogenic proteins involved in cellular growth, proliferation, migration, invasion, and angiogenesis. Angiogenesis is increased through EIF4E-mediated translation (e.g. HIF1α), as well as phosphorylation of NOS3 by AKT to increase NO production.
Inhibition: PTEN and SHIP each dephosphorylate PIP_3 at specific sites to generate PIP_2, where PTEN generates PI(4,5)-P_2 and SHIP generates PI(3,4)-P_2; INPP4B further dephosphorylates PI(3,4)-P_2 to PI3P; PPA2 and PHLPP dephosphorylate AKT at T308 and S473, respectively.
[Figure created with BioRender.com]

PI3Ks are a family of intracellular lipid kinases that phosphorylate the 3'-hydroxyl group of the inositol ring on intracellular membrane-bound phosphatidylinositol (PI). There are three PI3K classes, which serve both overlapping and distinct cellular functions through their phosphorylation of their respective PIs, though Class I PI3Ks are of primary interest in neoplastic processes and the focus of this text. PI3K classes and subunit isoforms are listed in **Table 1.01**. The roles of the other two classes of PI3Ks in various tissues and disease processes are reviewed in greater detail elsewhere, and are only mentioned herein in reference to mutations involved in certain tumors.[100-102] As a very brief summary of their roles in cellular processes, class II PI3Ks (PI3KC2α, PI3KC2β, and PI3KC2γ in vertebrates) and the single known class III PI3K, ubiquitously expressed in eukaryotes (known as vacuolar protein sorting 34, Vsp34), are involved in endocytosis, protein sorting, some receptor signaling, cellular migration, and promotion of autophagy.[100-102] While only catalytic subunits comprise class II PI3Ks, class I and class III PI3Ks have both catalytic and regulatory subunits. Class I PI3Ks serve their primary role through interaction with cell surface receptors and subsequent activation of signal transduction. Class IA PI3Ks are primarily activated by receptor tyrosine kinases (RTKs) and Ras GTPases, and class IB PI3Ks by G-protein-coupled receptors (GPCRs).[97] Class I PI3Ks are involved in receptor signaling, cell growth and metabolism, and inhibition of apoptosis and autophagy. Pertinent to the tumorigenic processes of PI3K-AKT-mTOR pathway, class I PI3Ks promote signal transduction when they phosphorylate phosphatidylinositol-(4,5)-bisphosphate (PIP_2) to phosphatidylinositol-(3,4,5)-trisphosphate (PIP_3).[103] In opposition of PI3K activity, phosphatase and tensin homolog (PTEN) regulates the signaling duration of PIP_3 by

dephosphorylating to PIP_2.[48,104,105] In its phosphorylated form, PIP_3 recruits AKT and phosphoinositide-dependent kinase-1 (PDPK1) to the plasma membrane, and binds to their Pleckstrin homology (PH) domains, where PDPK1 phosphorylates the T308 amino acid residue of AKT.[8,9,24,26,30] Partial phosphorylation of AKT at T308 is sufficient for activation of AKT to phosphorylate and inactivate tuberous sclerosis complex subunit 2 (TSC2) of the TSC1/TSC2 heterodimer, releasing the TSC1/TSC2 inhibition of Ras homolog, mTORC1 binding (RHEB).[79,83-85] Activated RHEB then leads to the subsequent activation of mTOR complex 1 (mTORC1).[86,87,106]

Table 1.01: PI3K isoforms.
In general, PI3K heterodimer isoforms are named and abbreviated for their catalytic subunits. In most cases, the regulatory subunits are paired with their corresponding catalytic subunit, such that regulatory p85α or p55α splicing variants and the catalytic p110α subunit dimerize to the PI3K isoform abbreviated as PI3Kα. The gamma heterodimer isoforms are the exception to the regulatory pairing, such that PI3Kγ is the abbreviation for the class I PI3K heterodimer with the p110γ subunit, regardless of whether the regulatory subunit is p84, p101, or p85γ. In the instances in which disambiguation between classes is required, it is common to simply use the catalytic subunit protein abbreviation for the heterodimer (e.g. PI3KC2β to indicate the beta isoform of a class II PI3K). The one known class III PI3K heterodimer is generally referred to as Vsp34 at the time of this writing. This and other alternate abbreviations commonly used for subunit isoforms are noted in brackets.

PI3K Class	Subunit	Gene	Subunit isoforms
Class I PI3K	catalytic	*PIK3CA*	p110α
		PIK3CB	p110β
		PIK3CD	p110δ
		PIK3CG	p110γ
	regulatory	*PIK3R1*	p85α, p55α, and p50α splicing variants
		PIK3R2	p85β
		PIK3R3	p85γ
		PIK3R5	p101
		PIK3R6	p84 [p87]
Class II PI3K	catalytic	*PIK3C2A*	PI3KC2α
		PIK3C2B	PI3KC2β
		PIK3C2G	PI3KC2γ
Class III PI3K	catalytic	*PIK3C3*	PI3KC3 [Vsp34]
	regulatory	*PIK3R4*	PI3KR4 [p150; Vsp15]

mTORC1 is noteworthy in itself, because of the large body of research focused on drugs targeting this rapamycin-sensitive complex formed with the regulatory-associated protein of mTOR (RAPTOR).[70] Upon activation of mTORC1, the resultant downstream effects are numerous and include promotion of translation of mRNA for protein synthesis and cellular proliferation, acting through eukaryotic translation initiation factor 4E (EIF4E)-binding protein 1 (4EBP1) and ribosomal protein S6 kinase beta-1 (S6K1; RPS6KB1) to phosphorylate ribosomal protein S6 (RPS6).[72,107]

With phosphorylation of AKT at the S473 position by mTOR complex 2 (mTORC2), AKT T308 phosphorylation is further potentiated and fully phosphorylated AKT (pAKT) is then capable of phosphorylating a diverse set of proteins containing RXXS/T motifs.[69,108,109] Of significant interest for survival of neoplastic cells, pAKT phosphorylates the Forkhead box transcription factors (including FOXO1 and FOXO3), promoting their nuclear export and ubiquitin-proteasome degradation.[110-116] This prevents FOXO transcription factors from promoting apoptosis via expression of death receptor ligands, Fas ligand (FASLG), and tumor necrosis factor-related apoptosis-inducing ligand (TRAIL), as well as modulating expression of apoptosis regulator proteins in the BCL2 family, including BCL2 interacting protein 3 (BNIP3), BCL2-like 1 (BCL2L1), and BIM).[111,117,118] pAKT also directly phosphorylates another pro-apoptotic BCL2 family member, BCL2 associated agonist of cell death (BAD), resulting in its inactivation and cell survival.[119,120]

In addition to inhibition of FOXO1 mediated apoptosis, pAKT promotes the pro-survival and proliferative activity of the transcription factor, nuclear factor kappa-light-chain-enhancer of activated B cells (NFκB).[121] NFκB mediates multiple oncogenic

phenotypes, which are described by Schlein et al. in a recent review.[122] PI3K-AKT signaling functions to promote NFκB activity in three ways: phosphorylating and thereby activating the alpha subunit of the inhibitor of nuclear factor kappa B (IκB) kinase (IKK), which allows NFκB to enter the nucleus for transcription; stimulation of IKK activity via signaling through mitogen-activated protein kinase kinase kinase 8 (MAP3K8); and promotion of NFκB transactivation via IKK and stimulation the mitogen-activated protein kinase (MAPK) signaling pathway.[123-125]

Pathway Feedback

Since mutations and/or overexpression of individual members of the signaling pathway are reported in multiple cancers, one might assume that inhibitors targeting one of these proteins could be sufficient. However, challenges to targeted pathway inhibition in tumors are presented by the presence of many points of feedback in PI3K-AKT-mTOR signal transduction well documented in human cancer studies, including those discussed below and diagrammed in **Figure 1.02**.

Under normal conditions, mTORC1 activation results in S6K1 negatively regulating IRS1 by phosphorylation. Inhibition of mTORC1, via rapamycin administration, mitigates this S6K1 activity toward IRS1, as demonstrated in human cells in vitro.[126] IRS1 then serves as an adaptor protein at RTKs to promote activation of PI3K.[127] IRS1 activation also causes increased mTORC2 activation, allowing for mTORC2 to phosphorylate AKT.[109] AKT can additionally be activated in mTORC2-independent mechanisms by other kinases, such as IκB kinase subunit epsilon (IKKε) and TANK-binding kinase 1 (TBK1), which are capable of phosphorylating AKT at the

hydrophobic motif and at the activation loop in a PI3K-dependent manner, even when mTORC2 is inhibited.[128]

While the canonical pathway to mTORC1 activation goes through AKT, PI3K signaling through other kinases can also activate mTORC1. Inhibition of the translation products of mTORC1 induces a feedback pathway that leads to PI3K activation of protein kinase C delta (PKCδ), which in turn phosphorylates TSC2, resulting in greater mTORC1 activation.[129,130] Further mTORC1 feedback activation can occur through mTORC2 phosphorylation of protein kinase N2 (PKN2). PKN2 then inactivates the class II PI3K isoform, PI3KC2β, which normally acts during starvation periods to negatively regulate mTORC1.[131] Thus, glucose starvation and/or RTK inhibitors that could potentially reduce mTORC1 activity are rendered less effective.[132]

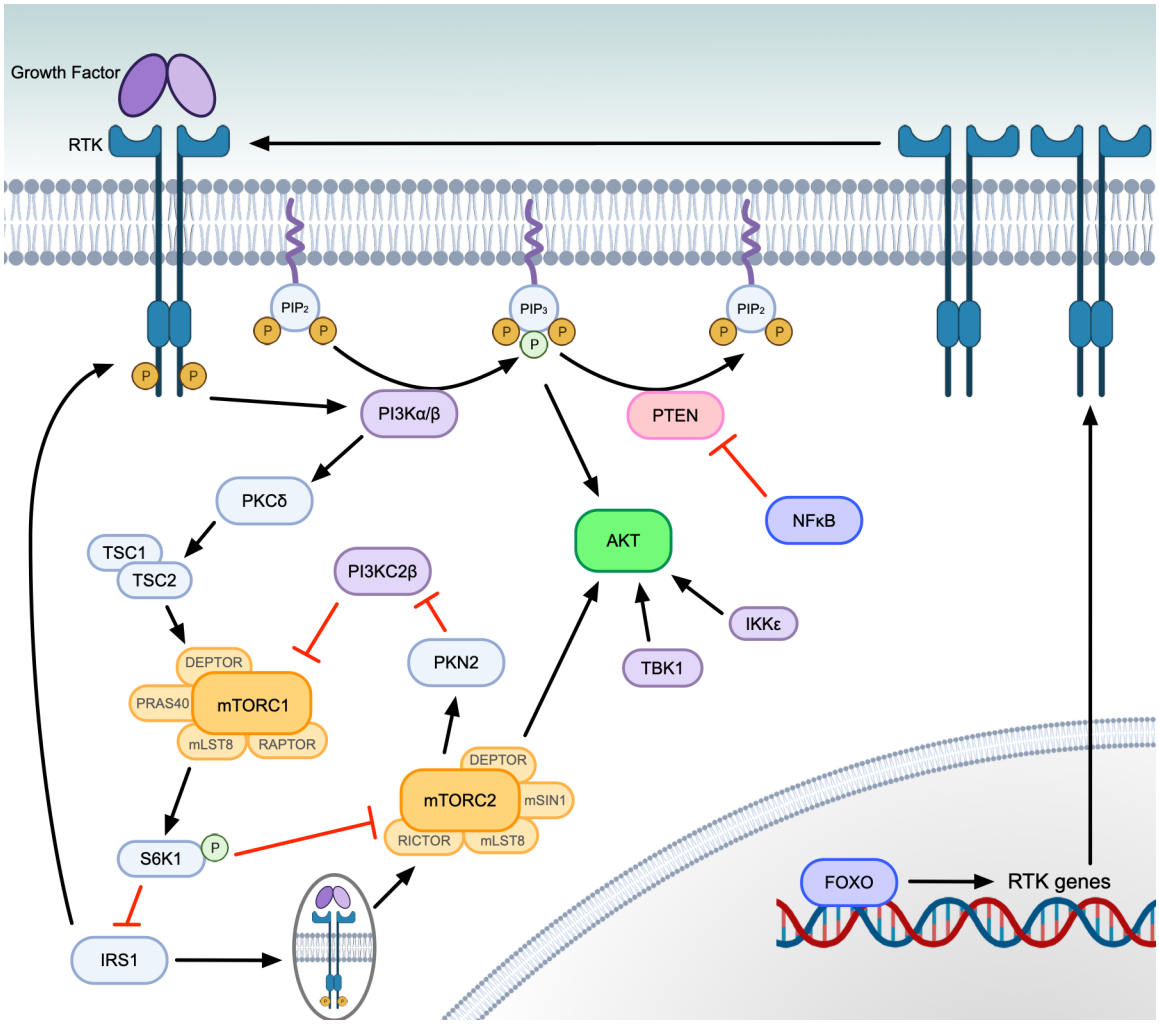

Figure 1.02: PI3K-AKT-mTOR signal transduction feedback pathways.
Inhibitors of the PI3K-AKT-mTOR typically target mTORC1, PI3K, specific PI3K isoforms, or less frequently AKT. Depicted here are feedback loops and alternate methods of pathway activation that can occur following inhibition of canonical PI3K-AKT-mTOR signal transduction. PI3Kα is the predominant isoform of the class IA PI3Ks, and activating mutations in *PIK3CA* (gene encoding p110α catalytic subunit of PI3Kα) are highly reported in cancer. PI3Kα isoform inhibition leads to greater activation of the PI3Kβ isoform and continued PIP_3 formation. PI3Kβ inhibition causes less significant isoform switching, but results in the same RTK expression as AKT inhibition. Both isoforms, when sufficiently expressed, are capable of activating TSC2 and mTORC1 through PKCδ, without the need for AKT. Inhibiting AKT allows FOXO-mediated transcription of genes to express RTKs, which also activate PI3K. mTORC1 inhibition removes S6K1 inhibition of IRS1. IRS1 then acts as an RTK/PI3K adaptor protein and removes p85 inhibition of PI3K p110. IRS1 also contributes to activation of mTORC2. Active mTORC2 reduces PI3KC2β inhibition of mTORC1, as well as activating AKT. AKT activation can also occur from proteins outside of the canonical PI3K-AKT-mTOR pathway, including TBK1 and IKKε. When activated by other signals (e.g. TNF or IL-1), NFκB also reduces *PTEN* transcription, which allows for PIP_3 accumulation and AKT activation. [Figure created with BioRender.com]

Broad inhibition of PI3K has proven difficult, because pan-PI3K inhibitors at doses required to block class I PI3K activity induced toxicities that have not allowed for efficacious treatment, with hepatotoxicity reported in canine patients.[133,134] Given that mutations in *PIK3CA*—the gene encoding the p110α catalytic subunit of the PI3K alpha isoform (PI3Kα)—or *PTEN* are among the most commonly reported mutations in canine cancer, one might presume better clinical results could be obtained by targeting specific isoforms of class I PI3Ks based on the type of mutations present (activating mutations for genes encoding RTKs or PI3K result in primarily PI3Kα signaling, and *PTEN* mutations result in predominantly PI3Kβ signaling in human studies).[133,135] However, treatment with a PI3Kα-specific inhibitor only yields an transient decrease in PIP_3 phosphorylation and AKT activation, due to G-protein coupled receptors (GPCRs) and feedback activation of widely expressed PI3Kβ.[136-138] While there is more robust inhibition with targeted PI3Kα inhibitors in canine cell lines *in vitro*, variability in efficacy indicates pathway activation in different tumor types that may be related to isoforms and feedback mechanisms in the canine patient, as well.[139] It has been well documented in human studies that PI3Kβ inhibition or direct AKT inhibition both result in greater expression of RTKs, including IR, ERBB3, and IGF1R, due to aforementioned feedback from mTORC1 inhibition, via IRS1, and greater FOXO transcriptional activation to increase RTK expression.[140] Likewise, mTOR inhibition by rapamycin increases the expression of RTKs to enhance PI3K-mTORC2 signaling.[132] Increased RTK expression allows for greater PI3Kα signal transduction, and re-activation of AKT.[138] NFκB signaling also indirectly represses transcription of *PTEN*, leading to increased PI3K signaling.[121,141,142]

PI3K-AKT-mTOR Pathway in Health and Cancer: Downstream Effectors

The sections below focus on the downstream targets and effectors of the PI3K-AKT-mTOR pathway in the modulation of cellular metabolism, survival, proliferation, and angiogenesis present in cancer development (**Table 1.02**). However, the broader downstream physiologic effects are not limited to these examples, and are more thoroughly reviewed by LoPiccolo et al. (2008), Revathidevi et al. (2019), and Tsai et al. (2022).[143-145] Some of the information below regarding general pathophysiologic mechanisms of this highly conserved pathway is extrapolated from human oncology, as there is evidence of PI3K-AKT-mTOR dysregulation in tumors of multiple species.

Table 1.02: AKT targets and effectors.
Effector proteins that are activated (+) or inhibited (–) by AKT are listed in the left column, with the resultant downstream effects promoting oncogenesis and tumor survival/progression denoted to the right. Where common or previously common abbreviations are used, current HGNC-approved abbreviations noted in brackets.

Target protein	Activate/Inhibit	Downstream effect	References
mTORC1 (via TSC2)	+	Protein synthesis (includes angiogenesis & metabolism)	146-148
RAF1 (a MAP3K)	+	ERK [MAPK1] pathway activation; evasion of apoptosis	149,150
MAP3K5 and MAPK8IP1	+	JNK [MAPK8] pathway inhibition; evasion of apoptosis	151-155
IKK	+	NFκB pathway activation → pro-survival gene transcription	123-125,156,157
SLC2A4 and TBC1D4	+	↑Vesicle glucose import (insulin/GF-responsive)	158-163
SLC2A1 (via mTORC1/4EBP1)	+	↑SLC2A1 expression → ↑glucose uptake (constitutive)	164-169
PFKM and PFKFB3	+	↑Glucose uptake; glycolytic activity	170,171
GSK3	–	↑Glycogen synthesis (via glycogen synthase); ↑Cell cycle (via cyclin D) ↑Lipogenesis & ↓gluconeogenesis (via SREBP1)	163,172-177
NOS3	+	↑NO; Angiogenesis	178-181
HIF1α (via mTORC1/4EBP1)	+	↑VEGF production; Angiogenesis	146,147,182,183
p21[CDKN1A] and p27[CDKN1B]	–	Cell cycle progression	184-187
MDM2	+	Cell cycle progression (p53 degradation)	187-189
CREB1	+	Survival gene transcription	190-195
BAD	–	↑Cell survival	154,196,197
FOXO1	–	Inhibition of apoptosis	111,196,198-201
Caspase 9	–	Inhibition of apoptosis	202,203
XIAP	+	Inhibition of apoptosis	204,205
NFκB (via IKK)	+	Promotion of proliferation Inhibition of PTEN and apoptosis	122,142,206-208

Cellular Glucose Metabolism, Lipogenesis, and Protein Synthesis

The PI3K-AKT-mTOR pathway regulates glucose metabolism by promoting cellular uptake and regulating gene expression. Many of these effects on glucose metabolism are mediated through the phosphorylation and inactivation of glycogen synthase kinase-3 (GSK3) by AKT.[209] Through GSK3 and directly, AKT promotes the translocation of the facilitated glucose transporter, solute carrier family 2 member 4 (SLC2A4), to the plasma membrane to increase insulin-responsive glucose uptake.[161,198] PI3K-AKT-mTOR pathway activation increases the translation of the cell surface glucose transporter, solute carrier family 2 member 1 (SLC2A1), through mTORC1-4EBP1 signaling, increasing constitutive glucose uptake.[161,167] The phosphorylation of GSK3 by AKT also decreases ubiquitin-mediated proteasomal degradation of sterol regulatory element-binding transcription factor 1 (SREBP1), thus inhibiting gluconeogenesis and promoting lipogenesis necessary in cellular proliferation.[174]

PI3K-AKT-mTOR signal transduction's ability to promote synthesis of proteins involved in metabolism and growth through mTORC1-4EBP1-EIF4E and mTORC1-S6K1 signaling activation is very well studied and is thoroughly reviewed elsewhere.[109,148,210] In addition to an increase in global protein translation, phosphorylation of 4EBP1 results in selective promotion of translation for specific pro-oncogenic and angiogenic transcripts, including fibroblast growth factor 2 (FGF2), vascular endothelial growth factor (VEGF), cyclin D, matrix metalloprotease 9 (MMP9), and MYC proto-oncogene basic helix-loop-helix transcription factor protein (MYC).[211] Phosphorylation of S6K1 leads to multiple effectors that promote processes including

mRNA biogenesis and translation initiation and elongation. mTORC1, through other downstream effectors, promotes expression of rRNA (via tripartite motif containing 24 (TRIM24) and RNA polymerase I) and transcription of 5S rRNA and tRNA (via MAF1 homolog, negative regulator of RNA polymerase III).[212-214]

Proliferation

The FOXO transcription factors are important targets of AKT activation in processes necessary for proliferation.[144,198,215] By modulating the expression of target genes, FOXO proteins are involved in regulating differentiation, apoptosis, resistance to oxidative stress, and cell cycle arrest.[199] FOXO proteins primarily modulate proliferation through increasing transcription of cyclin-dependent kinase inhibitors (CDKIs)—$p27^{Kip1}$, $p21^{Waf1/cip1}$, and p130—to prevent the G1/S transition of the cell cycle.[216-218] They additionally reduce expression of cyclin D1 and cyclin D2, resulting in G1 arrest.[219,220] When growth factors (GFs) and extracellular signals or oncogenic mutations activate the PI3K-AKT pathway, the subsequent nuclear export of FOXO proteins allows for mitotic progression to continue.[112,221]

PI3K-AKT-mTOR pathway activation resulting in the phosphorylation of 4EBP1 allows for EIF4E to selectively translate known oncogenic factors promoting proliferation, including: MYC, ornithine decarboxylase (ODC), cyclin D1, and cyclin D3.[222-225] PI3K-AKT-mTOR signaling also promotes mitogenesis through S6K1 inhibition of the $p16^{INK4a}$/CDK4/cyclin D1/RB pathway's induction of cell cycle arrest in G1 phase.[226-229]

Further proliferative effects of PI3K-AKT signal transduction are mediated through NFκB hyperphosphorylation of retinoblastoma protein (RB) and promotion of cyclin D1 expression, which is important for cell cycle progression from G1 to S phase.[230,231] NFκB also promotes proliferation through several downstream cytokines that act as GFs, including interleukins, IL-1 and IL-6, of particular importance in lymphoid neoplasms.[207,232]

Evasion of Apoptosis

PI3K-AKT signaling resulting in nuclear export of FOXO1 and FOXO3 prevents expression of pro-apoptotic BCL2 member, BIM, and subsequent release of mitochondrial cytochrome complex (cyt c) and activation and caspase-3 to induce apoptosis.[111,199,201,233,234] Concurrent inhibitory phosphorylation of BAD/BCL2L1 signaling by pAKT also prevents mitochondrial cyt c release and caspase activation.[119,120,202] AKT mediated degradation of FOXO1 and FOXO3a also reduces expression of FASLG and TRAIL, which are both death receptor ligands that function in paracrine and autocrine pathways.[235,236] FASLG inhibition prevents mitochondria-dependent apoptosis, as well as mitochondria-independent apoptosis through JNK pathway activation.[111,237] Reduced expression of TRAIL similarly results in evasion of apoptosis mediated by death receptors, DR4 and DR5.[238] In addition to inhibiting these apoptotic pathways, PI3K-AKT signal transduction also inhibits caspase-mediated apoptosis through IKK-IκB-NFκB signaling to increase expression of survival genes, including *BCL2L1*.[122]

Angiogenesis

One of the primary mechanisms through which tumor angiogenesis occurs is promotion of VEGF signaling. The PI3K-AKT-mTOR pathway is implicated on both sides of VEGF signaling for tumor angiogenesis: in the stimulation of angiogenesis through paracrine signals from neoplastic cells, and in endothelial cells themselves. VEGF and FGF2 are integral angiogenic factors that signal through the AKT-mTOR pathway in endothelial cells, to promote tumor vessel formation through endothelial proliferation, migration, and actin reorganization.[239] Activation of the PI3K-AKT pathway in tumor cells can increase VEGF secretion, through hypoxia-inducible factor 1 (HIF1)-dependent and HIF1-independent mechanisms, as well as modulating other angiogenic factors such as nitric oxide and angiopoietins.[240,241] PI3K-AKT-mTORC1 activation results in increased translation of the HIF1α subunit, through 4EBP1-EIF4G signaling.[146] Increased HIF1α and constitutively present HIF1β form a heterodimer that binds to hypoxia response elements, thus promoting transcription and expression of FGF2 and VEGF.[147,183] Angiogenic VEGF and IL-8 transcription is also upregulated through PI3K-AKT-NFκB signal transduction.[242,243] Additionally, phosphorylation of the endothelial and inducible isoforms of nitric oxide synthase (NOS3 and NOS2, respectively) by pAKT in tumor cells results in angiogenesis stimulated by nitric oxide synthesis.[179,240] Nitric oxide also serves as a signaling molecule that regulates processes involved in vasodilation, vascular permeability, microlymphatic flow, platelet aggregation, and leukocyte-endothelial cell interaction.[240,244]

Invasion and Metastasis

Among multiple mechanisms, PI3K-AKT-mTOR signal transduction promotes tumor invasion through the inhibition of 4EBP1, resulting in increased translation of invasion and metastasis mRNAs to proteins, including Y-box binding protein 1 (YB1), metastasis associated protein 1 (MTA1), CD44, and vimentin.[211,245] There is evidence that mTORC2 promotes cellular motility, increasing migration and invasion in tumor cells directly, in addition to activation of AKT and other kinases.[68,246] mTORC2 has been shown to control cytoskeletal F-actin polymerization for cellular spreading and motility, which is necessary for the migration and invasion of neoplastic cells.[247,248] mTORC1 also plays a role in promoting chemotactic, and IGF1-mediated, cellular migration by signaling through S6K1 and 4EBP1 for translation of proteins involved in regulation of F-actin reorganization and cell polarization.[249-251] S6K1 activation by mTORC1 is also involved in focal adhesion protein phosphorylation, which is necessary for de-adhesion from the extracellular matrix for migration.[250] In addition to migration, mTORC1-4EBP1-EIF4E signaling promotes invasion through increased translation of pro-invasive mRNAs, including matrix metalloproteinases (MMPs).[252,253] Tumor invasion is also promoted via PI3K-AKT signaling through NFκB to increase transcription of proteolytic enzymes, including MMPs and plasminogen activator, urokinase (PLAU).[254,255]

Tumor metastasis is enabled by increased translation to facilitate nutrient utilization and survival of neoplastic cells in the microenvironment of the metastatic site.[256] Constitutive activation of the PI3K-AKT-mTOR pathway results in increased translation signaling through S6K1 and 4EBP1, in response to nutrient deprivation or hypoxia and oxidative stress (which normally restrict mTORC1 activity).[257,258]

Pathway Activation Reported in Human Neoplasms

There are numerous reports of PI3K-AKT-mTOR dysregulation in multiple tumor types in human oncology. The literature review herein focuses on the role of mutations and dysregulation of PI3K-AKT-mTOR signaling in veterinary medicine and the research presented in the following chapters focuses on canine osteosarcoma and lymphoma. As such, pathway mutations and dysregulation specific to those tumors in human oncology are discussed below. For a broader discussion of the other human tumor types in which PI3K-AKT-mTOR dysregulation plays a role, the interested reader is referred to well-written review articles on the subject.[259,260]

Pathway Dysregulation in Human Osteosarcoma

Osteosarcoma (OSA) is a malignant mesenchymal tumor of bone with aggressive biologic behavior. In humans OSA accounts for less than 1% of all cancers diagnosed in the United States, but 20% of malignant bone tumors, which has a bimodal distribution that primarily affects children and young adults with a secondary population in people over 60.[261-264] Aberrations in expression and mutations within the PI3K-AKT-mTOR pathway itself are frequently reported in human OSA cases and have been associated with metastatic and/or chemoresistant tumors, which have spurred on the development and investigation of multiple targeted inhibitors in human oncology.[265-269] Among frequently reported dysregulation in human OSA are alterations in expression of oncogenes *HGFR*, *ERBB2* and activation of kinase pathways related to PDGF, mTOR, c-KIT and VEGF.[267] A recent study documented differential expression of 263 genes in metastatic OSA that were predominantly related to PI3K-AKT pathway

and dysregulated signaling.[270] Pathway analysis by Perry et al. revealed that there was alteration of PI3K-AKT-mTOR signaling proteins in 24% of patients.[271] Utilizing whole-exome, whole-genome, and RNA-sequencing, this study and others reported mutations in human OSA cases that are within, and/or direct upstream regulators of, the PI3K-AKT-mTOR pathway (listed in **Table 1.03**). In addition to finding recurrent somatic structural mutations in pediatric OSA, mutations reported Chen et. al reported untranslated regions for genes encoding members of the PI3K family and regulators of PI3K-AKT-mTOR signal transduction, including ERBB4 and PTPRD.[272] Outside the pathway, while there is an association of pediatric OSA to Li–Fraumeni syndrome (*TP53* mutation), retinoblastoma syndrome (*RB1* mutation), and Rothmund–Thomson type II syndrome (*RECQL4* mutation) that carry increased risk, the reader is referred to reviews of pediatric OSA for these, and other, molecular abnormalities in such cases.[273,274]

Table 1.03: Mutations within the PI3K-AKT-mTOR pathway in human tumors.
Summarized below are commonly reported mutations in OSA and lymphoid tumors, with specific mutations or additional context parenthetically noted where possible or indicated. Abbreviations: amp, amplification; del, deletion; fs, frame shift; mis, missense; ns, nonsense; pm, point mutation; SV, structural variant.

Tumor Type	Reported Mutations	References
Osteosarcoma	*AKT1* (amp, mis); *EGFR* (mis); *EIF4B* (mis); *IGF1R* (amp); *NF1* (del, fs, SV); *NF2* (fs, pm, SV); *PDGFRA* (amp, SV); *PDGFRB* (SV); *PDPK1* (mis); *PIK3CA* (mis, pm, SV); *PIK3C2B* (mis); *PIK3R1* (mis); *PIK3R4* (fs); *PIK3R6* (splice); *PIM1* (amp); *PTEN* (del, fs, ns, pm, SV); *TSC2* (mis, pm, SV)	267,271-273,275,276
Lymphoma and Chronic lymphocytic leukemia	BCL: *MTOR* (mis); *PDGFRA* (mis); *PIK3CA* (amp); *PIK3CD* (mis); *PIK3R1* (mis); *PTEN* (del) CLL: *NOTCH1* (resulting in PTEN inactivation) TCL: *AKT2* (mis); *INPPL1*; *INPP4A*; *INPP5J*; *MTOR* (mis, fs); *PHLPP1*; *PHLPP2; PIK3CA* (mis); *PIK3CB* (mis); *PIK3CD* (mis); *PIK3C2A*; *PIK3C2B*; *PIK3C2G*; *PIK3R5*; *PIK3R3*; *PTEN*; *TSC1* (splice); *TSC2* (mis)	277-283

Pathway Dysregulation in Human Lymphoma and Leukemia

The activity of the PI3K-AKT-mTOR pathway has been well studied in immunology and lymphocyte development, activation, and regulation.[284-286] The activation of PI3K-AKT signaling in response to the B-cell receptor (BCR), in conjunction with known dysregulation of the PI3K-AKT-mTOR pathway in diffuse large B-cell lymphoma (DLBCL) and chronic lymphocytic leukemia (CLL), generated interest in the potential for targeted inhibition in hematopoietic neoplasms.[287-289] Frequently reported mutations occurring in LSA and CLL are listed in **Table 1.03**. Interestingly, the direct oncogenic role of mutations in the PI3K-AKT-mTOR pathway is lower than one might expect for the frequency of signal transduction dysregulation and the efficacy of PI3Kδ inhibitors in the treatment of B-cell malignancies.[283] These malignancies often exhibit increased PI3K-AKT-mTOR signal transduction not because of mutations for proteins within the pathway, but rather due to the relationship of the BCR to PI3K activation.[290] For the purposes of this review, it is best to simplify the activity of the BCR—in conjunction with CD19 and GPCRs—by stating that it fills the same role as RTKs for PI3K activation, and the interested reader is referred to other reviews for more detailed signaling mechanisms.[283,284,290,291] As such, in neoplasms with high frequency of activating mutations in BCR signaling, like DLBCL, there is often increased activation of PI3K-AKT signaling, regardless of the mutation status for downstream proteins within the cascade.[283] Uddin et al. found that the PI3K-AKT pathway is constitutively activated in human DLBCL cell lines and pAKT overexpression in patient derived DLBCL samples is associated with poor outcome.[292] This is exacerbated by post-translational loss of *PTEN* expression reported in both DLBCL and CLL, which is correlated to lower survival

with concurrent AKT activation in DLBCL and more rapid disease progression with concurrent PI3K activation in CLL.[293,294] Yet, the variation in mutations and mechanisms of pathway activation in these tumors prevent broad generalization. Pfeifer et al. detected loss of *PTEN* expression in 55% germinal center B cell (GCB)-like DLBCL samples, but only in 14% of activated B cell (ABC)-like DLBCL samples, indicating the heterogeneity of genetic and molecular pathogenesis in various subtypes of DLBCL malignancies.[280] In CLL, the connection between BCR-related mutations and dysregulation of PI3K-AKT-mTOR signaling is less completely understood, and appears to be related to immunoglobulin mutations resulting in BCR activation through reaction to autoantigen, subsequent PI3K-AKT-mTOR overexpression, and expansion of the neoplastic population.[295] This is a more functional and dynamic process than a simple one-to-one relationship of mutation to dysregulation in other tumor types, but the resultant tumor promoting effects of pathway activation present an opportunity for targeted inhibition that has proven fruitful in the treatment of CLL.[296,297] While a full reporting is outside the scope of this review, a brief note should be made that PI3K-AKT-mTOR dysregulation is frequently reported in other lymphoid tumors in addition to BCL and CLL. In acute lymphoblastic leukemia, there is constitutive activation of the PI3K-AKT-mTOR pathway, which has also been found to be resistant to single-point inhibitors.[298,299] In subcutaneous panniculitis-like T-cell lymphoma samples, IHC demonstrated abundant AKT and 4EBP1 phosphorylation throughout neoplastic lymphocytes.[277] PI3K-AKT-mTOR and MYC signaling pathways are activated in Burkitt lymphoma and associated with poorer outcomes.[300,301] Needless to say, the frequent dysregulation of PI3K-AKT-mTOR signaling in LSA has motivated research into

targeted inhibitors, which has yielded varying success. As previously mentioned, specific classes and isoforms of PI3K are expressed differentially in various tissues. While class I PI3Ks are expressed systemically, the differential expression of PI3Kδ in particular is much greater in hematopoietic and lymphoid tissues than in other tissues, as compared to other PI3K isoforms.[302] This has led to greater focus on the development of isoform specific PI3Kδ inhibitors in the treatment of lymphoma. Detailed discussion of these and other pathway inhibitors in human oncology are outside the scope of this review, other than to state that this research has provided sound reasoning for similar investigation in canine LSA, which is discussed in subsequent sections.

Pathway Activation Reported in Canine Tumors

Given that activation of the PI3K-AKT-mTOR pathway results in many of the downstream effects that promote cancer development, it is not surprising that mutations and pathway enrichment are frequently reported and prognostically significant in human and canine neoplasms. The sections below highlight canine tumors that are associated with pathway activation with potential for diagnostic and therapeutic value in veterinary and comparative oncology. Mutations in the pathway reported in canine tumors are outlined in **Table 1.04** and additional signal transduction dysregulation for canine tumors with reported PI3K-AKT-mTOR activation is described below.

Table 1.04: PI3K-AKT-mTOR pathway mutations reported in canine tumors.
Abbreviations: +, activating; –, inactivating; amp, amplification; del, deletion; fs, frame shift; mis, missense; ns, nonsense; pm, point mutation; SV, structural variant.

Tumor Type	Reported Mutations	References
Hemangiosarcoma	*PIK3CA* (+, mis, fus); *FOXO3* (–); *PTEN* (–); *AKT3* (+, fus); *PIK3R1* (+, mis)	265,268,303-307
B-cell Lymphoma	*PTEN* (–); *PIK3CG* (+); *PLCB4* (+); *INPP4B* (–)	265,268,308
T-cell Lymphoma	*PTEN* (–, del); *MTOR* (+, mis)	265,268,309
Melanoma	*PIK3CA* (+, mis); *PTEN* (–, del)	265,268,310
Mammary Gland Tumor	*PIK3CA* (+, mis); *PTEN* (–, mis, del); *AKT1* (+, mis); *INPP5A* (–)	93,265,268,311-313
Osteosarcoma	*PIK3CA* (SV); *AKT2* (+, amp); *PIK3C2B* (+, amp); *PIK3C2A/G* (+, amp, mis); *PTEN* (–, del, SV)	266,268,314-317
Pulmonary Adenocarcinoma	*PTEN* (–, del, mis); *AKT1* (+, amp, mis); *ERBB2* (+, mis)	318

Canine Osteosarcoma

In dogs, the incidence of OSA is 27 times greater than in humans and the age distribution differs, yet it shares many of the clinicopathologic, genetic, and molecular features with the malignancy in humans, including the high metastatic rate and aggressive biologic behavior. In canine and human patients, the metastatic rate is high with radical resection alone, and the median survival time (MST) for dogs following limb amputation for OSA is 5 months, with a 1-year survival rate of 19.8%, which increases to 45% at 1 year and 20.9% at 2 years when amputation is followed by administration of the chemotherapeutic drugs doxorubicin, cisplatin, or carboplatin.[319-322] While an improvement over surgery alone, these survival times evidence the necessity for improvements in the treatment of this highly aggressive canine tumor.

PI3K-AKT-mTOR pathway enrichment and constitutive activation are reported in human and canine OSA, are associated with poorer prognosis, and represent a significant therapeutic target.[271,314,317,323] PI3K-AKT-mTOR pathway activation in canine

OSA promotes neoplastic survival, proliferation, and metabolic activity, as well as promoting migration and invasion.[324-326] Phosphorylated mTOR and S6K1, indicating pathway activation, are reported in canine OSA cells, and are inhibited by rapamycin administration *in vitro*.[324] Deletions and down-regulation of *PTEN* are frequently reported in canine OSA.[266,268,314,316,327] Genomic analysis of canine OSA has demonstrated *EGFR* and *PIK3CA* mutations, aberrant copy numbers of *TSC2*, and amplification of *PIK3CB* and *AKT2*.[266,268,314]

As RTKs are a primary mechanism of PI3K-AKT-mTOR pathway activation conserved across multiple species, several have been evaluated in canine tumors, in conjunction with AKT phosphorylation. Mutations and overexpression of RTKs are reported in canine OSA (*IGF1R*, *HGFR*, *PDGFR*, and *ERBB2*).[267,328-332] PDGF and PDGFR overexpression has been detected by immunoassays and quantitative PCR in canine OSA cell lines and tumors.[333] Canine OSA tumor sections have been shown to be robustly positive for IGF2R expression, by IHC.[334] Also reported in canine OSA are elevated serum IGF concentrations and expression of IGF and growth hormone mRNA within tumors.[335,336] IGF1R overexpression in canine appendicular OSA is correlated with greater AKT signaling and poorer prognosis.[337] Elevated serum VEGF is reported in cases of canine OSA, and is associated with shorter disease-free interval (DFI), radiation resistance, and poorer prognosis.[338,339]

Canine Hemangiosarcoma

Angiosarcoma (AS) is a rare neoplasm of humans, but the canine correlate, hemangiosarcoma (HSA), accounts for almost 2% of all cancer diagnoses in dogs and 5-7% of non-cutaneous primary canine malignancies.[340,341] Visceral AS and HSA are similar aggressive tumors of endothelial origin, characterized by marked local invasion and rapid hematogenous metastasis/dissemination. Canine visceral HSA is often multicentric by the time it is detected.[342,343] As a result, prognosis is poor, and the 1-year survival rate is no more than 10%.[344-347] Given the aforementioned role of PI3K-AKT-mTOR signaling in angiogenesis, neoplastic cell proliferation, survival and invasion, it is not surprising that pathway activation is reported in canine HSA. Previous studies have reported increased VEGF and FGF2 expression by HSA cells *in vitro*, and found that VEGF is detectable at significantly higher plasma concentrations in dogs with HSA as compared to healthy dogs.[348,349] Evaluation of canine vascular tumors by immunohistochemistry, in situ hybridization, and RT-PCR demonstrated elevated FGF2, VEGF, and VEGF receptors (VEGFR1 and VEGFR2) in HSA samples, as compared to hemangioma samples.[350] Through genomic and molecular analyses, mutations in *PIK3CA*, *PTEN*, *AKT3*, and *FOXO3* have been identified in canine HSA, similar to those reported in human AS.[265,303-307,351] Examination of canine HSA cell lines has demonstrated increased phosphorylation of AKT, mTORC1, and 4EBP1 that was not altered by *in vitro* serum-stimulation, indicating constitutive activation of the signaling pathway.[352] IHC examination of canine splenic and cutaneous HSA samples also demonstrated PI3K-AKT-mTOR pathway activation.[352,353] Moreover, pAKT immunoreactivity was found to be greater in cutaneous HSA sections as compared to

hemangioma samples, indicating an association of pathway activity to increased malignancy.[352] In our previous study of PI3K-AKT-mTOR dysregulation and targeted pathway inhibition in canine HSA *in vitro*, we confirmed the finding of increased pAKT and p4EBP1 expression in DEN-HSA, CIN-HSA, and SB-HSA cell lines.[354]

Canine Lymphoma and Leukemia

Lymphomas account for approximately 80% of all hematopoietic tumors in dogs. Approximately 60-70% of canine lymphomas are B-cell, and 30-40% are T-cell. Diffuse large B-cell lymphoma (DLBCL) accounts for 50% of canine lymphoma diagnoses.[355] Elevated expression and activation of components of the PI3K-AKT-mTOR pathway are reported in human activated B cell (ABC) DLBCL and canine DLBCL.[356-358] Canine peripheral T-cell lymphoma (PTCL) and human PTCL also share similar biologic behavior, *PTEN* mutation status, and activation of the PI3K-AKT-mTOR pathway.[90,359,360] Alterations in PTEN and PI3K-AKT-mTOR expression are reported in canine PTCL.[309] Mutations reported in canine lymphoma related to alterations in PI3K-AKT-mTOR expression include *MTOR*, *PIK3CG*, *PTEN*, *INPP4B*, and *PLCB4* (the gene encoding the β4 isoform of phospholipase C, which is involved in the phosphoinositide cycle).[265,268,308,309,361]

Canine Melanoma

In humans and dogs, malignant melanoma is an aggressive tumor, with frequent resistance to traditional cytotoxic chemotherapy. In dogs, oral melanoma is more common and more aggressive with a 90% metastatic rate.[362] In humans, cutaneous

melanoma is the more common malignancy, associated with UV exposure and activating *BRAF*^{V600E} mutation in 60% of patients.[363] Unlike the human neoplasm, *BRAF* mutations are infrequent in canine oral melanoma.[364] However, MAPK and PI3K-AKT-mTOR dysregulation are reported with similar differential gene expression in both species.[92,365] Alterations in PTEN expression and AKT phosphorylation have been demonstrated by immunoassays in canine melanoma tumor samples and cell lines.[366,367] A transcriptomic study comparing gene expression between canine malignant melanomas and melanocytomas found significant upregulation in signaling pathways for focal adhesion, extracellular matrix (ECM)-receptor interaction, and PI3K-AKT in the malignant tumors.[368] Interestingly, many of the upregulated ECM-receptor interaction genes are upstream regulators of PI3K-AKT signaling. In conjunction with reported *PIK3CA* and *PTEN* mutations, this likely contributes to the marked enrichment of the PI3K-AKT-mTOR pathway observed in canine melanoma.[265,268,310,368] Elevated serum VEGF is reported in cases of canine melanoma, and is associated with shorter disease-free interval, radiation resistance, and poorer prognosis.[338,339]

Canine Mammary Gland Tumor

Increased AKT activity has been reported in approximately 40% of breast, ovarian epithelial, prostate, and gastric cancers in humans.[144] Mutations in *PIK3CA* are the most commonly observed genetic alterations in the PI3K-AKT-mTOR pathway in mammary and ovarian tumors of humans.[98] Similar pathway mutations have also been identified in canine mammary gland tumors (cMGTs), including recurrent somatic *PIK3CA* variants and *PTEN* deletions with loss of heterozygosity associated with poor

prognosis.[93,311-313] There are also similarities in gene expression signatures, characterized by PI3K-AKT, PTEN, and MAPK pathway enrichment.[96] PI3K pathway alteration is reported in 50% of cMGT with the *PIK3CA* H1047R mutation affecting 26% of tumors examined.[265]

However, continued research is required to elucidate the indirect correlation between mutation status and PI3K-AKT-mTOR pathway dysregulation in cMGT.[313,369] In an immunohistochemical study of cMGTs, greater PI3K immunoreactivity was significantly associated with regional lymph node infiltration, distant metastasis, HER2+ tumors, triple-negative and luminal B phenotypes, and the lowest survival rate.[370] Similar studies have reported increased pAKT immunoreactivity, increased VEGF and phosphorylated mTOR immunolabeling in 78% of canine mammary carcinomas, as well as loss of PTEN immunoreactivity associated with poorer prognosis 33% of tumors.[371-374] While dysregulation in PI3K-AKT-mTOR signal transduction is apparent in cMGT and correlated with malignancy and poorer prognosis, it is not directly correlated to mutation status, which may be due to other factors including hypermethylation, post transcriptional expression regulation (e.g. miRNA), and aberrant RTK activation.[370] EGF promotes proliferation, migration, survival, VEGF production, and AKT phosphorylation in canine mammary carcinoma cells *in vitro*, which have been shown to highly express EGFR.[375] EGFR immunoreactivity is associated with malignancy in cMGT.[376]

Other Canine Tumor Types

PI3KCA and *PTEN* mutations are reported in a variety of other canine tumors, described by Alsaihati et al. (2021) and Wu et al. (2023).[265,268] A qRT-PCR study of canine thyroid tumors concluded that increased expression of several genes associated with PI3K-AKT-mTOR signaling—including *PIK3CA*, *AKT1*, and *AKT2*—suggests the involvement of this pathway in the pathogenesis of canine thyroid carcinoma, although pathway activation status was not directly interrogated.[377] Increased AKT and RPS6 phosphorylation have been demonstrated by IHC in canine cutaneous squamous cell carcinoma, indicating PI3K-AKT-mTOR pathway activation.[378] Canine glioma cells have been shown to overexpress *ERBB4* mRNA with concurrently downregulated microRNA (miR)-190a. Transfection with miR-190a inhibited ERBB4-induced AKT phosphorylation and cell growth of canine glioma cells *in vitro.*[379] A recent genomic study of canine pulmonary adenocarcinomas demonstrated *PTEN* deletion, *AKT1* amplification, and *ERBB2/HER2* activating mutations (at V659E) in 35% of tumor samples, which was correlated to constitutive AKT phosphorylation in $HER2^{V659E}$ cell lines.[318] EGFR overexpression is reported in canine transitional cell carcinomas and malignant nasal epithelial tumors, and authors comment that further investigation into PI3K-AKT pathway activation in these tumors is warranted.[380,381]

Diagnostic Applications

As genomic databases have expanded and clinical application has grown, commercially available genomic diagnostic and screening tests for mutation status in dogs have become available, which do screen for mutations of genes associated with PI3K-AKT-mTOR signal transduction.[268,382,383] However, it should be noted that mutational status does not necessarily correlate to aberrant PI3K-AKT-mTOR pathway activation or response to treatment with targeted inhibitors.[313] Further analysis of gene expression or transcriptomics and protein phosphorylation for functional pathway activation, and correlation of these findings with drug response *in vitro* and *in vivo* should be performed. Total and/or phosphorylated AKT, 4EBP1, and mTOR can be evaluated, and has been reported, using IHC for some tumor types.[313,371,372,384] Unfortunately, phospho-protein epitopes are often rendered difficult to detect by IHC following decalcification of OSAs. In such cases, unphosphorylated targets may be used as indirect indicators of pathway activation, such as intracellular immunolocalization of FOXO1, as demonstrated in human neoplasms.[385] Combining modalities for diagnostic purposes is often the most reliable means of identifying when PI3K-AKT-mTOR signal transduction is involved in tumor development.

Pathway Inhibition via Targeted Agents

Success in targeted PI3K-AKT-mTOR pathway inhibition has been promising, but also dependent on the genetic and molecular profiles of various tumors. mTOR inhibitors like rapamycin have been examined for cancer treatment over several decades. In some cases, they show promise, but more often efficacy is superior when

mTOR inhibition is combined with cytotoxic agents. In a murine OSA model, rapamycin was effective at inhibiting ezrin-mediated metastatic behavior related to AKT-mTOR-S6K1-4EBP1 signaling.[386] Rapamycin was also shown to be capable of reversing doxorubicin resistance in a murine lymphoma model.[387] However, some canine tumors are predominantly dependent upon PI3K-AKT signaling. Chen et al. found that *in vitro* PI3K inhibition (ZSTK474) and AKT inhibition (KP372-1) reduced proliferation, survival, and signal transduction more effectively than mTOR inhibition for canine HSA, MGT, DLBCL, glioblastoma, and mast cell tumor cell lines.[388] Inhibition of AKT phosphorylation induced cell death of canine T-cell lymphoma cells *in vitro*.[389] Specific PI3K isoform inhibition has shown success in canine B-cell and T-cell non-Hodgkin lymphoma. An orally bioavailable PI3Kδ inhibitor reduced phosphorylation of AKT and demonstrated clinically significant responses in a clinical trial.[134]

Upstream RTK inhibition of PI3K-AKT-mTOR signaling has also been examined. Research has demonstrated a variable reduction of HSA cell viability *in vitro*, using inhibitors of VEGFR, PDGFR, FGFR, KIT, PI3K, AKT, and mTOR, indicating a likely partial pathway blockade and partial cellular response.[353] Based on findings of overexpression of MET/HGFR with co-expression of hepatocyte growth factor (HGF) in human OSA, and reported HGFR signaling activating PI3K, HGFR inhibition was studied in canine OSA cell lines, demonstrating a reduction in AKT phosphorylation and malignant cellular behavior, *in vitro*.[390] PDGFR, EGFR, and VEGFR2 inhibitors have been studied in canine OSA and MGT cell lines, demonstrating variable degrees of inhibition of cell growth and AKT phosphorylation.[333,375,391] Previous research has documented the role of the molecular chaperone, heat shock protein 90 (HSP90), in KIT

activity and in maintaining phosphorylation of AKT in human cancer cells.[392,393] On this basis, HSP90 inhibition was examined in canine mast cell tumor lines, and found to inhibit KIT and AKT phosphorylation, but not PI3K activity.[394] Similarly, research finding BTK and PI3K inhibition in human LSA spurred study of BTK and specific PI3K inhibitors in canine LSA, showing decreased cellular proliferation, reduced AKT activation *in vitro*, and partial responses in clinical trials.[134,395] Additionally, differential baseline gene expression of components and regulators of PI3K-AKT-mTOR signaling are correlated with response to chemoimmunotherapy and targeted inhibitors in canine DLBCL cases, indicating the importance of understanding the specific expression profiles for successful treatment protocol in DLBCL cases.[396] In canine oral squamous cell carcinoma cell lines, PI3K inhibition using LY294002 resulted in decreased AKT phosphorylation and cell proliferation.[397]

Due to multiple points of activation and feedback, there is promise in multimodal inhibition. Dual-inhibition of PI3K and mTOR in canine HSA cell lines has demonstrated robust signaling blockade, with dose-dependent reductions in proliferation, migration, VEGF production, and increased apoptosis *in vitro*.[354] **Table 1.05** briefly summarizes research using PI3K-AKT-mTOR pathway inhibitors studied in the canine tumors covered in this review. It should be noted that studies that either did not demonstrate or did not specifically evaluate modulation of PI3K-AKT-mTOR signaling are not included in **Table 1.05**.[391,398]

Table 1.05: PI3K-AKT-mTOR inhibition in canine tumors.
Multiple studies have examined PI3K-AKT-mTOR inhibitors in canine in vivo and in vitro. Outlined here are combined findings for specific pathway inhibitors.

Cancer	Compound(s) and References	Target	Experiment/Model	Findings
HSA	Alpelisib (BYL719)[139] Rapamycin, Temsirolimus[399] VDC-597[354]	PI3Kα (p110-alpha) mTOR PI3K + mTOR	*in vitro*; Xenograft (athymic nude mouse)	*in vitro* suppression of AKT and 4EBP1 phosphorylation; inhibition of cell proliferation, migration, VEGF production; apoptosis induction. Sensitization to MEK inhibitors and doxorubicin in vitro and MEK inhibition in vivo.
LSA	AS-605240[395]	BTK + PI3Kγ	*in vitro*	AS-605240 and a BTK inhibitor (ibrutinib) acted synergistically; reduced DLBCL proliferation; increased apoptosis/necrosis; reduced phosphorylation of BTK, AKT, GSK3β, and ERK.
	RV1001[134,396]	PI3Kδ	*in vitro*; Phase I (21 dogs); Phase II (35 dogs)	*in vitro*: suppression of AKT phosphorylation in tumor cells collected from dogs with B- and T-cell NHL. Phase I/II: Objective response rate 62-77% (mostly partial responses) *in vivo*: differential gene expression of PI3KCD, AKT3, PTEN, and NRAS was correlated with response to treatment in canine DLBCL.
MCT	STA-9090[394]	Hsp90	*in vitro*; Xenograft (SCID mouse)	*in vitro*: cell growth inhibition; apoptosis induction; inhibition of AKT and Kit phosphorylation; loss of cell surface Kit expression; no change in PI3K expression. *in vivo*: tumor growth inhibition.
Mel	Sapanisertib[400] Rapamycin, Everolimus[92,401,402] Dactolisib (NVP-BEZ235)[367]	mTORC1/2 mTOR PI3K + mTOR	*in vitro*; Xenograft (nu/nu mouse)	*in vitro*: suppression of mTOR, S6K1, RPS6, and 4EBP1 phosphorylation; inhibition of proliferation and cell cycle progression; promotion of apoptosis; canine and human melanoma cell lines exhibit similar MAPK and mTOR pathway activation and similar sensitivity to respective inhibitors; Synergistic carboplatin or MEK inhibitor, with additional suppression of AKT phosphorylation, in vitro. *in vivo*: sensitization to MEK inhibitor.
MGT	Alpelisib (BYL719)[139] Rapamycin[403] Metformin[404,405]	PI3Kα (p110-alpha) mTOR AMPK	*in vitro*; Xenograft (BALB/c-nu/nu mouse)	*in vitro*: suppression of AKT, S6K1, and 4EBP1 phosphorylation without change in *AKT*, *MTOR*, *PTEN*, or *4EBP1* gene expression; inhibition of proliferation; promotion of cell cycle arrest and apoptosis; differential effects to metastatic and non-metastatic cell lines. *in vivo*: inhibition of primary tumor growth; suppression of AKT, S6K1, and 4EBP1 phosphorylation.

	Vandetanib (ZD6474)[375]	EGFR + VEGFR-2	*in vitro*	Dose-dependent inhibition of: EGFR phosphorylation; PI3K-AKT activation; and all EGF-mediated proliferation, chemotaxis, resistance to apoptosis, and VEGF production.
	Everolimus, Temsirolimus[406]	mTOR	*in vitro*; Xenograft (BLAB/c nude mouse)	*in vitro*: dose-dependent reductions in mTOR phosphorylation and viability of sphere-forming cancer stem cells and adherent neoplastic cells with everolimus and temsirolimus administration. *in vivo*: Reduced tumor growth/volume with everolimus administration.
OSA	Luteolin[407]	PI3K/AKT	*in vitro*; Clinical trial	*in vitro*: suppression of AKT, mTOR, S6K1, and RPS6 phosphorylation; inhibition of proliferation; promotion of apoptosis and reactive oxygen species. Clinical trial: parenteral rapamycin suppressed RPS6 phosphorylation in tumor and PBMC; disease free interval not increased.
	Quercetin[408]	PI3K		
	Rapamycin[324,409,410]	mTOR		
	Tepoxalin[411]	COX + 5-LOX	*in vitro*	Increased caspase-dependent apoptosis; induction of oxidative stress; increased PTEN homolog activity by preventing alkylation or oxidation.
	AG1296[333]	PDGFR	*in vitro*	Dose-dependent and time-dependent decrease in AKT phosphorylation without significant differences in apoptotic activity, cell cycle, or cytotoxicity.
	PF2362376[390]	MET/HGFR	*in vitro*	Inhibition of cellular proliferation, migration, invasion, branching morphogenesis and colony formation; induction of cell death; inhibition of HGFR/MET, GAB1, ERK, and AKT phosphorylation.

Conclusions

With increased availability of molecular diagnostic tools for veterinary oncology, a greater understanding of the role of PI3K-AKT-mTOR pathway activation in canine cancer continues to develop, much as it has in human oncology. Similarities in mutations and pathway activation of both species provides evidence for a comparative approach in studying PI3K-AKT-mTOR signal transduction in canine companions. The relatively higher incidence of some canine tumors can provide valuable spontaneous animal models, and veterinary oncology can benefit from targeted pathway inhibitors developed in human medicine. Continued research into the role of PI3K-AKT-mTOR activity in canine tumors will help hone sensitivity and specificity of diagnostic tests and efficacy targeted therapy.

Project Rationale and Specific Aims

The rationale behind the investigation presented in Chapters 2 and 3 of this text is based on: the tumorigenic role of PI3K-AKT-mTOR pathway dysregulation; the value of dogs as spontaneous animal models for human tumors with similar biologic behavior and mechanisms; the frequency of pathway activation in tumors of both species; and the need for advancement in treatment of canine tumors. The findings presented in the subsequent chapters can provide a basis for further investigation and clinical trials that may lead to improvements in chemotherapeutic protocols for the canine patient, as well as a potential contribution to comparative oncology. The primary goal of this research was to evaluate whether dual-inhibition of PI3K and mTOR with VDC597 is a viable component of treatment for canine OSA and lymphoid tumors. The specific aims of the study for this purpose were:

1. Evaluate alterations in PI3K-Akt-mTOR pathway activation in canine cell lines treated with VDC597.
2. Characterize expression of phosphoproteins indicating pathway activity in formalin fixed paraffin embedded sections of spontaneous osteosarcoma and lymphoma tumor collected from canine patients.
3. Assess the antineoplastic activity of VDC597, alone and in combination with standard-of-care chemotherapy drugs, in canine osteosarcoma and lymphoid tumor cell lines.
4. Evaluate the *in vivo* safety and efficacy of VDC597, alone and in combination with carboplatin, in a xenograft mouse model for osteosarcoma.

References

1. Staal SP, Hartley JW, Rowe WP. Isolation of transforming murine leukemia viruses from mice with a high incidence of spontaneous lymphoma. *Proc Natl Acad Sci U S A*. 1977;74(7):3065–3067. https://doi.org/10.1073/pnas.74.7.3065

2. Staal SP, Hartley JW. Thymic lymphoma induction by the AKT8 murine retrovirus. *J Exp Med*. 1988;167(3):1259–1264. https://doi.org/10.1084/jem.167.3.1259

3. Staal SP. Molecular cloning of the akt oncogene and its human homologues AKT1 and AKT2: amplification of AKT1 in a primary human gastric adenocarcinoma. *Proc Natl Acad Sci U S A*. 1987;84(14):5034–5037. https://doi.org/10.1073/pnas.84.14.5034

4. Jones PF, Jakubowicz T, Pitossi FJ, Maurer F, Hemmings BA. Molecular cloning and identification of a serine/threonine protein kinase of the second-messenger subfamily. *Proc Natl Acad Sci U S A*. 1991;88(10):4171–4175. https://doi.org/10.1073/pnas.88.10.4171

5. Bellacosa A, Testa, Staal SP, Tsichlis PN. A retroviral oncogene, akt, encoding a serine-threonine kinase containing an SH2-like region. *Science*. 1991;254(5029):274–277. https://doi.org/10.1126/science.254.5029.274

6. Coffer PJ, Woodgett JR. Molecular cloning and characterisation of a novel putative protein-serine kinase related to the cAMP-dependent and protein kinase C families. *European Journal of Biochemistry*. 1991;201(2):475–481. https://doi.org/10.1111/j.1432-1033.1991.tb16305.x

7. Jones PF, Jakubowicz T, Hemmings BA. Molecular cloning of a second form of rac protein kinase. *Cell Regul*. 1991;2(12):1001–1009. https://doi.org/10.1091/mbc.2.12.1001

8. Harlan JE, Yoon HS, Hajduk PJ, Fesik SW. Structural characterization of the interaction between a pleckstrin homology domain and phosphatidylinositol 4,5-bisphosphate. *Biochemistry*. 1995;34(31):9859–9864. https://doi.org/10.1021/bi00031a006

9. Frech M, Andjelkovic M, Ingley E, Reddy KK, Falck JR, Hemmings BA. High affinity binding of inositol phosphates and phosphoinositides to the pleckstrin homology domain of RAC/protein kinase B and their influence on kinase activity. *J Biol Chem*. 1997;272(13):8474–8481. https://doi.org/10.1074/jbc.272.13.8474

10. Datta K, Franke TF, Chan TO, et al. AH/PH domain-mediated interaction between Akt molecules and its potential role in Akt regulation. *Mol Cell Biol*. 1995;15(4):2304–2310. https://doi.org/10.1128/MCB.15.4.2304

11. Cohen P, Alessi DR, Cross DAE. PDK1, one of the missing links in insulin signal transduction? *FEBS Letters*. 1997;410(1):3–10. https://doi.org/10.1016/s0014-5793(97)00490-0

12. Berridge MJ. Inositol trisphosphate and diacylglycerol as second messengers. *Biochem J*. 1984;220(2):345–360. https://doi.org/10.1042/bj2200345

13. Stone RM, Weber BL, Spriggs DR, Kufe DW. Phospholipase C activates protein kinase C and induces monocytic differentiation of HL-60 cells. *Blood*. 1988;72(2):739–744. https://doi.org/10.1182/blood.v72.2.739.bloodjournal722739

14. Berridge MJ, Irvine RF. Inositol trisphosphate, a novel second messenger in cellular signal transduction. *Nature*. 1984;312(5992):315–321. https://doi.org/10.1038/312315a0

15. Sugimoto Y, Whitman M, Cantley LC, Erikson RL. Evidence that the Rous sarcoma virus transforming gene product phosphorylates phosphatidylinositol and diacylglycerol. *Proc Natl Acad Sci U S A*. 1984;81(7):2117–2121. https://doi.org/10.1073/pnas.81.7.2117

16. Whitman M, Kaplan DR, Schaffhausen B, Cantley L, Roberts TM. Association of phosphatidylinositol kinase activity with polyoma middle-T competent for transformation. *Nature*. 1985;315(6016):239–242. https://doi.org/10.1038/315239a0

17. Kaplan DR, Whitman M, Schaffhausen B, et al. Phosphatidylinositol metabolism and polyoma-mediated transformation. *Proc Natl Acad Sci U S A*. 1986;83(11):3624–3628. https://doi.org/10.1073/pnas.83.11.3624

18. Whitman M, Kaplan D, Roberts T, Cantley L. Evidence for two distinct phosphatidylinositol kinases in fibroblasts. Implications for cellular regulation. *Biochem J*. 1987;247(1):165–174. https://doi.org/10.1042/bj2470165

19. Whitman M, Downes CP, Keeler M, Keller T, Cantley L. Type I phosphatidylinositol kinase makes a novel inositol phospholipid, phosphatidylinositol-3-phosphate. *Nature*. 1988;332(6165):644–646. https://doi.org/10.1038/332644a0

20. Auger KR, Serunian LA, Soltoff SP, Libby P, Cantley LC. PDGF-dependent tyrosine phosphorylation stimulates production of novel polyphosphoinositides in intact cells. *Cell*. 1989;57(1):167–175. https://doi.org/10.1016/0092-8674(89)90182-7

21. Carpenter CL, Duckworth BC, Auger KR, Cohen B, Schaffhausen BS, Cantley LC. Purification and characterization of phosphoinositide 3-kinase from rat liver. *Journal of Biological Chemistry*. 1990;265(32):19704–19711. https://doi.org/10.1016/s0021-9258(17)45429-9

22. Stephens LR, Hughes KT, Irvine RF. Pathway of phosphatidylinositol(3,4,5)-trisphosphate synthesis in activated neutrophils. *Nature*. 1991;351(6321):33–9. https://doi.org/10.1038/351033a0

23. Stephens LR, Jackson TR, Hawkins PT. Agonist-stimulated synthesis of phosphatidylinositol(3,4,5)-trisphosphate. *Biochimica et Biophysica Acta (BBA) - Molecular Cell Research*. 1993;1179(1):27–75. https://doi.org/10.1016/0167-4889(93)90072-w

24. Harlan JE, Hajduk PJ, Yoon HS, Fesik SW. Pleckstrin homology domains bind to phosphatidylinositol-4,5-bisphosphate. *Nature*. 1994;371(6493):168–170. https://doi.org/10.1038/371168a0

25. Haslam RJ, Koide HB, Hemmings BA. Pleckstrin domain homology. *Nature*. 1993;363(6427):309–310. https://doi.org/10.1038/363309b0

26. Mayer BJ, Ren R, Clark KL, Baltimore D. A putative modular domain present in diverse signaling proteins. *Cell*. 1993;73(4):629–630. https://doi.org/10.1016/0092-8674(93)90244-k

27. Burgering BMT, Coffer PJ. Protein kinase B (c-Akt) in phosphatidylinositol-3-OH kinase signal transduction. *Nature*. 1995;376(6541):599–602. https://doi.org/10.1038/376599a0

28. James SR, Downes CP, Gigg R, Grove SJ, Holmes AB, Alessi DR. Specific binding of the Akt-1 protein kinase to phosphatidylinositol 3,4,5-trisphosphate without subsequent activation. *Biochem J*. 1996;315 (Pt 3)(Pt 3):709–713. https://doi.org/10.1042/bj3150709

29. Stokoe D, Stephens LR, Copeland T, et al. Dual Role of Phosphatidylinositol-3,4,5-trisphosphate in the Activation of Protein Kinase B. *Science*. 1997;277(5325):567–570. https://doi.org/10.1126/science.277.5325.567

30. Alessi DR, James SR, Downes CP, et al. Characterization of a 3-phosphoinositide-dependent protein kinase which phosphorylates and activates protein kinase Bα. *Curr Biol*. 1997;7(4):261–269. https://doi.org/10.1016/s0960-9822(06)00122-9

31. McManus EJ, Collins BJ, Ashby PR, et al. The in vivo role of PtdIns(3,4,5)P3 binding to PDK1 PH domain defined by knockin mutation. *EMBO J*. 2004;23(10):2071–82. https://doi.org/10.1038/sj.emboj.7600218

32. Manning BD, Toker A. AKT/PKB Signaling: Navigating the Network. *Cell*. 2017;169(3):381–405. https://doi.org/10.1016/j.cell.2017.04.001

33. Steck PA, Pershouse MA, Jasser SA, et al. Identification of a candidate tumour suppressor gene, MMAC1, at chromosome 10q23.3 that is mutated in multiple advanced cancers. *Nat Genet*. 1997;15(4):356–62. https://doi.org/10.1038/ng0497-356

34. Li DM, Sun H. TEP1, encoded by a candidate tumor suppressor locus, is a novel protein tyrosine phosphatase regulated by transforming growth factor beta. *Cancer Res*. 1997;57(11):2124–9.

35. Maehama T, Dixon JE. The tumor suppressor, PTEN/MMAC1, dephosphorylates the lipid second messenger, phosphatidylinositol 3,4,5-trisphosphate. *J Biol Chem*. 1998;273(22):13375–8. https://doi.org/10.1074/jbc.273.22.13375

36. Li DM, Sun H. PTEN/MMAC1/TEP1 suppresses the tumorigenicity and induces G1 cell cycle arrest in human glioblastoma cells. *Proc Natl Acad Sci U S A*. 1998;95(26):15406–11. https://doi.org/10.1073/pnas.95.26.15406

37. Wu X, Senechal K, Neshat MS, Whang YE, Sawyers CL. The PTEN/MMAC1 tumor suppressor phosphatase functions as a negative regulator of the phosphoinositide 3-kinase/Akt pathway. *Proc Natl Acad Sci U S A*. 1998;95(26):15587–91. https://doi.org/10.1073/pnas.95.26.15587

38. Andjelković M, Jakubowicz T, Cron P, Ming XF, Han JW, Hemmings BA. Activation and phosphorylation of a pleckstrin homology domain containing protein

kinase (RAC-PK/PKB) promoted by serum and protein phosphatase inhibitors. *Proc Natl Acad Sci U S A*. 1996;93(12):5699–704. https://doi.org/10.1073/pnas.93.12.5699

39. Gao T, Furnari F, Newton AC. PHLPP: a phosphatase that directly dephosphorylates Akt, promotes apoptosis, and suppresses tumor growth. *Mol Cell*. 2005;18(1):13–24. https://doi.org/10.1016/j.molcel.2005.03.008

40. Dempke WCM, Uciechowski P, Fenchel K, Chevassut T. Targeting SHP-1, 2 and SHIP Pathways: A Novel Strategy for Cancer Treatment? *Oncology*. 2018;95(5):257–269. https://doi.org/10.1159/000490106

41. Li H, Marshall AJ. Phosphatidylinositol (3,4) bisphosphate-specific phosphatases and effector proteins: A distinct branch of PI3K signaling. *Cell Signal*. 2015;27(9):1789–98. https://doi.org/10.1016/j.cellsig.2015.05.013

42. Li Chew C, Lunardi A, Gulluni F, et al. In Vivo Role of INPP4B in Tumor and Metastasis Suppression through Regulation of PI3K-AKT Signaling at Endosomes. *Cancer Discov*. 2015;5(7):740–51. https://doi.org/10.1158/2159-8290.Cd-14-1347

43. Fedele CG, Ooms LM, Ho M, et al. Inositol polyphosphate 4-phosphatase II regulates PI3K/Akt signaling and is lost in human basal-like breast cancers. *Proc Natl Acad Sci U S A*. 2010;107(51):22231–6. https://doi.org/10.1073/pnas.1015245107

44. Carver DJ, Aman MJ, Ravichandran KS. SHIP inhibits Akt activation in B cells through regulation of Akt membrane localization. *Blood*. 2000;96(4):1449–56.

45. Aman MJ, Lamkin TD, Okada H, Kurosaki T, Ravichandran KS. The inositol phosphatase SHIP inhibits Akt/PKB activation in B cells. *J Biol Chem*. 1998;273(51):33922–8. https://doi.org/10.1074/jbc.273.51.33922

46. Guilherme A, Klarlund JK, Krystal G, Czech MP. Regulation of Phosphatidylinositol 3,4,5-Trisphosphate 5′-Phosphatase Activity by Insulin*. *Journal of Biological Chemistry*. 1996;271(47):29533–29536. https://doi.org/https://doi.org/10.1074/jbc.271.47.29533

47. Gewinner C, Wang ZC, Richardson A, et al. Evidence that Inositol Polyphosphate 4-Phosphatase Type II Is a Tumor Suppressor that Inhibits PI3K Signaling. *Cancer Cell*. 2009;16(2):115–125. https://doi.org/https://doi.org/10.1016/j.ccr.2009.06.006

48. Lopez SM, Hodgson MC, Packianathan C, et al. Determinants of the tumor suppressor INPP4B protein and lipid phosphatase activities. *Biochem Biophys Res Commun*. 2013;440(2):277–282. https://doi.org/https://doi.org/10.1016/j.bbrc.2013.09.077

49. Stephens L, Anderson K, Stokoe D, et al. Protein Kinase B Kinases That Mediate Phosphatidylinositol 3,4,5-Trisphosphate-Dependent Activation of Protein Kinase B. *Science*. 1998;279(5351):710–714. https://doi.org/10.1126/science.279.5351.710

50. Alessi DR, Deak M, Casamayor A, et al. 3-Phosphoinositide-dependent protein kinase-1 (PDK1): structural and functional homology with the Drosophila DSTPK61 kinase. *Current Biology*. 1997;7(10):776–789. https://doi.org/10.1016/s0960-9822(06)00336-8

51. Powers T. The origin story of rapamycin: systemic bias in biomedical research and cold war politics. *Mol Biol Cell*. 2022;33(13)https://doi.org/10.1091/mbc.E22-08-0377

52. Heitman J, Movva NR, Hall MN. Targets for Cell Cycle Arrest by the Immunosuppressant Rapamycin in Yeast. *Science*. 1991;253(5022):905–909. https://doi.org/10.1126/science.1715094

53. Marks AR. Cellular functions of immunophilins. *Physiol Rev*. 1996;76(3):631–49. https://doi.org/10.1152/physrev.1996.76.3.631

54. Sigal NH, Dumont FJ. Cyclosporin A, FK-506, and Rapamycin: Pharmacologic Probes of Lymphocyte Signal Transduction. *Annual Review of Immunology*. 1992;10(1):519–560. https://doi.org/10.1146/annurev.iy.10.040192.002511

55. Terada N, Lucas JJ, Szepesi A, Franklin RA, Domenico J, Gelfand EW. Rapamycin blocks cell cycle progression of activated T cells prior to events characteristic of the middle to late G1 phase of the cycle. *Journal of Cellular Physiology*. 1993;154(1):7–15. https://doi.org/10.1002/jcp.1041540103

56. Morice WG, Brunn GJ, Wiederrecht G, Siekierka JJ, Abraham RT. Rapamycin-induced inhibition of p34cdc2 kinase activation is associated with G1/S-phase growth arrest in T lymphocytes. *Journal of Biological Chemistry*. 1993;268(5):3734–3738. https://doi.org/10.1016/s0021-9258(18)53755-8

57. Brown EJ, Albers MW, Bum Shin T, et al. A mammalian protein targeted by G1-arresting rapamycin–receptor complex. *Nature*. 1994;369(6483):756–758. https://doi.org/10.1038/369756a0

58. Chen J, Zheng XF, Brown EJ, Schreiber SL. Identification of an 11-kDa FKBP12-rapamycin-binding domain within the 289-kDa FKBP12-rapamycin-associated protein and characterization of a critical serine residue. *Proc Natl Acad Sci U S A*. 1995;92(11):4947–4951. https://doi.org/10.1073/pnas.92.11.4947

59. Sabers CJ, Martin MM, Brunn GJ, et al. Isolation of a Protein Target of the FKBP12-Rapamycin Complex in Mammalian Cells. *Journal of Biological Chemistry*. 1995;270(2):815–822. https://doi.org/10.1074/jbc.270.2.815

60. Choi J, Chen J, Schreiber SL, Clardy J. Structure of the FKBP12-Rapamycin Complex Interacting with Binding Domain of Human FRAP. *Science*. 1996;273(5272):239–242. https://doi.org/10.1126/science.273.5272.239

61. Sabatini DM, Erdjument-Bromage H, Lui M, Tempst P, Snyder SH. RAFT1: A mammalian protein that binds to FKBP12 in a rapamycin-dependent fashion and is homologous to yeast TORs. *Cell*. 1994;78(1):35–43. https://doi.org/10.1016/0092-8674(94)90570-3

62. Chiu MI, Katz H, Berlin V. RAPT1, a mammalian homolog of yeast Tor, interacts with the FKBP12/rapamycin complex. *Proc Natl Acad Sci U S A*. 1994;91(26):12574–12578. https://doi.org/10.1073/pnas.91.26.12574

63. Brown EJ, Beal PA, Keith CT, Chen J, Bum Shin T, Schreiber SL. Control of p70 S6 kinase by kinase activity of FRAP in vivo. *Nature*. 1995;377(6548):441–446. https://doi.org/10.1038/377441a0

64. Burnett PE, Barrow RK, Cohen NA, Snyder SH, Sabatini DM. RAFT1 phosphorylation of the translational regulators p70 S6 kinase and 4E-BP1. *Proc Natl Acad Sci U S A*. 1998;95(4):1432–1437. https://doi.org/10.1073/pnas.95.4.1432

65. Brunn GJ, Williams J, Sabers C, Wiederrecht G, Lawrence JC, Abraham RT. Direct inhibition of the signaling functions of the mammalian target of rapamycin by the phosphoinositide 3-kinase inhibitors, wortmannin and LY294002. *EMBO J*. 1996;15(19):5256–5267. https://doi.org/10.1002/j.1460-2075.1996.tb00911.x

66. Loewith R, Jacinto E, Wullschleger S, et al. Two TOR Complexes, Only One of which Is Rapamycin Sensitive, Have Distinct Roles in Cell Growth Control. *Molecular Cell*. 2002;10(3):457–468. https://doi.org/10.1016/s1097-2765(02)00636-6

67. Kim D-H, Sarbassov DD, Ali SM, et al. GβL, a Positive Regulator of the Rapamycin-Sensitive Pathway Required for the Nutrient-Sensitive Interaction between Raptor and mTOR. *Molecular Cell*. 2003;11(4):895–904. https://doi.org/10.1016/s1097-2765(03)00114-x

68. Sarbassov DD, Ali SM, Kim D-H, et al. Rictor, a novel binding partner of mTOR, defines a rapamycin-insensitive and raptor-independent pathway that regulates the cytoskeleton. *Curr Biol*. 2004;14(14):1296–1302. https://doi.org/10.1016/j.cub.2004.06.054

69. Sarbassov DD, Guertin DA, Ali SM, Sabatini DM. Phosphorylation and Regulation of Akt/PKB by the Rictor-mTOR Complex. *Science*. 2005;307(5712):1098–1101. https://doi.org/10.1126/science.1106148

70. Hara K, Maruki Y, Long X, et al. Raptor, a Binding Partner of Target of Rapamycin (TOR), Mediates TOR Action. *Cell*. 2002;110(2):177–189. https://doi.org/10.1016/s0092-8674(02)00833-4

71. Kim D-H, Sarbassov DD, Ali SM, et al. mTOR Interacts with Raptor to Form a Nutrient-Sensitive Complex that Signals to the Cell Growth Machinery. *Cell*. 2002;110(2):163–175. https://doi.org/10.1016/s0092-8674(02)00808-5

72. Nojima H, Tokunaga C, Eguchi S, et al. The mammalian target of rapamycin (mTOR) partner, raptor, binds the mTOR substrates p70 S6 kinase and 4E-BP1 through their TOR signaling (TOS) motif. *J Biol Chem*. 2003;278(18):15461–15464. https://doi.org/10.1074/jbc.c200665200

73. Gingras AC, Kennedy SG, O'Leary MA, Sonenberg N, Hay N. 4E-BP1, a repressor of mRNA translation, is phosphorylated and inactivated by the Akt(PKB) signaling pathway. *Genes Dev*. 1998;12(4):502–513. https://doi.org/10.1101/gad.12.4.502

74. Miron M, Lasko P, Sonenberg N. Signaling from Akt to FRAP/TOR targets both 4E-BP and S6K in Drosophila melanogaster. *Mol Cell Biol*. 2003;23(24):9117–9126. https://doi.org/10.1128/MCB.23.24.9117-9126.2003

75. Peng X-D, Xu P-Z, Chen M-L, et al. Dwarfism, impaired skin development, skeletal muscle atrophy, delayed bone development, and impeded adipogenesis in mice lacking Akt1 and Akt2. *Genes Dev*. 2003;17(11):1352–1365. https://doi.org/10.1101/gad.1089403

76. Dufner A, Andjelkovic M, Burgering BM, Hemmings BA, Thomas G. Protein kinase B localization and activation differentially affect S6 kinase 1 activity and eukaryotic translation initiation factor 4E-binding protein 1 phosphorylation. *Mol Cell Biol*. 1999;19(6):4525–4534. https://doi.org/10.1128/MCB.19.6.4525

77. Potter CJ, Huang H, Xu T. Drosophila Tsc1 Functions with Tsc2 to Antagonize Insulin Signaling in Regulating Cell Growth, Cell Proliferation, and Organ Size. *Cell*. 2001;105(3):357–368. https://doi.org/10.1016/s0092-8674(01)00333-6

78. Potter CJ, Pedraza LG, Xu T. Akt regulates growth by directly phosphorylating Tsc2. *Nature Cell Biology*. 2002;4(9):658–665. https://doi.org/10.1038/ncb840

79. Inoki K, Li Y, Zhu T, Wu J, Guan K-L. TSC2 is phosphorylated and inhibited by Akt and suppresses mTOR signalling. *Nat Cell Biol*. 2002;4(9):648–657. https://doi.org/10.1038/ncb839

80. Tee AR, Fingar DC, Manning BD, Kwiatkowski DJ, Cantley LC, Blenis J. Tuberous sclerosis complex-1 and -2 gene products function together to inhibit mammalian target of rapamycin (mTOR)-mediated downstream signaling. *Proc Natl Acad Sci U S A*. 2002;99(21):13571–13576. https://doi.org/10.1073/pnas.202476899

81. Xiao G-H, Shoarinejad F, Jin F, Golemis EA, Yeung RS. The Tuberous Sclerosis 2 Gene Product, Tuberin, Functions as a Rab5 GTPase Activating Protein (GAP) in Modulating Endocytosis. *Journal of Biological Chemistry*. 1997;272(10):6097–6100. https://doi.org/10.1074/jbc.272.10.6097

82. Hodges AK. Pathological mutations in TSC1 and TSC2 disrupt the interaction between hamartin and tuberin. *Human Molecular Genetics*. 2001;10(25):2899–2905. https://doi.org/10.1093/hmg/10.25.2899

83. Inoki K, Li Y, Xu T, Guan K-L. Rheb GTPase is a direct target of TSC2 GAP activity and regulates mTOR signaling. *Genes Dev*. 2003;17(15):1829–1834. https://doi.org/10.1101/gad.1110003

84. Garami A, Zwartkruis FJT, Nobukuni T, et al. Insulin activation of Rheb, a mediator of mTOR/S6K/4E-BP signaling, is inhibited by TSC1 and 2. *Mol Cell*. 2003;11(6):1457–1466. https://doi.org/10.1016/s1097-2765(03)00220-x

85. Tee AR, Manning BD, Roux PP, Cantley LC, Blenis J. Tuberous sclerosis complex gene products, Tuberin and Hamartin, control mTOR signaling by acting as a GTPase-activating protein complex toward Rheb. *Curr Biol*. 2003;13(15):1259–1268. https://doi.org/10.1016/s0960-9822(03)00506-2

86. Tabancay AP, Gau C-L, Machado IMP, et al. Identification of dominant negative mutants of Rheb GTPase and their use to implicate the involvement of human Rheb in the activation of p70S6K. *J Biol Chem*. 2003;278(41):39921–39930. https://doi.org/10.1074/jbc.m306553200

87. Castro AF, Rebhun JF, Clark GJ, Quilliam LA. Rheb binds tuberous sclerosis complex 2 (TSC2) and promotes S6 kinase activation in a rapamycin- and farnesylation-dependent manner. *J Biol Chem*. 2003;278(35):32493–32496. https://doi.org/10.1074/jbc.c300226200

88. Schiffman JD, Breen M. Comparative oncology: what dogs and other species can teach us about humans with cancer. *Philos Trans R Soc Lond B Biol Sci*. 2015;370(1673):20140231. https://doi.org/10.1098/rstb.2014.0231

89. Gardner HL, Fenger JM, London CA. Dogs as a model for cancer. *Annu Rev Anim Biosci*. 2016;4:199–222. https://doi.org/10.1146/annurev-animal-022114-110911

90. Avery AC. The genetic and molecular basis for canine models of human leukemia and lymphoma. *Front Oncol*. 2020;10:23–23. https://doi.org/10.3389/fonc.2020.00023

91. Dhawan D, Ramos-Vara JA, Utturkar SM, et al. Identification of a naturally-occurring canine model for early detection and intervention research in high grade urothelial carcinoma. *Front Oncol*. 2022;12:1011969. https://doi.org/10.3389/fonc.2022.1011969

92. Fowles JS, Denton CL, Gustafson DL. Comparative analysis of MAPK and PI3K/AKT pathway activation and inhibition in human and canine melanoma. *Vet Comp Oncol*. 2013;13(3):288–304. https://doi.org/10.1111/vco.12044

93. Kim T-M, Yang IS, Seung B-J, et al. Cross-species oncogenic signatures of breast cancer in canine mammary tumors. *Nat Commun*. 2020;11(1):3616–3616. https://doi.org/10.1038/s41467-020-17458-0

94. Liu D, Xiong H, Ellis AE, et al. Canine spontaneous head and neck squamous cell carcinomas represent their human counterparts at the molecular level. *PLoS Genet*. 2015;11(6):e1005277. https://doi.org/10.1371/journal.pgen.1005277

95. Pinho SS, Carvalho S, Cabral J, Reis CA, Gärtner F. Canine tumors: a spontaneous animal model of human carcinogenesis. *Transl Res*. 2012;159(3):165–72. https://doi.org/10.1016/j.trsl.2011.11.005

96. Uva P, Aurisicchio L, Watters J, et al. Comparative expression pathway analysis of human and canine mammary tumors. *BMC Genomics*. 2009;10:135–135. https://doi.org/10.1186/1471-2164-10-135

97. Engelman JA, Luo J, Cantley LC. The evolution of phosphatidylinositol 3-kinases as regulators of growth and metabolism. *Nat Rev Genet*. 2006;7(8):606–619. https://doi.org/10.1038/nrg1879

98. Mayer IA, Arteaga CL. The PI3K/AKT pathway as a target for cancer treatment. *Annu Rev Med*. 2016;67(1):11–28. https://doi.org/10.1146/annurev-med-062913-051343

99. Geltz NR, Augustine JA. The p85 and p110 subunits of phosphatidylinositol 3-kinase-α are substrates, in vitro, for a constitutively associated protein tyrosine kinase in platelets. *Blood*. 1998;91(3):930–939. https://doi.org/10.1182/blood.v91.3.930.930_930_939

100. Jean S, Kiger AA. Classes of phosphoinositide 3-kinases at a glance. *J Cell Sci*. 2014;127(Pt 5):923–8. https://doi.org/10.1242/jcs.093773

101. Safaroghli-Azar A, Sanaei MJ, Pourbagheri-Sigaroodi A, Bashash D. Phosphoinositide 3-kinase (PI3K) classes: From cell signaling to endocytic recycling and autophagy. *Eur J Pharmacol*. 2023;953:175827. https://doi.org/10.1016/j.ejphar.2023.175827

102. Bilanges B, Posor Y, Vanhaesebroeck B. PI3K isoforms in cell signalling and vesicle trafficking. *Nat Rev Mol Cell Biol*. 2019;20(9):515–534. https://doi.org/10.1038/s41580-019-0129-z

103. Funaki M, Katagiri H, Kanda A, et al. p85/p110-type phosphatidylinositol kinase phosphorylates not only the D-3, but also the D-4 position of the inositol ring. *J Biol Chem*. 1999;274(31):22019–22024. https://doi.org/10.1074/jbc.274.31.22019

104. Bunney TD, Katan M. Phosphoinositide signalling in cancer: beyond PI3K and PTEN. *Nat Rev Cancer*. 2010;10(5):342–352. https://doi.org/10.1038/nrc2842

105. Stambolic V, Suzuki A, de la Pompa JL, et al. Negative regulation of PKB/Akt-dependent cell survival by the tumor suppressor PTEN. *Cell*. 1998;95(1):29–39. https://doi.org/10.1016/s0092-8674(00)81780-8

106. Haar EV, Lee S-i, Bandhakavi S, Griffin TJ, Kim D-H. Insulin signalling to mTOR mediated by the Akt/PKB substrate PRAS40. *Nat Cell Biol*. 2007;9(3):316–323. https://doi.org/10.1038/ncb1547

107. Chauvin C, Koka V, Nouschi A, et al. Ribosomal protein S6 kinase activity controls the ribosome biogenesis transcriptional program. *Oncogene*. 2013;33(4):474–483. https://doi.org/10.1038/onc.2012.606

108. Feng J, Park J, Cron P, Hess D, Hemmings BA. Identification of a PKB/Akt hydrophobic motif Ser-473 kinase as DNA-dependent protein kinase. *J Biol Chem*. 2004;279(39):41189–41196. https://doi.org/10.1074/jbc.m406731200

109. Szwed A, Kim E, Jacinto E. Regulation and metabolic functions of mTORC1 and mTORC2. *Physiol Rev*. 2021;101(3):1371–1426. https://doi.org/10.1152/physrev.00026.2020

110. Biggs WH, 3rd, Meisenhelder J, Hunter T, Cavenee WK, Arden KC. Protein kinase B/Akt-mediated phosphorylation promotes nuclear exclusion of the winged helix transcription factor FKHR1. *Proc Natl Acad Sci U S A*. 1999;96(13):7421–7426. https://doi.org/10.1073/pnas.96.13.7421

111. Brunet A, Bonni A, Zigmond MJ, et al. Akt promotes cell survival by phosphorylating and inhibiting a forkhead transcription factor. *Cell*. 1999;96(6):857–868. https://doi.org/10.1016/s0092-8674(00)80595-4

112. Brunet A, Kanai F, Stehn J, et al. 14-3-3 transits to the nucleus and participates in dynamic nucleocytoplasmic transport. *J Cell Biol*. 2002;156(5):817–828. https://doi.org/10.1083/jcb.200112059

113. Cahill CM, Tzivion G, Nasrin N, et al. Phosphatidylinositol 3-kinase signaling inhibits DAF-16 DNA binding and function via 14-3-3-dependent and 14-3-3-independent pathways. *J Biol Chem*. 2001;276(16):13402–13410. https://doi.org/10.1074/jbc.m010042200

114. Guertin DA, Stevens DM, Thoreen CC, et al. Ablation in mice of the mTORC components raptor, rictor, or mLST8 reveals that mTORC2 is required for signaling to Akt-FOXO and PKCalpha, but not S6K1. *Dev Cell*. 2006;11(6):859–871. https://doi.org/10.1016/j.devcel.2006.10.007

115. Matsuzaki H, Daitoku H, Hatta M, Tanaka K, Fukamizu A. Insulin-induced phosphorylation of FKHR (Foxo1) targets to proteasomal degradation. *Proc Natl Acad Sci U S A*. 2003;100(20):11285–11290. https://doi.org/10.1073/pnas.1934283100

116. Rena G, Prescott AR, Guo S, Cohen P, Unterman TG. Roles of the forkhead in rhabdomyosarcoma (FKHR) phosphorylation sites in regulating 14-3-3 binding, transactivation and nuclear targetting. *Biochem J*. 2001;354(3):605–612. https://doi.org/10.1042/bj3540605

117. Fu Z, Tindall DJ. FOXOs, cancer and regulation of apoptosis. *Oncogene*. 2008;27(16):2312–2319. https://doi.org/10.1038/onc.2008.24

118. Furuyama T, Nakazawa T, Nakano I, Mori N. Identification of the differential distribution patterns of mRNAs and consensus binding sequences for mouse DAF-16 homologues. *Biochem J*. 2000;349(2):629–634. https://doi.org/10.1042/bj3490629

119. Yang E, Zha J, Jockel J, Boise LH, Thompson CB, Korsmeyer SJ. Bad, a heterodimeric partner for Bcl-xL and Bcl-2, displaces bax and promotes cell death. *Cell*. 1995;80(2):285–291. https://doi.org/10.1016/0092-8674(95)90411-5

120. Zha J, Harada H, Osipov K, Jockel J, Waksman G, Korsmeyer SJ. BH3 domain of BAD is required for heterodimerization with BCL-XL and pro-apoptotic activity. *J Biol Chem*. 1997;272(39):24101–24104. https://doi.org/10.1074/jbc.272.39.24101

121. Bader AG, Kang S, Zhao L, Vogt PK. Oncogenic PI3K deregulates transcription and translation. *Nat Rev Cancer*. 2005;5(12):921–929. https://doi.org/10.1038/nrc1753

122. Schlein LJ, Thamm DH. Review: NF-kB activation in canine cancer. *Vet Pathol*. 2022;59(5):724–732. https://doi.org/10.1177/03009858221092017

123. Kane LP, Mollenauer MN, Xu Z, Turck CW, Weiss A. Akt-dependent phosphorylation specifically regulates Cot induction of NF-kappa B-dependent transcription. *Mol Cell Biol*. 2002;22(16):5962–5974. https://doi.org/10.1128/MCB.22.16.5962-5974.2002

124. Madrid LV, Mayo MW, Reuther JY, Baldwin AS. Akt stimulates the transactivation potential of the RelA/p65 subunit of NF-kappa B through utilization of the Ikappa B kinase and activation of the mitogen-activated protein kinase p38. *J Biol Chem*. 2001;276(22):18934–18940. https://doi.org/10.1074/jbc.m101103200

125. Romashkova JA, Makarov SS. NF-κB is a target of AKT in anti-apoptotic PDGF signalling. *Nature*. 1999;401(6748):86–90. https://doi.org/10.1038/43474

126. Harrington LS, Findlay GM, Lamb RF. Restraining PI3K: mTOR signalling goes back to the membrane. *Trends Biochem Sci*. 2005;30(1):35–42. https://doi.org/10.1016/j.tibs.2004.11.003

127. Simpson A, Petnga W, Macaulay VM, Weyer-Czernilofsky U, Bogenrieder T. Insulin-like growth factor (IGF) pathway targeting in cancer: role of the IGF axis and opportunities for future combination studies. *Target Oncol*. 2017;12(5):571–597. https://doi.org/10.1007/s11523-017-0514-5

128. Xie X, Zhang D, Zhao B, et al. IkappaB kinase epsilon and TANK-binding kinase 1 activate AKT by direct phosphorylation. *Proc Natl Acad Sci U S A*. 2011;108(16):6474–6479. https://doi.org/10.1073/pnas.1016132108

129. Ghomlaghi M, Hart A, Hoang N, Shin S, Nguyen LK. Feedback, crosstalk and competition: ingredients for emergent non-linear behaviour in the PI3K/mTOR signalling network. *Int J Mol Sci*. 2021;22(13):6944. https://doi.org/10.3390/ijms22136944

130. Zhan J, Chitta RK, Harwood FC, Grosveld GC. Phosphorylation of TSC2 by PKC-δ reveals a novel signaling pathway that couples protein synthesis to mTORC1 activity. *Mol Cell Biochem*. 2019;456(1-2):123–134. https://doi.org/10.1007/s11010-019-03498-8

131. Wallroth A, Koch PA, Marat AL, Krause E, Haucke V. Protein kinase N controls a lysosomal lipid switch to facilitate nutrient signalling via mTORC1. *Nat Cell Biol*. 2019;21(9):1093–1101. https://doi.org/10.1038/s41556-019-0377-3

132. O'Reilly KE, Rojo F, She Q-B, et al. mTOR inhibition induces upstream receptor tyrosine kinase signaling and activates Akt. *Cancer Res*. 2006;66(3):1500–1508. https://doi.org/10.1158/0008-5472.CAN-05-2925

133. Fruman DA, Rommel C. PI3K and cancer: lessons, challenges and opportunities. *Nat Rev Drug Discov*. 2014;13(2):140–156. https://doi.org/10.1038/nrd4204

134. Gardner HL, Rippy SB, Bear MD, et al. Phase I/II evaluation of RV1001, a novel PI3Kδ inhibitor, in spontaneous canine lymphoma. *PLoS One*. 2018;13(4):e0195357–e0195357. https://doi.org/10.1371/journal.pone.0195357

135. Zhang M, Jang H, Nussinov R. PI3K inhibitors: review and new strategies. *Chem Sci*. 2020;11(23):5855–5865. https://doi.org/10.1039/d0sc01676d

136. Backer JM. The regulation of class IA PI 3-kinases by inter-subunit interactions. *Curr Top Microbiol Immunol*. 2010;346:87–114. https://doi.org/10.1007/82_2010_52

137. Bresnick AR, Backer JM. PI3Kβ—A versatile transducer for GPCR, RTK, and small GTPase signaling. *Endocrinology*. 2019;160(3):536–555. https://doi.org/10.1210/en.2018-00843

138. Schwartz S, Wongvipat J, Trigwell CB, et al. Feedback suppression of PI3Kα signaling in PTEN-mutated tumors is relieved by selective inhibition of PI3Kβ. *Cancer Cell*. 2015;27(1):109–122. https://doi.org/10.1016/j.ccell.2014.11.008

139. Maeda M, Ochiai K, Michishita M, et al. In vitro anticancer effects of alpelisib against PIK3CA-mutated canine hemangiosarcoma cell lines. *Oncol Rep*. 2022;47(4):84. https://doi.org/10.3892/or.2022.8295

140. Chandarlapaty S, Sawai A, Scaltriti M, et al. AKT inhibition relieves feedback suppression of receptor tyrosine kinase expression and activity. *Cancer Cell*. 2011;19(1):58–71. https://doi.org/10.1016/j.ccr.2010.10.031

141. Kim S, Domon-Dell C, Kang J, Chung DH, Freund J-N, Evers BM. Down-regulation of the tumor suppressor PTEN by the tumor necrosis factor-alpha/nuclear factor-kappaB (NF-kappaB)-inducing kinase/NF-kappaB pathway is linked to a default IkappaB-alpha autoregulatory loop. *J Biol Chem*. 2004;279(6):4285–4291. https://doi.org/10.1074/jbc.m308383200

142. Vasudevan KM, Gurumurthy S, Rangnekar VM. Suppression of PTEN expression by NF-kappa B prevents apoptosis. *Mol Cell Biol*. 2004;24(3):1007–1021. https://doi.org/10.1128/MCB.24.3.1007-1021.2004

143. LoPiccolo J, Blumenthal GM, Bernstein WB, Dennis PA. Targeting the PI3K/Akt/mTOR pathway: effective combinations and clinical considerations. *Drug Resist Updat*. 2008;11(1-2):32–50. https://doi.org/10.1016/j.drup.2007.11.003

144. Revathidevi S, Munirajan AK. Akt in cancer: mediator and more. *Semin Cancer Biol*. 2019;59:80–91. https://doi.org/10.1016/j.semcancer.2019.06.002

145. Tsai P-J, Lai Y-H, Manne RK, Tsai Y-S, Sarbassov D, Lin H-K. Akt: a key transducer in cancer. *J Biomed Sci*. 2022;29(1):76–76. https://doi.org/10.1186/s12929-022-00860-9

146. Braunstein S, Karpisheva K, Pola C, et al. A hypoxia-controlled cap-dependent to cap-independent translation switch in breast cancer. *Mol Cell*. 2007;28(3):501–512. https://doi.org/10.1016/j.molcel.2007.10.019

147. Forsythe JA, Jiang BH, Iyer NV, et al. Activation of vascular endothelial growth factor gene transcription by hypoxia-inducible factor 1. *Mol Cell Biol*. 1996;16(9):4604–4613. https://doi.org/10.1128/MCB.16.9.4604

148. Laplante M, Sabatini DM. mTOR signaling in growth control and disease. *Cell*. 2012;149(2):274–293. https://doi.org/10.1016/j.cell.2012.03.017

149. King WG, Mattaliano MD, Chan TO, Tsichlis PN, Brugge JS. Phosphatidylinositol 3-kinase is required for integrin-stimulated AKT and Raf-1/mitogen-activated protein kinase pathway activation. *Mol Cell Biol*. 1997;17(8):4406–4418. https://doi.org/10.1128/MCB.17.8.4406

150. Majewski M, Nieborowska-Skorska M, Salomoni P, et al. Activation of mitochondrial Raf-1 is involved in the antiapoptotic effects of Akt. *Cancer Res*. 1999;59(12):2815–2819.

151. Dajas-Bailador F, Bantounas I, Jones EV, Whitmarsh AJ. Regulation of axon growth by the JIP1-AKT axis. *J Cell Sci*. 2014;127(Pt 1):230–239. https://doi.org/10.1242/jcs.137208

152. Kim AH, Khursigara G, Sun X, Franke TF, Chao MV. Akt phosphorylates and negatively regulates apoptosis signal-regulating kinase 1. *Mol Cell Biol*. 2001;21(3):893–901. https://doi.org/10.1128/MCB.21.3.893-901.2001

153. Pan J, Chang Q, Wang X, et al. Reactive oxygen species-activated Akt/ASK1/p38 signaling pathway in nickel compound-induced apoptosis in BEAS 2B cells. *Chem Res Toxicol*. 2010;23(3):568–577. https://doi.org/10.1021/tx9003193

154. Zha J, Harada H, Yang E, Jockel J, Korsmeyer SJ. Serine phosphorylation of death agonist BAD in response to survival factor results in binding to 14-3-3 not BCL-X(L). *Cell*. 1996;87(4):619–628. https://doi.org/10.1016/s0092-8674(00)81382-3

155. Zhao H-F, Wang J, To S-ST. The phosphatidylinositol 3-kinase/Akt and c-Jun N-terminal kinase signaling in cancer: alliance or contradiction? (Review). *Int J Oncol*. 2015;47(2):429–436. https://doi.org/10.3892/ijo.2015.3052

156. Karin M, Cao Y, Greten FR, Li Z-W. NF-κB in cancer: from innocent bystander to major culprit. *Nat Rev Cancer*. 2002;2(4):301–310. https://doi.org/10.1038/nrc780

157. Nidai Ozes O, Mayo LD, Gustin JA, Pfeffer SR, Pfeffer LM, Donner DB. NF-κB activation by tumour necrosis factor requires the Akt serine–threonine kinase. *Nature*. 1999;401(6748):82–85. https://doi.org/10.1038/43466

158. Brumfield A, Chaudhary N, Molle D, Wen J, Graumann J, McGraw TE. Insulin-promoted mobilization of GLUT4 from a perinuclear storage site requires RAB10. *Mol Biol Cell*. 2021;32(1):57–73. https://doi.org/10.1091/mbc.E20-06-0356

159. Calera MR, Martinez C, Liu H, Jack AKE, Birnbaum MJ, Pilch PF. Insulin increases the association of Akt-2 with Glut4-containing vesicles. *J Biol Chem*. 1998;273(13):7201–7204. https://doi.org/10.1074/jbc.273.13.7201

160. Eickelschulte S, Hartwig S, Leiser B, et al. AKT/AMPK-mediated phosphorylation of TBC1D4 disrupts the interaction with insulin-regulated aminopeptidase. *J Biol Chem*. 2021;296:100637–100637. https://doi.org/10.1016/j.jbc.2021.100637

161. Kohn AD, Summers SA, Birnbaum MJ, Roth RA. Expression of a constitutively active Akt Ser/Thr kinase in 3T3-L1 adipocytes stimulates glucose uptake and glucose transporter 4 translocation. *J Biol Chem*. 1996;271(49):31372–31378. https://doi.org/10.1074/jbc.271.49.31372

162. Kupriyanova TA, Kandror KV. Akt-2 binds to Glut4-containing vesicles and phosphorylates their component proteins in response to insulin. *J Biol Chem*. 1999;274(3):1458–1464. https://doi.org/10.1074/jbc.274.3.1458

163. Raun SH, Knudsen JR, Han X, Jensen Thomas E, Sylow L. Cancer causes dysfunctional insulin signaling and glucose transport in a muscle-type-specific manner. *FASEB J*. 2022;36(3)https://doi.org/10.1096/fj.202101759r

164. Guo X-H, Jiang S-S, Zhang L-L, et al. Berberine exerts its antineoplastic effects by reversing the Warburg effect via downregulation of the Akt/mTOR/GLUT1 signaling pathway. *Oncol Rep*. 2021;46(6):253. https://doi.org/10.3892/or.2021.8204

165. Liu X, Yamaguchi K, Takane K, et al. Cancer-associated IDH mutations induce Glut1 expression and glucose metabolic disorders through a PI3K/Akt/mTORC1-Hif1α axis. *PLoS One*. 2021;16(9):e0257090–e0257090. https://doi.org/10.1371/journal.pone.0257090

166. Makinoshima H, Takita M, Saruwatari K, et al. Signaling through the phosphatidylinositol 3-kinase (PI3K)/mammalian target of rapamycin (mTOR) axis Is responsible for aerobic glycolysis mediated by glucose transporter in epidermal growth factor receptor (EGFR)-mutated lung adenocarcinoma. *J Biol Chem*. 2015;290(28):17495–17504. https://doi.org/10.1074/jbc.M115.660498

167. Taha C, Liu Z, Jin J, Al-Hasani H, Sonenberg N, Klip A. Opposite translational control of GLUT1 and GLUT4 glucose transporter mRNAs in response to insulin. Role of mammalian target of rapamycin, protein kinase b, and phosphatidylinositol 3-kinase in GLUT1 mRNA translation. *J Biol Chem*. 1999;274(46):33085–33091. https://doi.org/10.1074/jbc.274.46.33085

168. Weng H-C, Sung C-J, Hsu J-L, et al. The combination of a novel GLUT1 inhibitor and cisplatin synergistically inhibits breast cancer cell growth by enhancing the DNA damaging effect and modulating the Akt/mTOR and MAPK signaling pathways. *Front Pharmacol*. 2022;13:879748–879748. https://doi.org/10.3389/fphar.2022.879748

169. Wieman HL, Wofford JA, Rathmell JC. Cytokine stimulation promotes glucose uptake via phosphatidylinositol-3 kinase/Akt regulation of Glut1 activity and trafficking. *Mol Biol Cell*. 2007;18(4):1437–1446. https://doi.org/10.1091/mbc.e06-07-0593

170. Mattaini KR, Vander Heiden MG. Glycosylation to adapt to stress. *Science*. 2012;337(6097):925–926. https://doi.org/10.1126/science.1227513

171. Yi W, Clark PM, Mason DE, et al. Phosphofructokinase 1 glycosylation regulates cell growth and metabolism. *Science*. 2012;337(6097):975–980. https://doi.org/10.1126/science.1222278

172. Cross DAE, Alessi DR, Cohen P, Andjelkovich M, Hemmings BA. Inhibition of glycogen synthase kinase-3 by insulin mediated by protein kinase B. *Nature*. 1995;378(6559):785–789. https://doi.org/10.1038/378785a0

173. Cross DAE, Watt PW, Shaw M, et al. Insulin activates protein kinase B, inhibits glycogen synthase kinase-3 and activates glycogen synthase by rapamycin-insensitive pathways in skeletal muscle and adipose tissue. *FEBS Lett*. 1997;406(1-2):211–215. https://doi.org/10.1016/s0014-5793(97)00240-8

174. Krycer JR, Sharpe LJ, Luu W, Brown AJ. The Akt–SREBP nexus: cell signaling meets lipid metabolism. *Trends Endocrinol Metab*. 2010;21(5):268–276. https://doi.org/10.1016/j.tem.2010.01.001

175. Moule SK, Welsh GI, Edgell NJ, Foulstone EJ, Proud CG, Denton RM. Regulation of protein kinase B and glycogen synthase kinase-3 by insulin and β-adrenergic agonists in rat epididymal fat cells. *J Biol Chem*. 1997;272(12):7713–7719. https://doi.org/10.1074/jbc.272.12.7713

176. Pap M, Cooper GM. Role of glycogen synthase kinase-3 in the phosphatidylinositol 3-Kinase/Akt cell survival pathway. *J Biol Chem*. 1998;273(32):19929–19932. https://doi.org/10.1074/jbc.273.32.19929

177. Shao J, Sheng H, DuBois RN, Beauchamp RD. Oncogenic Ras-mediated cell growth arrest and apoptosis are associated with increased ubiquitin-dependent cyclin D1 degradation. *J Biol Chem*. 2000;275(30):22916–22924. https://doi.org/10.1074/jbc.m002235200

178. Fulton D, Gratton JP, McCabe TJ, et al. Regulation of endothelium-derived nitric oxide production by the protein kinase Akt. *Nature*. 1999;399(6736):597–601. https://doi.org/10.1038/21218

179. Hamada K, Sasaki T, Koni PA, et al. The PTEN/PI3K pathway governs normal vascular development and tumor angiogenesis. *Genes Dev*. 2005;19(17):2054–2065. https://doi.org/10.1101/gad.1308805

180. Koistinen P, Siitonen T, Mäntymaa P, et al. Regulation of the acute myeloid leukemia cell line OCI/AML-2 by endothelial nitric oxide synthase under the control of a vascular endothelial growth factor signaling system. *Leukemia*. 2001;15(9):1433–1441. https://doi.org/10.1038/sj.leu.2402217

181. Michell BJ, Griffiths JE, Mitchelhill KI, et al. The Akt kinase signals directly to endothelial nitric oxide synthase. *Curr Biol*. 1999;9(15):845–848. https://doi.org/10.1016/s0960-9822(99)80371-6

182. Gong J, Zhou S, Yang S. Vanillic acid suppresses HIF-1α expression via inhibition of mTOR/p70S6K/4E-BP1 and Raf/MEK/ERK pathways in human colon cancer HCT116 cells. *Int J Mol Sci*. 2019;20(3)https://doi.org/10.3390/ijms20030465

183. Kevil C, Carter P, Hu B, DeBenedetti A. Translational enhancement of FGF-2 by eIF-4 factors, and alternate utilization of CUG and AUG codons for translation initiation. *Oncogene*. 1995;11(11):2339–48.

184. Blagosklonny MV. Are p27 and p21 cytoplasmic oncoproteins? *Cell Cycle*. 2002;1(6):391–393. https://doi.org/10.4161/cc.1.6.262

185. Chen Y, Liu X, Wang H, Liu S, Hu N, Li X. Akt regulated phosphorylation of GSK-3β/cyclin D1, p21 and p27 contributes to cell proliferation through cell cycle progression from G1 to S/G2M phase in low-dose arsenite exposed HaCat cells. *Front Pharmacol*. 2019;10:1176–1176. https://doi.org/10.3389/fphar.2019.01176

186. Fang Y, Yu S, Braley-Mullen H. TGF-β promotes proliferation of thyroid epithelial cells in IFN-γ(-/-) mice by down-regulation of p21 and p27 via AKT pathway. *Am J Pathol*. 2012;180(2):650–660. https://doi.org/10.1016/j.ajpath.2011.10.009

187. Zhou BP, Hung M-C. Novel targets of Akt, p21(Cipl/WAF1), and MDM2. *Semin Oncol*. 2002;29(3 Suppl 11):62–70. https://doi.org/10.1053/sonc.2002.34057

188. Chibaya L, Karim B, Zhang H, Jones SN. Mdm2 phosphorylation by Akt regulates the p53 response to oxidative stress to promote cell proliferation and tumorigenesis. *Proc Natl Acad Sci U S A*. 2021;118(4):e2003193118. https://doi.org/10.1073/pnas.2003193118

189. Ogawara Y, Kishishita S, Obata T, et al. Akt enhances Mdm2-mediated ubiquitination and degradation of p53. *J Biol Chem*. 2002;277(24):21843–21850. https://doi.org/10.1074/jbc.m109745200

190. Du K, Montminy M. CREB Is a regulatory target for the protein kinase Akt/PKB. *J Biol Chem*. 1998;273(49):32377–32379. https://doi.org/10.1074/jbc.273.49.32377

191. Caravatta L, Sancilio S, di Giacomo V, Rana R, Cataldi A, Di Pietro R. PI3-K/Akt-dependent activation of cAMP-response element-binding (CREB) protein in Jurkat T leukemia cells treated with TRAIL. *J Cell Physiol*. 2007;214(1):192–200. https://doi.org/10.1002/jcp.21186

192. Gu T, Zhang Z, Wang J, Guo J, Shen WH, Yin Y. CREB is a novel nuclear target of PTEN phosphatase. *Cancer Res*. 2011;71(8):2821–2825. https://doi.org/10.1158/0008-5472.CAN-10-3399

193. Kumar AP, Bhaskaran S, Ganapathy M, et al. Akt/cAMP-responsive element binding protein/cyclin D1 network: a novel target for prostate cancer inhibition in transgenic adenocarcinoma of mouse prostate model mediated by Nexrutine, a Phellodendron amurense bark extract. *Clin Cancer Res*. 2007;13(9):2784–2794. https://doi.org/10.1158/1078-0432.CCR-06-2974

194. Tao X, Finkbeiner S, Arnold DB, Shaywitz AJ, Greenberg ME. Ca2+ influx regulates BDNF transcription by a CREB family transcription factor-dependent mechanism. *Neuron*. 1998;20(4):709–726. https://doi.org/10.1016/s0896-6273(00)81010-7

195. Wan X, Zhou M, Huang F, et al. AKT1-CREB stimulation of PDGFRα expression is pivotal for PTEN deficient tumor development. *Cell Death Dis*. 2021;12(2):172–172. https://doi.org/10.1038/s41419-021-03433-0

196. Datta SR, Dudek H, Tao X, et al. Akt phosphorylation of BAD couples survival signals to the cell-intrinsic death machinery. *Cell*. 1997;91(2):231–241. https://doi.org/10.1016/s0092-8674(00)80405-5

197. Peso Ld, González-García M, Page C, Herrera Rn, Nuñez G. Interleukin-3-induced phosphorylation of BAD through the protein kinase Akt. *Science*. 1997;278(5338):687–689. https://doi.org/10.1126/science.278.5338.687

198. Datta SR, Brunet A, Greenberg ME. Cellular survival: a play in three Akts. *Genes Dev*. 1999;13(22):2905–2927. https://doi.org/10.1101/gad.13.22.2905

199. Huang H, Tindall DJ. Dynamic FoxO transcription factors. *J Cell Sci*. 2007;120(15):2479–2487. https://doi.org/10.1242/jcs.001222

200. Nicholson KM, Anderson NG. The protein kinase B/Akt signalling pathway in human malignancy. *Cell Signal*. 2002;14(5):381–395. https://doi.org/10.1016/s0898-6568(01)00271-6

201. Zhang X, Tang N, Hadden TJ, Rishi AK. Akt, FoxO and regulation of apoptosis. *Biochim Biophys Acta*. 2011;1813(11):1978–1986. https://doi.org/10.1016/j.bbamcr.2011.03.010

202. Korsmeyer SJ. Regulators of cell death. *Trends Genet*. 1995;11(3):101–105. https://doi.org/10.1016/s0168-9525(00)89010-1

203. Uddin S, Hussain AR, Al-Hussein KA, et al. Inhibition of phosphatidylinositol 3'-kinase/AKT signaling promotes apoptosis of primary effusion lymphoma cells. *Clin Cancer Res*. 2005;11(8):3102–3108. https://doi.org/10.1158/1078-0432.ccr-04-1857

204. Gagnon V, St-Germain M-E, Parent S, Asselin E. Akt activity in endometrial cancer cells: regulation of cell survival through cIAP-1. *Int J Oncol*. 2003;23(3):803–810. https://doi.org/10.3892/ijo.23.3.803

205. Jeong JC, Kim MS, Kim TH, Kim YK. Kaempferol induces cell death through ERK and Akt-dependent down-regulation of XIAP and survivin in human glioma cells. *Neurochem Res*. 2009;34(5):991–1001. https://doi.org/10.1007/s11064-008-9868-5

206. Liptay S, Weber CK, Ludwig L, Wagner M, Adler G, Schmid RM. Mitogenic and antiapoptotic role of constitutive NF-kappaB/Rel activity in pancreatic cancer. *Int J Cancer*. 2003;105(6):735–746. https://doi.org/10.1002/ijc.11081

207. Sizemore N, Lerner N, Dombrowski N, Sakurai H, Stark GR. Distinct roles of the IκB kinase α and β subunits in liberating nuclear factor κB (NF-κB) from IκB and in phosphorylating the p65 subunit of NF-κB. *J Biol Chem*. 2002;277(6):3863–3869. https://doi.org/10.1074/jbc.m110572200

208. Sizemore N, Leung S, Stark GR. Activation of phosphatidylinositol 3-kinase in response to interleukin-1 leads to phosphorylation and activation of the NF-kappaB p65/RelA subunit. *Mol Cell Biol*. 1999;19(7):4798–4805. https://doi.org/10.1128/MCB.19.7.4798

209. Yu JSL, Cui W. Proliferation, survival and metabolism: the role of PI3K/AKT/mTOR signalling in pluripotency and cell fate determination. *Development*. 2016;143(17):3050–3060. https://doi.org/10.1242/dev.137075

210. Ma XM, Blenis J. Molecular mechanisms of mTOR-mediated translational control. *Nat Rev Mol Cell Biol*. 2009;10(5):307–318. https://doi.org/10.1038/nrm2672

211. Musa J, Orth MF, Dallmayer M, et al. Eukaryotic initiation factor 4E-binding protein 1 (4E-BP1): a master regulator of mRNA translation involved in tumorigenesis. *Oncogene*. 2016;35(36):4675–4688. https://doi.org/10.1038/onc.2015.515

212. Kantidakis T, Ramsbottom BA, Birch JL, Dowding SN, White RJ. mTOR associates with TFIIIC, is found at tRNA and 5S rRNA genes, and targets their repressor Maf1. *Proc Natl Acad Sci U S A*. 2010;107(26):11823–11828. https://doi.org/10.1073/pnas.1005188107

213. Mayer C, Zhao J, Yuan X, Grummt I. mTOR-dependent activation of the transcription factor TIF-IA links rRNA synthesis to nutrient availability. *Genes Dev*. 2004;18(4):423–434. https://doi.org/10.1101/gad.285504

214. Shor B, Wu J, Shakey Q, et al. Requirement of the mTOR kinase for the regulation of Maf1 phosphorylation and control of RNA polymerase III-dependent transcription in cancer cells. *J Biol Chem*. 2010;285(20):15380–15392. https://doi.org/10.1074/jbc.M109.071639

215. Hay N. Interplay between FOXO, TOR, and Akt. *Biochim Biophys Acta*. 2011;1813(11):1965–1970. https://doi.org/10.1016/j.bbamcr.2011.03.013

216. El-Deiry WS, Tokino T, Velculescu VE, et al. WAF1, a potential mediator of p53 tumor suppression. *Cell*. 1993;75(4):817–825. https://doi.org/10.1016/0092-8674(93)90500-p

217. Graña X, Garriga J, Mayol X. Role of the retinoblastoma protein family, pRB, p107 and p130 in the negative control of cell growth. *Oncogene*. 1998;17(25):3365–3383. https://doi.org/10.1038/sj.onc.1202575

218. Medema RH, Kops GJPL, Bos JL, Burgering BMT. AFX-like Forkhead transcription factors mediate cell-cycle regulation by Ras and PKB through p27kip1. *Nature*. 2000;404(6779):782–787. https://doi.org/10.1038/35008115

219. Ramaswamy S, Nakamura N, Sansal I, Bergeron L, Sellers WR. A novel mechanism of gene regulation and tumor suppression by the transcription factor FKHR. *Cancer Cell*. 2002;2(1):81–91. https://doi.org/10.1016/s1535-6108(02)00086-7

220. Schmidt M, Fernandez de Mattos S, van der Horst A, et al. Cell cycle inhibition by FoxO forkhead transcription factors involves downregulation of cyclin D. *Mol Cell Biol*. 2002;22(22):7842–7852. https://doi.org/10.1128/MCB.22.22.7842-7852.2002

221. Tzivion G, Dobson M, Ramakrishnan G. FoxO transcription factors; Regulation by AKT and 14-3-3 proteins. *Biochim Biophys Acta*. 2011;1813(11):1938–1945. https://doi.org/10.1016/j.bbamcr.2011.06.002

222. Dowling RJO, Topisirovic I, Alain T, et al. mTORC1-mediated cell proliferation, but not cell growth, controlled by the 4E-BPs. *Science*. 2010;328(5982):1172–1176. https://doi.org/10.1126/science.1187532

223. Rosenwald IB, Kaspar R, Rousseau D, et al. Eukaryotic translation initiation factor 4E regulates expression of cyclin D1 at transcriptional and post-transcriptional levels. *J Biol Chem*. 1995;270(36):21176–21180. https://doi.org/10.1074/jbc.270.36.21176

224. Rousseau D, Kaspar R, Rosenwald I, Gehrke L, Sonenberg N. Translation initiation of ornithine decarboxylase and nucleocytoplasmic transport of cyclin D1 mRNA are increased in cells overexpressing eukaryotic initiation factor 4E. *Proc Natl Acad Sci U S A*. 1996;93(3):1065–1070. https://doi.org/10.1073/pnas.93.3.1065

225. Shantz LM, Hu RH, Pegg AE. Regulation of ornithine decarboxylase in a transformed cell line that overexpresses translation initiation factor eIF-4E. *Cancer Res*. 1996;56(14):3265–9.

226. Gao N, Flynn DC, Zhang Z, et al. G1 cell cycle progression and the expression of G1 cyclins are regulated by PI3K/AKT/mTOR/p70S6K1 signaling in human ovarian cancer cells. *Am J Physiol Cell Physiol*. 2004;287(2):C281–91. https://doi.org/10.1152/ajpcell.00422.2003

227. Lukas J, Bartkova J, Rohde M, Strauss M, Bartek J. Cyclin D1 is dispensable for G1 control in retinoblastoma gene-deficient cells independently of cdk4 activity. *Mol Cell Biol*. 1995;15(5):2600–2611. https://doi.org/10.1128/MCB.15.5.2600

228. Matsushime H, Quelle DE, Shurtleff SA, Shibuya M, Sherr CJ, Kato JY. D-type cyclin-dependent kinase activity in mammalian cells. *Mol Cell Biol*. 1994;14(3):2066–2076. https://doi.org/10.1128/mcb.14.3.2066-2076.1994

229. Meyerson M, Harlow E. Identification of G1 kinase activity for cdk6, a novel cyclin D partner. *Mol Cell Biol*. 1994;14(3):2077–2086. https://doi.org/10.1128/mcb.14.3.2077-2086.1994

230. Guttridge DC, Albanese C, Reuther JY, Pestell RG, Baldwin AS, Jr. NF-kappaB controls cell growth and differentiation through transcriptional regulation of cyclin D1. *Mol Cell Biol*. 1999;19(8):5785–5799. https://doi.org/10.1128/MCB.19.8.5785

231. Hinz M, Krappmann D, Eichten A, Heder A, Scheidereit C, Strauss M. NF-kappaB function in growth control: regulation of cyclin D1 expression and G0/G1-to-S-phase transition. *Mol Cell Biol*. 1999;19(4):2690–2698. https://doi.org/10.1128/MCB.19.4.2690

232. Aggarwal BB. Nuclear factor-kappaB: the enemy within. *Cancer Cell*. 2004;6(3):203–208. https://doi.org/10.1016/j.ccr.2004.09.003

233. Dijkers PF, Medema† RH, Lammers J-WJ, Koenderman L, Coffer PJ. Expression of the pro-apoptotic Bcl-2 family member Bim is regulated by the forkhead transcription factor FKHR-L1. *Curr Biol*. 2000;10(19):1201–1204. https://doi.org/10.1016/s0960-9822(00)00728-4

234. Shukla S, Rizvi F, Raisuddin S, Kakkar P. FoxO proteins' nuclear retention and BH3-only protein Bim induction evoke mitochondrial dysfunction-mediated apoptosis in berberine-treated HepG2 cells. *Free Radic Biol Med*. 2014;76:185–199. https://doi.org/10.1016/j.freeradbiomed.2014.07.039

235. Alikhani M, Alikhani Z, Graves DT. FOXO1 functions as a master switch that regulates gene expression necessary for tumor necrosis factor-induced fibroblast apoptosis. *J Biol Chem*. 2005;280(13):12096–12102. https://doi.org/10.1074/jbc.m412171200

236. Marfè G, Tafani M, Fiorito F, Pagnini U, Iovane G, De Martino L. Involvement of FOXO transcription factors, TRAIL-FasL/Fas, and sirtuin proteins family in canine coronavirus type II-induced apoptosis. *PLoS One*. 2011;6(11):e27313–e27313. https://doi.org/10.1371/journal.pone.0027313

237. Kischkel FC, Hellbardt S, Behrmann I, et al. Cytotoxicity-dependent APO-1 (Fas/CD95)-associated proteins form a death-inducing signaling complex (DISC) with the receptor. *EMBO J*. 1995;14(22):5579–5588. https://doi.org/10.1002/j.1460-2075.1995.tb00245.x

238. Artykov AA, Yagolovich AV, Dolgikh DA, Kirpichnikov MP, Trushina DB, Gasparian ME. Death receptors DR4 and DR5 undergo spontaneous and ligand-mediated endocytosis and recycling regardless of the sensitivity of cancer cells to TRAIL. *Front Cell Dev Biol*. 2021;9:733688–733688. https://doi.org/10.3389/fcell.2021.733688

239. Morales-Ruiz M, Fulton D, Sowa G, et al. Vascular endothelial growth factor-stimulated actin reorganization and migration of endothelial cells is regulated via the serine/threonine kinase Akt. *Circ Res*. 2000;86(8):892–896. https://doi.org/10.1161/01.res.86.8.892

240. Fukumura D, Kashiwagi S, Jain RK. The role of nitric oxide in tumour progression. *Nat Rev Cancer*. 2006;6(7):521–534. https://doi.org/10.1038/nrc1910

241. Jiang BH, Liu LZ. PI3K/PTEN signaling in angiogenesis and tumorigenesis. *Adv Cancer Res*. 2009;102:19–65. https://doi.org/10.1016/s0065-230x(09)02002-8

242. Levine L, Lucci JA, 3rd, Pazdrak B, et al. Bombesin stimulates nuclear factor kappa B activation and expression of proangiogenic factors in prostate cancer cells. *Cancer Res*. 2003;63(13):3495–502.

243. Zhao K, Song X, Huang Y, et al. Wogonin inhibits LPS-induced tumor angiogenesis via suppressing PI3K/Akt/NF-κB signaling. *Eur J Pharmacol*. 2014;737:57–69. https://doi.org/10.1016/j.ejphar.2014.05.011

244. Fukumura D, Gohongi T, Kadambi A, et al. Predominant role of endothelial nitric oxide synthase in vascular endothelial growth factor-induced angiogenesis and vascular permeability. *Proc Natl Acad Sci U S A*. 2001;98(5):2604–2609. https://doi.org/10.1073/pnas.041359198

245. Hsieh AC, Liu Y, Edlind MP, et al. The translational landscape of mTOR signalling steers cancer initiation and metastasis. *Nature*. 2012;485(7396):55–61. https://doi.org/10.1038/nature10912

246. Masri J, Bernath A, Martin J, et al. mTORC2 activity is elevated in gliomas and promotes growth and cell motility via overexpression of rictor. *Cancer Res*. 2007;67(24):11712–11720. https://doi.org/10.1158/0008-5472.can-07-2223

247. Collins SE, Wiegand ME, Werner AN, et al. Ras-mediated activation of mTORC2 promotes breast epithelial cell migration and invasion. *Mol Biol Cell*. 2023;34(2):ar9–ar9. https://doi.org/10.1091/mbc.E22-06-0236

248. Jacinto E, Loewith R, Schmidt A, et al. Mammalian TOR complex 2 controls the actin cytoskeleton and is rapamycin insensitive. *Nat Cell Biol*. 2004;6(11):1122–1128. https://doi.org/10.1038/ncb1183

249. Jeong Y-J, Hwang S-K, Magae J, Chang Y-C. Ascofuranone suppresses invasion and F-actin cytoskeleton organization in cancer cells by inhibiting the mTOR complex 1 signaling pathway. *Cell Oncol (Dordr)*. 2020;43(5):793–805. https://doi.org/10.1007/s13402-020-00520-w

250. Liu L, Chen L, Chung J, Huang S. Rapamycin inhibits F-actin reorganization and phosphorylation of focal adhesion proteins. *Oncogene*. 2008;27(37):4998–5010. https://doi.org/10.1038/onc.2008.137

251. Liu L, Li F, Cardelli JA, Martin KA, Blenis J, Huang S. Rapamycin inhibits cell motility by suppression of mTOR-mediated S6K1 and 4E-BP1 pathways. *Oncogene*. 2006;25(53):7029–7040. https://doi.org/10.1038/sj.onc.1209691

252. Graff JR, Boghaert ER, De Benedetti A, et al. Reduction of translation initiation factor 4E decreases the malignancy of ras-transformed cloned rat embryo fibroblasts. *Int J Cancer*. 1995;60(2):255–263. https://doi.org/https://doi.org/10.1002/ijc.2910600221

253. Graff JR, Zimmer SG. Translational control and metastatic progression: Enhanced activity of the mRNA cap-binding protein eIF-4E selectively enhances translation of metastasis-related mRNAs. *Clin Exp Metastasis*. 2003;20(3):265–273. https://doi.org/10.1023/A:1022943419011

254. Bond M, Fabunmi RP, Baker AH, Newby AC. Synergistic upregulation of metalloproteinase-9 by growth factors and inflammatory cytokines: an absolute requirement for transcription factor NF-κB. *FEBS Lett*. 1998;435(1):29–34. https://doi.org/10.1016/s0014-5793(98)01034-5

255. Wang W, Abbruzzese JL, Evans DB, Chiao PJ. Overexpression of urokinase-type plasminogen activator in pancreatic adenocarcinoma is regulated by constitutively activated RelA. *Oncogene*. 1999;18(32):4554–4563. https://doi.org/10.1038/sj.onc.1202833

256. Chambers AF, Groom AC, MacDonald IC. Dissemination and growth of cancer cells in metastatic sites. *Nat Rev Cancer*. 2002;2(8):563–572. https://doi.org/10.1038/nrc865

257. Leprivier G, Rotblat B, Khan D, Jan E, Sorensen PH. Stress-mediated translational control in cancer cells. *Biochim Biophys Acta*. 2015;1849(7):845–860. https://doi.org/10.1016/j.bbagrm.2014.11.002

258. Morrow JJ, Mendoza A, Koyen A, et al. mTOR inhibition mitigates enhanced mRNA translation associated with the metastatic phenotype of osteosarcoma cells in vivo. *Clin Cancer Res*. 2016;22(24):6129–6141. https://doi.org/10.1158/1078-0432.CCR-16-0326

259. Glaviano A, Foo ASC, Lam HY, et al. PI3K/AKT/mTOR signaling transduction pathway and targeted therapies in cancer. *Mol Cancer*. 2023;22(1):138. https://doi.org/10.1186/s12943-023-01827-6

260. Vanhaesebroeck B, Perry MWD, Brown JR, André F, Okkenhaug K. PI3K inhibitors are finally coming of age. *Nat Rev Drug Discov*. 2021;20(10):741–769. https://doi.org/10.1038/s41573-021-00209-1

261. Corre I, Verrecchia F, Crenn V, Redini F, Trichet V. The Osteosarcoma Microenvironment: A Complex But Targetable Ecosystem. *Cells*. 2020;9(4)https://doi.org/10.3390/cells9040976

262. Rathore R, Van Tine BA. Pathogenesis and Current Treatment of Osteosarcoma: Perspectives for Future Therapies. *J Clin Med*. 2021;10(6)https://doi.org/10.3390/jcm10061182

263. Pu F, Guo H, Shi D, et al. The generation and use of animal models of osteosarcoma in cancer research. *Genes Dis*. 2024;11(2):664–674. https://doi.org/10.1016/j.gendis.2022.12.021

264. Mirabello L, Troisi RJ, Savage SA. Osteosarcoma incidence and survival rates from 1973 to 2004: data from the Surveillance, Epidemiology, and End Results Program. *Cancer*. 2009;115(7):1531–1543. https://doi.org/10.1002/cncr.24121

265. Alsaihati BA, Ho K-L, Watson J, et al. Canine tumor mutational burden is correlated with TP53 mutation across tumor types and breeds. *Nat Commun*. 2021;12(1):4670–4670. https://doi.org/10.1038/s41467-021-24836-9

266. Angstadt AY, Motsinger-Reif A, Thomas R, et al. Characterization of canine osteosarcoma by array comparative genomic hybridization and RT-qPCR: Signatures of genomic imbalance in canine osteosarcoma parallel the human counterpart. *Genes Chromosomes Cancer*. 2011;50(11):859–874. https://doi.org/10.1002/gcc.20908

267. Morello E, Martano M, Buracco P. Biology, diagnosis and treatment of canine appendicular osteosarcoma: Similarities and differences with human osteosarcoma. *Vet J*. 2011;189(3):268–277. https://doi.org/10.1016/j.tvjl.2010.08.014

268. Wu K, Rodrigues L, Post G, et al. Analyses of canine cancer mutations and treatment outcomes using real-world clinico-genomics data of 2119 dogs. *NPJ Precis Oncol*. 2023;7(1):8–8. https://doi.org/10.1038/s41698-023-00346-3

269. Sadrkhanloo M, Paskeh MDA, Hashemi M, et al. New emerging targets in osteosarcoma therapy: PTEN and PI3K/Akt crosstalk in carcinogenesis. *Pathol Res Pract*. 2023;251:154902. https://doi.org/10.1016/j.prp.2023.154902

270. Wiratnaya IGE, Ismail MD, Hasan F. Identification of potential genes associated with metastasis in osteosarcoma: an integrated bioinformatics analysis. *Musculoskelet Surg*. 2025;109(4):417–428. https://doi.org/10.1007/s12306-025-00891-z

271. Perry JA, Kiezun A, Tonzi P, et al. Complementary genomic approaches highlight the PI3K/mTOR pathway as a common vulnerability in osteosarcoma. *Proc Natl Acad Sci U S A*. 2014;111(51):E5564–E5573. https://doi.org/10.1073/pnas.1419260111

272. Chen X, Bahrami A, Pappo A, et al. Recurrent somatic structural variations contribute to tumorigenesis in pediatric osteosarcoma. *Cell Rep*. 2014;7(1):104–12. https://doi.org/10.1016/j.celrep.2014.03.003

273. Czarnecka AM, Synoradzki K, Firlej W, et al. Molecular biology of osteosarcoma. *Cancers (Basel)*. 2020;12(8):2130. https://doi.org/10.3390/cancers12082130

274. Rickel K, Fang F, Tao J. Molecular genetics of osteosarcoma. *Bone*. 2017;102:69–79. https://doi.org/10.1016/j.bone.2016.10.017

275. Sayles LC, Breese MR, Koehne AL, et al. Genome-Informed Targeted Therapy for Osteosarcoma. *Cancer Discov*. 2019;9(1):46–63. https://doi.org/10.1158/2159-8290.Cd-17-1152

276. Behjati S, Tarpey PS, Haase K, et al. Recurrent mutation of IGF signalling genes and distinct patterns of genomic rearrangement in osteosarcoma. *Nat Commun*. 2017;8:15936. https://doi.org/10.1038/ncomms15936

277. Li Z, Lu L, Zhou Z, et al. Recurrent mutations in epigenetic modifiers and the PI3K/AKT/mTOR pathway in subcutaneous panniculitis-like T-cell lymphoma. *Br J Haematol*. 2018;181(3):406–410. https://doi.org/10.1111/bjh.14611

278. Psyrri A, Papageorgiou S, Liakata E, et al. Phosphatidylinositol 3'-kinase catalytic subunit alpha gene amplification contributes to the pathogenesis of mantle cell lymphoma. *Clin Cancer Res*. 2009;15(18):5724–32. https://doi.org/10.1158/1078-0432.Ccr-08-3215

279. Zhang J, Grubor V, Love CL, et al. Genetic heterogeneity of diffuse large B-cell lymphoma. *Proc Natl Acad Sci U S A*. 2013;110(4):1398–403. https://doi.org/10.1073/pnas.1205299110

280. Pfeifer M, Grau M, Lenze D, et al. PTEN loss defines a PI3K/AKT pathway-dependent germinal center subtype of diffuse large B-cell lymphoma. *Proc Natl Acad Sci U S A*. 2013;110(30):12420–5. https://doi.org/10.1073/pnas.1305656110

281. Bouska A, Zhang W, Sharma S, et al. Integrative Genomic and Transcriptomic Analysis Reveals Targetable Vulnerabilities in Angioimmunoblastic T-Cell Lymphoma. *Am J Hematol*. 2025;100(9):1486–1501. https://doi.org/10.1002/ajh.27736

282. Özçalımlı A, Erdoğdu İ H, Turgutkaya A, Yavaşoğlu İ, Döger FK, Bolaman AZ. The evaluation of gene mutation profiles by next-generation sequencing in diffuse large B-cell lymphoma. *Int J Lab Hematol*. 2023;45(3):310–316. https://doi.org/10.1111/ijlh.14012

283. Pauls SD, Lafarge ST, Landego I, Zhang T, Marshall AJ. The phosphoinositide 3-kinase signaling pathway in normal and malignant B cells: activation mechanisms, regulation and impact on cellular functions. *Front Immunol*. 2012;3:224. https://doi.org/10.3389/fimmu.2012.00224

284. Okkenhaug K, Vanhaesebroeck B. PI3K in lymphocyte development, differentiation and activation. *Nat Rev Immunol*. 2003;3(4):317–30. https://doi.org/10.1038/nri1056

285. Patel RK, Mohan C. PI3K/AKT signaling and systemic autoimmunity. *Immunol Res*. 2005;31(1):47–55. https://doi.org/10.1385/ir:31:1:47

286. Jellusova J, Rickert RC. The PI3K pathway in B cell metabolism. *Crit Rev Biochem Mol Biol*. 2016;51(5):359–378. https://doi.org/10.1080/10409238.2016.1215288

287. Troutman TD, Hu W, Fulenchek S, et al. Role for B-cell adapter for PI3K (BCAP) as a signaling adapter linking Toll-like receptors (TLRs) to serine/threonine kinases PI3K/Akt. *Proc Natl Acad Sci U S A*. 2012;109(1):273–8. https://doi.org/10.1073/pnas.1118579109

288. Castello A, Gaya M, Tucholski J, et al. Nck-mediated recruitment of BCAP to the BCR regulates the PI(3)K-Akt pathway in B cells. *Nat Immunol*. 2013;14(9):966–75. https://doi.org/10.1038/ni.2685

289. Patil S, Rajput S, Patil S, Mhaiskar A. B-cell lymphoma: Advances in pathogenesis, diagnosis, and targeted therapies. *Pathol Res Pract*. 2025;271:156036. https://doi.org/10.1016/j.prp.2025.156036

290. Buchner M. Insights into PI3K/AKT signaling in B cell development and chronic lymphocytic leukemia. *FEBS Lett*. 2025;599(20):2896–2910. https://doi.org/10.1002/1873-3468.15079

291. Burger JA, Wiestner A. Targeting B cell receptor signalling in cancer: preclinical and clinical advances. *Nat Rev Cancer*. 2018;18(3):148–167. https://doi.org/10.1038/nrc.2017.121

292. Uddin S, Hussain AR, Siraj AK, et al. Role of phosphatidylinositol 3'-kinase/AKT pathway in diffuse large B-cell lymphoma survival. *Blood*. 2006;108(13):4178–86. https://doi.org/10.1182/blood-2006-04-016907

293. Wang X, Cao X, Sun R, et al. Clinical Significance of PTEN Deletion, Mutation, and Loss of PTEN Expression in De Novo Diffuse Large B-Cell Lymphoma. *Neoplasia*. 2018;20(6):574–593. https://doi.org/10.1016/j.neo.2018.03.002

294. Schmid VK, Khadour A, Ahmed N, et al. B-cell antigen receptor expression and phosphatidylinositol 3-kinase signaling regulate genesis and maintenance of mouse chronic lymphocytic leukemia. *Haematologica*. 2022;107(8):1796–1814. https://doi.org/10.3324/haematol.2021.279924

295. Vardi A, Agathangelidis A, Sutton LA, Ghia P, Rosenquist R, Stamatopoulos K. Immunogenetic studies of chronic lymphocytic leukemia: revelations and speculations about ontogeny and clinical evolution. *Cancer Res*. 2014;74(16):4211–6. https://doi.org/10.1158/0008-5472.Can-14-0630

296. Khoury R, Raffoul C, Khater C, Hanna C. Precision Medicine in Hematologic Malignancies: Evolving Concepts and Clinical Applications. *Biomedicines*. 2025;13(7)https://doi.org/10.3390/biomedicines13071654

297. Nayyar M, Menezes RCB, Ailawadhi S, Parrondo RD. Chronic Lymphocytic Leukemia: Novel Therapeutic Targets Under Investigation. *Cancers (Basel)*. 2025;17(14)https://doi.org/10.3390/cancers17142298

298. Ehm P, Grottke A, Bettin B, Jücker M. Investigation of the function of the PI3-Kinase / AKT signaling pathway for leukemogenesis and therapy of acute childhood lymphoblastic leukemia (ALL). *Cell Signal*. 2022;93:110301. https://doi.org/10.1016/j.cellsig.2022.110301

299. Ehm P, Jücker M. The Inositol-5-Phosphatase SHIP1: Expression, Regulation and Role in Acute Lymphoblastic Leukemia. *Int J Mol Sci*. 2025;26(14)https://doi.org/10.3390/ijms26146935

300. Gehringer F, Weissinger SE, Möller P, Wirth T, Ushmorov A. Physiological levels of the PTEN-PI3K-AKT axis activity are required for maintenance of Burkitt lymphoma. *Leukemia*. 2020;34(3):857–871. https://doi.org/10.1038/s41375-019-0628-0

301. Bhatti M, Ippolito T, Mavis C, et al. Pre-clinical activity of targeting the PI3K/Akt/mTOR pathway in Burkitt lymphoma. *Oncotarget*. 2018;9(31):21820–21830. https://doi.org/10.18632/oncotarget.25072

302. Blachly JS, Baiocchi RA. Targeting PI3-kinase (PI3K), AKT and mTOR axis in lymphoma. *Br J Haematol*. 2014;167(1):19–32. https://doi.org/10.1111/bjh.13065

303. Dickerson EB, Thomas R, Fosmire SP, et al. Mutations of phosphatase and tensin homolog deleted from chromosome 10 in canine hemangiosarcoma. *Vet Pathol*. 2005;42(5):618–632. https://doi.org/10.1354/vp.42-5-618

304. Kim JH, Megquier K, Thomas R, et al. Genomically complex human angiosarcoma and canine hemangiosarcoma establish convergent angiogenic

transcriptional programs driven by novel gene fusions. *Mol Cancer Res*. 2021;19(5):847–861. https://doi.org/10.1158/1541-7786.MCR-20-0937

305. Megquier K, Turner-Maier J, Swofford R, et al. Comparative genomics reveals shared mutational landscape in canine hemangiosarcoma and human angiosarcoma. *Mol Cancer Res*. 2019;17(12):2410–2421. https://doi.org/10.1158/1541-7786.MCR-19-0221

306. Wang G, Wu M, Durham AC, et al. Molecular subtypes in canine hemangiosarcoma reveal similarities with human angiosarcoma. *PLoS One*. 2020;15(3):e0229728–e0229728. https://doi.org/10.1371/journal.pone.0229728

307. Wang G, Wu M, Maloneyhuss MA, et al. Actionable mutations in canine hemangiosarcoma. *PLoS One*. 2017;12(11):e0188667–e0188667. https://doi.org/10.1371/journal.pone.0188667

308. Zamani-Ahmadmahmudi M, Najafi A, Nassiri SM. Reconstruction of canine diffuse large B-cell lymphoma gene regulatory network: detection of functional modules and hub genes. *J Comp Pathol*. 2015;152(2-3):119–130. https://doi.org/10.1016/j.jcpa.2014.11.008

309. Elvers I, Turner-Maier J, Swofford R, et al. Exome sequencing of lymphomas from three dog breeds reveals somatic mutation patterns reflecting genetic background. *Genome Res*. 2015;25(11):1634–1645. https://doi.org/10.1101/gr.194449.115

310. Wong K, van der Weyden L, Schott CR, et al. Cross-species genomic landscape comparison of human mucosal melanoma with canine oral and equine melanoma. *Nature Commun*. 2019;10(1):353–353. https://doi.org/10.1038/s41467-018-08081-1

311. Borge KS, Nord S, Van Loo P, et al. Canine mammary tumours are affected by frequent copy number aberrations, including amplification of MYC and loss of PTEN. *PLoS One*. 2015;10(5):e0126371–e0126371. https://doi.org/10.1371/journal.pone.0126371

312. Arendt ML, Sakthikumar S, Melin M, et al. PIK3CA is recurrently mutated in canine mammary tumors, similarly to in human mammary neoplasia. *Sci Rep*. 2023;13(1):632–632. https://doi.org/10.1038/s41598-023-27664-7

313. Kim S-H, Seung B-J, Cho S-H, Lim H-Y, Bae M-K, Sur J-H. Dysregulation of PI3K/Akt/PTEN pathway in canine mammary tumor. *Animals (Basel)*. 2021;11(7):2079. https://doi.org/10.3390/ani11072079

314. Chu S, Skidmore ZL, Kunisaki J, et al. Unraveling the chaotic genomic landscape of primary and metastatic canine appendicular osteosarcoma with current sequencing technologies and bioinformatic approaches. *PLoS One*. 2021;16(2):e0246443–e0246443. https://doi.org/10.1371/journal.pone.0246443

315. Gardner HL, Sivaprakasam K, Briones N, et al. Canine osteosarcoma genome sequencing identifies recurrent mutations in DMD and the histone methyltransferase gene SETD2. *Commun Biol*. 2019;2:266–266. https://doi.org/10.1038/s42003-019-0487-2

316. Levine RA, Forest T, Smith C. Tumor suppressor PTEN is mutated in canine osteosarcoma cell lines and tumors. *Vet Pathol*. 2002;39(3):372–378. https://doi.org/10.1354/vp.39-3-372

317. Megquier K, Turner-Maier J, Morrill K, et al. The genomic landscape of canine osteosarcoma cell lines reveals conserved structural complexity and pathway alterations. *PLoS One*. 2022;17(9):e0274383–e0274383. https://doi.org/10.1371/journal.pone.0274383

318. Lorch G, Sivaprakasam K, Zismann V, et al. Identification of Recurrent Activating HER2 Mutations in Primary Canine Pulmonary Adenocarcinoma. *Clin Cancer Res*. 2019;25(19):5866–5877. https://doi.org/10.1158/1078-0432.Ccr-19-1145

319. Berg J, Weinstein MJ, Schelling SH, Rand WM. Treatment of dogs with osteosarcoma by administration of cisplatin after amputation or limb-sparing surgery: 22 cases (1987-1990). *J Am Vet Med Assoc*. 1992;200(12):2005–2008. https://doi.org/10.2460/javma.1992.200.12.2005

320. Bergman PJ, MacEwen EG, Kurzman ID, et al. Amputation and carboplatin for treatment of dogs with osteosarcoma: 48 cases (1991 to 1993). *J Vet Intern Med*. 1996;10(2):76–81. https://doi.org/10.1111/j.1939-1676.1996.tb02031.x

321. Spodnick GJ, Berg J, Rand WM, et al. Prognosis for dogs with appendicular osteosarcoma treated by amputation alone: 162 cases (1978-1988). *J Am Vet Med Assoc*. 1992;200(7):995–999. https://doi.org/10.2460/javma.1992.200.07.995

322. Straw RC, Withrow SJ, Richter SL, et al. Amputation and cisplatin for treatment of canine osteosarcoma. *J Vet Intern Med*. 1991;5(4):205–210. https://doi.org/10.1111/j.1939-1676.1991.tb00950.x

323. Zhou Q, Deng Z, Zhu Y, Long H, Zhang S, Zhao J. mTOR/p70S6K signal transduction pathway contributes to osteosarcoma progression and patients' prognosis. *Med Oncol*. 2010;27(4):1239–1245. https://doi.org/10.1007/s12032-009-9365-y

324. Gordon IK, Ye F, Kent MS. Evaluation of the mammalian target of rapamycin pathway and the effect of rapamycin on target expression and cellular proliferation in osteosarcoma cells from dogs. *Am J Vet Res*. 2008;69(8):1079–1084. https://doi.org/10.2460/ajvr.69.8.1079

325. Mauchle U, Selvarajah GT, Mol JA, Kirpensteijn J, Verheije MH. Identification of anti-proliferative kinase inhibitors as potential therapeutic agents to treat canine osteosarcoma. *Vet J*. 2015;205(2):281–287. https://doi.org/10.1016/j.tvjl.2014.08.006

326. Meuten T, Rose BJ, Thamm DH. Evaluation of efficacy of dual PI3K/Akt/mTOR pathway inhibition in canine osteosarcoma cells in vitro and xenograft mouse model. 2017:

327. Thomas R, Wang HJ, Tsai PC, et al. Influence of genetic background on tumor karyotypes: evidence for breed-associated cytogenetic aberrations in canine appendicular osteosarcoma. *Chromosome Res*. 2009;17(3):365–377. https://doi.org/10.1007/s10577-009-9028-z

328. De Maria R, Miretti S, Iussich S, et al. Met oncogene activation qualifies spontaneous canine osteosarcoma as a suitable pre-clinical model of human osteosarcoma. *J Pathol*. 2009;218(3):399–408. https://doi.org/10.1002/path.2549

329. Ferracini R, Angelini P, Cagliero E, et al. MET oncogene aberrant expression in canine osteosarcoma. *J Orthop Res*. 2000;18(2):253–6. https://doi.org/10.1002/jor.1100180213

330. Fieten H, Spee B, Ijzer J, Kik MJ, Penning LC, Kirpensteijn J. Expression of hepatocyte growth factor and the proto-oncogenic receptor c-Met in canine osteosarcoma. *Vet Pathol*. 2009;46(5):869–877. https://doi.org/10.1354/vp.08-VP-0155-F-FL

331. Flint AF, U'Ren L, Legare ME, Withrow SJ, Dernell W, Hanneman WH. Overexpression of the erbB-2 proto-oncogene in canine osteosarcoma cell lines and tumors. *Vet Pathol*. 2004;41(3):291–6. https://doi.org/10.1354/vp.41-3-291

332. MacEwen EG, Pastor J, Kutzke J, et al. IGF-1 receptor contributes to the malignant phenotype in human and canine osteosarcoma. *J Cell Biochem*. 2004;92(1):77–91. https://doi.org/10.1002/jcb.20046

333. Maniscalco L, Iussich S, Morello E, et al. PDGFs and PDGFRs in canine osteosarcoma: new targets for innovative therapeutic strategies in comparative oncology. *Vet J*. 2013;195(1):41–47. https://doi.org/10.1016/j.tvjl.2012.05.003

334. Karkare S, Allen KJH, Jiao R, et al. Detection and targeting insulin growth factor receptor type 2 (IGF2R) in osteosarcoma PDX in mouse models and in canine osteosarcoma tumors. *Sci Rep*. 2019;9(1):11476. https://doi.org/10.1038/s41598-019-47808-y

335. Khanna C, Prehn J, Hayden D, et al. A randomized controlled trial of octreotide pamoate long-acting release and carboplatin versus carboplatin alone in dogs with naturally occurring osteosarcoma: evaluation of insulin-like growth factor suppression and chemotherapy. *Clin Cancer Res*. 2002;8(7):2406–12.

336. Kirpensteijn J, Timmermans-Sprang EP, van Garderen E, Rutteman GR, Lantinga-van Leeuwen IS, Mol JA. Growth hormone gene expression in canine normal growth plates and spontaneous osteosarcoma. *Mol Cell Endocrinol*. 2002;197(1-2):179–185. https://doi.org/10.1016/s0303-7207(02)00269-1

337. Maniscalco L, Iussich S, Morello E, et al. Increased expression of insulin-like growth factor-1 receptor is correlated with worse survival in canine appendicular osteosarcoma. *Vet J*. 2015;205(2):272–280. https://doi.org/10.1016/j.tvjl.2014.09.005

338. Thamm DH, O'Brien MG, Vail DM. Serum vascular endothelial growth factor concentrations and postsurgical outcome in dogs with osteosarcoma. *Vet Comp Oncol*. 2008;6(2):126–32. https://doi.org/10.1111/j.1476-5829.2007.00153.x

339. Wergin MC, Ballmer-Hofer K, Roos M, et al. Preliminary study of plasma vascular endothelial growth factor (VEGF) during low- and high-dose radiation therapy of dogs with spontaneous tumors. *Vet Radiol Ultrasound*. 2004;45(3):247–54. https://doi.org/10.1111/j.1740-8261.2004.04045.x

340. Smith AN. Hemangiosarcoma in dogs and cats. *Vet Clin North Am Small Anim Pract*. 2003;33(3):533–552. https://doi.org/10.1016/s0195-5616(03)00002-0

341. Vail DM, Thamm DH, Liptak JM. Miscellaneous Tumors: Hemangiosarcoma. In: Withrow SJ, Vail DM, Page RL, eds. *Withrow and MacEwen's Small Animal Clinical Oncology*. 5th ed. St. Louis, MO; Elsevier/Saunders; 2013:773–810. https://doi.org/10.1016/b978-0-323-59496-7.00034-7

342. Shiu K-B, Flory AB, Anderson CL, et al. Predictors of outcome in dogs with subcutaneous or intramuscular hemangiosarcoma. *J Am Vet Med Assoc*. 2011;238(4):472–479. https://doi.org/10.2460/javma.238.4.472

343. Waters DJ, Caywood DD, Hayden DW, Klausner JS. Metastatic pattern in dogs with splenic haemangiosarcoma: clinical implications. *J Small Anim Pract*. 1988;29(12):805–814. https://doi.org/10.1111/j.1748-5827.1988.tb01907.x

344. Faulhaber EA, Janik E, Thamm DH. Adjuvant carboplatin for treatment of splenic hemangiosarcoma in dogs: Retrospective evaluation of 18 cases (2011-2016) and comparison with doxorubicin-based chemotherapy. *J Vet Intern Med*. 2021;35(4):1929–1934. https://doi.org/10.1111/jvim.16212

345. Finotello R, Stefanello D, Zini E, Marconato L. Comparison of doxorubicin–cyclophosphamide with doxorubicin–dacarbazine for the adjuvant treatment of canine hemangiosarcoma. *Vet Comp Oncol*. 2017;15(1):25–35. https://doi.org/https://doi.org/10.1111/vco.12139

346. Gardner HL, London CA, Portela RA, et al. Maintenance therapy with toceranib following doxorubicin-based chemotherapy for canine splenic hemangiosarcoma. *BMC Vet Res*. 2015;11:131–131. https://doi.org/10.1186/s12917-015-0446-1

347. Matsuyama A, Poirier VJ, Mantovani F, Foster RA, Mutsaers AJ. Adjuvant doxorubicin with or without metronomic cyclophosphamide for canine splenic hemangiosarcoma. *J Am Anim Hosp Assoc*. 2017;53(6):304–312. https://doi.org/10.5326/jaaha-ms-6540

348. Clifford CA, Hughes D, Beal MW, et al. Plasma vascular endothelial growth factor concentrations in healthy dogs and dogs with hemangiosarcoma. *J Vet Intern Med*. 2001;15(2):131–135. https://doi.org/10.1111/j.1939-1676.2001.tb01244.x

349. Thamm DH, Dickerson EB, Akhtar N, et al. Biological and molecular characterization of a canine hemangiosarcoma-derived cell line. *Res Vet Sci*. 2006;81(1):76–86. https://doi.org/10.1016/j.rvsc.2005.09.005

350. Yonemaru K, Sakai H, Murakami M, Yanai T, Masegi T. Expression of vascular endothelial growth factor, basic fibroblast growth factor, and their receptors (flt-1, flk-1, and flg-1) in canine vascular tumors. *Vet Pathol*. 2006;43(6):971–980. https://doi.org/10.1354/vp.43-6-971

351. Kim JH. PIK3CA mutations matter for cancer in dogs. *Res Vet Sci*. 2020;133:39–41. https://doi.org/10.1016/j.rvsc.2020.09.001

352. Murai A, Asa SA, Kodama A, Hirata A, Yanai T, Sakai H. Constitutive phosphorylation of the mTORC2/Akt/4E-BP1 pathway in newly derived canine hemangiosarcoma cell lines. *BMC Vet Res*. 2012;8:128–128. https://doi.org/10.1186/1746-6148-8-128

353. Adachi M, Hoshino Y, Izumi Y, Sakai H, Takagi S. Effects of inhibitors of vascular endothelial growth factor receptor 2 and downstream pathways of receptor tyrosine kinases involving phosphatidylinositol 3-kinase/Akt/mammalian target of rapamycin or mitogen-activated protein kinase in canine hemangiosarcoma cell lines. *Can J Vet Res*. 2016;80(3):209–16.

354. Pyuen AA, Meuten T, Rose BJ, Thamm DH. In vitro effects of PI3K/mTOR inhibition in canine hemangiosarcoma. *PLoS One*. 2018;13(7):e0200634–e0200634. https://doi.org/10.1371/journal.pone.0200634

355. Valli VE, Bienzle D, Meuten DJ. Tumors of the Hemolymphatic System. In: Meuten DJ, ed. *Tumors in Domestic Animals*. 5th edition ed. Ames, Iowa; John Wiley & Sons, Inc.; 2017:203–321. https://doi.org/10.1002/9781119181200.ch7

356. Aresu L, Ferraresso S, Marconato L, et al. New molecular and therapeutic insights into canine diffuse large B-cell lymphoma elucidates the role of the dog as a model for human disease. *Haematologica*. 2019;104(6):e256–e259. https://doi.org/10.3324/haematol.2018.207027

357. Mooney M, Bond J, Monks N, et al. Comparative RNA-Seq and microarray analysis of gene expression changes in B-cell lymphomas of Canis familiaris. *PLoS One*. 2013;8(4):e61088–e61088. https://doi.org/10.1371/journal.pone.0061088

358. Xu Z-Z, Xia Z-G, Wang A-H, et al. Activation of the PI3K/AKT/mTOR pathway in diffuse large B cell lymphoma: clinical significance and inhibitory effect of rituximab. *Ann Hematol*. 2013;92(10):1351–1358. https://doi.org/10.1007/s00277-013-1770-9

359. Harris LJ, Hughes KL, Ehrhart EJ, Labadie JD, Yoshimoto J, Avery AC. Canine CD4+ T-cell lymphoma identified by flow cytometry exhibits a consistent histomorphology and gene expression profile. *Vet Comp Oncol*. 2019;17(3):253–264. https://doi.org/10.1111/vco.12460

360. Shan X, Czar MJ, Bunnell SC, et al. Deficiency of PTEN in Jurkat T cells causes constitutive localization of Itk to the plasma membrane and hyperresponsiveness to CD3 stimulation. *Mol Cell Biol*. 2000;20(18):6945–6957. https://doi.org/10.1128/MCB.20.18.6945-6957.2000

361. Owusu Obeng E, Rusciano I, Marvi MV, et al. Phosphoinositide-dependent signaling in cancer: a focus on phospholipase C isozymes. *Int J Mol Sci*. 2020;21(7):2581. https://doi.org/10.3390/ijms21072581

362. Bergman PJ, Kent MS, Farese JP. Melanoma. In: Withrow SJ, Vail DM, Page RL, eds. *Withrow and MacEwen's Small Animal Clinical Oncology*. 5th ed. St. Louis, MO; Elsevier/Saunders; 2013:321–334. https://doi.org/10.1016/B978-1-4377-2362-5.00019-0

363. Colombino M, Capone M, Lissia A, et al. BRAF/NRAS mutation frequencies among primary tumors and metastases in patients with melanoma. *J Clin Oncol*. 2012;30(20):2522–2529. https://doi.org/10.1200/jco.2011.41.2452

364. Mochizuki H, Kennedy K, Shapiro SG, Breen M. BRAF mutations in canine cancers. *PLoS One*. 2015;10(6):e0129534–e0129534. https://doi.org/10.1371/journal.pone.0129534

365. Brocca G, Ferraresso S, Zamboni C, et al. Array comparative genomic hybridization analysis reveals significantly enriched pathways in canine oral melanoma. *Front Oncol*. 2019;9:1397–1397. https://doi.org/10.3389/fonc.2019.01397

366. Koenig A, Bianco SR, Fosmire S, Wojcieszyn J, Modiano JF. Expression and significance of p53, rb, p21/waf-1, p16/ink-4a, and PTEN tumor suppressors in canine melanoma. *Vet Pathol*. 2002;39(4):458–472. https://doi.org/10.1354/vp.39-4-458

367. Wei B-R, Michael HT, Halsey CHC, et al. Synergistic targeted inhibition of MEK and dual PI3K/mTOR diminishes viability and inhibits tumor growth of canine melanoma underscoring its utility as a preclinical model for human mucosal melanoma. *Pigment Cell Melanoma Res*. 2016;29(6):643–655. https://doi.org/10.1111/pcmr.12512

368. Brachelente C, Cappelli K, Capomaccio S, et al. Transcriptome analysis of canine cutaneous melanoma and melanocytoma reveals a modulation of genes regulating extracellular matrix metabolism and cell cycle. *Sci Rep*. 2017;7(1):6386–6386. https://doi.org/10.1038/s41598-017-06281-1

369. Kanae Y, Endoh D, Yokota H, Taniyama H, Hayashi M. Expression of the PTEN tumor suppressor gene in malignant mammary gland tumors of dogs. *Am J Vet Res*. 2006;67(1):127–133. https://doi.org/10.2460/ajvr.67.1.127

370. Perossi IFS, Saito MM, Varallo GR, de Godoy BLV, Colombo J, Zuccari DAPC. Protein expression of PI3K/AKT/mTOR pathway targets validated by gene expression and its correlation with prognosis in canine mammary cancer. *J Mammary Gland Biol Neoplasia*. 2022;27(3-4):241–252. https://doi.org/10.1007/s10911-022-09527-5

371. Asproni P, Millanta F, Ressel L, et al. An immunohistochemical study of the PTEN/AKT pathway involvement in canine and feline mammary tumors. *Animals (Basel)*. 2021;11(2):365. https://doi.org/10.3390/ani11020365

372. Delgado L, Gärtner F, Dias Pereira P. Activation of mammalian target of rapamycin in canine mammary carcinomas: an immunohistochemical study. *J Comp Pathol*. 2015;152(2-3):138–144. https://doi.org/10.1016/j.jcpa.2014.12.004

373. Qiu CW, Lin DG, Wang JQ, Li CY, Deng GZ. Expression and significance of PTEN and VEGF in canine mammary gland tumours. *Vet Res Commun*. 2008;32(6):463–472. https://doi.org/10.1007/s11259-008-9049-7

374. Ressel L, Millanta F, Caleri E, Innocenti VM, Poli A. Reduced PTEN protein expression and Its prognostic implications in canine and feline mammary tumors. *Vet Pathol*. 2009;46(5):860–868. https://doi.org/10.1354/vp.08-vp-0273-p-fl

375. Kennedy KC, Qurollo BA, Rose BJ, Thamm DH. Epidermal growth factor enhances the malignant phenotype in canine mammary carcinoma cell lines. *Vet Comp Oncol*. 2011;9(3):196–206. https://doi.org/10.1111/j.1476-5829.2010.00248.x

376. Gama A, Gärtner F, Alves A, Schmitt F. Immunohistochemical expression of Epidermal Growth Factor Receptor (EGFR) in canine mammary tissues. *Res Vet Sci*. 2009;87(3):432–7. https://doi.org/10.1016/j.rvsc.2009.04.016

377. Campos M, Kool MMJ, Daminet S, et al. Upregulation of the PI3K/Akt pathway in the tumorigenesis of canine thyroid carcinoma. *J Vet Intern Med*. 2014;28(6):1814–1823. https://doi.org/10.1111/jvim.12435

378. Sanz Ressel BL, Massone AR, Barbeito CG. Immunohistochemical expression of selected phosphoproteins of the mTOR signalling pathway in canine cutaneous squamous cell carcinoma. *Vet J*. 2019;245:41–48. https://doi.org/10.1016/j.tvjl.2018.12.024

379. Noguchi S, Inoue M, Ichikawa T, et al. The NRG3/ERBB4 signaling cascade as a novel therapeutic target for canine glioma. *Exp Cell Res*. 2021;400(2):112504. https://doi.org/10.1016/j.yexcr.2021.112504

380. Hanazono K, Fukumoto S, Kawamura Y, et al. Epidermal growth factor receptor expression in canine transitional cell carcinoma. *J Vet Med Sci*. 2015;77(1):1–6. https://doi.org/10.1292/jvms.14-0032

381. Shiomitsu K, Johnson CL, Malarkey DE, Pruitt AF, Thrall DE. Expression of epidermal growth factor receptor and vascular endothelial growth factor in malignant canine epithelial nasal tumours. *Vet Comp Oncol*. 2009;7(2):106–14. https://doi.org/10.1111/j.1476-5829.2009.00178.x

382. Flory A, Kruglyak KM, Tynan JA, et al. Clinical validation of a next-generation sequencing-based multi-cancer early detection "liquid biopsy" blood test in over 1,000 dogs using an independent testing set: The CANcer Detection in Dogs (CANDiD) study. *PLoS One*. 2022;17(4):e0266623–e0266623. https://doi.org/10.1371/journal.pone.0266623

383. Tate JG, Bamford S, Jubb HC, et al. COSMIC: the catalogue of somatic mutations in cancer. *Nucleic Acids Res*. 2019;47(D1):D941–D947. https://doi.org/10.1093/nar/gky1015

384. Rivera-Calderón LG, Fonseca-Alves CE, Kobayashi PE, Carvalho M, Vasconcelos RO, Laufer-Amorim R. p-mTOR, p-4EBP-1 and eIF4E expression in canine prostatic carcinoma. *Res Vet Sci*. 2019;122:86–92. https://doi.org/10.1016/j.rvsc.2018.11.006

385. Maekawa T, Maniwa Y, Doi T, et al. Expression and localization of FOXO1 in non-small cell lung cancer. *Oncol Rep*. 2009;22(1):57–64.

386. Wan X, Mendoza A, Khanna C, Helman LJ. Rapamycin inhibits ezrin-mediated metastatic behavior in a murine model of osteosarcoma. *Cancer Res*. 2005;65(6):2406–2411. https://doi.org/10.1158/0008-5472.can-04-3135

387. Wendel H-G, Stanchina Ed, Fridman JS, et al. Survival signalling by Akt and eIF4E in oncogenesis and cancer therapy. *Nature*. 2004;428(6980):332–337. https://doi.org/10.1038/nature02369

388. Chen Y-T, Tan KA, Pang LY, Argyle DJ. The class I PI3K/Akt pathway is critical for cancer cell survival in dogs and offers an opportunity for therapeutic intervention. *BMC Vet Res*. 2012;8:73–73. https://doi.org/10.1186/1746-6148-8-73

389. Tsuji S, Yabe R, Usui T, Mizuno T, Ohama T, Sato K. Anti-tumor effects of perphenazine on canine lymphoma. *J Vet Med Sci*. 2016;78(8):1293–1298. https://doi.org/10.1292/jvms.15-0707

390. Liao AT, McCleese J, Kamerling S, Christensen J, London CA. A novel small molecule Met inhibitor, PF2362376, exhibits biological activity against osteosarcoma. *Vet Comp Oncol*. 2007;5(3):177–96. https://doi.org/10.1111/j.1476-5829.2007.00137.x

391. Mantovani FB, Morrison JA, Mutsaers AJ. Effects of epidermal growth factor receptor kinase inhibition on radiation response in canine osteosarcoma cells. *BMC Vet Res*. 2016;12:82. https://doi.org/10.1186/s12917-016-0707-7

392. Sato S, Fujita N, Tsuruo T. Modulation of Akt kinase activity by binding to Hsp90. *Proc Natl Acad Sci U S A*. 2000;97(20):10832–7. https://doi.org/10.1073/pnas.170276797

393. Solit DB, Basso AD, Olshen AB, Scher HI, Rosen N. Inhibition of heat shock protein 90 function down-regulates Akt kinase and sensitizes tumors to Taxol. *Cancer Res*. 2003;63(9):2139–44.

394. Lin TY, Bear M, Du Z, et al. The novel HSP90 inhibitor STA-9090 exhibits activity against Kit-dependent and -independent malignant mast cell tumors. *Exp Hematol*. 2008;36(10):1266–77. https://doi.org/10.1016/j.exphem.2008.05.001

395. Kong W, Sender S, Taher L, et al. BTK and PI3K inhibitors reveal synergistic inhibitory anti-tumoral effects in canine diffuse large B-cell lymphoma cells. *Int J Mol Sci*. 2021;22(23):12673. https://doi.org/10.3390/ijms222312673

396. Dittrich K, Yıldız-Altay Ü, Qutab F, et al. Baseline tumor gene expression signatures correlate with chemoimmunotherapy treatment responsiveness in canine B cell lymphoma. *PLoS One*. 2023;18(8):e0290428. https://doi.org/10.1371/journal.pone.0290428

397. Smolensky D, Rathore K, Bourn J, Cekanova M. Inhibition of the PI3K/AKT Pathway Sensitizes Oral Squamous Cell Carcinoma Cells to Anthracycline-Based Chemotherapy In Vitro. *J Cell Biochem*. 2017;118(9):2615–2624. https://doi.org/10.1002/jcb.25747

398. Sánchez-Céspedes R, Accornero P, Miretti S, et al. In vitro and in vivo effects of toceranib phosphate on canine osteosarcoma cell lines and xenograft orthotopic models. *Vet Comp Oncol*. 2020;18(1):117–127. https://doi.org/10.1111/vco.12562

399. Andersen NJ, Boguslawski EB, Kuk CY, Chambers CM, Duesbery NS. Combined inhibition of MEK and mTOR has a synergic effect on angiosarcoma tumorgrafts. *Int J Oncol*. 2015;47(1):71–80. https://doi.org/10.3892/ijo.2015.2989

400. Wei B-R, Hoover SB, Peer CJ, et al. Efficacy, tolerability, and pharmacokinetics of combined targeted MEK and dual mTORC1/2 inhibition in a preclinical model of mucosal melanoma. *Mol Cancer Ther*. 2020;19(11):2308–2318. https://doi.org/10.1158/1535-7163.MCT-19-0858

401. Bernard S, Poon AC, Tam PM, Mutsaers AJ. Investigation of the effects of mTOR inhibitors rapamycin and everolimus in combination with carboplatin on canine malignant melanoma cells. *BMC Vet Res*. 2021;17(1):382–382. https://doi.org/10.1186/s12917-021-03089-0

402. Kent MS, Collins CJ, Ye F. Activation of the AKT and mammalian target of rapamycin pathways and the inhibitory effects of rapamycin on those pathways in canine malignant melanoma cell lines. *Am J Vet Res*. 2009;70(2):263–269. https://doi.org/10.2460/ajvr.70.2.263

403. Lainetti PF, Leis-Filho AF, Kobayashi PE, et al. Proteomics approach of rapamycin anti-tumoral effect on primary and metastatic canine mammary tumor Cells in vitro. *Molecules*. 2021;26(5):1213. https://doi.org/10.3390/molecules26051213

404. Fan Y, Ren X, Wang Y, et al. Metformin inhibits the proliferation of canine mammary gland tumor cells through the AMPK/AKT/mTOR signaling pathway in vitro. *Oncol Lett*. 2021;22(6):852–852. https://doi.org/10.3892/ol.2021.13113

405. Saeki K, Watanabe M, Tsuboi M, et al. Anti-tumour effect of metformin in canine mammary gland tumour cells. *Vet J*. 2015;205(2):297–304. https://doi.org/10.1016/j.tvjl.2015.04.026

406. Michishita M, Ochiai K, Nakahira R, et al. mTOR pathway as a potential therapeutic target for cancer stem cells in canine mammary carcinoma. *Front Oncol*. 2023;13:1100602. https://doi.org/10.3389/fonc.2023.1100602

407. Ryu S, Park S, Lim W, Song G. Effects of luteolin on canine osteosarcoma: suppression of cell proliferation and synergy with cisplatin. *J Cell Physiol*. 2018;234(6):9504–9514. https://doi.org/10.1002/jcp.27638

408. Ryu S, Park S, Lim W, Song G. Quercetin augments apoptosis of canine osteosarcoma cells by disrupting mitochondria membrane potential and regulating PKB and MAPK signal transduction. *J Cell Biochem*. 2019;120(10):17449–17458. https://doi.org/10.1002/jcb.29009

409. LeBlanc AK, Mazcko CN, Cherukuri A, et al. Adjuvant sirolimus does not improve outcome in pet dogs receiving standard-of-care therapy for appendicular osteosarcoma: a prospective, randomized trial of 324 dogs. *Clin Cancer Res*. 2021;27(11):3005–3016. https://doi.org/10.1158/1078-0432.CCR-21-0315

410. Paoloni MC, Mazcko C, Fox E, et al. Rapamycin pharmacokinetic and pharmacodynamic relationships in osteosarcoma: a comparative oncology study in dogs. *PLoS One*. 2010;5(6):e11013–e11013. https://doi.org/10.1371/journal.pone.0011013

411. Loftus JP, Cavatorta D, Bushey JJ, Levine CB, Sevier CS, Wakshlag JJ. The 5-lipoxygenase inhibitor tepoxalin induces oxidative damage and altered PTEN status prior to apoptosis in canine osteosarcoma cell lines. *Vet Comp Oncol*. 2016;14(2):e17–e30. https://doi.org/https://doi.org/10.1111/vco.12094

CHAPTER 2: PI3K/mTOR DUAL INHIBITOR, VDC597, AS A THERAPEUTIC AGENT FOR CANINE OSTEOSARCOMA[iii]

Overview

Canine osteosarcoma (OSA) presents a significant clinical challenge in veterinary oncology. Due to the similarities in aggressive biologic behavior, mutation status, and gene expression profiles, the canine patient also provides a spontaneous animal model for OSA in humans. Advancements in the treatment of OSA have been slow to progress. The phosphatidylinositol 3-kinase (PI3K), AKT serine/threonine kinase (AKT), and mechanistic target of rapamycin (mTOR) signal transduction pathway is implicated in canine and human OSA, and presents a potentially valuable therapeutic target. The present study investigated PI3K-AKT-mTOR signaling activity in canine OSA cells, and the *in vitro* and *in vivo* efficacy of a PI3K/mTOR dual-inhibitor alone and in combination with cytotoxic chemotherapy drugs for treatment of canine OSA. The results of this study demonstrate: reduced signal transduction; increased cell death; reduced cell proliferation, migration, invasion, and vascular endothelial growth factor production *in vitro*; as well as reduced tumor growth and greater survival times with inhibition of PI3K-AKT-mTOR signaling in a xenograft mouse model. We also examined patient derived tumors for immunoreactivity of forkhead box O1 (FOXO1), a downstream target of AKT activation, but found that, unlike the xenograft tumors which were treated with a PI3K/mTOR inhibitor, a correlation between tumor biologic behavior

[iii] This chapter has been previously published in:
Meuten T, Farrell KB, Rose BJ, Brill SA, Brady RV, Schlein LJ, Thamm DH. Phosphatidylinositol 3-kinase and mechanistic target of rapamycin dualinhibitor, VDC597, as a therapeutic agent for canine osteosarcoma. *J Pharmacol Exp Ther*. 2025;392(10):103715. https://doi.org/10.1016/j.jpet.2025.103715

and FOXO1 immunoreactivity was not present in the patient derived tumor sections. These findings indicate both the potential benefits of PI3K/mTOR dual-inhibitors in chemotherapeutic protocols and the need for further study of patient-derived tumors to better understand the extent of PI3K-AKT-mTOR activation for the application of such targeted inhibitors.

Introduction

Canine osteosarcoma (OSA) is a malignant mesenchymal neoplasm of bone with aggressive biologic behavior and a high metastatic rate. Appendicular OSA accounts for 75% of OSA cases and is a significant cause of death in large and giant breed dogs.[1,2] While only 10% of canine OSA cases have radiographically apparent pulmonary metastases at the time of diagnosis, as many as 90% already have microscopic metastases, which rapidly progress and are the primary cause of death.[1-4] In dogs treated for OSA by limb amputation alone, the one-year survival rate is 11.5% with a median survival time (MST) of 5 months or less.[5] When amputation is combined with chemotherapy, the survival rate increases to approximately 45% at 1 year and 20% at 2 years.[5-7] While conventional chemotherapy agents improve progression free and overall survival times, there have not been significant improvements in patient outcome over recent decades.[4] There is a need for improved adjuvant therapies for canine OSA.

The development of targeted signal transduction inhibitors presents an opportunity for advancement in canine OSA treatment. Studies in human OSA signaling have provided potential targets, due to the similarities in pathogenesis, biological behavior, genetic and proteomic characteristics, and the applicability of dogs as a useful

spontaneous animal model for human OSA.[8-10] Among strong candidate targets is the phosphatidylinositol 3-kinase (PI3K), AKT serine/threonine kinase (AKT), and mechanistic target of rapamycin (mTOR) signal transduction pathway (PI3K-AKT-mTOR), which is highly conserved across mammalian species and dysregulated in multiple tumor types, including human and canine OSA.[11-13] PI3K-AKT-mTOR pathway activation has been reported in canine OSA and promotes tumor survival, proliferation, migration, and invasion.[14,15] Mutations and aberrations in expression of *PTEN, PIK3CA, PIK3CB, PIK3C2A/G, PIK3R1/4, AKT2*, and upstream receptor tyrosine kinases responsible for pathway activation have been reported in canine OSA and are associated with poorer prognosis.[16-19] The authors have previously reviewed the PI3K-AKT-mTOR signaling cascade and its involvement in canine cancers, including OSA.[20]

Given the involvement of PI3K-AKT-mTOR signaling in OSA, inhibiting pathway activity has been an area of veterinary research with some potentially promising results.[20] Rapamycin, a long-studied inhibitor of mTOR complex 1 (mTORC1), has been investigated for its efficacy against OSA *in vitro* and in canine patients.[21] These studies demonstrated a decrease in the expression of the phosphorylated forms of mTOR and phosphorylated ribosomal protein S6 kinase beta 1 (S6K1) in peripheral blood, indicating decreased pathway activation.[21-23] However, no concurrent decrease in AKT phosphorylation was observed, and patient outcome was not significantly improved with rapamycin.[21-23] This is likely to be due in part to known feedback mechanisms through which PI3K-AKT-mTOR signaling can be reactivated.[24,25] PI3K inhibitors have also been investigated *in vitro*, demonstrating decreased proliferation and increased apoptosis of canine OSA cells along with decreased AKT and S6K1 phosphorylation.[26,27] However,

these may face similar challenges *in vivo* due to feedback mechanisms shown to reactivate the pathway.[28,29]

For a more robust blockade of PI3K-AKT-mTOR signaling, inhibition of the pathway at multiple points is necessary. Preclinical murine and *in vitro* studies have demonstrated efficacy of PI3K/mTOR dual-inhibitors in reducing pathway activation, decreasing tumor progression, and increasing survival times.[30-32] The purpose of the present study is to evaluate the efficacy of VDC597, a dual PI3K/mTOR inhibitor, for the treatment of canine OSA, alone and in combination with cytotoxic chemotherapy drugs. A simplified diagram of the PI3K-AKT-mTOR pathway, showing points at which VDC597 is active in inhibition is shown in **Figure 2.01A**. Cell based assays were utilized to evaluate *in vitro* efficacy of VDC597 on canine OSA cell lines for reduction in cell growth and angiogenic paracrine signaling, induction of cell death, and inhibition of migration and invasion. Immunoassays were used to evaluate the inhibition of signal transduction, by examining the phosphorylation of AKT, as an indicator of PI3K signaling and a crucial component of pathway activation, and the phosphorylation of eukaryotic translation initiation factor 4E-binding protein 1 (4EBP1), as an indicator of mTORC1 signaling. A xenograft mouse model was used to evaluate the efficacy of VDC597 for *in vivo* canine OSA tumor growth inhibition and survival times. We also evaluated immunolocalization of forkhead box O1 (FOXO1) as a proxy for PI3K-AKT-mTOR activity in formalin fixed, paraffin embedded (FFPE) primary canine OSA tissues, which was the first such investigation to the authors' knowledge. Where we did observe correlations with prognostic indicators, those observations did not support this application of FOXO1 as a pathway activity indicator, but rather presented correlations

inverse of expectations. However, the findings may indicate interesting directions for future investigation, focused on more thorough examination of the relationship between AKT activity, FOXO1 degradation, and other regulators of FOXO1, including exportin 1 (XPO1) in spontaneous canine OSA.

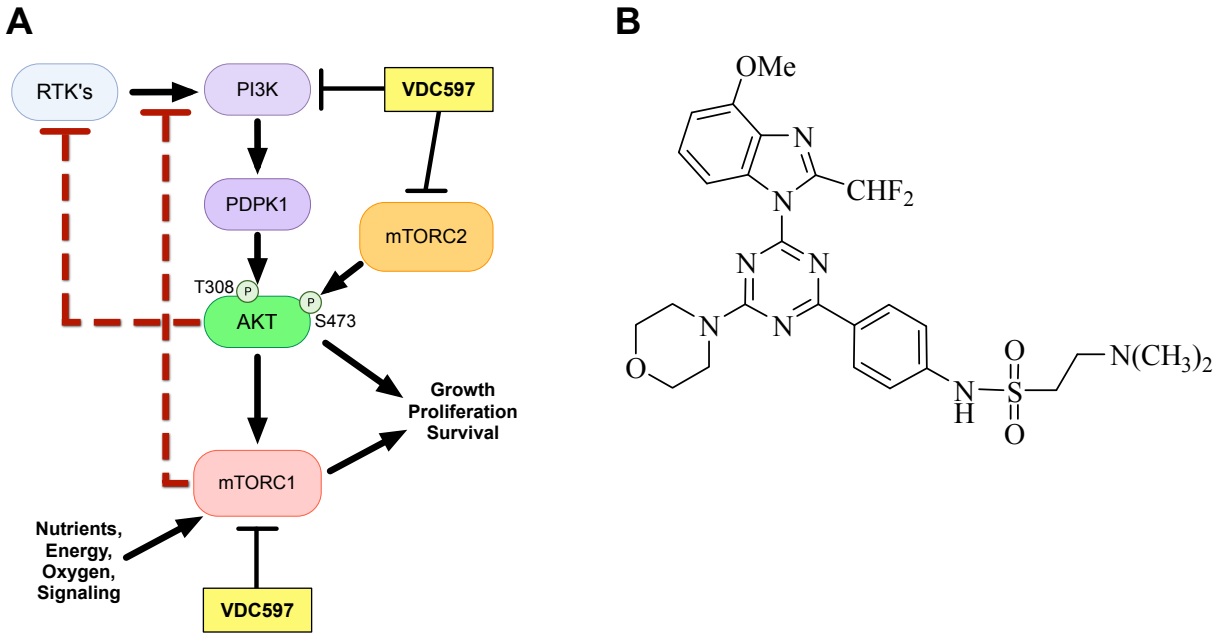

Figure 2.01: VDC597. (**A**) Simplified PI3K-AKT-mTOR signal transduction pathway, showing points at which VDC597 is active in pathway inhibition. With single-point inhibition of mTORC1 by drugs like rapamycin, the normal feedback inhibition is disrupted and alternate reactivation of RTKs and PI3K occurs. Other feedback mechanisms not depicted here also induce resumption of signal transduction, when there is single-point inhibition of PI3K, RTKs or mTORC2. By inhibiting signaling at PI3K, mTORC1, and mTORC2, there is a more robust signal transduction blockade that prevents feedback reactivation of the PI3K-AKT-mTOR signaling cascade, as compared to single-point inhibitors. (**B**) Structure of VDC597; molecular formula: $C_{26}H_{30}F_2N_8O_4S$.

Materials and Methods

Cell Lines and Conditions

The cell lines included in the Flint Animal Cancer Center Canine Tumor Cell Line panel are described in detail by Fowles et al.[33] OSA cell lines were established from dogs with spontaneously occurring OSA. The canine OSA cell lines Gracie, MacKinley, and Vogel were sourced from Colorado State University (CSU). Canine OSA cell lines

sourced from outside collections include: Abrams (University of Wisconsin-Madison, UWM); D17 (American Type Culture Collection); HMPOS (University of Tokyo); Moresco (UWM); and OSA8 (University of California-San Francisco). All cell lines were serially passaged by trypsinization and maintained in complete (C10) Dulbecco's Modified Eagle Medium (DMEM) (Corning, Henderson, VA), which was supplemented with nonessential amino acids, 1x minimum essential medium vitamin solution (Corning), 2 mM L-glutamine (Corning), 1 mM sodium pyruvate (Corning), and 10% heat-inactivated fetal bovine serum (FBS) (Peak, Wellington, CO). Cells were maintained in standard conditions (37°C and 5% CO_2 in a humidified atmosphere). All cell lines were confirmed to be of canine origin and unique by microsatellite PCR and a multiplex species-specific PCR technique, as previously described.[34] All *in vitro* protocols below were replicated in at least three independent experiments for each cell line.

Reagents

VDC597, a dual-inhibitor of PI3K and mechanistic target of rapamycin complexes 1 and 2 (mTORC1/2), was provided by VetDC Inc. (Fort Collins, CO), as a dry powder (**Figure 2.01B**). Stock solution aliquots were prepared in sterile dimethylsulfoxide (DMSO) for *in vitro* experiments. An aqueous suspension was prepared for *in vivo* experiments, at the time of administration. United States Pharmacopeia (USP) doxorubicin and USP carboplatin were obtained from commercial vendors through the CSU Veterinary Teaching Hospital pharmacy.

Viral Transduction of Cell Lines

OSA cell lines were virally transduced, according to the manufacturer's directions, with Incucyte® NucLight™ Red Lentivirus Reagent (Essen Bioscience, Ann Arbor, MI), for nuclear labeling of cells with a red fluorescent protein to facilitate real-time microscopy. Puromycin selection was used to isolate the transduced population.

Cell Lysates

Cells were grown to 70% confluence in C10 DMEM and standard conditions and were washed with phosphate-buffered saline (PBS). Cells were then incubated for 24 hours in C10 DMEM with DMSO vehicle or varying concentrations of VDC597 (0, 0.1, 0.2, 0.3, 1.0, and 3.0 μM). For examination of dose-response, cells were incubated for 24 hours under these conditions before lysate collection. To examine inhibition of pathway activity over time, cells were treated with 1 μM VDC597 or DMSO vehicle control and incubated for varying times (0.5–24 hours) before lysate collection. To examine persistence of pathway inhibition following clearance of drug from media, cells were incubated in media with DMSO vehicle control or 1 μM VDC597 for one hour then rinsed with PBS and placed in fresh media for varying times (10–240 minutes) before lysate collection.

At the time of lysate collection and preparation, cells were washed with PBS and lysed with mammalian protein extraction reagent (Thermo Fisher Scientific) containing 1 mM activated sodium orthovanadate (Sigma Aldrich, St. Louis, MO), 1 mM phenylmethylsulfonyl fluoride (Sigma Aldrich) solubilized in isopropanol, and protease inhibitor cocktail tablet at the manufacturer's recommended concentration (Complete

Mini, Roche Diagnostics, Mannheim, Germany). Lysed cells were collected in Eppendorf tubes and homogenized using a 25-gauge needle, then centrifuged at 4°C, and supernatants were aliquoted and frozen at -20°C for storage. Total protein concentration was determined using a bicinchoninic acid (BCA) Protein Assay Kit (Thermo Fisher Scientific) according to manufacturer instructions.

Western Blot Analysis

The degree of activation of the PI3K-AKT-mTOR pathway was evaluated by western immunoblot analysis of AKT phosphorylated at the serine 473 (S473) site (pAKT) and total AKT in canine OSA cell lines following treatment with VDC597. Cell lysates were diluted with lysis buffer as indicated by BCA assay results to reach approximately the same concentration for all samples, not exceeding 20 µg protein per 17 µL total volume. Sodium dodecyl sulfate loading dye was added to lysates to reach a total volume of 20 µL per sample. Then cell lysates and Precision Plus Protein™ Kaleidoscope™ ladder (Bio-Rad Laboratories, Hercules, CA) were heated to 95°C and then run on a 1.0–1.5 mm, 4-12% NuPAGE™ bis-tris precast gel (Invitrogen, Carlsbad, CA) in a NOVEX XCell SureLock™ Mini-Cell System (Invitrogen) and transferred to a polyvinylidene difluoride (PVDF) membrane (Bio-Rad). The membrane was then blocked using SuperBlock™ blocking buffer with Tween 20 (T20) (Thermo Fisher Scientific). PVDF membranes were cut into sections by protein size for primary antibody incubation. Primary antibodies were diluted in SuperBlock™ T20 and applied to PVDF membranes to be incubated overnight at 4°C. Antibodies and concentrations are listed in **Table A1 in the Appendix**. Membranes were then washed using TBST and

incubated with goat anti-rabbit horseradish peroxidase (HRP) conjugated secondary antibody (Thermo Fisher Scientific) diluted in SuperBlock™ T20 for 1 hour at room temperature. They were then developed using SuperSignal™ West Pico or SuperSignal™ West Femto chemiluminescent substrate (Thermo Fisher Scientific) and bands visualized using a ChemiDoc XRS+ System (Bio-Rad). Densitometric image analysis of western blots was performed using ImageJ (v. 1.54h; National Institutes of Health, Bethesda, MD) following previously described methods.[35-37] Background subtraction was applied by the ImageJ software before band intensity measurements. Band intensity for AKT was expressed as a fraction of total AKT and resultant fractions were normalized as percentage of controls before statistical analysis, which is described below in the *Data and Statistical Analysis* subsection (*Data & Stats*) of the Materials and Methods section.

Cellular Fixation for Histochemistry and Immunohistochemistry

Cells were cultured in C10 DMEM in T175 culture flasks. When cells reached 75-80% confluency, cells were rinsed in PBS and were incubated overnight in fresh C10 DMEM with VD597 at concentrations of 0.2 μM or 1.0 μM, or with DMSO vehicle control. Cells were collected by scraping and pelleted by centrifugation for 5 minutes at 400xG relative centrifugal force. Cells were then washed and resuspended in PBS, transferred to a 1.7 mL Eppendorf tube, and pelleted by centrifugation for 5 minutes at approximately 400xG. The cell pellet was resuspended in 1 mL 10% v/v neutral buffered formalin (NBF) (Cancer Diagnostics Inc., Durham, NC) and fixed overnight at 4°C. Following fixation, cells were pelleted by centrifugation for 5 minutes at 400xG, formalin

was removed, and cells were suspended in 1% agarose reconstituted with PBS. Agarose-embedded cells were then dissected into thin sections for processing. Sections were affixed with specimen sponges in tissue cassettes and submitted to the CSU Histology Laboratory in 10% NBF for overnight automated histologic processing using a VIP® 6 vacuum infiltration tissue processor (Sakura Finetek USA Inc., Torrance, CA) before manual paraffin embedding. Four-micrometer sections were examined by histochemistry (hematoxylin and eosin stains) and immunohistochemistry (3,3'-diaminobenzidine chromogen and hematoxylin counterstain). Standard hematoxylin and eosin sections were made by the CSU Histology Laboratory using an automated stainer following paraffin embedding. Immunohistochemical staining was performed manually, as described below.

Immunohistochemistry

The degree of activation of the PI3K-AKT-mTOR pathway was evaluated by immunohistochemical (IHC) analysis of pAKT (S473) expression in canine OSA cell lines, following treatment with VDC597 *in vitro*. To verify that VDC597 inhibits signal transduction beyond AKT to mTORC1 *in vitro*, we also used IHC to evaluate deactivating phosphorylation at the threonine 46 (T46) site of 4EBP1, which is a downstream target of PI3K-AKT-mTOR signaling. Phosphorylated 4EBP1 (p4EBP1) is an indicator of mTORC1 activity, and a reduction in p4EBP1 (T46) was used to examine inhibition of mTORC1 by VDC597. For *in vivo* xenograft specimens, marker of proliferation Kiel 67 (Ki67) and FOXO1 IHC was also examined. For all IHC experiments, following cell or tissue collection, FFPE sections were deparaffinized and

rehydrated in sequential 5-minute baths of xylene, xylol, ethanol (100%, 95%, 75%, 50%), and deionized water. Following rehydration, antigen retrieval was performed using Dako Target Antigen Retrieval® solution at pH 6.10 (Agilent, Santa Clara, CA) in a decloaking chamber, set to 118°C for 15 minutes, followed by slow cooling (approximately 1-hour total time of antigen retrieval). Sections were rinsed in deionized water and placed in 3% hydrogen peroxide for 10 minutes to quench endogenous peroxidases, and rinsed in deionized water. Following endogenous peroxidase quenching, all subsequent rinses between blocking and antibody incubation were in three 5-minute baths of TBST (tris-buffered saline (TBS) with 0.5% T20). Sections were blocked for non-specific immunoreactivity for 1 hour at room temperature in SuperBlock™ T20. Normal rabbit serum, isotype controls, and no primary antibody controls were included for each experiment. Primary antibodies and isotype controls were diluted in PBS or TBS with 1% bovine serum albumin (BSA). Antibodies and assay concentrations are listed in **Table A1**. Approximately 80 µL of diluted primary antibody were placed on sections, and slides were coverslipped to prevent evaporation. Primary antibody incubation was performed in a humidity chamber at 4°C overnight. Secondary antibody was either a goat anti rabbit HRP-conjugated antibody (Thermo Fisher Scientific) diluted in PBS with 1% BSA or Dako EnVision® Dual-Link HRP (Agilent), as indicated to avoid cross-reactivity with the species from which tissue was obtained (**Table A1**). Secondary antibody was added to sections and sections were incubated for 1 hour at room temperature in a humidity chamber. Dako 3,3'-diaminobenzidine (DAB) chromogen (Agilent) was used for visualization of immunoreactivity, incubating sections for approximately 2-5 minutes. Sections were then rinsed in deionized water and

counterstained with Mayer's hematoxylin for 30 seconds. Sections were then dehydrated in reverse order of that described above, before coverslips were affixed with Cytoseal™ XYL mounting media (Thermo Fisher Scientific). Sections from both *in vitro* and *in vivo* experiments were examined microscopically and IHC scoring was applied where applicable, as described below in *Data & Stats*.

Growth Inhibition Assay

For analysis of growth inhibition when treated with with VDC597, canine OSA cells were suspended in C10 DMEM, seeded in 96-well plates at a concentration of 2,000 cells per 200 µL per well, and allowed to adhere overnight. The following day, the plates were washed with PBS and media was replaced with fresh C10 DMEM containing serially diluted concentrations of VDC597, or DMSO vehicle control in quintuplicate. Cells were then incubated for 72 hours at 37°C with 5% CO_2. Following incubation, relative cell viability was determined using a resazurin fluorometric assay to detect metabolically active cells, and detected (530 nm excitation, 590 nm emission) with a Synergy™ HT microplate reader and associated KC4™ software (Gen5™, v. 3.11.19; BioTek Instruments).[38] Results were imported to Prism 10, relative cell viability was expressed as a percentage of vehicle control-treated cells, and the VDC597 concentration was log-transformed. The IC_{50} and growth inhibition curves were determined mathematically using non-linear curve fitting with the "log(inhibitor) vs. normalized response" function in Prism 10 software.

For examination of growth inhibition when treated with a combination of VDC597 and cytotoxic chemotherapy drugs, OSA cells were plated as above. The following day, the plates were washed with PBS and fresh C10 DMEM was added, containing: DMSO vehicle control; serially diluted concentrations of VDC597; serially diluted concentrations of doxorubicin or carboplatin; or varying concentrations of VDC597 and cytotoxic drug together. The plates were then incubated for an additional 72 hours, followed by determination of relative viable cell number as above. Relative viable cell number was standardized to that of cells incubated in C10 DMEM with DMSO vehicle control and expressed as a percentage of that control. Concentration of doxorubicin or carboplatin was log-transformed and growth inhibition curves were determined mathematically using non-linear curve fitting with the "log(inhibitor) vs. normalized response" function in Prism 10 software. Cell viability data were imported to CompuSyn software (ComboSyn Inc., Paramus, NJ), which uses the Chou-Talalay method to calculate drug combination indices and evaluate for potential synergism or antagonism.[39-41]

Cell Viability and Death Assay

To examine the degree to which cell death was induced by VDC597, we tracked viable cell proliferation and death over 48 hours of multiple NucLight™ Red expressing canine OSA cell lines, using Incucyte® Live-Cell Analysis System, calibrated to detect and count red cellular nuclei and green nucleic acids of dead cells labeled by the cell-impermeant dye, YOYO®-1 (Thermo Fisher Scientific). NucLight™ Red (Essen BioScience, Ann Arbor, MI) expressing cells were seeded at a density of 2,000 cells/200 uL/well in a 96-well plate and incubated overnight in standard conditions. Media was

replaced with C10 DMEM containing 100 nM YOYO®-1 iodide fluorescent dimeric cyanine nucleic acid stain (excitation 491 nm; emission 509 nm) and DMSO vehicle control or serially diluted concentrations of VDC597. The plate was placed in the Incucyte® ZOOM or Incucyte® SX5 Live Cell Imaging device (Essen BioScience) in standard incubation conditions and images of viable cells (red fluorescing; excitation 567-607 nm; emission 622-704 nm) and dead cells (green fluorescing; excitation 441-481 nm; emission 503-544 nm) were captured over a 48-hour period. Images captured from each well were analyzed with Incucyte® ZOOM (v. 2015A Rev1) or Incucyte® SX5 (v. 2023A Rev2) Live Cell Imaging software and total numbers of live and dead cells were exported for statistical analysis.[42,43] Red object (live cell) and green object (dead cell) counts were exported from Incucyte® software to a spreadsheet and green object count was expressed as a percentage of red object count per well at all time points. Resultant values were normalized to controls as percent of control wells and imported to Graphpad Prism 10 for statistical analysis, as described below in *Data & Stats*.

Vascular Endothelial Growth Factor ELISA

Due to the known role of PI3K-AKT-mTOR signaling in promotion of tumor angiogenesis, we evaluated the effects of PI3K/mTOR inhibition by VDC597 on vascular endothelial growth factor (VEGF) production in three canine OSA cell lines. Cells were plated at $1x10^5$ cells/well in 12-well plates with 800 µL C10 DMEM for 24 hours under standard conditions. Cells were then washed and incubated for 24 hours in C10 DMEM with VDC597 (0.25, 0.5, or 1 µM) or DMSO vehicle control. The supernatant was then collected and for VEGF quantification, fresh C10 DMEM was then

added to the plate, and the resazurin fluorometric assay was used to determine relative viable cell number, as described above. The VEGF concentrations of the supernatant were evaluated using a R&D Systems (Minneapolis, MN) canine ELISA, according to manufacturer's specifications. VEGF ELISA absorbance values were fitted to a linear regression, using known standards to interpolate sample VEGF concentrations (picograms per mL). Relative viable cell number for each sample well was normalized as a percentage of control wells and VEGF concentrations were corrected for cell numbers by dividing VEGF concentration by the resulting percentage before statistical evaluation, as below in *Data & Stats*.

Scratch Assay

Given that cytoskeletal reorganization for motility is mediated by rapamycin-insensitive mTORC2, and that mTORC1 and 4EBP1 play roles in cellular migration and invasion (see Discussion), we hypothesized that migration may be inhibited by VDC597, further contributing to reduced neoplastic migration.[20] To assess the inhibition of canine OSA cell motility by VDC597, OSA cells were plated at a density of 25,000 cells/200uL/well in a 96-well ImageLock™ plate (Essen BioScience) and incubated overnight in standard conditions. A uniform defect (scratch wound) was then created in the monolayer cells in the 96-well plate using the Essen BioScience WoundMaker™ and wells were rinsed with PBS to eliminate detached cells. Media was replaced with C10 DMEM containing serially diluted concentrations of VDC597 or DMSO vehicle control. The plate was placed within the IncuCyte® SX5 imaging device in standard conditions and the percent wound confluence, was recorded via IncuCyte® SX5

imaging software over 48 hours.[42] Cell counts within the scratch wound were reported as a percent confluence of the wound. All percentage confluence values were baseline-corrected for any cells present within the scratch wound at the beginning of the observation period, with the formula: corrected confluence = $(x_t-x_0)/x_0$, where x_0 = percent confluence at time 0; x_t = percent confluence at time *t*. Baseline-corrected values were then normalized as a percentage of the control groups. Area under the curve (AUC) was calculated for each treatment condition over the 48-hour period. For each cell line, the AUC values from 3 independent experiments were found to be normally distributed and evaluated for statistically significant differences, as described below in the *Data & Stats*.

Chemotactic Migration and Invasion (Boyden Chamber) Assay

To simulate the migration and invasion of canine OSA cells through basement membranes to nutrient-rich environments *in vivo,* we evaluated the *in vitro* chemotactic migration and invasion of canine OSA cells in Boyden chambers in the presence of VDC597. Cells were incubated in DMEM with 0.1% FBS for 1.5 days, then plated at a density of $2x10^5$ cells per well in 100 µL of 0.1% FBS DMEM in a 24-well Boyden chamber plate with 8-micron pore diameter cell culture inserts (Falcon, Corning, NY) and 30 µL of Matrigel (Corning, Glendale, AZ) diluted at a 1:5 ratio in DMEM, which was allowed to solidify before plating cells. Following adherence of cells to the well overnight, cells were treated in duplicate with DMSO vehicle control, 0.2 µM VDC597, or 1 µM VDC597. Two control wells were left untreated. At the time of treatment, C10 DMEM was placed in the outer chambers, separated from the cells by the 8-micron pore

diameter semipermeable membranes and Matrigel to simulate a chemotactic gradient across a semipermeable basement membrane layer. Two wells per treatment condition were maintained with serum-free DMEM on both sides of the membranes as non-chemotactic gradient controls. Cells were allowed to migrate for 24 hours post-treatment. At experiment completion, cells that had not migrated were removed, wells were washed, and lower compartment wells were fixed with 4% paraformaldehyde for 10 minutes on ice, stained with 3% crystal violet (Sigma-Aldrich, St. Louis, MO), rinsed with distilled water, and allowed to air-dry overnight. Boyden chamber membranes were then cut from the cell culture inserts and mounted on Superfrost® Plus glass slides and coverslips were affixed with Cytoseal™ XYL mounting media (Thermo Fisher Scientific). Two replicate membranes were collected and five 400x fields per membrane were counted, and the mean number of cells per field was determined for each membrane. Subsequent replicate means were found to be normally distributed and variance between groups was evaluated as described below in *Data & Stats*.

Subcutaneous Xenograft

To study oral bioavailability, safety, and efficacy of VDC597 for inhibition of tumor growth *in vivo* a xenograft model was used. For development of the xenograft model in this specific application, multiple canine OSA cell lines were subcutaneously implanted in athymic nude (nu/nu) mice. During this process, the Gracie canine OSA cell line was found to develop tumors most reliably, and was used for subsequent *in vivo* experiments. To examine tumor growth, sixteen female, 6–8-week-old, athymic nu/nu mice were purchased from Jackson Laboratories (Bar Harbor, ME), housed in

microisolation cages at a density of four mice per cage, and allowed to acclimate for 1 week prior to the initiation of experimentation. All procedures were approved by the CSU Institutional Animal Care and Use Committee (IACUC) before experimentation. Mice were implanted with $1x10^6$ canine OSA cells (Gracie), which were suspended in sterile PBS at a concentration of $1x10^6$ cells per 100 µL and implanted subcutaneously overlying the right proximal hindlimb. Mice were identified with metal ear tags at the time of tumor implantation and 8 mice per group were randomized by weight into sham vehicle-control or VDC597 treatment groups. For mice receiving VDC597, a 20 mg/mL aqueous suspension of VDC597 was administered *per os* (PO) every 24 hours (q24h) for 5 days per week at a dose of 50 mg/kg, using a gavage syringe. For mice in the control group, water was administered PO via gavage at equivalent volumes by weight, and at the same frequency. The observation period lasted 80 days from time of implantation. Mice were euthanized when tumor length exceeded 20 mm, when tumor diameter exceeded 15 mm, or otherwise inhibited free mobility, when there was weight loss exceeding 15% body weight, or when other indications for euthanasia arose, including hunched posture for 24 hours or failure to right, according to IACUC protocols. Mice were weighed and tumors were measured at least 3 times, weekly. Animals were euthanized by cervical dislocation after isoflurane anesthetization. Following euthanasia for the above criteria or at the end of the study, samples of the tumor and organs were fixed in 10% NBF (Thermo Fisher Scientific) and submitted to the CSU Histology Lab for paraffin embedding and sectioning, as described above. Sections were stained for histochemical and immunohistochemical examination as described above.

To study the survival of time of mice with xenograft tumors that had grown to a substantial size before the initiation of treatment, forty-four female, 6–8-week-old, athymic nu/nu mice were purchased from Jackson Laboratories (Bar Harbor, ME), were housed and acclimated under the conditions described above, and all experimental procedures were approved by the CSU IACUC before experimentation. Canine OSA cells were implanted as described above. Treatment was initiated after approximately 30 days, when the implanted cells formed solid tumors with a mean tumor diameter at least 6 mm. Mice were randomized by initial tumor size to one of four treatment groups: control; VDC597; carboplatin; or both VDC597 and carboplatin. At that time, 11 mice had tumors that exceeded maximal diameter for treatment initiation and those mice were excluded from the study. Group sizes at the time of initiation of the study and randomization for treatment were as follows: control (n = 9); VDC597 (n = 8); carboplatin (n = 8); VDC597 + carboplatin (n = 8). For mice receiving carboplatin, a sterile 10 mg/mL injectable solution of carboplatin was administered intraperitoneal (IP) every 7 days at a dose of 40 mg/kg. For mice receiving VDC597 and mice in the control group, treatment was as described above. Additionally, for mice in the control group, sterile PBS was administered IP at equivalent volumes and frequency to the carboplatin group. The total observation period was 75 days. Treatment and data collection frequency, euthanasia criteria, and tissue sampling were as described above. The end-point for each subject was at the time of euthanasia, when one of the following criteria for euthanasia was met: 20 mm tumor length; 15mm tumor diameter; 15% weight loss; ulceration over the tumor site; hunched posture for 24 hours or more; or inability to right. Tumor tissues collected following euthanasia were microscopically evaluated for pAKT

(S473), p4EBP1 (T46), and FOXO1 immunolabeling and Ki67 proliferation indices.[44] Following manual assessment of immunolabeling, sections were scanned and converted into digital images for artificial intelligence analysis and IHC scoring, as described below. Specific statistical methodology for comparisons of resultant scoring is outlined in *Data and Stats*.

FOXO1 expression in canine OSA tissue specimens

Anonymized FFPE samples of spontaneous canine OSA tumors from a previously conducted prospective clinical trial with outcome data were provided by Gustafson et al.[45] Samples from this study were obtained from canine oncology patients at the CSU Veterinary Teaching Hospital diagnosed with appendicular OSA being treated at the FACC. The study protocol was approved by the CSU Clinical Trials Review Board (protocol number 428), and signed informed consent was obtained from owners for the study. Using FFPE sections from this study, histochemical and IHC processing were as described above with antibody concentrations listed in **Table A1**. Validation of an antibody for detection of FOXO1 was performed by western analysis using the protocol described above. Following antibody specificity validation by western blot, the sensitivity and specificity of the FOXO1 antibody in FFPE tissue sections was verified, and antibody concentrations were optimized, using sections of xenograft canine OSA tumors, mouse tissues, and sections of canine lymph nodes, which served as positive canine tissue controls.[46,47] Following the verification of applicability in FFPE sections, we tested for the correlation of FOXO1 immunolocalization to PI3K-AKT-mTOR signaling activity by comparing the immunolabeling for FOXO1, pAKT (S473),

and p4EBP1 (T46) in a subset of xenograft tumor samples, which did not require decalcification. After finding the expected correlation, sections of the anonymized decalcified FFPE clinical canine OSA samples were processed for IHC as described above and converted to digital images for artificial intelligence analysis of IHC as described below.

Artificial Intelligence Analysis of Immunohistochemistry

Sections of clinical canine OSA samples and xenograft tumor samples were scanned at 400x magnification, using an Olympus VS200 slide scanner (ASW-4.1.1, build 29408; Evident Corporation, Tokyo, Japan) with an Olympus iDS VS-264C (firmware v. 3.1.18303; Olympus Corporation, Center Valley, PA) camera with cellSens™ software (v. 1.17; Olympus Corporation, Center Valley, PA) and analyzed using Visiopharm software (v. 2023.09.7.16662 x64; Visiopharm A/S, Hoersholm, Denmark) at a resolution of approximately 5 pixels/µm.[48,49] For Visiopharm evaluation of patient-derived spontaneous OSA sections, osteoid spicules, regions of necrosis or hemorrhage, and any tissue folds present in the sections were omitted, and all remaining sections of tumor tissue were analyzed.[49] To identify nuclei in the tumor sections, software employed an artificial intelligence (AI) U-Net deep learning classification method that was trained using 3 regions of interest (ROI) per image in 20 specimens (approximately 60 unique images), with a 50% initial minimum probability of identification as the criterion for pixel classification (and progressively higher minimum probabilities for inclusion in subsequent iterations), over 330,000 iterations until loss function reached ≤ 0.06 (approximately equivalent to 2.5% error rate).[50,51] Thresholds

for DAB intensity scoring were set manually and remained constant for all subsequent analysis. From each nucleus, an area expanding 2.5 μm radially was designated as corresponding cytoplasm and thresholds for DAB intensity scoring were set manually. All scanned images were then analyzed by the AI algorithm, using the above parameters and demonstrated in **Supplemental Figure S2.01**. These same parameters were used for FOXO1 IHC analysis in tumor sections from xenograft mouse experiments. For Visiopharm IHC analysis of pAKT (S473), p4EBP1 (T46), and Ki67 in xenograft tumor sections, the cytoplasmic and nuclear labels were merged to capture total cellular immunolabeling. U-Net deep learning classification training was continued through additional iterations until loss function was ≤ 0.06 and thresholds for DAB intensity scoring were adjusted appropriately for the immunolabeling properties of each target antigen. All scanned images were analyzed by the AI algorithm using the parameters as set for each target antigen. Histochemical scoring (H-scoring), which is a metric based on number and intensity of immunopositive cells or subcellular compartments, was applied to the nuclei and cytoplasms (for FOXO1) or to whole cells (for pAKT, p4EBP1, and Ki67) for all cells in the sections, based on DAB intensity. The formula for H-scoring is outlined below. Hematoxylin and eosin-stained sections of the samples were examined and graded by two canine OSA grading methods.[52,53]

$$\text{H-score} = (0 \times P_0) + (1 \times P_1) + (2 \times P_2) + (3 \times P_3)$$

where: P_i = percentage of cells of DAB staining intensity ***i*** (range 0-3)

Data and Statistical Analysis

Data from all *in vitro* and *in vivo* experiments were imported to GraphPad Prism 10 (v. 10.4.1; GraphPad Software LLC, Boston, MA) for statistical analysis and P-values less than 0.05 were considered statistically significant.[54] For *in vitro* assays, any baseline-correction, normalization as percentage of controls, and data transformations are outlined below. Following control-normalization or transformation, data were tested for normality using the Shapiro-Wilk test. Normally distributed data were then compared using ANOVA with Tukey's or Dunnett's multiple comparisons tests, as appropriate. In cases where data were not normally distributed or when other statistical analyses were indicated, those methods are discussed under the subheadings for their respective experiments.[20,35-37,39-41,49,54-56]

For *in vivo* experiments, survival times and tumor diameters were recorded and imported to Graphpad Prism 10 for statistical analysis. For both *in vivo* experiments, mice were euthanized according to the criteria outlined above. In the first experiment, tumor measurements per group were recorded for the duration of the experiment, and mean tumor measurements were compared between groups up to the time of the first euthanized subject, which was in the control group on day 42. In this experiment, maximal tumor size was the reason for euthanasia in all experimental subjects. Tumor measurements were evaluated for variance by repeated measures two-way ANOVA, comparing treatment group to the control group (n = 8 per group) with Bonferroni multiple comparison test for statistical significance. In the second experiment, which examined survival time, differences in experimental design, including later initiation of treatment and inclusion of carboplatin and combined VDC597 + carboplatin, are as

described above and all euthanasia criteria remained the same. Throughout the 75-day observation period, survival times for each subject were recorded at the time of euthanasia. At the end of the experiment, all survival times were imported to Graphpad Prism for statistical analysis. Survival times were evaluated for statistically significant differences, comparing each treatment group (n = 8) to the control group (n = 9), using a log-rank (Mantel-Cox) test with Bonferroni correction for multiple comparisons (α = 0.01667). Xenograft tumor sections were examined by IHC. Resultant immunopositive cell counts and H-scoring from Visiopharm for IHC of pAKT (S473), p4EBP1 (T46), and FOXO1 were imported to Graphpad Prism 10 for statistical analysis. Distribution was found to be normal by Shapiro-Wilk normality test and immunolabeling differences between treatment groups and controls were evaluated by ANOVA with Šidák test for multiple comparisons.

Results

VDC597 inhibits activation of AKT/mTOR signal transduction in canine OSA cells

In multiple canine OSA cell lines, we used western immunoblots to examine expression of total AKT and pAKT (S473), which is a phosphorylated form required for full activation of AKT in signal transduction. In all four cell lines, there was a dose-dependent reduction in pAKT (S473) following 24-hour incubation with VDC597 (P-values: 0.0004 to < 0.0001) (**Figure 2.01, A and B**). At pharmacologically achievable concentrations of 1 μM, this reduction in AKT phosphorylation was rapid in onset and was robustly maintained over a 24-hour period, which correlates to a clinically relevant PO dosing interval (**Figure 2.01, C and D**). In washout experiments, in which cells were

treated with 1 μM VDC597 for one hour and then placed in fresh media, VDC597 maintained suppression of AKT phosphorylation at S473 ($P < 0.0001$) for greater than 4 hours (**Figures 2.01, E and F**).

Correlating to AKT phosphorylation demonstrated in western blot analysis, three canine OSA cell lines were also examined by IHC for p4EBP1 (T46), as an indicator of the degree of PI3K-AKT-mTOR signal transduction. Compared to DMSO vehicle-control, in cells incubated with 1 μM VDC597 for 24 hours, there was a marked decrease in perinuclear and cytoplasmic pAKT (S473) immunoreactivity, which is demonstrated in **Figure 2.01, G and H**, for the D17 cell line, and is shown in **Supplemental Figure S2.01** for all three canine OSA cell lines examined: D17, Gracie, and Abrams. In addition to a reduction in pAKT (S473) immunoreactivity, there was also a marked decrease in cytoplasmic p4EBP1 (T46) immunoreactivity in the Gracie, D17, and Abrams canine OSA cell lines (**Supplemental Figure S2.03**), following a 24-hour incubation with 1 μM VDC597.

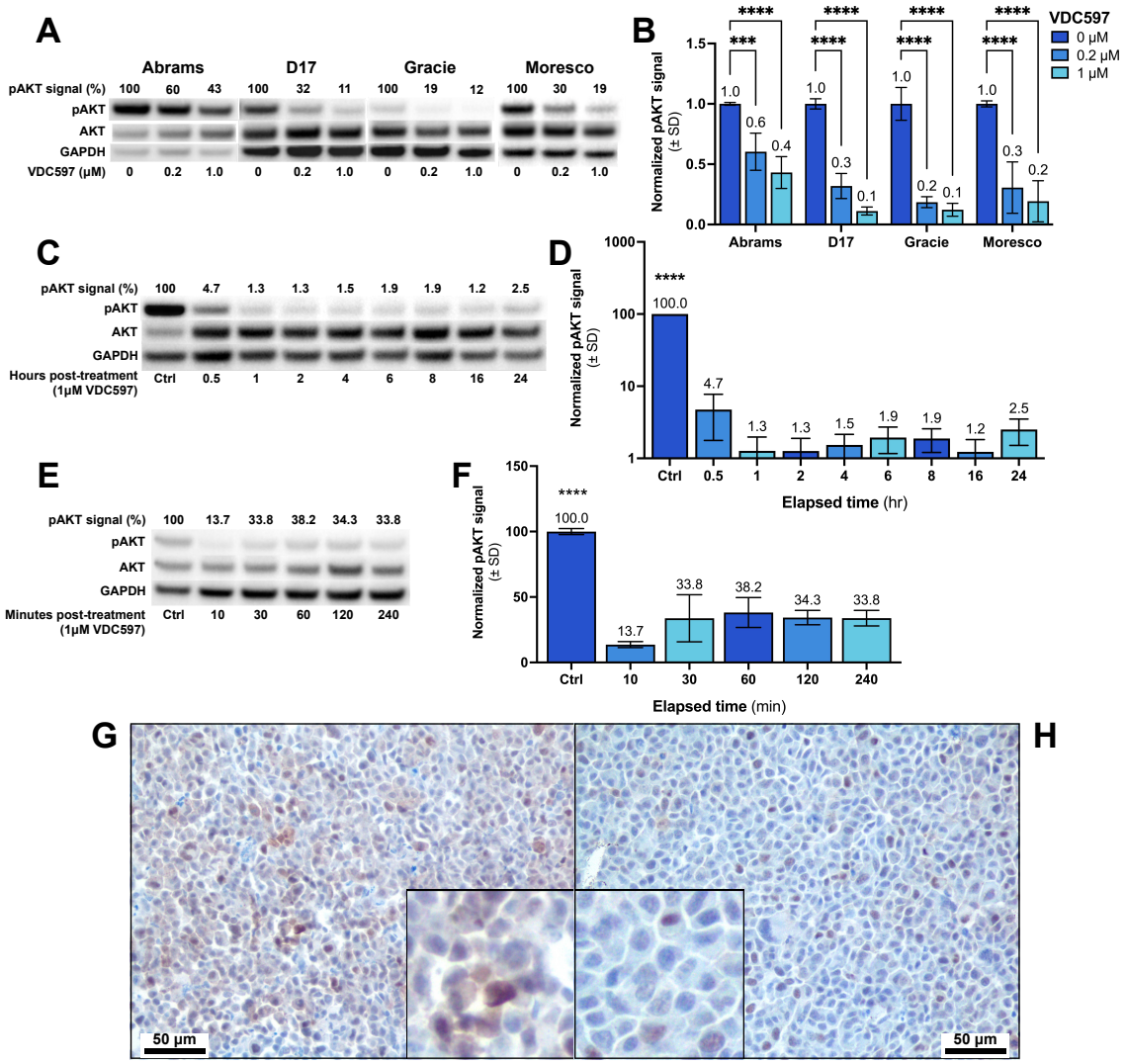

Figure 2.01: *in vitro* pAKT (S473) inhibition by VDC597 in canine osteosarcoma (OSA) cells. (**A**) Western blots for pAKT (S473) in various canine OSA cell lines following 24-hour incubation with varying concentrations of VDC597, normalized to total AKT and expressed as a percentage of DMSO vehicle controls. (**B**) Quantification of three experimental replicates of western blots shown in (A), expressed as a fraction of controls. (**C**) Western blot of a canine OSA cell line (Gracie) incubated with 1 μM VDC597 for varying times, with pAKT (S473) normalized to total AKT and expressed as a percentage of control. (**D**) Quantification of three experimental replicates of western blots shown in (C); for all comparisons to control, $p < 0.0001$. (**E**) Western blot of a canine OSA cell line (Gracie) incubated with 1 μM VDC597 for 1 hour, then rinsed with PBS and placed in fresh, untreated media for varying times, with pAKT (S473) normalized to total AKT and expressed as a percentage of control. (**F**) Quantification of three experimental replicates of western blots shown in (E); for all comparisons to control, $p < 0.0001$. (**G**) 400X magnification photomicrograph of formalin fixed paraffin embedded canine OSA cells (D17) with abundant perinuclear and cytoplasmic pAKT (S473) immunoreactivity; DAB chromogen and hematoxylin counterstain. (**H**) D17 canine OSA cells after incubation with 1 μM VDC597 for 24 hours, with markedly reduced cytoplasmic and perinuclear pAKT (S473) immunoreactivity; DAB chromogen and hematoxylin counterstain; insets of both images are enlarged approximately 2.5X to show immunolocalization detail. All error bars represent standard deviation and significance indicators are as follows: * $p < 0.05$; ** $p < 0.005$; *** $p < 0.0005$; **** $p < 0.0001$.

VDC597 inhibits cell proliferation and promotes cell death in canine OSA cell lines, showing variable responses in combination with doxorubicin and carboplatin

Following evaluation of inhibition of pAKT activity, *in vitro* sensitivity to VDC597 was assessed in nine canine OSA cell lines using fluorescent quantification of metabolically active cells. In unpublished pharmacokinetic studies, following oral administration of VDC597 to dogs at 30 mg/kg, the mean peak plasma concentration was 2.1-2.3 μM and was maintained over 600 ng/mL (1 μM) for greater than 8 hours (A. Kousba, MD, PhD, G.N. Lam, PhD, and D.F. Beyerlein, written personal communication, March 2011). In a phase-I clinical trial in tumor bearing dogs, 20 mg/kg oral administration of VDC597 5 days per week was found to be the most efficacious dosing schedule with few adverse effects. In this study, the mean peak plasma concentrations for doses examined were 885.3 ng/mL (1.5 μM) at 20 mg/kg. In a subset of dogs in the 15 mg/kg group for which tumors were sampled, the concentration of VDC597 within the tumors was above the threshold for a reduction in end-point cell viability, indicating growth inhibition.[57] According to this pharmacokinetic limitation, in 6 of the 9 OSA cell lines the half maximum inhibitory concentration (IC_{50}) was at or below the pharmacologically achievable concentration, with IC_{50} concentrations ranging from approximately 0.4 to 1.1 μM (**Figure 2.02A**). In 3 of the canine OSA cell lines, the IC_{50} was 1.2 μM or greater, which was considered partially resistant or resistant. Growth inhibition curves for all canine OSA cell lines examined are shown in **Supplemental Figure S2.04**.

In addition to single-agent analysis, for a subset of canine OSA cell lines, *in vitro* reduction in growth inhibition was examined when cells were treated with a combination of VDC597 and doxorubicin or carboplatin. In all three cell lines, growth was inhibited and the IC_{50} values reduced to a greater extent for both doxorubicin and carboplatin with the addition of VDC597 at pharmacologically achievable doses (**Supplemental Figure S2.05**). The combination indices (CI) distributed near CI = 1 indicate that the effect of combined treatment with VDC597 was additive, but largely not synergistic (CI < 1), for both doxorubicin and carboplatin (**Figure 2.02B**), though effects were stronger when VDC597 and doxorubicin were combined.

The bioreductive method utilized above cannot discriminate between cell growth inhibition and induction of cell death. Therefore, in addition to growth inhibition assays, the degree to which cell death was induced over time with VDC597 administration was examined by using the Incucyte® live cell tracking system with YOYO®-1 cell death indicator dye. There was a dose dependent increase in the proportion of YOYO®-1 positive cells over the 72-hour incubation period, which was most significant at and above 1 μM for the Abrams ($P = 0.0050$), MacKinley ($P = 0.0077$), and Vogel ($P < 0.0001$) canine OSA cell lines, indicating cytotoxicity of VDC597 for OSA cells *in vitro* (**Figure 2.02C**).

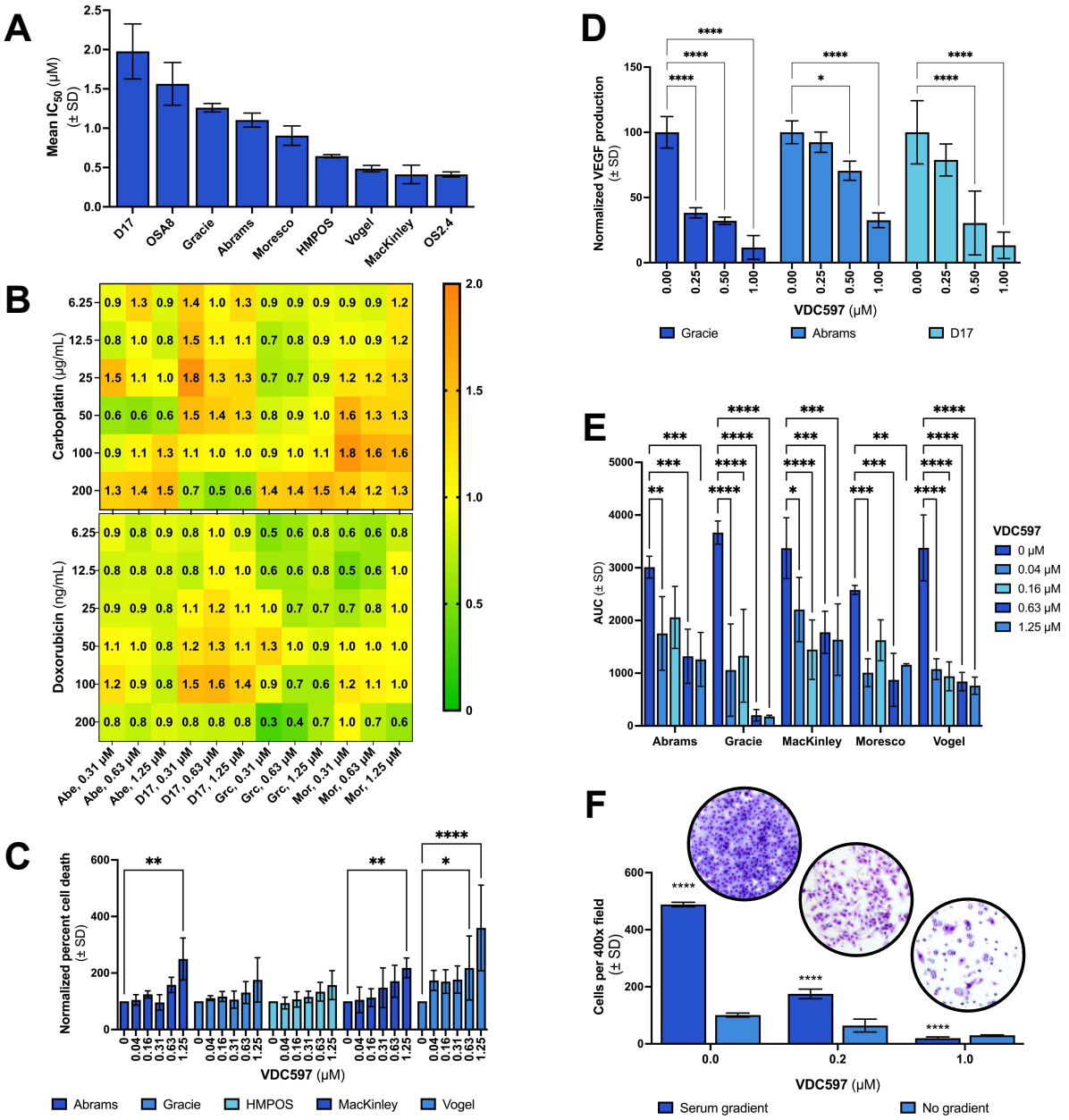

Figure 2.02: *in vitro* antineoplastic activity of VDC597 in canine osteosarcoma (OSA) cells. (**A**) Mean half maximum inhibitory micromolar concentrations (IC_{50}) of VDC597 for multiple canine OSA cell lines from three experimental replicates, demonstrating that IC_{50} values for six of the nine cell lines tested are at or below pharmacologically achievable concentrations (approximately 1.2 μM). (**B**) Mean drug combination indices (CI) for VDC597 with carboplatin (top) or doxorubicin (bottom), from three experimental replicates, demonstrating effects closer to synergism (CI < 1) for doxorubicin than for carboplatin; cell lines and VDC597 concentrations are listed at the bottom; cell line abbreviations: Abe (Abrams), Grc (Gracie), Mor (Moresco). (**C**) Mean percent cell death at the end of a 48-hour incubation period, from three experimental replicates and normalized to vehicle control, for multiple canine OSA cell lines treated with VDC597; significant difference is primarily at the 1.25 μM concentration; differences were not significant for Gracie and HMPOS cell lines in this experiment. (**D**) Mean VEGF concentration from three experimental replicates, expressed relative to cellularity and normalized to vehicle control, for three

canine OSA cell lines following 24-hour incubation with varying concentrations of VDC597. (**E**) Migration inhibition of canine OSA cells treated with varying concentrations of VDC597 from three scratch assay experimental replicates, measured as cell confluence in the scratch wound over a 48-hour period and converted to area under the curve (AUC) for each treatment condition. (**F**) Mean cell counts from two fields per treatment condition, representing inhibition of chemotactic migration and invasion along a serum gradient through a basement membrane layer (Matrigel) and porous membrane, following 24-hour incubation of canine OSA cells (Gracie) in varying concentrations of VDC597; inset images above the graph are representative images from 0 μM (vehicle control), 0.2 μM, and 1 μM concentrations of VDC597. In the graphs above, all error bars represent standard deviation and significance indicators are as follows: * $p < 0.05$; ** $p < 0.005$; *** $p < 0.0005$; **** $p < 0.0001$.

VDC597 inhibits angiogenesis, migration, and invasion in canine OSA cells

Due to the role of VEGF production in promotion of tumor angiogenesis, the effect of VDC597 on VEGF production in three canine OSA cell lines was also examined. There was observable dose-dependent reduction in VEGF production following 24-hour incubation with varying concentrations of VDC597 (**Figure 2.02D**). All statistically significant comparisons to vehicle control carried a P-value < 0.0001, except the 0.5 μM VDC597 concentration for the Abrams cell line (P = 0.0229).

Along with the promotion of neovascularization of the tumor microenvironment, we sought to the effects of VDC597 on migratory and invasive features of malignancy in canine OSA cells, using scratch assays (migration) and Boyden chamber assays (chemotactic migration and invasion). There was a dose-dependent reduction of OSA cells migrating into the scratch wound over a 48-hour period in all cell lines examined (**Figure 2.02E**). To quantify cellular migration into the scratch wound, the percent wound coverage was plotted (**Supplemental Figure S2.06**) and area under the curve (AUC) was used to examine differences between treatment groups. For canine OSA cells incubated in Boyden chambers with a chemotactic gradient, migration through the membrane and invasion through Matrigel coatings were inhibited by VDC597 in a dose-dependent manner (P < 0.0001) (**Figure 2.02F**).

VDC597 contributes to in vivo tumor growth inhibition in xenografts of canine OSA cells

Xenograft canine OSA tumor (Gracie cell line) growth was recorded over time, to measure the *in vivo* effect of orally administered VDC597 on neoplastic progression. Tumors in mice treated with VDC597 (n = 8) grew slower than those in untreated mice of the control group (n = 8), with statistically significant differences in tumor diameter on days 27, 30, 39, and 42 (treatment P-value = 0.0004). **Figure 2.03A** reports mean tumor diameter up to the timepoint at which the first mouse was euthanized due to tumor size, on day 42.

In a second xenograft experiment, following subcutaneous implantation of Gracie canine OSA cells, and after allowing the tumor to reach 6mm diameter before treatment with VDC597, carboplatin, VDC597 and carboplatin, or vehicle controls, we found significant differences between treatment and control survival times before tumor growth necessitated euthanasia ($\alpha = 0.01667$). Mice treated with VDC597 (n = 8; P = 0.0070) or carboplatin (n = 8; P = 0.0253) survived longer than mice in the control group (n = 9), and mice in the group treated with both VDC597 and carboplatin (n = 8) survived numerically longer than any other group (**Figure 2.03B**). The median survival time (MST) for mice in the control group was 41 days. MST for mice treated with VDC597 was 55 days. The MST for mice treated with carboplatin was 60.5 days. The MST for mice treated with carboplatin and VDC 597 was 65 days (**Figure 2.03B**). One mouse in the control group and one mouse in the VDC597 + carboplatin group was each euthanized on day 29, due to trauma from other mice and those subjects were censored in survival data. One mouse in the carboplatin group, and two mice in the VDC597 +

carboplatin group, survived to the end of the 75-day observation period and those mice were censored in the survival data. All other mice were euthanized due to maximal tumor size being reached, without other negative clinical signs, such as weight loss, being indicating a need for euthanasia. A scatter plot of subject weights and mean percent weight change per group over time is provided in **Supplemental Figure S2.07**, demonstrating similar median weights and mean percent weight changes over time between groups.

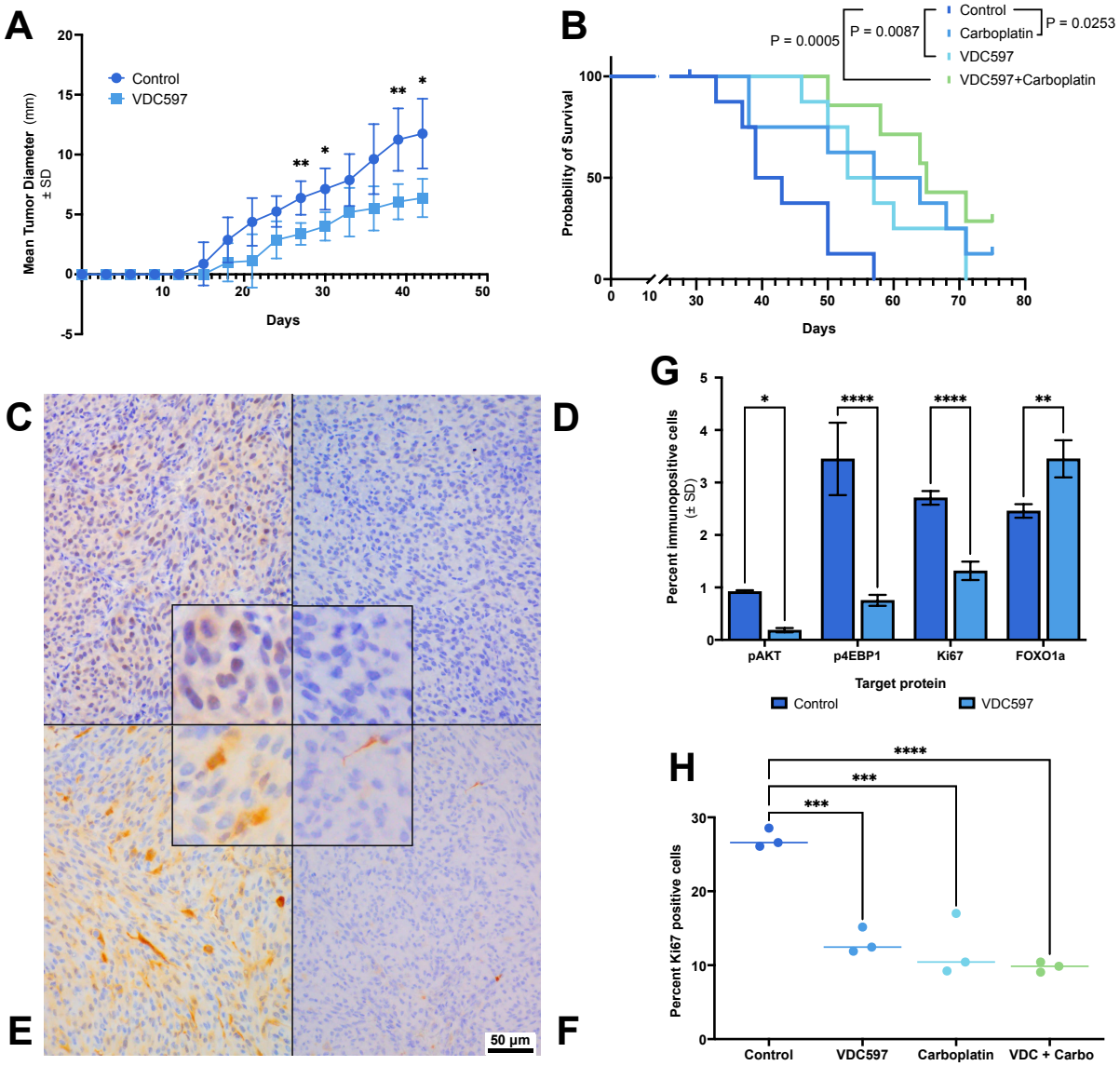

Figure 2.03: *in vivo* antineoplastic activity of VDC597 in canine osteosarcoma (OSA) xenograft tumors. (**A**) Mean tumor diameter of mice treated with VDC597 oral gavage (n = 8) or aqueous vehicle control (n = 8) over a 42-day period, at which point the first mouse in the control group was euthanized due to tumor size. (**B**) Kaplan-Meier survival curves for mice treated with vehicle controls (water and sterile isotonic saline; n = 9), VDC597 (n = 8), carboplatin (n = 8), or VDC597 and carboplatin (n = 8); median survival times for each group were control = 41 days, VDC597 = 55 days, carboplatin = 60.5 days, VDC597 + carboplatin = 65 days; following log-rank Mantel-Cox comparison of treatment to control groups, and Bonferroni correction for multiple comparisons (α = 0.01667), there were significant differences between the control group and the VDC597 group (P = 0.0087) and the VDC597 + carboplatin group (P = 0.0005), but not between control and carboplatin group (P = 0.0253). (**C-F**) 400X magnification photomicrographs of formalin fixed paraffin embedded sections of canine OSA (Gracie) xenograft tumors from mice, demonstrating: (**C**) diffuse perinuclear and cytoplasmic pAKT immunoreactivity in a section from a mouse in the vehicle control group; (**D**) markedly reduced pAKT immunoreactivity characterized by very rare weak perinuclear immunolocalization in a tumor section from a mouse treated with VDC597; (**E**) multifocally extensive moderate cytoplasmic p4EBP1 immunoreactivity with scattered strongly immunopositive cells in a section from a mouse in the control group; (**F**) infrequent mild p4EBP1 immunoreactivity with rare moderate to strong cytoplasmic immunolocalization in a section from a mouse

treated with VDC597; insets of images are enlarged approximately 2.5X to show immunolocalization detail; DAB chromogen and hematoxylin counterstain. (**G**) Percent immunopositive cells in sections from xenograft canine OSA tumors in mice treated with vehicle control or VDC597, demonstrating decreased immunoreactivity for pAKT, p4EBP1, and Ki67 with increased FOXO1a immunoreactivity in mice treated with VDC597. (**H**) Percent cells immunopositive for Ki67 in xenograft canine OSA tumors in mice treated with vehicle control, VDC597, carboplatin, or both VDC597 and carboplatin. In the graphs above, all error bars represent standard deviation and significance indicators are as follows: * $p < 0.05$; ** $p < 0.005$; *** $p < 0.0005$; **** $p < 0.0001$.

VDC597 contributes to in vivo inhibition of pAKT, p4EBP1 immunoreactivity in xenograft canine OSA tissue specimens

Following euthanasia of mice, FFPE sections of the subcutaneously implanted canine OSA tumors (Gracie cell line) were examined by IHC for pAKT (S473), p4EBP1 (T46) immunoreactivity. In tissues collected from the control group, pAKT perinuclear and cytoplasmic immunopositivity was abundant throughout neoplastic cells. There was frequent moderate, and infrequent strong, cytoplasmic p4EBP1 throughout the tumor cells. In the carboplatin treated tumors, there was mild subjective reduction in pAKT immunolabeling. In the tumors from mice treated with VDC597, there was reduction in both the number of pAKT positive cells and the intensity of pAKT immunolabeling (**Figure 2.03, C and D**). Immunoreactivity was also decreased for p4EBP1 (**Figure 2.03, E and F**). Photomicrographs of IHC isotype controls for all IHC antibodies used in these experiments are shown in **Supplemental Figure S2.08**. These microscopic findings were correlated to immunolabeling throughout tumor sections that were scanned and analyzed by Visiopharm software. In the scanned images of tumor sections from mice treated with VDC597, there was a marked reduction of p4EBP1 immunopositivity ($P < 0.0001$), as well as reduction in pAKT immunopositivity ($P = 0.0273$) (**Figure 2.03G**).

In canine xenograft OSA tissues, in vivo reduction in p4AKT and p4EBP1 immunoreactivity correlates to decreased Ki67 immunoreactivity and increased intranuclear FOXO1 immunolocalization

With the xenograft canine OSA specimens, we also sought to evaluate the correlation between pAKT (S473) and p4EBP1 (T46) activity and indicators of proliferation and evasion of apoptosis, *in vivo*. Sections were examined by IHC for the well-established proliferation marker, Ki67, as well as FOXO1 immunolocalization as an indicator of dysregulation of apoptosis and cellular immortality. We found that there was scattered moderate specific intranuclear Ki67 immunoreactivity throughout canine OSA sections from mice in the control group, while there were very rare Ki67 immunopositive cells in sections from mice treated with VDC597 (**Supplemental Figure S2.09**).

Previous to IHC evaluation of FOXO1, we validated the specificity of the FOXO1 antibody being used by western blot, which demonstrated discrete bands at the level of the 70 kDa molecular weight without any nonspecific signal (**Supplemental Figure S2.10**). Following initial validation of specificity, the efficacy for IHC application was tested in sections of FFPE canine lymph nodes. In the lymph node sections, we found strong specific discrete FOXO1 intranuclear immunoreactivity in cells predominantly confined to germinal centers, which is consistent with B-lymphocytes (**Supplemental Figure S2.11**).[46,47] FOXO1 immunoreactivity was markedly reduced outside of germinal centers, and did not label (or rarely weakly labeled) sinusoids, capillaries, plasma cells, macrophages, and lymphocytes consistent with T-cells in morphology and in distribution through the paracortex and outside of germinal centers.

Following antibody validation, we evaluated the xenograft canine OSA for FOXO1 immunolocalization, hypothesizing that there would be an inverse correlation between pAKT immunoreactivity and intranuclear FOXO1 immunoreactivity. In control sections examined, FOXO1 immunoreactivity was scant, without an apparent increase in cytoplasmic immunolocalization, which was hypothesized to be present previous to ubiquitin degradation. Throughout tumor sections from mice treated with VDC597, intranuclear FOXO1 immunolabeling was increased in comparison to specimens from the control group (**Supplemental Figure S2.12**). These findings were confirmed and quantified, when sections were analyzed using Visiopharm software. In the sections from mice treated with VDC597, there was a decrease in Ki67 immunoreactivity ($P = 0.0004$), and an increase in FOXO1 nuclear immunopositivity ($P = 0.0028$), when compared to tumors from the control group (**Figure 2.03, G and H**). A reduction in the percent of cells with Ki67 immunopositivity was also present in tumor sections from mice treated with carboplatin ($P = 0.0003$) or VDC597 + carboplatin ($P < 0.0001$), when compared to the control group (**Figure 2.03H**). As with pAKT and p4EBP1, photomicrographs of sections of isotype controls for Ki67 and FOXO1 are shown in (**Supplemental Figure S2.08**).

FOXO1 expression in canine OSA tissue sections

We sought to evaluate patient-derived FFPE canine OSA samples for pAKT and p4EBP1 expression by IHC to study correlation between these markers of pathway activation and survival time, as well as the previously reported and clinically useful prognostic indicators in the canine patient following diagnosis of OSA: age; weight;

serum alkaline phosphatase (ALP) concentration; and circulating monocyte count.[55,56,58] However, we found that the decalcification process made IHC probing for phospho-specific proteins unfeasible. As such, we looked to downstream targets for which detection in FFPE sections is not phospho-specific, including FOXO1. FOXO1 is trafficked out of the nucleus to the cytoplasm and undergoes ubiquitin-degradation as a result of activated pAKT.[20] For this reason, we hypothesized that intranuclear FOXO1 immunoreactivity would be inversely correlated to pAKT immunoreactivity. For the clinically derived canine OSA samples, FOXO1 nuclear and cytoplasmic immunoreactivity and H-scores were analyzed for correlation to survival time and prognostic indicators (age, weight, ALP concentration, and circulating monocyte count).[55,56,58] Following assessment of H&E sections to confirm diagnostic specimens were included and, following IHC processing of the sections available from the study, there were 37 cases with samples of good cellularity that lacked excessive processing artifact, which considered to be of adequate quality for digital analysis within the capabilities of the software being used. In the sections examined, the percentage of nuclei immunopositive for FOXO1 was approximately 59% with 27% cytoplasmic FOXO1 immunopositivity (**Figure 2.04A**), with a median nuclear H-score of 87 and a median cytoplasmic H-score of 18 (**Figure 2.04B**). There was a strong positive correlation between nuclear immunopositivity and cytoplasmic immunopositivity ($P < 0.0001$). The number of circulating monocytes was positively correlated to nuclear FOXO1 immunopositivity and H-score ($P = 0.0491$) and serum ALP concentration was positively correlated to nuclear FOXO1 H-score ($P = 0.0254$) (**Figure 2.04, C and D**). Nuclear/cytoplasmic immunoreactivity did not have a significant impact on progression

free interval or overall survival in this patient cohort. However, there was a trend toward shorter survival times for dogs with lower nuclear FOXO1 H-scores (**Supplemental Figure S2.13**). The correlations between nuclear FOXO1 immunoreactivity and mitotic rates or survival times were also the inverse of expectations, although these trends did not reach statistical significance (P = 0.3211). There was no correlation of FOXO1 immunolabeling with tumor grade in the sections examined. The mitotic rate within 2.37 mm^2 was positively correlated to the percent of cells with cytoplasmic FOXO1 immunoreactivity (P = 0.0430) and to the cytoplasmic H-score (P = 0.0159) by simple linear regression. FOXO1 nuclear H-score was also positively correlated to the mitotic rate within 2.37 mm^2 (P = 0.0133) by simple linear regression (**Supplemental Figure S2.14**).

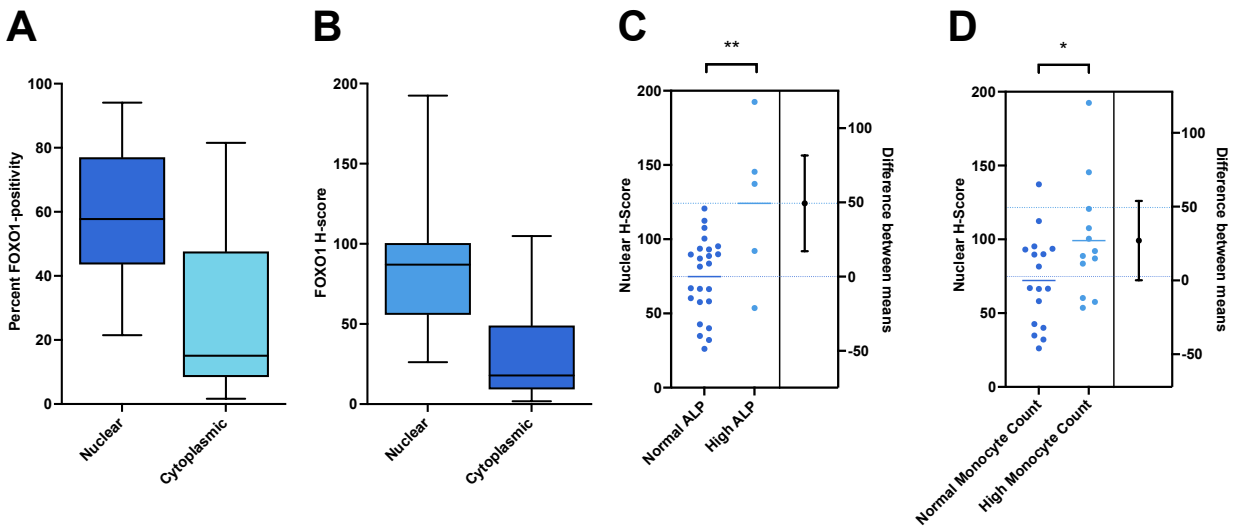

Figure 2.04: FOXO1 and prognostic indicators in spontaneous canine osteosarcomas. (**A**) Plots of FOXO1 immunoreactivity in sections of patient-derived spontaneous canine OSA tumors, expressed as percent positive cells and (**B**) histochemical scores (H-scores); boxes represent the interquartile range, with a line at the median and whiskers to minimum and maximum values. (**C**) Estimation plot of the distribution of nuclear FOXO1 H-scores relative to normal and high total serum ALP concentrations. (**D**) Estimation plot of the distribution of nuclear FOXO1 H-scores relative to normal and high circulating monocyte counts. Significance indicators are as follows: * $p < 0.05$; ** $p < 0.005$

Discussion

The PI3K-AKT-mTOR pathway is frequently dysregulated in cancer and involved in neoplastic cell growth, proliferation, survival, increased cellular metabolism, increased cellular migration/invasion, and angiogenesis in both human and canine OSA.[20] Previous studies examined the PI3K-AKT-mTOR signaling inhibition in canine neoplasms.[20] In the present study, we evaluated the *in vitro* and *in vivo* activity of VDC597 against multiple canine OSA cell lines, alone and in combination with cytotoxic chemotherapy drugs.

PI3K-AKT-mTOR signaling is known to be: involved in cellular survival and proliferation; correlated with higher histopathologic grades, higher Ki67 indices, and poorer prognosis; and variably responsive to rapamycin in tumors.[20,22,59] Multi-nodal inhibition at PI3K, mTORC2, and mTORC1 potentially provides a more robust blockade of PI3K-AKT-mTOR signaling. Our findings of dose-dependent growth inhibition and induction of cell death within pharmacologically achievable concentrations indicate potential clinical application of VDC597 for tumor growth inhibition and induction of cell death in pulmonary metastases.

Human studies have shown that the addition of PI3K/AKT/mTOR inhibition to chemotherapy protocols decreases resistance to chemotherapy and radiotherapy, as well as producing growth inhibition and cell death at equivalent levels to higher drug/radiation doses.[32,60-65] Previous studies have also examined inhibitors of PI3K, AKT, and mTOR signaling in canine tumors, including hemangiosarcoma, lymphoma, mast cell tumor, melanoma, mammary gland tumor, and osteosarcoma.[20] However, the majority of these investigations have focused on single-target inhibitors and/or inhibition

of upstream receptor tyrosine kinases (RTKs). Studies utilizing inhibitors of more than one component of the signaling cascade have observed a more robust blockade of signal transduction and greater efficacy against neoplastic cell proliferation, survival, and features of malignancy.[20] The authors refer the interested reader to our review of PI3K/AKT/mTOR inhibition in canine neoplasms for more information about these studies.[20] We have previously evaluated the *in vitro* efficacy of VDC597 in canine hemangiosarcoma, and found that there was significant reduction in many of the neoplastic processes examined in the present study, indicating a potentially beneficial application of this inhibitor to clinical treatment of canine hemangiosarcoma.[66] Our findings in the present study indicate that VDC597 may be able to fill a similar role for the canine OSA patient.

Cellular migration and invasion are promoted through multiple mechanisms by PI3K-AKT-mTOR signaling, including activating phosphorylation of mTORC1 and inactivating phosphorylation of 4EBP1 in human OSA and other neoplasms, and can be reduced with targeted inhibitors.[11,20,67-71] To the authors' knowledge, the role of pathway inhibition in canine OSA migration or invasion has not previously been examined. The dose-dependent reduction in cells that transited the membrane when incubated with VDC597 indicates that the addition of VDC597 to chemotherapy regimens as a component of canine OSA treatment may inhibit neoplastic migration and invasion for metastasis.

In correlation to the findings above, western immunoblot analysis of pAKT and total AKT in canine OSA cell lines demonstrated a dose-dependent reduction in pAKT at pharmacologically relevant concentrations of VDC597. Time to peak inhibition and

duration of inhibition following removal of the drug also indicated pharmacologically attainable maintenance of concentrations sufficient for likely *in vivo* efficacy. These findings were also supported by IHC results, and indicate that the *in vitro* growth inhibition, induction of cell death, and decreased cellular migration we observed is correlated to inhibition of the PI3K-AKT-mTOR signaling by VDC597.

Growth of a vascular network within solid tumors is an integral component of neoplastic growth beyond a few millimeters in diameter without becoming necrotic.[72-74] The involvement of PI3K-AKT-mTOR in promoting the production of angiogenic factors, including VEGF, has been well established in human neoplasms and murine models.[20,75] Elevated serum VEGF is reported in canine OSA cases, and is associated with radiation therapy resistance, shorter disease-free intervals, and poorer prognosis.[20] Research has also demonstrated *in vitro* reduction of VEGF production by canine hemangiosarcoma and mammary cancer cell lines treated with PI3K-AKT-mTOR pathway inhibitors.[66,76]

The dose-dependent decrease in VEGF expression by canine OSA cell lines that we observed indicates that there may be potential for decreased OSA angiogenesis in patients treated with VDC597. However, it should be noted that the *in vivo* efficacy of VDC597 for inhibition of VEGF-mediated angiogenesis is not addressed in the present study, and may be affected by other components of the tumor microenvironment. Further investigation is needed to evaluate the potential for clinically applicable antiangiogenic benefits. Additionally, sensitivity to VDC597 varies between cell lines, indicating the value in evaluating patients' tumors for pathway activation in clinical application.

For clinical trials of targeted PI3K/mTOR inhibition to be considered, it was necessary to evaluate VDC597 *in vivo*. During experimental mouse model development, multiple canine OSA cell lines were implanted subcutaneously in athymic nude mice, and the Gracie cell line was found to grow best in this model. Following SQ implantation of canine OSA cells (Gracie), athymic nude mice treated with VDC597 were found to have slower tumor growth and longer survival times, without overt clinical signs of toxicity or excessive weight loss. Compared to controls, IHC of FFPE tumor sections from mice treated with VDC597 exhibited reduced immunoreactivity for pAKT, p4EBP1, and Ki67, as well as increased intranuclear FOXO1 immunolocalization. These findings indicate that inhibition of PI3K-AKT-mTOR signaling is correlated with reduced proliferation indices, possible restoration of FOXO1 mediated cell death, reduced tumor growth, and increased survival times. The reduction of Ki67 immunoreactivity in mice treated with carboplatin, or both VDC597 and carboplatin was also expected. While there was also a trend toward slowest tumor growth in the group treated with both carboplatin and VDC597 compared to those treated with a single agent, the lack of statistical significance may be due to the limited power resultant from the low number of animals used in this trial. However, the trend indicates good biological activity of VDC597 in this limited scope experiment. Larger scale xenograft studies are needed for a more thorough examination of the efficacy of this combined treatment modality.

In light of the negative correlation of FOXO1 and pAKT by IHC in the xenograft experiments, it was surprising to find that the correlations between FOXO1 immunoreactivity and prognostic indicators of serum ALP and circulating monocytes were the inverse of the authors' expectations in the spontaneous canine OSA samples

examined.[55,56] The correlations between nuclear FOXO1 immunoreactivity and mitotic rates or survival times were also the inverse of expectations, although these trends did not reach statistical significance (P = 0.3211). We hypothesize that these ambiguous results may be due to the relative insensitivity of artificial intelligence (AI) for identifying and differentiating subcellular immunolocalization in brightfield images, as compared to analysis by trained observers. As such, the authors caution against over-interpreting the cytoplasmic immunoreactivity in this experiment, despite the reported benefits of AI regarding observer variability.[77] Additional limitations include: challenges for AI analysis of brightfield, as opposed to immunofluorescent images; variation in tumor, stroma, and matrix density; and variable degrees of decalcification and occasional tissue folding, which produced image artifacts. Ongoing rapid progress in AI technology and optimization with larger training sets may produce more accurate results.[78]

Beyond AI limitations for brightfield IHC analysis in OSA sections, additional mechanisms are known to play a role in FOXO1 activity and promotion of neoplastic progression, including S-phase kinase-associated protein 2, microRNAs, and exportin-1 (XPO1).[79,80] XPO1 dysregulation has been demonstrated in multiple human neoplasms and presents a potentially valuable target for therapy in canine cancers, including canine OSA.[80]

It is the authors' opinion that application of genomic and proteomic testing could yield strategies for the use of a combination of such targeted inhibitors with chemotherapy to yield the greater therapeutic benefit. This further emphasizes the importance of including gene expression for the consideration of targeted therapy in

clinical cases. We hope that further study will yield affordable diagnostic opportunities for clients and canine patients.

There are significant limitations to the scope of this study, and further research is warranted to better characterize, refine, and expand upon the findings herein. The scope of the *in vivo* experiments was limited by small sample size, indicating a greater number of subjects could increase statistical power. It is the authors' opinion that the effects of treatment could also be better examined after pilot studies examining growth of these canine OSA cell lines in mice allows for refined times of treatment initiation and duration. Additionally, examination of *in vivo* activity against metastatic disease is warranted. The biological activity of VDC597 against canine OSA cells *in vitro* appears promising. However, established cell lines are known to variably exhibit atypical features as compared to spontaneous tumors. More complete examination of a larger sample of patient derived canine OSA cells for PI3K/AKT/mTOR status for potential applicability of this compound would be valuable. It would be desirable to further characterize rapid and affordable clinically applicable detection methods for PI3K-AKT-mTOR signaling activity in patient tumors. While our findings confounded the use of FOXO1 as a proxy, it was beyond the scope of this study to fully examine other candidate downstream targets for detection of pathway activity in decalcified FFPE tissues, due to the limitations on expense and time.

Conclusions

In conclusion, there is evidence for constitutive PI3K-AKT-mTOR signaling activity in canine OSA cells, as is in the case in human OSA and other canine tumors. There is evidence that VDC597 decreases PI3K-AKT-mTOR signaling activation and tumor growth in canine derived OSA cells both *in vitro* and *in vivo*, as well as increasing cell death, decreasing VEGF production, decreasing cellular migration, and acting in an additive fashion with chemotherapeutic drugs *in vitro*. There is also evidence that oral administration of VDC597 is well tolerated and is associated with greater survival time both alone and in combination with carboplatin i*n vivo*, indicating oral bioavailability of the compound. These findings provide a worthwhile rationale for further investigation of PI3K/mTOR inhibition with VDC597 as a component of chemotherapeutic treatment of canine OSA, as well as a basis for investigation of PI3K-AKT-mTOR signaling and the efficacy of this compound in other canine cancers.

Supplementary Materials

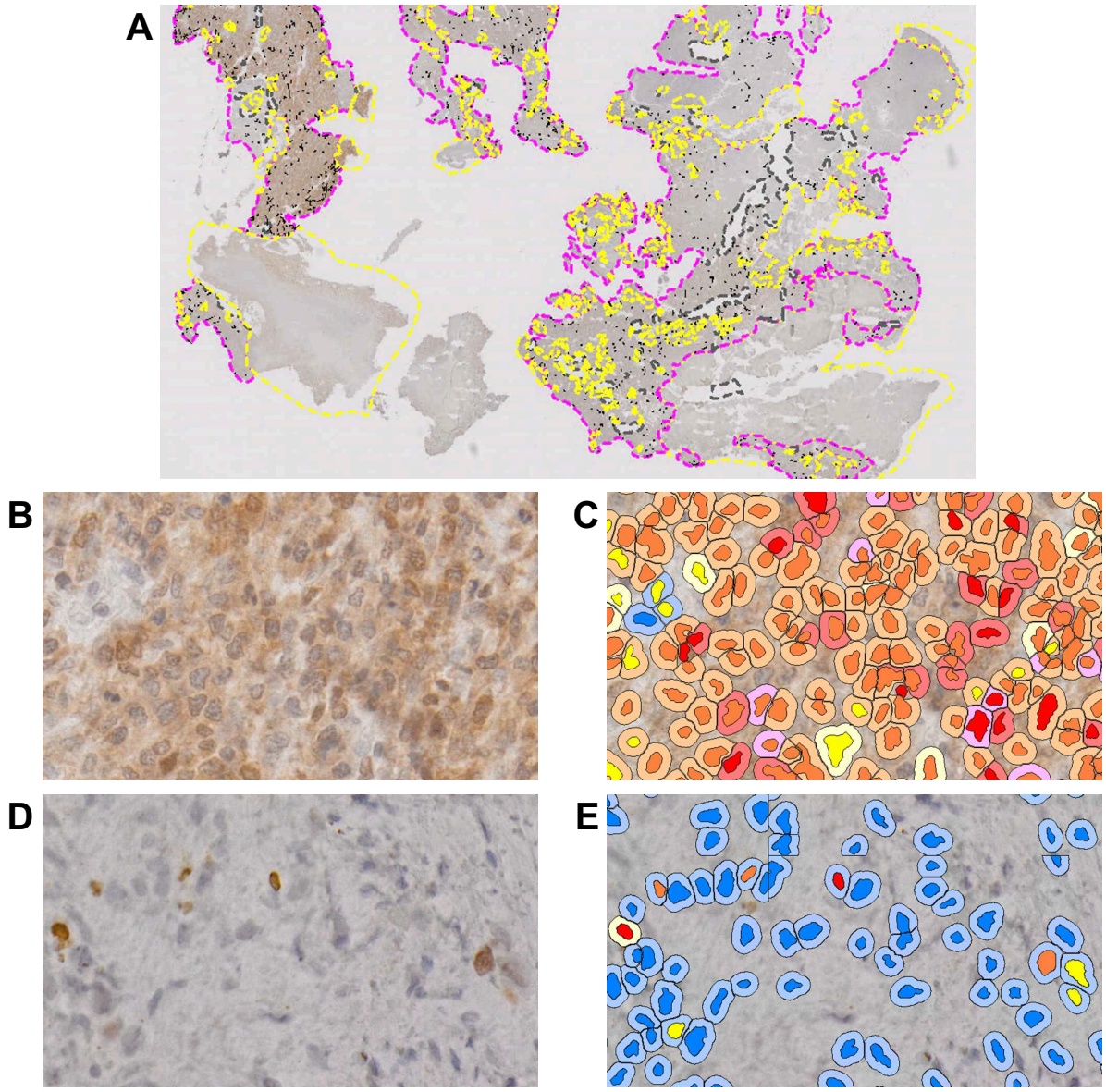

Supplemental Figure S2.01: Image examples of sections examined with Visiopharm software and resultant region and object identification. (**A**) Example of areas selected by a tissue detection algorithm for analysis outlined in pink and areas omitted due to low cellularity, poor focus, or heavy matrix deposition. (**B**) Image of a heavily FOXO1-immunopositive region; (**C**) corresponding nuclear identification, cytoplasmic approximation, and colors indicating classification of 1+, 2+, 3+, and negative FOXO1 IHC intensities. (**D**) An area with low cellularity and infrequent immunoreactivity; (**E**) corresponding nuclear identification and labeling as described above. Visible in these examples are scattered cells that were not identified by the AI algorithm, as well as examples of the challenges that brightfield IHC presents to AI algorithms for consistent separation of nuclear and cytoplasmic compartments for IHC scoring.

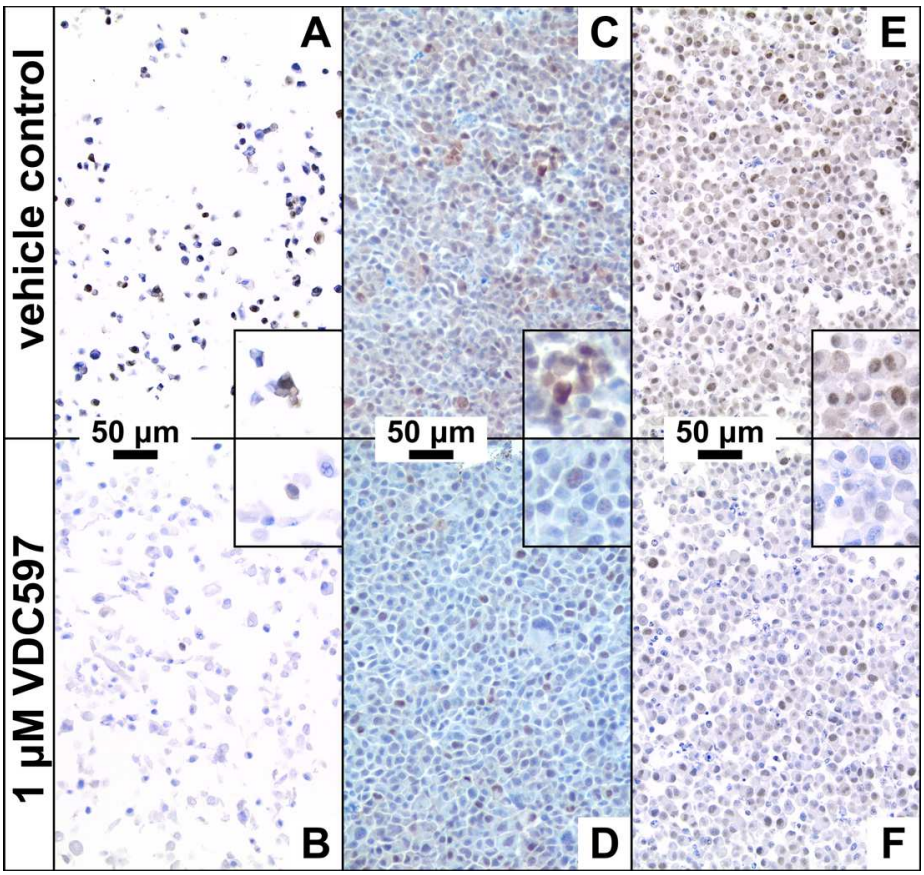

Supplemental Figure S2.02: S473 phosphorylated AKT (pAKT) immunolabeling in canine OSA cell lines, Gracie (**A** and **B**), D17 (**C** and **D**), and Abrams (**E** and **F**), following a 24-hour incubation with 1 µM VDC597 (**bottom row**) or DMSO vehicle control (**top row**). Following incubation, cells were either pelleted or dispersed in agarose before formalin fixation and paraffin embedding. In later experiments, cell suspensions were more frequently used, as it allowed for more sections to be made from a single paraffin block. In the vehicle control sections, there is frequent discrete, specific perinuclear and cytoplasmic pAKT immunoreactivity. Following incubation with VDC597, there are reduced numbers and intensity of immunopositive cells. Compared to other cell lines, in the Gracie cell line (**A** and **B**) there was a somewhat lower percentage of cells that were strongly immunoreactive for pAKT (**A**), resulting in very rare weak pAKT immunopositivity following incubation with VDC597 (**B**). A reduction in number and intensity of pAKT immunoreactivity was also present in the D17 (**C** and **D**) and Abrams (**E** and **F**) cell lines. While there is a marked reduction in all cell lines, the number of immunopositive cells remains higher than in Gracie cells, which correlates to the relative reduction in pAKT signal measured by western blot, as demonstrated in **Figures 1A-B**. Photomicrographs are 200x magnification. Insets are 400x magnification to show immunolocalization detail. DAB chromogen and hematoxylin counterstain. For all photomicrographs, all acquisition and image settings were maintained identical between control and treated groups.

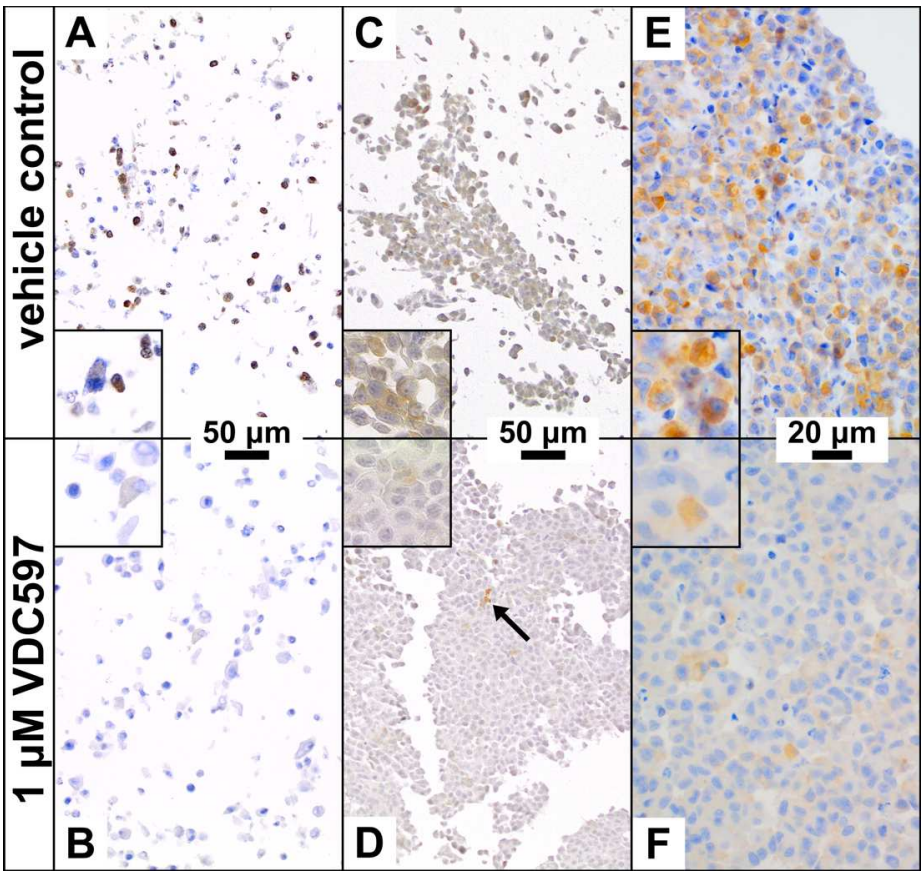

Supplemental Figure S2.03: phosphorylated 4EBP1 (p4EBP1) immunolabeling in canine OSA cell lines, Gracie (**A** and **B**), D17 (**C** and **D**), and Abrams (**E** and **F**), following a 24-hour incubation with 1 µM VDC597 (**bottom row**) or DMSO vehicle control (**top row**). Cells were suspended or pelleted in agarose before fixation and paraffin embedding. Following 24-hour incubation with DMSO vehicle-control (0 µM VDC597), there is frequent strong discrete specific cytoplasmic p4EBP1 immunoreactivity in all 3 cell lines, indicating abundant inactivating phosphorylation of 4EBP1 (via mTORC1), which is correlated to PI3K-AKT-mTOR pathway activity. As with pAKT immunolabeling, the number and intensity of immunopositive cells in the Gracie cell line (**A**) was less than D17 (**C**) and Abrams (**E**). Following incubation with VDC597, there is infrequent weak to moderate discrete specific cytoplasmic p4EBP1 immunoreactivity, indicating reduced signal transduction for the inactivating phosphorylation of 4EBP1. In the VDC597 treated D17 cell line (**D**), there are occasional cells with strong discrete cytoplasmic p4EBP1 immunoreactivity (**arrow**), but that was far less common than the weakly immunopositive cells demonstrated in the **inset** of **D**. Photomicrographs are 200x magnification with 400x insets (**A-D**) or 400x magnification with 800x insets (**E-F**) in order to best show detail and overall immunolabeling, based on cell density. DAB chromogen and hematoxylin counterstain. For all photomicrographs, all acquisition and image settings were maintained identical between control and treated groups.

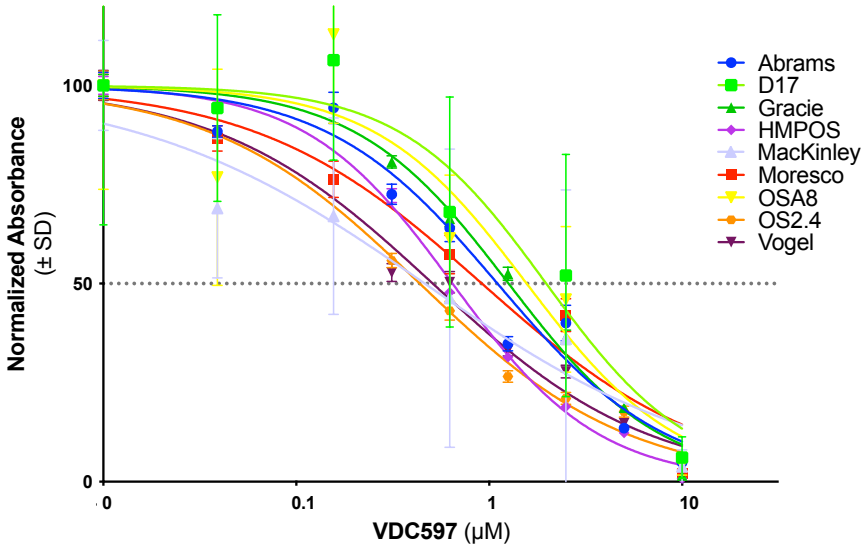

Supplemental Figure S2.04: Growth inhibition assay dose-response curves for multiple canine OSA cell lines, following 72-hour incubation with varying concentrations of VDC597. All absorbance values were normalized to the control group. Curves represent the results of three experimental replicates. VDC597 concentrations are 0-10 μM. Error bars represent standard deviation.

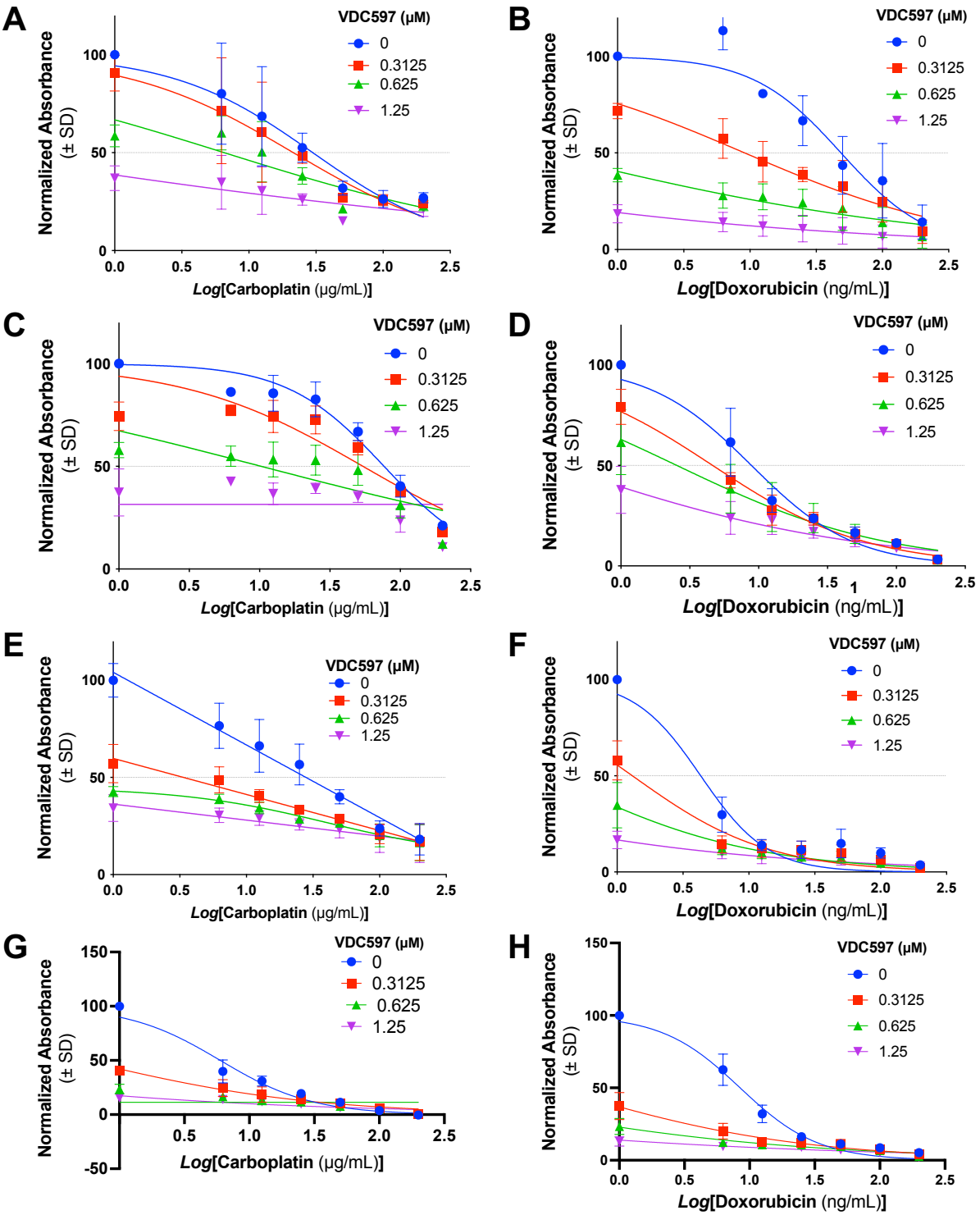

Supplemental Figure S2.05: Growth inhibition assay dose-response curves for varying concentrations of VDC597 (0 = vehicle control) and carboplatin (left column) or doxorubicin (right column). Cell lines in the figure: Abrams (**A-B**); D17 (**C-D**); Gracie (**E-F**); Moresco (**G-H**). Curves represent the results of three experimental replicates. The x-axis indicating carboplatin or doxorubicin is in the Log_{10} scale. VDC597 concentrations are represented in the legends. Error bars represent standard deviation.

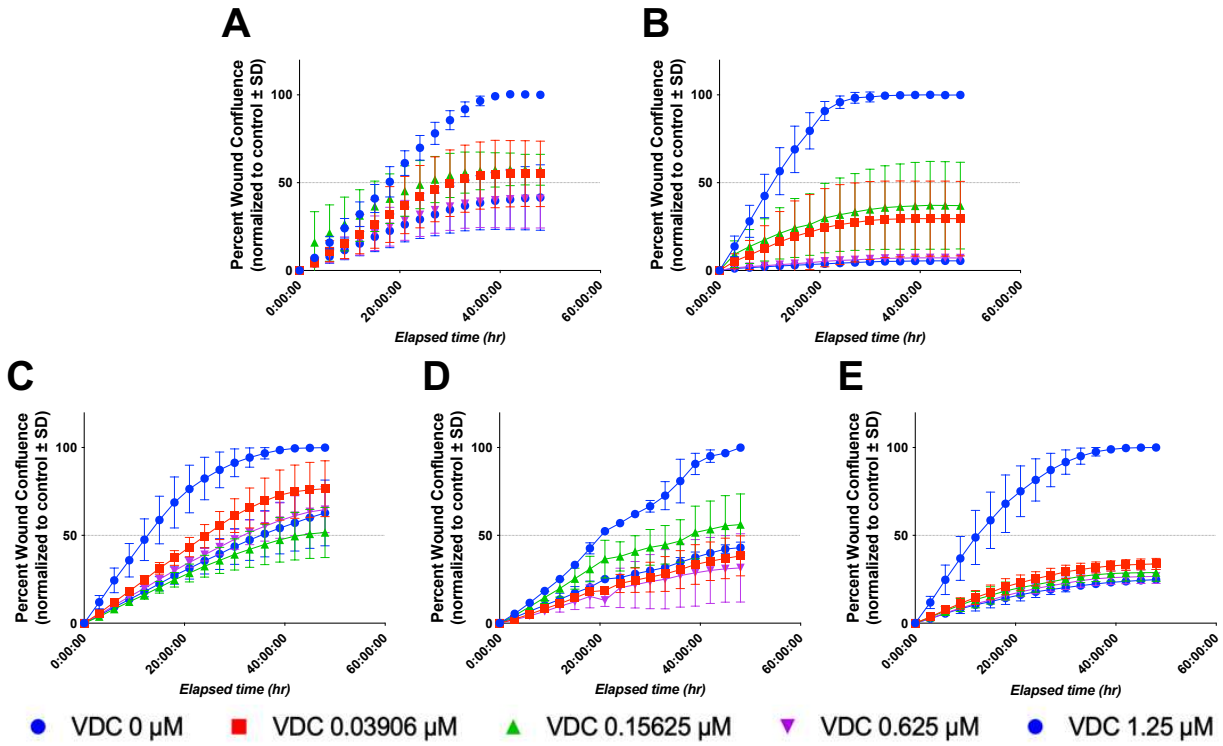

Supplemental Figure S2.06: Scratch assay percent wound confluence curves over a 48-hour period for multiple canine OSA cell lines, with varying concentrations of VDC597 (VDC 0 µM = vehicle control). Cell lines are as follows: (**A**) Abrams; (**B**) Gracie; (**C**) MacKinley; (**D**) Moresco; (**E**) Vogel. Curves are the combined results of 3 experimental replicates. Error bars represent standard deviation.

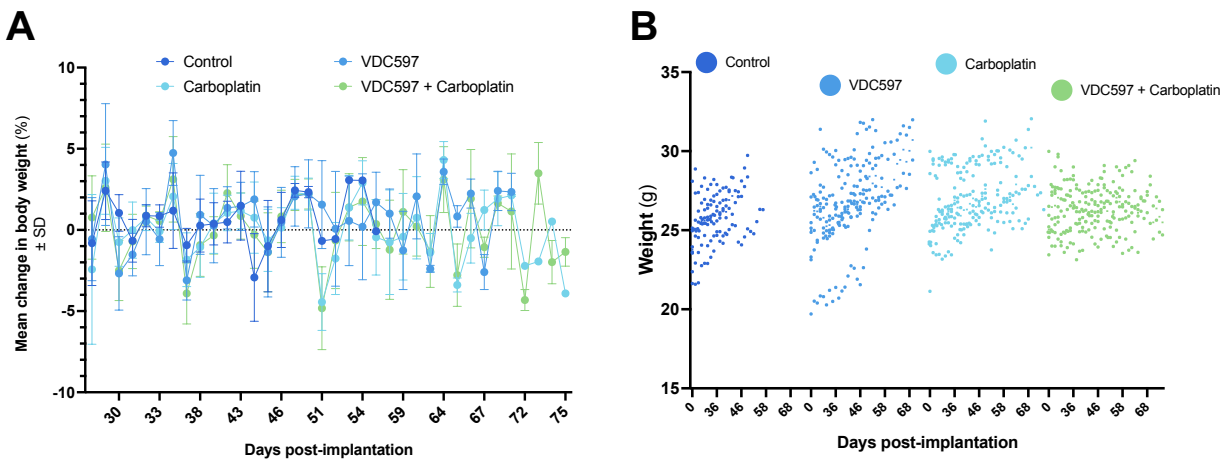

Supplemental Figure S2.07: Mouse weight over time. (**A**) Mean percent change in body weight over time for all treatment groups, demonstrating a fluctuation of the mean between -5% and 5% change over time for each group. (**B**) Scatter plot of individual subject body weight over time per treatment group. Median weights shared a similar upward trend over time and were within 1-2 grams between groups. Listed below are median weights and ranges by group on day 23 (initiation of treatment), day 33 (first euthanasia), and day 47 (last day with n ≥ 3 for all groups).

	Median body weight ± range (g)		
Treatment group	Day 23	Day 33	Day 47
Control	25.01 (28.87, 21.58)	25.97 (28.21, 23.68)	27.76 (28.94, 24.58)
VDC597	26.23 (29.29, 20.52)	25.11 (29.63, 20.50)	27.29 (31.77, 22.63)
Carboplatin	25.25 (29.51, 23.58)	26.26 (29.52, 23.44)	27.15 (30.78, 26.11)
VDC597+Carbo.	26.46 (27.89, 24.00)	26.55 (28.23, 24.20)	26.79 (28.31, 24.43)

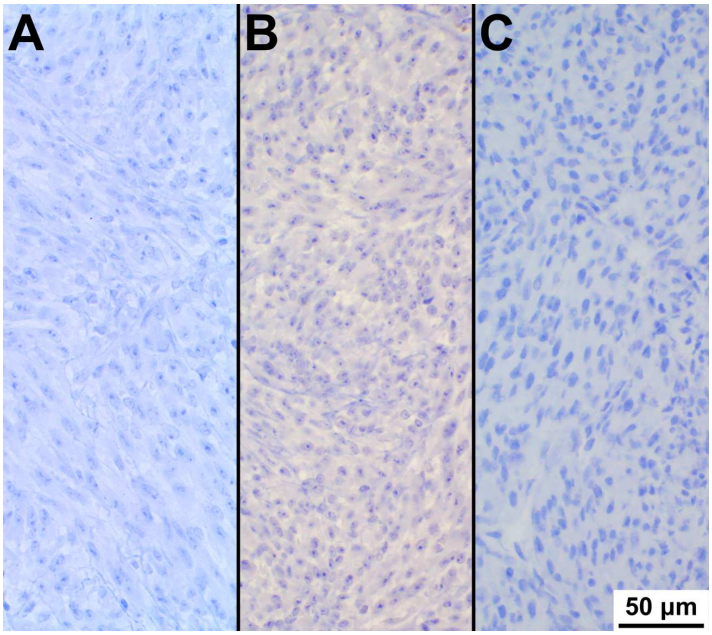

Supplemental Figure S2.08: Isotype control sections. 400x magnification photomicrographs of xenograft canine OSA (Gracie) tumor sections from mice, demonstrating an absence of non-specific binding of immunohistochemical isotype controls for (**A**) Ki67, (**B**) FOXO1, (**C**) pAKT and p4EBP1. DAB chromogen and hematoxylin counterstain.

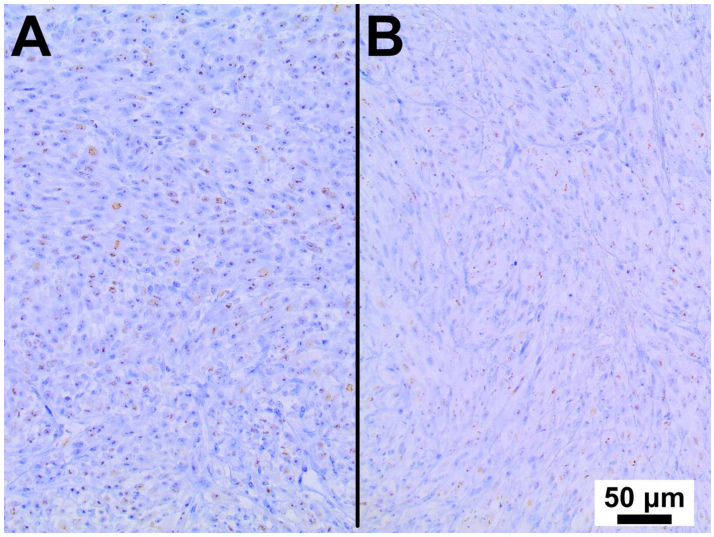

Supplemental Figure S2.09: Ki67 immunolabeling. 200X photomicrographs of xenograft canine OSA (Gracie) tumor sections from mice, demonstrating (**A**) control group section with scattered punctate to diffusely intranuclear Ki67 immunoreactivity, and (**B**) VDC597 treatment group section with rare fine punctate intranuclear Ki67 immunoreactivity. DAB chromogen and hematoxylin counterstain.

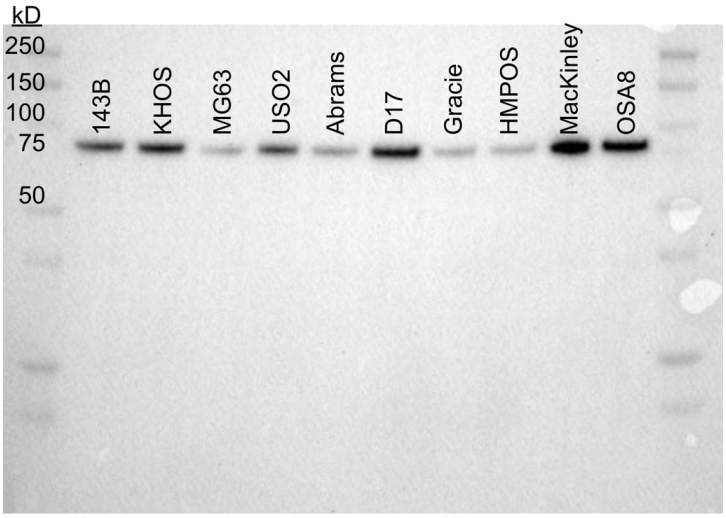

Supplemental Figure S2.10: Western blot for validation of antibody specificity against the forkhead box O1 transcription factor (FOXO1) before immunohistochemical application, with discrete specific bands at the level of the 70 kilodalton (kDa) molecular weight (kDa values are listed on the left). Cell line names are above the corresponding bands.

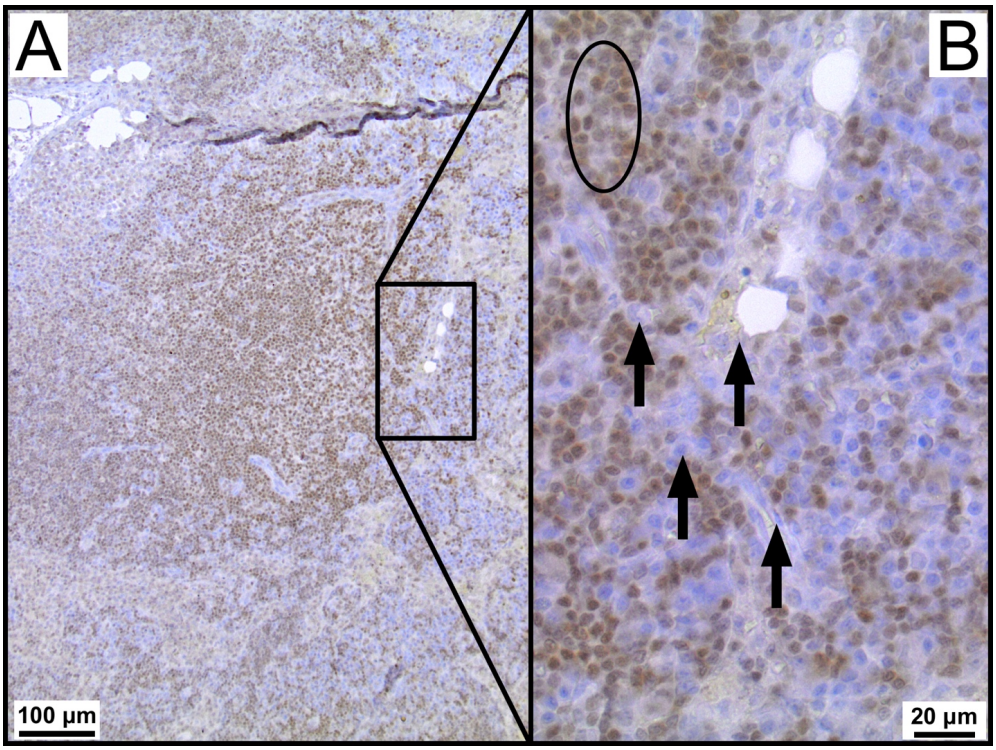

Supplemental Figure S2.11: Immunohistochemical labeling of FOXO1 in a FFPE section of a canine lymph node. (**A**) 100x magnification, demonstrating specific discrete predominantly intranuclear FOXO1 immunoreactivity in lymphocytes, most concentrated in germinal centers, which is consistent with B-cell localization. (**B**) 400x magnification, with FOXO1 immunoreactivity in lymphocytes, consistent with B-cells (circle), and decreased to absent immunolabeling of plasma cells, macrophages and endothelial cells of postcapillary venules. These findings are consistent with the reported role of FOXO1 in B-cells of germinal centers. Immunoreactivity is consistent with expectations of FOXO1 distribution in lymph nodes. DAB chromogen and hematoxylin counterstain.

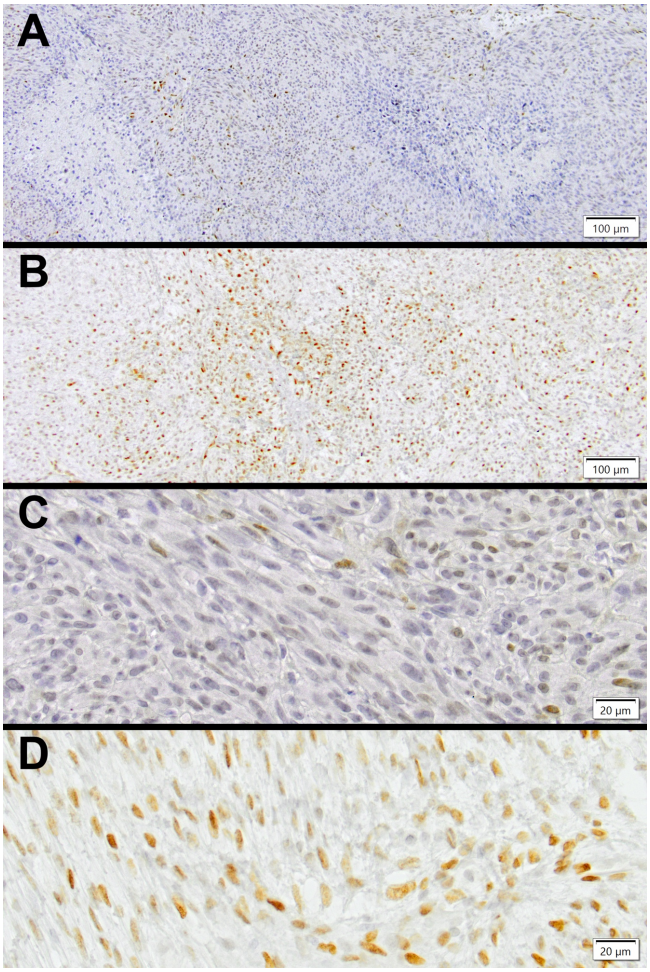

Supplemental Figure S2.12: FOXO1 immunolabeling. Photomicrographs of xenograft canine OSA (Gracie) tumor sections from mice, demonstrating nuclear FOXO1 immunoreactivity. (**A**) 100X magnification of a tumor from the control group with scattered immunopositive nuclei. (**B**) 100X magnification of a tumor from the VDC597 treatment group with greater numbers of immunopositive nuclei. (**C**) 400X magnification of a tumor from the control group with scattered specific discrete moderately immunopositive nuclei. (**D**) 400X magnification of a tumor from the VDC597 treatment group with specific discrete strong intranuclear FOXO1 immunoreactivity. DAB chromogen and hematoxylin counterstain. Note: the difference in hematoxylin intensity is due to hematoxylin solution that had been become weak (VDC597 group), which was replaced with fresh hematoxylin for staining of the control group.

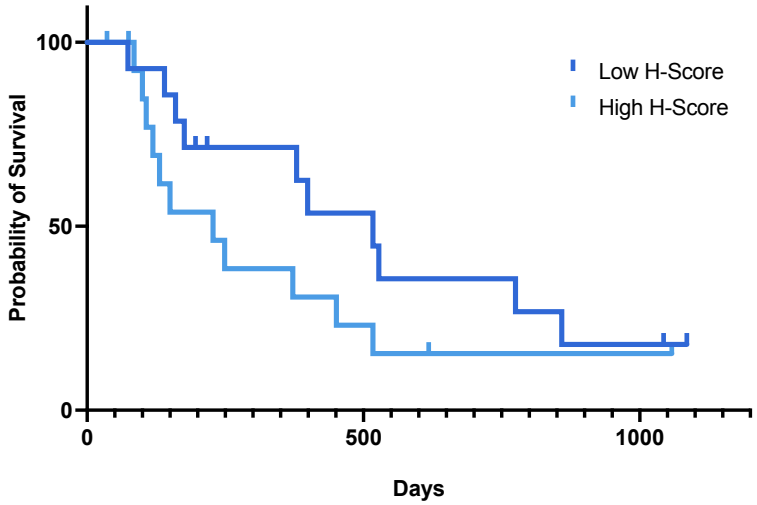

Supplemental Figure S2.13: Kaplan-Meier survival curves for dogs with osteosarcoma, categorized by high or low histochemical score (H-score) for FOXO1 nuclear immunoreactivity. It is noteworthy that the relationship between survival and nuclear FOXO1 immunoreactivity is inverted from the expected correlation, if PI3K-AKT-mTOR signal transduction activity is the primary explanation. This finding is addressed in the discussion section. While a trend is present, these correlations were not found to be statistically significant.

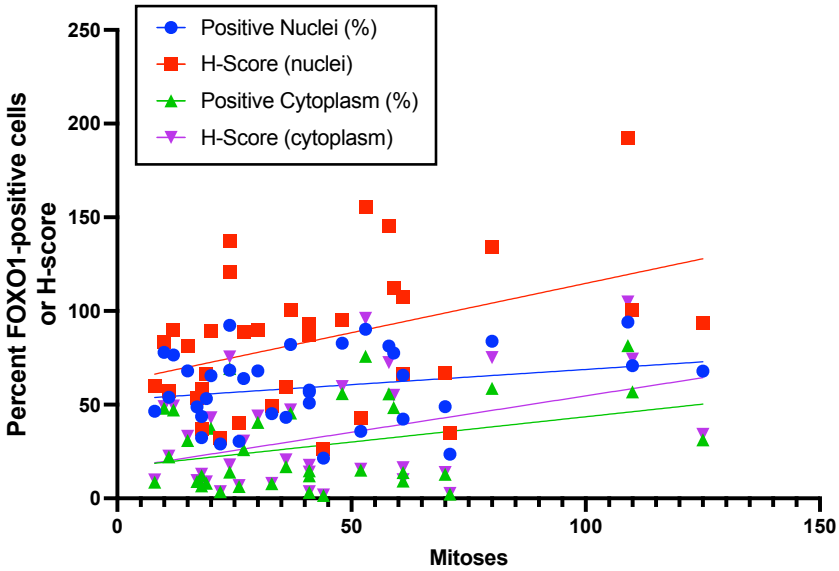

Supplemental Figure S2.14: Simple linear regression, correlating FOXO1 immunoreactivity and number of mitoses per 2.37 mm^2. There was a positive correlation to mitoses for both cytoplasmic and nuclear FOXO1 immunoreactivity.

References

1. Ehrhart NP, Ryan SD, Fan TM. Tumors of the Skeletal System. In: Withrow SJ, Vail DM, Page RL, eds. *Withrow and MacEwen's Small Animal Clinical Oncology*. 5th ed. St. Louis, MO; Elsevier/Saunders; 2013:463–503. https://doi.org/10.1016/B978-1-4377-2362-5.00024-4

2. Thompson KG, Dittmer KE. Tumors of Bone. In: Meuten DJ, ed. *Tumors in Domestic Animals*. 5th ed. Ames, IA; John Wiley & Sons, Inc.; 2017:356–424. https://doi.org/10.1002/9781119181200.ch10

3. Boston SE, Ehrhart NP, Dernell WS, Lafferty M, Withrow SJ. Evaluation of survival time in dogs with stage III osteosarcoma that undergo treatment: 90 cases (1985-2004). *J Am Vet Med Assoc*. 2006;228(12):1905–1908. https://doi.org/10.2460/javma.228.12.1905

4. Saam DE, Liptak JM, Stalker MJ, Chun R. Predictors of outcome in dogs treated with adjuvant carboplatin for appendicular osteosarcoma: 65 cases (1996-2006). *J Am Vet Med Assoc*. 2011;238(2):195–206. https://doi.org/10.2460/javma.238.2.195

5. Spodnick GJ, Berg J, Rand WM, et al. Prognosis for dogs with appendicular osteosarcoma treated by amputation alone: 162 cases (1978-1988). *J Am Vet Med Assoc*. 1992;200(7):995–999. https://doi.org/10.2460/javma.1992.200.07.995

6. Berg J, Weinstein MJ, Schelling SH, Rand WM. Treatment of dogs with osteosarcoma by administration of cisplatin after amputation or limb-sparing surgery: 22 cases (1987-1990). *J Am Vet Med Assoc*. 1992;200(12):2005–2008. https://doi.org/10.2460/javma.1992.200.12.2005

7. Bergman PJ, MacEwen EG, Kurzman ID, et al. Amputation and carboplatin for treatment of dogs with osteosarcoma: 48 cases (1991 to 1993). *J Vet Intern Med*. 1996;10(2):76–81. https://doi.org/10.1111/j.1939-1676.1996.tb02031.x

8. Beck J, Ren L, Huang S, et al. Canine and murine models of osteosarcoma. *Vet Pathol*. 2022;59(3):399–414. https://doi.org/10.1177/03009858221083038

9. Morello E, Martano M, Buracco P. Biology, diagnosis and treatment of canine appendicular osteosarcoma: Similarities and differences with human osteosarcoma. *Vet J*. 2011;189(3):268–277. https://doi.org/10.1016/j.tvjl.2010.08.014

10. Paoloni M, Davis S, Lana S, et al. Canine tumor cross-species genomics uncovers targets linked to osteosarcoma progression. *BMC Genomics*. 2009;10:625. https://doi.org/10.1186/1471-2164-10-625

11. Jiang N, Dai Q, Su X, Fu J, Feng X, Peng J. Role of PI3K/AKT pathway in cancer: the framework of malignant behavior. *Mol Biol Rep*. 2020;47(6):4587–4629. https://doi.org/10.1007/s11033-020-05435-1

12. Kim JH. PIK3CA mutations matter for cancer in dogs. *Res Vet Sci*. 2020;133:39–41. https://doi.org/10.1016/j.rvsc.2020.09.001

13. Perry JA, Kiezun A, Tonzi P, et al. Complementary genomic approaches highlight the PI3K/mTOR pathway as a common vulnerability in osteosarcoma. *Proc Natl Acad Sci U S A*. 2014;111(51):E5564–E5573. https://doi.org/10.1073/pnas.1419260111

14. Das S, Idate R, Cronise KE, Gustafson DL, Duval DL. Identifying candidate druggable targets in canine cancer cell lines using whole-exome sequencing. *Mol Cancer Ther*. 2019;18(8):1460–1471. https://doi.org/10.1158/1535-7163.Mct-18-1346

15. Wang K, Zhuang Y, Liu C, Li Y. Inhibition of c-Met activation sensitizes osteosarcoma cells to cisplatin via suppression of the PI3K-Akt signaling. *Arch Biochem Biophys*. 2012;526(1):38–43. https://doi.org/10.1016/j.abb.2012.07.003

16. Chu S, Skidmore ZL, Kunisaki J, et al. Unraveling the chaotic genomic landscape of primary and metastatic canine appendicular osteosarcoma with current sequencing technologies and bioinformatic approaches. *PLoS One*. 2021;16(2):e0246443–e0246443. https://doi.org/10.1371/journal.pone.0246443

17. Fieten H, Spee B, Ijzer J, Kik MJ, Penning LC, Kirpensteijn J. Expression of hepatocyte growth factor and the proto-oncogenic receptor c-Met in canine osteosarcoma. *Vet Pathol*. 2009;46(5):869–877. https://doi.org/10.1354/vp.08-VP-0155-F-FL

18. Maniscalco L, Iussich S, Morello E, et al. Increased expression of insulin-like growth factor-1 receptor is correlated with worse survival in canine appendicular osteosarcoma. *Vet J*. 2015;205(2):272–280. https://doi.org/10.1016/j.tvjl.2014.09.005

19. Megquier K, Turner-Maier J, Morrill K, et al. The genomic landscape of canine osteosarcoma cell lines reveals conserved structural complexity and pathway

alterations. *PLoS One*. 2022;17(9):e0274383–e0274383. https://doi.org/10.1371/journal.pone.0274383

20. Meuten TK, Dean GA, Thamm DH. Review: The PI3K-AKT-mTOR signal transduction pathway in canine cancer. *Vet Pathol*. 2023;6(3)(3):339–356. https://doi.org/10.1177/03009858231207021

21. Paoloni MC, Mazcko C, Fox E, et al. Rapamycin pharmacokinetic and pharmacodynamic relationships in osteosarcoma: a comparative oncology study in dogs. *PLoS One*. 2010;5(6):e11013–e11013. https://doi.org/10.1371/journal.pone.0011013

22. Gordon IK, Ye F, Kent MS. Evaluation of the mammalian target of rapamycin pathway and the effect of rapamycin on target expression and cellular proliferation in osteosarcoma cells from dogs. *Am J Vet Res*. 2008;69(8):1079–1084. https://doi.org/10.2460/ajvr.69.8.1079

23. LeBlanc AK, Mazcko CN, Cherukuri A, et al. Adjuvant sirolimus does not improve outcome in pet dogs receiving standard-of-care therapy for appendicular osteosarcoma: a prospective, randomized trial of 324 dogs. *Clin Cancer Res*. 2021;27(11):3005–3016. https://doi.org/10.1158/1078-0432.CCR-21-0315

24. O'Reilly KE, Rojo F, She Q-B, et al. mTOR inhibition induces upstream receptor tyrosine kinase signaling and activates Akt. *Cancer Res*. 2006;66(3):1500–1508. https://doi.org/10.1158/0008-5472.CAN-05-2925

25. Rodrik-Outmezguine VS, Chandarlapaty S, Pagano NC, et al. mTOR kinase inhibition causes feedback-dependent biphasic regulation of AKT signaling. *Cancer Discov*. 2011;1(3):248–259. https://doi.org/10.1158/2159-8290.Cd-11-0085

26. Ryu S, Park S, Lim W, Song G. Effects of luteolin on canine osteosarcoma: suppression of cell proliferation and synergy with cisplatin. *J Cell Physiol*. 2018;234(6):9504–9514. https://doi.org/10.1002/jcp.27638

27. Ryu S, Park S, Lim W, Song G. Quercetin augments apoptosis of canine osteosarcoma cells by disrupting mitochondria membrane potential and regulating PKB and MAPK signal transduction. *J Cell Biochem*. 2019;120(10):17449–17458. https://doi.org/10.1002/jcb.29009

28. Schwartz S, Wongvipat J, Trigwell CB, et al. Feedback suppression of PI3Kα signaling in PTEN-mutated tumors is relieved by selective inhibition of PI3Kβ. *Cancer Cell*. 2015;27(1):109–122. https://doi.org/10.1016/j.ccell.2014.11.008

29. Mi W, Ye Q, Liu S, She QB. AKT inhibition overcomes rapamycin resistance by enhancing the repressive function of PRAS40 on mTORC1/4E-BP1 axis. *Oncotarget*. 2015;6(16):13962–13977. https://doi.org/10.18632/oncotarget.3920

30. Gobin B, Battaglia S, Lanel R, et al. NVP-BEZ235, a dual PI3K/mTOR inhibitor, inhibits osteosarcoma cell proliferation and tumor development in vivo with an improved survival rate. *Cancer Lett*. 2014;344(2):291–298. https://doi.org/10.1016/j.canlet.2013.11.017

31. Gupte A, Baker EK, Wan SS, et al. Systematic Screening Identifies Dual PI3K and mTOR Inhibition as a Conserved Therapeutic Vulnerability in Osteosarcoma. *Clin Cancer Res*. 2015;21(14):3216–3229. https://doi.org/10.1158/1078-0432.Ccr-14-3026

32. Huang JC, Cui ZF, Chen SM, et al. NVP-BEZ235 synergizes cisplatin sensitivity in osteosarcoma. *Oncotarget*. 2018;9(12):10483–10496. https://doi.org/10.18632/oncotarget.23711

33. Fowles JS, Dailey DD, Gustafson DL, Thamm DH, Duval DL. The Flint Animal Cancer Center (FACC) Canine Tumour Cell Line Panel: a resource for veterinary drug discovery, comparative oncology and translational medicine. *Vet Comp Oncol*. 2017;15(2):481–492. https://doi.org/https://doi.org/10.1111/vco.12192

34. O'Donoghue LE, Rivest JP, Duval DL. Polymerase chain reaction-based species verification and microsatellite analysis for canine cell line validation. *J Vet Diagn Invest*. 2011;23(4):780–5. https://doi.org/10.1177/1040638711408064

35. Schneider CA, Rasband WS, Eliceiri KW. NIH Image to ImageJ: 25 years of image analysis. *Nature Methods*. 2012;9(7):671–675. https://doi.org/10.1038/nmeth.2089

36. Ferreira T, Rasband W. ImageJ user guide. *USA: National Institutes of Health*. 2011;IJ 1.46r

37. National Institutes of Health. ImageJ (Version 1.54m; Java 1.8.0_172 (64bit)) [computer software]. 2023. http://imagej.org

38. BioTek Instruments. Gen5 (Version 3.11.19) [computer software]. Agilent BioTek; 2019. https://www.agilent.com/

39. Chou TC, Talalay P. Quantitative analysis of dose-effect relationships: the combined effects of multiple drugs or enzyme inhibitors. *Adv Enzyme Regul*. 1984;22:27–55. https://doi.org/10.1016/0065-2571(84)90007-4

40. Chou T-C, Martin N. CompuSyn For Drug Combinations User's Guide. A computer program for quantitation of synergism and Antagonism in drug combinations, and the determination of IC50 and ED50 values. Paramus, NJ: ComboSyn, Inc.; 2004. p. 1–65.

41. Chou TC, Martin N. CompuSyn (Version 1.0) [computer software]. ComboSyn Inc.; 2014. https://www.combosyn.com/

42. Sartorius BioAnalytical Instruments Inc. Incucyte SX5 Controller and GUI (Version 2023A Rev2) [computer software]. 2023. https://www.sartorius.com/

43. Sartorius BioAnalytical Instruments Inc. Incucyte ZOOM Controller and GUI (Version 2015A Rev1) [computer software]. 2015. https://www.sartorius.com/

44. Veronese SM, Gambacorta M, Gottardi O, Scanzi F, Ferrari M, Lampertico P. Proliferation index as a prognostic marker in breast cancer. *Cancer*. 1993;71(12):3926–3931. https://doi.org/10.1002/1097-0142(19930615)71:12<3926::aid-cncr2820711221>3.0.co;2-2

45. Gustafson DL, Collins KP, Fowles JS, et al. Prospective clinical trial testing COXEN-based gene expression models of chemosensitivity in dogs with spontaneous osteosarcoma. *Cancer Chemother Pharmacol*. 2021;88(4):699–712. https://doi.org/10.1007/s00280-021-04325-y

46. Dominguez-Sola D, Kung J, Holmes AB, et al. The FOXO1 Transcription Factor Instructs the Germinal Center Dark Zone Program. *Immunity*. 2015;43(6):1064–74. https://doi.org/10.1016/j.immuni.2015.10.015

47. Sander S, Chu VT, Yasuda T, et al. PI3 Kinase and FOXO1 Transcription Factor Activity Differentially Control B Cells in the Germinal Center Light and Dark Zones. *Immunity*. 2015;43(6):1075–86. https://doi.org/10.1016/j.immuni.2015.10.021

48. Olympus Corporation. cellSens (Version 1.17) [computer software]. Evident Scientific; 2017. www.olympus-lifescience.com.

49. Visiopharm A/S. Visiopharm Software (Version 2023.09.7.16662 x64) [computer software]. 2023. www.visiopharm.com

50. Ronneberger O, Fischer P, Brox T. U-Net: Convolutional Networks for Biomedical Image Segmentation. Springer International Publishing; 2015:234–241.

51. Terven J, Cordova-Esparza DM, Ramirez-Pedraza A, Chavez-Urbiola EA. Loss functions and metrics in deep learning. A review. *arXiv preprint arXiv:230702694*. 2023;

52. Kirpensteijn J, Kik M, Rutteman GR, Teske E. Prognostic significance of a new histologic grading system for canine osteosarcoma. *Vet Pathol*. 2002;39(2):240–246. https://doi.org/10.1354/vp.39-2-240

53. Straw RC, Powers BE, Klausner J, et al. Canine mandibular osteosarcoma: 51 cases (1980-1992). *J Am Anim Hosp Assoc*. 1996;32(3):257–262. https://doi.org/10.5326/15473317-32-3-257

54. GraphPad Software LLC. GraphPad Prism (Version 10.4.1 (532)) [computer software]. 2024. https://www.graphpad.com/

55. Garzotto CK, Berg J, Hoffmann WE, Rand WM. Prognostic significance of serum alkaline phosphatase activity in canine appendicular osteosarcoma. *J Vet Intern Med*. 2000;14(6):587–592. https://doi.org/10.1892/0891-6640(2000)014<0587:psosap>2.3.co;2

56. Sottnik JL, Rao S, Lafferty MH, et al. Association of blood monocyte and lymphocyte count and disease-free interval in dogs with osteosarcoma. *J Vet Intern Med*. 2010;24(6):1439–1444. https://doi.org/10.1111/j.1939-1676.2010.0591.x

57. Thamm DH, Weishaar K, Meuten TK, Gustafson DL. Phase-I clinical trial of the dual PI3K/mTOR inhibitor VDC-597 in dogs with spontaneous neoplasia. 2018:

58. Boerman I, Selvarajah GT, Nielen M, Kirpensteijn J. Prognostic factors in canine appendicular osteosarcoma - a meta-analysis. *BMC Vet Res*. 2012;8:56. https://doi.org/10.1186/1746-6148-8-56

59. Miyanishi K, Nururrozi A, Igase M, et al. Activation of the Akt signalling pathway as a prognostic indicator in canine soft tissue sarcoma. *J Comp Pathol*. 2023;206:44–52. https://doi.org/10.1016/j.jcpa.2023.08.007

60. Chen C, Guo Y, Huang Q, et al. PI3K inhibitor impairs tumor progression and enhances sensitivity to anlotinib in anlotinib-resistant osteosarcoma. *Cancer Lett*. 2022;536:215660. https://doi.org/10.1016/j.canlet.2022.215660

61. Jia N, Che X, Jiang Y, Zhu M, Yang T, Feng W. Synergistic effects of a combined treatment of PI3K/mTOR dual inhibitor LY3023414 and carboplatin on human endometrial carcinoma. *Gynecol Oncol*. 2021;162(3):788–796. https://doi.org/10.1016/j.ygyno.2021.06.015

62. Li J, Wang X, Ma C, et al. Dual PI3K/mTOR inhibitor NVP-BEZ235 decreases the proliferation of doxorubicin-resistant K562 cells. *Mol Med Rep*. 2021;23:301. https://doi.org/10.3892/mmr.2021.11940

63. Liu H, Zang C, Schefe JH, et al. The mTOR inhibitor RAD001 sensitizes tumor cells to the cytotoxic effect of carboplatin in breast cancer in vitro. *Anticancer Res*. 2011;31(9):2713–2722.

64. Shariati M, Meric-Bernstam F. Targeting AKT for cancer therapy. *Expert Opin Investig Drugs*. 2019;28(11):977–988. https://doi.org/10.1080/13543784.2019.1676726

65. Xie G, Wang Z, Chen Y, et al. Dual blocking of PI3K and mTOR signaling by NVP-BEZ235 inhibits proliferation in cervical carcinoma cells and enhances therapeutic response. *Cancer Lett*. 2017;388:12–20. https://doi.org/10.1016/j.canlet.2016.11.024

66. Pyuen AA, Meuten T, Rose BJ, Thamm DH. In vitro effects of PI3K/mTOR inhibition in canine hemangiosarcoma. *PLoS One*. 2018;13(7):e0200634–e0200634. https://doi.org/10.1371/journal.pone.0200634

67. Chen D, Lei C, Liu W, et al. Reduction-responsive nucleic acid nanocarrier-mediated miR-22 inhibition of PI3K/AKT pathway for the treatment of patient-derived tumor xenograft osteosarcoma. *Bioact Mater*. 2023;28:376–385. https://doi.org/10.1016/j.bioactmat.2023.05.012

68. Hjelmeland AB, Lattimore KP, Fee BE, et al. The combination of novel low molecular weight inhibitors of RAF (LBT613) and target of rapamycin (RAD001)

decreases glioma proliferation and invasion. *Mol Cancer Ther*. 2007;6(9):2449–2457. https://doi.org/10.1158/1535-7163.Mct-07-0155

69. Sadrkhanloo M, Paskeh MDA, Hashemi M, et al. New emerging targets in osteosarcoma therapy: PTEN and PI3K/Akt crosstalk in carcinogenesis. *Pathol Res Pract*. 2023;251:154902. https://doi.org/10.1016/j.prp.2023.154902

70. Sakuma H, Tomiyasu H, Tani A, et al. Antitumor effects of inhibitors of ERK and Akt pathways in canine histiocytic sarcoma cell lines. *Vet J*. 2024;308:106264. https://doi.org/10.1016/j.tvjl.2024.106264

71. Wei Z, Xia K, Zheng D, Gong C, Guo W. RILP inhibits tumor progression in osteosarcoma via Grb10-mediated inhibition of the PI3K/AKT/mTOR pathway. *Mol Med*. 2023;29(1):133. https://doi.org/10.1186/s10020-023-00722-6

72. Bouck N, Stellmach V, Hsu SC. How tumors become angiogenic. *Adv Cancer Res*. 1996;69:135–174. https://doi.org/10.1016/s0065-230x(08)60862-3

73. Gimbrone MA, Jr., Leapman SB, Cotran RS, Folkman J. Tumor dormancy in vivo by prevention of neovascularization. *J Exp Med*. 1972;136(2):261–276. https://doi.org/10.1084/jem.136.2.261

74. Hanahan D, Folkman J. Patterns and emerging mechanisms of the angiogenic switch during tumorigenesis. *Cell*. 1996;86(3):353–364. https://doi.org/10.1016/s0092-8674(00)80108-7

75. Karar J, Maity A. PI3K/AKT/mTOR Pathway in Angiogenesis. *Front Mol Neurosci*. 2011;4:doi: 10.3389/fnmol.2011.00051. https://doi.org/10.3389/fnmol.2011.00051

76. Moschetta MG, Leonel C, Maschio-Signorini LB, et al. Evaluation of Angiogenesis Process after Metformin and LY294002 Treatment in Mammary Tumor. *Anticancer Agents Med Chem*. 2019;19(5):655–666. https://doi.org/10.2174/1871520619666181218164050

77. Poalelungi DG, Neagu AI, Fulga A, et al. Revolutionizing Pathology with Artificial Intelligence: Innovations in Immunohistochemistry. *J Pers Med*. 2024;14(7):693. https://doi.org/10.3390/jpm14070693

78. Acs B, Rantalainen M, Hartman J. Artificial intelligence as the next step towards precision pathology. *J Intern Med*. 2020;288(1):62–81. https://doi.org/10.1111/joim.13030

79. Xing YQ, Li A, Yang Y, Li XX, Zhang LN, Guo HC. The regulation of FOXO1 and its role in disease progression. *Life Sci*. 2018;193:124–131. https://doi.org/10.1016/j.lfs.2017.11.030

80. Breitbach JT, Louke DS, Tobin SJ, Watts MR, Davies AE, Fenger JM. The selective inhibitor of nuclear export (SINE) verdinexor exhibits biologic activity against canine osteosarcoma cell lines. *Vet Comp Oncol*. 2021;19(2):362–373. https://doi.org/10.1111/vco.12680

CHAPTER 3: *IN VITRO* EFFECTS OF THE PI3K/MTOR DUAL-INHIBITOR, VDC597, IN CANINE LYMPHOMA AND LEUKEMIA[iv]

Overview

Canine hematopoietic tumors are among the most common tumors in dogs and advancements in treatment are necessary to improve outcomes. The phosphatidylinositol-4,5-bisphosphate 3-kinase (PI3K), AKT serine/threonine kinase (AKT), mechanistic target of rapamycin (mTOR) signaling pathway is frequently dysregulated in canine hematopoietic tumors and contributes to poorer outcomes. Targeted signal transduction inhibition offers a potentially beneficial avenue for improving treatment of these tumors. The purpose of this study was to investigate the efficacy of a PI3K/mTOR dual-inhibitor, VDC597, against canine lymphoma and leukemia cells *in vitro* and to immunohistochemically evaluate this signaling pathway in spontaneous canine B-cell lymphoma. Our results demonstrate that VDC597 inhibited PI3K/AKT/mTOR signal transduction, reduced cell viability and proliferation, promoted cell death, and inhibited angiogenic factor production in a dose dependent manner in canine lymphoma/leukemia cells *in vitro*. Expression of phosphorylated proteins indicating pathway activation was variable in samples of spontaneous canine B-cell lymphoma. In these samples, phospho-protein expression correlated in the hypothesized manner to two prognostic indicators, but not to outcome data. Major histocompatibility complex class II expression and post-treatment relapse status were

[iv] Submitted for publication:
Meuten T, Farrell KB, Rose BJ, Brill SA, Brady RV, Schlein LJ, Thamm DH. in vitro effects of the PI3K/mTOR dual-inhibitor, VDC597, in canine lymphoma and leukemia. [Article under review, *BMC Veterinary Oncology*, 2026]

correlated to phosphorylated AKT and phosphorylated eukaryotic translation initiation factor 4E-binding protein 1 expression, respectively. These results suggest that PI3K/mTOR inhibition may be a useful anti-cancer strategy for the treatment of canine lymphoma and leukemia. However, immunohistochemical results suggest that signaling pathway activation is variable in canine B-cell lymphoma and that more research is needed to elucidate the prognostic role of pathway activation in this tumor type.

Introduction

Lymphoma (LSA) represents one of the most common tumor types in dogs, accounting for 7-24% of all canine neoplasms and 80% of canine hematopoietic tumors, with many subtypes and heterogeneous biological behavior.[1,2] Approximately 60-70% of canine LSA diagnoses are B-cell lymphoma (BCL) and 30-40% are T-cell lymphoma (TCL), with diffuse large B-cell lymphoma (DLBCL) comprising 50% of cases.[3] Canine DLBCL is also a valuable spontaneous animal model for non-Hodgkin lymphoma (NHL) in humans.[4]

Unlike LSA, the true incidence of canine chronic lymphocytic leukemia (CLL) is not accurately known, due in part to the difficulty in differentiating it from stage V LSA. In dogs, there are three primary types of CLL differentiated by immunophenotype: T-CLL, which is the most common; B-CLL; and atypical CLL. Treatment of canine CLL rarely achieves remission due to the indolent nature of the disease. The current standard of care revolves around palliative goals, and includes chlorambucil and prednisone, with vincristine or cyclophosphamide for refractory cases.[1] While standard of veterinary care in chemotherapeutic protocols for the treatment of LSA—including cyclophosphamide,

doxorubicin, vincristine, and prednisone (CHOP)—have been successful in inducing short-term responses to treatment, there has not been significant progress in recent years, beyond a 12-month median survival time and 20-25% 2-year survival rates for LSA cases, and advances in chemotherapy have largely centered on modifications of the CHOP protocol.[1,5] These modifications are primarily applied to rescue protocols following relapse, which often result in lower response rates over shorter durations than the initial treatment from which the patient relapsed.[6]

Despite the slow progression of advances in treatment for canine LSA and CLL, there has been expansion in our understanding of the mutations and aberrations in signal transduction pathways over the last decade, which has allowed for investigation of targeted signal transduction inhibitors. Mutations and aberrant activation of the phosphatidylinositol-3 kinase, AKT serine/threonine kinase, mechanistic target of rapamycin (PI3K-AKT-mTOR) pathway have been reported in multiple canine tumor types, including lymphoma.[7] The similarities between human and canine BCL in mutation status and PI3K-AKT-mTOR signaling aberrations with prognostic significance for humans have helped to motivate further investigation of the mutations involved in canine BCL. Such studies have found mutations in *MTOR*, *PTEN*, *PIK3CG*, *PIK3R1*, *PLCB4* and *INPP4B*, all of which are involved in of PI3K-AKT-mTOR signal transduction.[7-9] Epigenetic and transcriptomic studies have also found increased enrichment and expression in genes encoding upstream regulators and components of the PI3K-AKT-mTOR pathway in canine DLBCL.[7,10-12] As is the case in human TCL, canine TCL exhibits genetic and transcriptomic alterations implicated in PI3K-AKT-

mTOR signal transduction dysregulation, including *MTOR* and *PTEN*.[4,13] Additionally, *in vitro* inhibition of AKT has been found to induce cell death in canine TCL cell lines.[14]

Resistance to chemotherapy is commonly encountered in LSA, as with other tumor types. Numerous studies have examined mutations and alterations in expression of genes involved in chemotherapeutic resistance, modifications in CHOP protocols for chemoresistant cases, and the addition of various lymphocytolytic agents and targeted inhibitors of commonly altered signal transduction pathways for LSA cases that are refractory to treatment, relapsed, or chemotherapy resistant.[6,15,16] The role of PI3K-AKT-mTOR signaling in chemotherapy resistance has been well documented in other canine tumors, and is being investigated to a greater degree in canine LSA. At this juncture, there are conflicting findings regarding the correlation between chemotherapy resistance and mutations or expression alteration of the PI3K-AKT-mTOR pathway, yet studies involving the use of pathway inhibitors has indicated potentially beneficial avenues for intervention.[17-19] Investigation of new PI3K-AKT-mTOR pathway inhibitors for the treatment of in human and canine LSA is ongoing and indicates potentially benefit of pathway inhibition in these tumors.[20,21]

The findings outlined above highlight the indication for further examination of the potential efficacy of PI3K-AKT-mTOR pathway inhibitors for canine LSA. Indeed, there is presently good *in vitro* and *in vivo* evidence for the benefits of PI3K-AKT-mTOR signaling inhibitors in canine LSA for their capacity to reduce neoplastic survival and proliferation as well as synergistic effects when used in combination with other targeted inhibitors and sensitization to other targeted inhibitors and chemotherapeutic drugs.[7,10,22,23] Due to the role in B cell development and involvement in PI3K activation

in B cells, Bruton's tyrosine kinase (BTK) inhibitors and PI3K inhibitors have been examined in canine DLBCL cells *in vitro*, and *in vivo*, respectively.[10,23] Specifically, inhibition of PI3Kδ in BCL and TCL has been examined, demonstrating AKT suppression *in vitro* and a response rate of 62-77% in Phase I and II clinical trials, predominated by partial responses.[24] The authors state that the observed partial responses in these clinical trials are due to development of resistance to PI3K inhibition and hypothesize that it is due in part to well-known feedback mechanisms within the PI3K-AKT-mTOR signaling pathway.[7,24] For a more complete and durable blockade of signal transduction in the face of such feedback mechanisms, multi-nodal inhibition is beneficial. VDC597 is an inhibitor of PI3K, mTORC1, and mTORC2, which may be useful due to the inhibition at multiple points involved in feedback along this pathway. The structure of VDC597 and a diagram of the PI3K-AKT-mTOR pathway and points of inhibition can be found in our previous publication evaluating the efficacy of VDC597 against canine osteosarcoma.[25]

The purpose of the present study was to investigate the *in vitro* effects of VDC597 on canine BCL and CLL cell lines, which have been previously documented to have either mutations related to PI3K-AKT-mTOR signaling or constitutively express phosphorylated AKT (pAKT).[9] Cell based assays were used to evaluate the effect of VDC597 in reduction of neoplastic cell viability, induction of cell death, and inhibition of angiogenic paracrine signaling. Western blots and immunohistochemistry (IHC) were used to examine the efficacy of VDC597 for the inhibition of PI3K-AKT-mTOR pathway activity, by evaluating the phosphorylation of AKT and eukaryotic translation initiation factor 4E binding protein 1 (4EBP1), a downstream target of mTORC1, as indicators of

signal transduction. The degree of AKT and 4EBP1 phosphorylation was also evaluated by IHC in patient derived samples of spontaneous canine BCL to examine for correlation to outcome data and the prognostic indicators of World Health Organization (WHO) tumor stage, substage, MHC-II expression, and specific immunophenotypic markers.[26-28]

Materials and Methods

Reagents

VDC597, a dual-inhibitor of PI3K and mechanistic target of rapamycin complexes 1 and 2 (mTORC1/2), was provided by VetDC Inc. (Fort Collins, CO), as a dry powder (for structure and points of inhibition, see **Figure 2.01** in Chapter 2). Stock solution aliquots were prepared in sterile dimethylsulfoxide (DMSO) for *in vitro* experiments. United States Pharmacopeia (USP) doxorubicin, dexamethasone, and vincristine were obtained from commercial vendors through the Colorado State University (CSU) Veterinary Teaching Hospital pharmacy. Antibodies and concentrations used in the experiments reported herein are outlined in **Table A1** in the Appendix.

Cell Lines and Conditions

Lymphoma (LSA) and chronic lymphocytic leukemia (CLL) cell lines were established from dogs with spontaneously occurring LSA and CLL. Cell lines were confirmed to be of canine origin and unique by microsatellite PCR and a multiplex species-specific PCR technique, as previously described.[29] The canine BCL cell line, 1771, was sourced from Dr. K. Ann Jeglum at the University of Pennsylvania and the

canine leukemia cell line, CLL1390, was sourced from Dr. Peter Moore at the University of California, Davis. Cell lines were maintained in Roswell Park Memorial Institute 1640 culture medium (RPMI) (Corning, Henderson, VA), which was supplemented with nonessential amino acids, 1x minimum essential medium vitamin solution (Corning), 2 mM L-glutamine (Corning), 1 mM sodium pyruvate (Corning), and 10% heat-inactivated fetal bovine serum (Peak, Wellington, CO) to make a complete (C10) RPMI culture medium. Cells were incubated in standard conditions (37 °C and 5% CO_2 in a humidified atmosphere) and passaged in suspension using density gradient centrifugation. All *in vitro* protocols below were replicated in at least three independent experiments for each cell line.

Viral Transduction of Cell Lines

Cell lines were virally transduced, according to the manufacturer's directions, with Incucyte® NucLight™ Red Lentivirus Reagent (Essen Bioscience, Ann Arbor, MI), for nuclear labeling of cells with a red fluorescent protein to facilitate real-time microscopy. Puromycin selection was used to isolate the transduced population.

Cell Lysates

Cells were grown to 70% confluence in C10 RPMI under standard conditions and were collected and washed with phosphate buffered saline (PBS). Cells were then resuspended and incubated for 24 hours in C10 RPMI with DMSO vehicle or varying concentrations of VDC597 (0, 0.2, 0.5, and 1.0 μM). For examination of dose-response, cells were incubated for 24 hours under these conditions before lysate collection. To

examine inhibition of pathway activity over time, cells were treated with 1 μM VDC597 or DMSO vehicle control and incubated for varying times (0.5–24 hours) before lysate collection.

At the time of lysate collection and preparation, cells were collected and washed with PBS, resuspended in 1 mL PBS, transferred to 1.7 mL Eppendorf tubes, centrifuged at 400xG for 5 minutes, decanted, and lysed with mammalian protein extraction reagent (Thermo Fisher Scientific) containing 1 mM activated sodium orthovanadate (Sigma-Aldrich, St. Louis, MO), 1 mM phenylmethylsulfonyl fluoride (Sigma-Aldrich) solubilized in isopropanol, and cOmplete™ Mini protease inhibitor cocktail tablet (Roche Diagnostics, Mannheim, Germany) at the manufacturer's recommended concentration. Lysed cells were homogenized using a 25-gauge needle, then centrifuged at 1600xG for 15 minutes at 4 °C, and supernatants were aliquoted and frozen at -20 °C for short term storage (or at -80 °C for storage of up to 6 months). Total protein concentration was determined using a bicinchoninic acid protein assay kit (Thermo Fisher Scientific) according to manufacturer instructions.

Western Blot Analysis

The degree of activation of the PI3K-AKT-mTOR pathway was evaluated by western immunoblot analysis of pAKT and p4EBP1 following treatment with VDC597. Cell lysates were diluted with lysis buffer as indicated by bicinchoninic acid assay results to reach approximately the same concentration for all samples, not exceeding 20 μg protein per 17 μL total volume. Sodium dodecyl sulfate loading dye was added to lysates to reach a total volume of 20 μL per sample. Cell lysate samples and Precision

Plus Protein™ Kaleidoscope™ ladder (Bio-Rad Laboratories, Hercules, CA) were heated to 95°C and then run on a 1.0–1.5 mm, 4-12% NuPAGE™ bis-tris precast gel (Invitrogen, Carlsbad, CA) in a NOVEX Xcell SureLock™ Mini-Cell System (Invitrogen) and transferred to a polyvinylidene difluoride membrane (Bio-Rad). The membrane was then blocked using SuperBlock™ blocking buffer with Tween 20 (T20) (Thermo Fisher Scientific). Membranes were cut into sections by protein size for primary antibody incubation. Primary antibodies were diluted in SuperBlock™ T20 and applied to membranes to be incubated overnight at 4°C. Antibodies and concentrations are listed in **Table A1**. Membranes were then washed using TBST and incubated with goat anti-rabbit horseradish peroxidase (HRP) conjugated secondary antibody (Thermo Fisher Scientific) diluted in SuperBlock™ T20 for 1 hour at room temperature. They were then developed using SuperSignal™ West Pico or SuperSignal™ West Femto chemiluminescent substrate (Thermo Fisher Scientific) and bands visualized using a ChemiDoc XRS+ System (Bio-Rad). Densitometric image analysis of western blots, including background subtraction and band intensity measurements, was performed using Image Lab software, following manufacturer instructions.[30] For each image analyzed: all lane widths and band measurement regions were set to the same size; all background subtractions used the same subtraction disk size; a report was generated; and the adjusted band volumes (intensity) were used for relative densitometric calculations.

Final normalized relative densitometric values were calculated by expressing pAKT phosphorylated at the serine 473 amino acid residue (S473) or p4EBP1 phosphorylated at the threonine 46 amino acid residue (T46) as a fraction of total AKT

or total 4EBP1, respectively, and then normalizing each resultant value as a percentage of the control value for that experiment. Resulting normalized values from three independent experimental replicates were imported into Prism 10 (GraphPad Software, La Jolla, CA) for statistical analysis.[31]

Cellular Fixation for Histochemistry and Immunohistochemistry

Cells were cultured in C10 RPMI in T175 culture flasks, collected and rinsed in PBS, and incubated overnight in fresh C10 RPMI with VD597 at concentrations of 0.2 μM or 1.0 μM, or with DMSO vehicle control. Cells were pelleted by centrifugation for 5 minutes at 400xG, then washed and resuspended in PBS, transferred to a 1.7 mL Eppendorf tube, and pelleted by centrifugation for 5 minutes at approximately 400xG. The cell pellet was resuspended in 1 mL 10% v/v neutral buffered formalin (NBF) (Cancer Diagnostics Inc., Durham, NC) and fixed overnight at 4°C. Following fixation, cells were pelleted by centrifugation for 5 minutes at 400xG, formalin was removed, and cells were suspended in 1% agarose reconstituted with PBS. Agarose-embedded cells were then dissected into thin sections for processing. Sections were affixed with specimen sponges in tissue cassettes and submitted to the CSU Histology Laboratory in 10% NBF for overnight automated histologic processing using a VIP® 6 vacuum infiltration tissue processor (Sakura Finetek USA Inc., Torrance, CA) before manual paraffin embedding. Four-micrometer (4 μm) sections of formalin fixed paraffin embedded (FFPE) cell suspensions were stained for examination by hematoxylin and eosin (H&E) and stained for IHC evaluation by 3,3'-diaminobenzidine chromogen (DAB) and Mayer's hematoxylin counterstain (ScyTek Laboratories, Inc., Logan, UT). Standard

H&E sections were made by the CSU Histology Laboratory using an automated stainer following paraffin embedding. IHC staining was performed manually, as described below.

Immunohistochemistry

The degree of activation of the PI3K-AKT-mTOR pathway was evaluated by IHC for pAKT (S473) expression in both 1771 and CLL1390 canine cell lines, following treatment with VDC597 *in vitro*. To verify that VDC597 inhibits signal transduction of the entire PI3K-AKT-mTOR pathway *in vitro,* we also used IHC to evaluate expression of p4EBP1 (T46), a downstream target of PI3K-AKT-mTOR signaling. Following cell collection and paraffin embedding, or tissue microarray (TMA) preparation described below, FFPE sections were deparaffinized and rehydrated in sequential 5-minute baths of xylene, xylol, ethanol (100%, 95%, 75%, 50%), and deionized water. Following rehydration, antigen retrieval was performed using Dako Target Antigen Retrieval® solution at pH 6.10 (Agilent, Santa Clara, CA) in a decloaking chamber, set to 118°C for 15 minutes, followed by slow cooling (approximately 1-hour total time of antigen retrieval). Sections were rinsed in deionized water and placed in 3% hydrogen peroxide for 10 minutes to quench endogenous peroxidases, and rinsed in deionized water. Following endogenous peroxidase quenching, all subsequent rinses between blocking and antibody incubation were in three 5-minute baths of TBST (tris-buffered saline (TBS) with 0.5% T20). Sections were blocked for non-specific immunoreactivity for 1 hour at room temperature in SuperBlock™ T20. Isotype controls and no primary antibody controls were included as negative controls for each experiment. Primary

antibodies and isotype controls were diluted in PBS or TBS with 1% bovine serum albumin (BSA). Antibodies and assay concentrations are listed in **Table A1**. Approximately 80 µL of diluted primary antibody were placed on sections, and slides were coverslipped to prevent evaporation. Primary antibody incubation was performed in a humidity chamber at 4°C overnight. Secondary antibody was either a goat anti rabbit HRP-conjugated antibody (Thermo Fisher Scientific) diluted in PBS with 1% BSA or ready-to-use Dako EnVision® Dual-Link HRP (Agilent) (**Table A1**). Secondary antibody was added to sections and sections were incubated for 1 hour at room temperature in a humidity chamber. Dako DAB chromogen (Agilent) was used for visualization of immunoreactivity, incubating sections for approximately 2-5 minutes. Sections were then rinsed in deionized water and counterstained with Mayer's hematoxylin (ScyTek Laboratories, Inc.) for 30 seconds, followed by a warm tap water wash and submersion in deionized water. For tissue sections, slides were submerged for approximately 30 seconds in 0.08% ammonium hydroxide aqueous solution for additional bluing of Mayer's hematoxylin followed by submersion in deionized water. Sections were then dehydrated in reverse order of that described above, before coverslips were affixed with Cytoseal™ XYL mounting media (Thermo Fisher Scientific). Sections from both were examined microscopically and IHC scoring was applied where applicable, as described below.

Tissue Microarray Preparation and Visiopharm Immunohistochemistry Analysis

Anonymized FFPE samples of lymph nodes from CSU Veterinary Teaching Hospital patients with clinically diagnosed BCL enrolled in a previously published prospective study were provided for IHC analysis.[32] For inclusion in this study, dogs were cytologically and histologically diagnosed with multicentric BCL by a board-certified pathologist, did not receive previous treatment, and were enrolled in the 19-week CHOP therapy protocol for the study. Inclusion criteria are outlined in greater detail by Wolf-Ringwall et al. in their publication.[32] The study for which the samples were collected was performed under approval of the Colorado State University Institutional Animal Care and Use Committee (IACUC number 13-4330A), which followed ethical guidelines for standard of care and animals were enrolled with informed consent from the owners. Using FFPE specimens from this study-set, paraffin blocks for tissue microarrays (TMA's) were prepared, using a 150-core TMA kit (Arraymold LLC, Ogden UT), according to the manufacturer directions. Core samples of FFPE tissues were extracted with a 1.5 mm diameter Miltex® biopsy punch (Integra LifeSciences, Princeton, NJ). Core samples were transferred to an empty paraffin TMA block in an 8x13 array, leaving the outer row on all sides empty. The empty outer cores and any additional empty cores of the array were filled with paraffin before heating the array according to manufacturer directions. TMA blocks were submitted to the CSU Histology Laboratory for sectioning into 4 μm sections for IHC examination. Histochemical and IHC processing of the TMA's was performed as described above with antibody concentrations listed in **Table A1**. Following processing, TMA slides immunostained for pAKT (S473) and p4EBP1 (T46) were then scanned at 400X magnification, using an

Olympus VS200 slide scanner (ASW-4.1.1, build 29408; Evident Corporation, Tokyo, Japan) with an Olympus iDS VS-264C (firmware v. 3.1.18303; Olympus Corporation, Center Valley, PA) camera with cellSens™ software (v. 1.17; Olympus Corporation, Center Valley, PA) and analyzed using Visiopharm software (v. 2023.09.7.16662 x64; Visiopharm A/S, Hoersholm, Denmark) at a resolution of approximately 5 pixels/μm.[33,34] Visiopharm software used AI algorithms to analyze scanned tissue sections.

For Visiopharm evaluation of patient-derived FFPE sections of lymph nodes diagnosed with canine BCL, vasculature, stroma, fascia, regions of necrosis or hemorrhage, and any tissue folds present in the sections were omitted from regions to be analyzed. Remaining sections of tumor tissue were assigned unique numbered regions of interest (ROI) for each TMA core, corresponding to patient/sample ID. To identify nuclei, Visiopharm software employed an artificial intelligence (AI) U-Net deep learning classification method that was trained using 3 ROI per image in 20 specimens (approximately 60 unique images), with a 50% initial minimum probability of identification as the criterion for pixel classification (and progressively higher minimum probabilities for inclusion in subsequent iterations), over 300,000 iterations until loss function reached ≤ 0.05 (approximately equivalent to 2% error rate).[34] This classification algorithm was then trained on 10 ROIs of varying staining intensity for an additional 100,000 iterations using the TMA sections, and criteria refined for inclusion of nuclei as objects to be analyzed included: size limits, eccentricity limits, and separators. To capture both cytoplasmic and nuclear immunoreactivity, each label for a detected nucleus was expanded radially from the by up to 30 μm from the label border, until contacting another nucleus. Thresholds for DAB staining intensity scoring were set

manually. All scanned images were then analyzed by the AI algorithm, using the above parameters. Histochemical scoring (H-scoring) was applied to detected cells based on DAB intensity and counts and scores were calculated for each ROI. Resultant values were used to calculate Allred scores. Histochemical scoring (H-scoring) was applied based on DAB intensity, using the H-score formula below.[35] Instead of using ten random fields for H-scoring, the software analyzed the entire section of each TMA sample. Additional criteria and procedures involved in AI training and analysis of tissue sections can be found in the supplementary Materials. The TMA's were also examined manually to record percent positive cells and Allred scores.[35-37] To do so, all cells in three randomly selected fields at 400X (approximately 0.237 mm^2/field) were counted and mean Allred scores were calculated from the scores for each field, based on the Allred score formula below. Additionally, for comparison of manual Allred scores to whole section Allred scoring, the results from AI analysis of the TMA's were used to calculate an Allred score for each sample. To do so, percentages of positive cells from 0 to 100 were assigned a proportion score, in increments of 20%. Intensity score of 0-3 was assigned, based on the relative numbers of cells with an intensity score of 0-3.

$$\text{H-score} = (0 \times P_0) + (1 \times P_1) + (2 \times P_2) + (3 \times P_3)$$

where: P_i = percentage of cells of DAB staining intensity i (range 0-3)

$$\text{Allred score} = P_x + I_x$$

where: P_x = proportion score (range 0-5), corresponding to the percentage of immunopositive cells in field x; I_x = intensity score (range 0-3), corresponding to the DAB staining intensity of immunopositive cells in field x.

Resultant pAKT (S473) and p4EBP1 (T46) immunopositive cell counts, Allred scores, and H-scores were imported to Prism 10 for statistical analysis.

Allred scores and H-scores were evaluated for correlation to progression free interval (PFI) and prognostic indicators, MHC-II expression, WHO stage and substage,

immunophenotypic markers detected by flow cytometry, and percentages of infiltrating lymphocytes by immunophenotype.[27,28,32,38] IHC scores from samples before CHOP therapy and those from the same patients that relapsed after CHOP therapy were also compared.

Cell Growth Inhibition and Cell Death Assays

For analysis of *in vitro* single-agent growth inhibition by VDC597, as measured by end-point cell viability, canine LSA and leukemia cells were suspended in C10 RPMI, containing serially diluted concentrations of VDC597, or DMSO vehicle control in quintuplicate. Cells were then incubated for 72 hours at 37°C with 5% CO_2. Following incubation, relative cell viability was determined using a resazurin fluorometric assay to detect metabolically active cells, and detected (530 nm excitation, 590 nm emission) with a Synergy™ HT microplate reader and associated KC4™ software (Gen5™, v. 3.11.19; BioTek Instruments, Winooski, VT).[39] Resultant mean replicate fluorometric values normalized as a percentage of vehicle control-treated cells and the VDC597 concentration was log-transformed using Prism 10 software. The half-maximal inhibitory concentration (IC_{50}) values and growth inhibition curves were determined mathematically using non-linear curve fitting with the “log(inhibitor) vs. normalized response” function in Prism 10 software and evaluated for statistical significance between treatment groups.

For examination of *in vitro* growth inhibition by a combination of VDC597 and chemotherapy drugs used to treat canine LSA, 1771 cells were plated as above in C10 RPMI, containing: DMSO vehicle control; serially diluted concentrations of VDC597;

serially diluted concentrations of dexamethasone, doxorubicin, vincristine; or varying concentrations of VDC597 and a chemotherapeutic drug together. The plates were then incubated for 72 hours, followed by determination of relative viable cell number as described above. To generate growth inhibition curves for combined agent assays, relative viable cell number was expressed as a percentage of vehicle control-treated cells as above and the concentration of dexamethasone, doxorubicin, or vincristine was log-transformed. Normalized mean cell viability data from each experiment were then imported to CompuSyn software (ComboSyn Inc., Paramus, NJ), which uses the Chou-Talalay method to calculate drug combination indices (CI's) and evaluate for potential synergism or antagonism.[40-42] Mean CI values from three independent experiments are reported herein.

To examine the degree to which cell death was induced by VDC597, we tracked the cell proliferation and death over 48 hours of a canine LSA cell line (1771) expressing NucLight™ Red (Essen BioScience, Ann Arbor, MI), using Incucyte® Live-Cell Analysis System (Essen BioScience, Ann Arbor, MI), calibrated to detect and count red cellular nuclei and green nucleic acids of dead cells labeled by the cell-impermeant dye, YOYO®-1 (Thermo Fisher Scientific). NucLight™ Red expressing cells were seeded at a density of 2,000 cells/200 uL/well in a 96-well plate with C10 RPMI containing 100 nM YOYO®-1 iodide fluorescent dimeric cyanine nucleic acid stain (excitation 491 nm; emission 509 nm) and DMSO vehicle control or serially diluted concentrations of VDC597. The plate was placed in the Incucyte® ZOOM or Incucyte® SX5 Live Cell Imaging device (Essen BioScience) in standard incubation conditions and images of viable cells (red fluorescing; excitation 567-607 nm; emission 622-704 nm)

and dead cells (green fluorescing; excitation 441-481 nm; emission 503-544 nm) were captured over a 48-hour period. Images captured from each well were analyzed with Incucyte® SX5 (v. 2023A Rev2) Live Cell Imaging software and total numbers of red objects (live cells) and green objects (dead cells) were exported for statistical analysis.[43,44] Green object count (GOC) was expressed as a percentage of red object count (ROC) per well at all time points. All percentage values were normalized by baseline-correction and expressed as a percentage of controls. The baseline-corrected mean and SD at the 48-hour timepoint for each treatment condition from each experiment was imported to Prism 10 for statistical analysis.

Vascular Endothelial Growth Factor ELISA

Due to the known role of PI3K-AKT-mTOR signaling in promotion of tumor angiogenesis, we evaluated the effects of PI3K/mTOR inhibition by VDC597 on vascular endothelial growth factor (VEGF) production in the 1771 and CLL1390 cell lines. Cells were plated at $1x10^5$ cells/well in 12-well plates with 800 µL C10 RPMI with varying concentrations of VDC597 (0.25, 0.5, or 1 µM) or DMSO vehicle control. Plates were centrifuged for 5 minutes at 400xG and the supernatant was then collected from each well for VEGF quantification. Fresh C10 RPMI was then added to wells, and the resazurin fluorometric assay was used to determine relative viable cell number, as described above for growth inhibition assays. The VEGF concentrations of the supernatant were evaluated using a R&D Systems (Minneapolis, MN) canine ELISA, according to manufacturer's specifications, and using a Synergy™ HT microplate reader and associated KC4™ software (Gen5™, v. 3.11.19; BioTek Instruments) to read

absorbance at the 405 nm wavelength.[39] VEGF ELISA absorbance values were fitted to a linear regression, using known standards to interpolate sample VEGF concentrations (pg/mL). Relative viable cell fluorometric values for each sample well was normalized as a percentage of control wells and VEGF concentrations were corrected for cell numbers by dividing VEGF concentration by the corresponding percentage before statistical evaluation. Resultant values from 3 independent experiments were normalized as percentage of the mean values at each treatment level and imported to Prism 10 for statistical analysis.

Data and Statistical Analysis

Following importation to Prism 10 (Graphpad), data were assessed for normality or log-normality by D'Agostino and Pearson test or Shapiro-Wilk test. When found to be normally distributed, multiple groups were compared to control values and evaluated for statistically significant differences by one-way ANOVA with Dunnett's test for multiple comparisons. When data used for multiple group comparison were found to be non-normally distributed, comparisons were made using a Kruskal-Wallis test with Dunn's multiple comparisons. For IHC scoring assessment, Allred scores and H-scores were evaluated for correlation to continuous variables by simple linear regression. For categorical variables where distributions were found to be Gaussian, statistically significant differences were evaluated with an unpaired two tailed t-test when SD was equal or a Welch's t-test when SD was unequal. For categorical variables with non-normal distributions, either a Kruskal-Wallis test with Dunn's test for multiple comparisons between more than two groups, or a Mann-Whitney test was used to

compare ranks between two groups. Patient PFI was estimated using the Kaplan-Meier method and differences between groups evaluated using a log-rank (Mantel-Cox) test. P-values less than 0.05 were considered statistically significant.

Results

VDC597 inhibits PI3K-AKT-mTOR signal transduction in canine lymphoma and leukemia cells

Expression of pAKT (S473) and total AKT was examined by western immunoblot. In both cell lines, there was a dose-dependent reduction in pAKT (S473) following 24-hour incubation with VDC597. The reduction in pAKT was greater for CLL1390 at both the 0.2 μM ($p = 0.0004$) and 1 μM ($p < 0.0001$) concentrations than for 1771. The 1771 cell line exhibited a significant reduction in pAKT (S473) expression at the 1 μM concentration ($p = 0.0046$) (**Figures 3.01 A and B**).

We also evaluated the time to onset of AKT and 4EBP1 phosphorylation inhibition, as well as duration of effect following a pharmacologically achievable 1 μM concentration of VDC597 in the 1771 cell line. Reduction in AKT phosphorylation in the 1771 cell line was rapid in onset and maintained at approximately the same range of one half of control values over a 24-hour period. The reduction in phosphorylated 4EBP1 (p4EBP1) was more pronounced immediately following treatment, during the timepoints: 0.5 hour ($P = 0.0060$); 1 hour ($P = 0.0016$); 2 hours ($P = 0.0405$), indicating inhibition of the PI3K-AKT-mTOR pathway as well as downstream targets activated through the signaling cascade (**Figures 3.01 C and D**). Correlating to AKT and 4EBP1 phosphorylation demonstrated in western blot analysis, canine LSA and CLL cell lines

were also examined by IHC for expression of pAKT (S473) and p4EBP1 (T46) as indicators of the degree of PI3K-AKT-mTOR signal transduction. Following a 24-hour incubation with 1 μM VDC597, there was a decrease in perinuclear and cytoplasmic pAKT (S473) immunoreactivity, as well as a decrease in cytoplasmic p4EBP1 (T46) immunoreactivity in both cell lines as compared to DMSO vehicle-control treated cells (**Figure 3.02**). This reduction in pAKT (S473) and p4EBP1 (T46) was less in 1771 cells (**Figures 3.02A–D**) than in CLL1390 cells (**Figures 3.02E–H**), which correlates to the reduction in pAKT (S473) demonstrated by western blots. A sample photomicrograph of IHC controls is shown in **Supplemental Figure S3.01**.

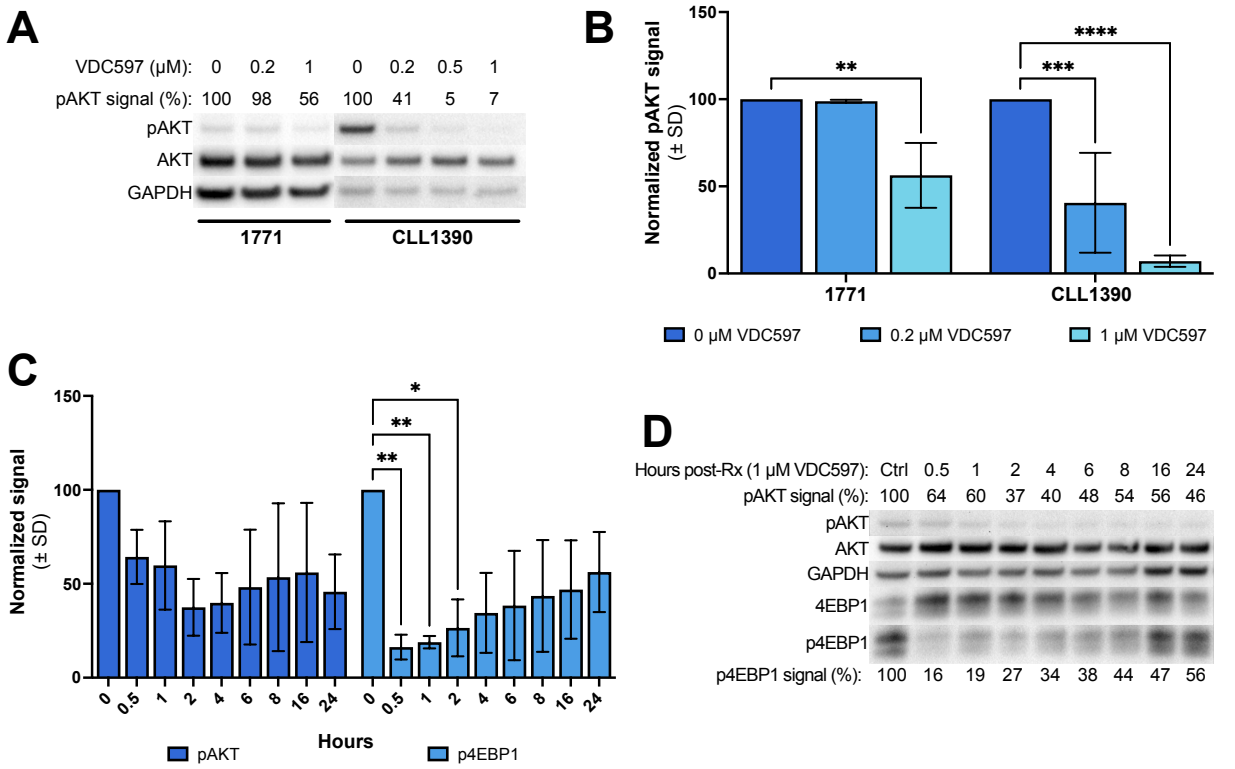

Figure 3.01: VDC597 inhibits pAKT (S473) and p4EBP1 (T46) signal in canine lymphoma and lymphocytic leukemia cells *in vitro*. (**A** and **B**) Western blot results demonstrating dose-dependent *in vitro* inhibition of PI3K-AKT-mTOR signal transduction in 1771 and CLL1390 cell lines following 24-hour incubation with VDC597. (**A**) Representative images of western blots with dose-dependent reduction in pAKT (S473) signal relative to total AKT in both cell lines. (**B**) In both cell lines, there was a significant reduction in AKT phosphorylation at the S473 site following incubation at the 1 μM VDC597 concentration, with CLL1390 being more sensitive with markedly reduced pAKT (S473) at both the 1 μM and 0.2 μM concentrations. (**C** and **D**) Western blot results demonstrating *in vitro* inhibition of both pAKT (S473) and p4EBP1 (T46) signal in 1771 cells, followed by maintenance of inhibition over 24 hours, when treated with a single dose of 1 μM VDC597. (**C**) Inhibition of 4EBP1 phosphorylation (T46) was statistically significant through 2 hours following treatment. (**D**) Representative images of western blots with reduced pAKT (S473) and p4EBP1 (T46) over a 24-hour observation period. Results are representative of 3 experimental replicates. Error bars represent standard deviation and significance indicators are as follows: * $P < 0.05$; ** $P < 0.005$; *** $P < 0.0005$; **** $P < 0.0001$.

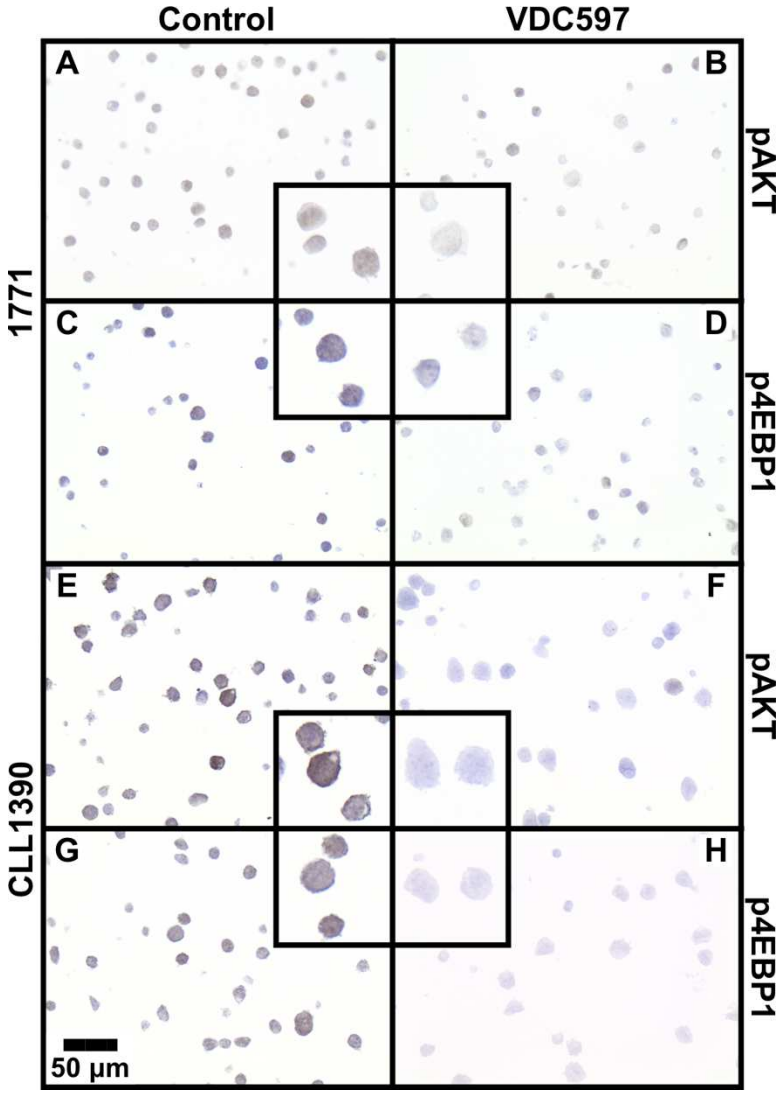

Figure 3.02: *in vitro* pAKT (S473) and p4EBP1 (T46) expression inhibition by VDC597 in canine lymphoma and lymphocytic leukemia cells. 400x magnification photomicrographs of FFPE suspensions of 1771 (**A**–**D**) and CLL1390 (**E**–**H**) cells incubated for 24 hours with either DMSO vehicle control (**left column**) or 1 µM VDC597 (**right column**). In both cell lines, there is a marked reduction in perinuclear and cytoplasmic immunoreactivity for pAKT (S473) and p4EBP1 (T46) following treatment with VDC597, as compared to vehicle control treated cells. Insets are magnified to 800x to show cellular morphology and staining. Images are corrected for background white-balance using the same adjustment for all images, and were otherwise unmodified. DAB chromogen and hematoxylin counterstain.

Immunohistochemical evaluation of pAKT and p4EBP1 expression in spontaneous canine lymphomas

We also sought to evaluate patient-derived FFPE samples of spontaneous B-cell LSA for pAKT (S473) and p4EBP1 (T46) expression by IHC, utilizing two scoring methods. H-scores were applied by AI analysis and Allred scores were manually applied, as well as calculated from AI analysis. Manually applied Allred scores, AI analyzed Allred scores, and H-scores were found to be well correlated. There was not a strong correlation between pAKT and p4EBP1 IHC scores, by any of the three methods. Examples of sections with high and low immunopositivity are shown in **Figure 3.03**. Photomicrographs of H&E-stained sections and control sections are in **Supplemental Figure S3.02**. Sample images of photomicrographs analyzed by Visiopharm AI software are in **Supplemental Figure S3.03**.

Allred-scores and H-scores from anonymized TMA sections were correlated to corresponding prognostic, treatment, and outcome information for each patient. Parameters that were examined for correlation to either H-scores and/or Allred scores of tumor sections included: patient survival time; progression free interval; MHC-II expression measured by flow cytometry; immunophenotypic markers measured by flow cytometry; and comparison of pre-treatment samples to those taken from patients relapsing after CHOP therapy. Lower MHC-II levels, as detected by flow cytometry, were associated with higher pAKT H-scores ($P = 0.0303$), higher manually assessed Allred scores ($P = 0.0358$), and higher whole slide AI calculated Allred scores ($P = 0.0258$) (**Figure 3.04**).

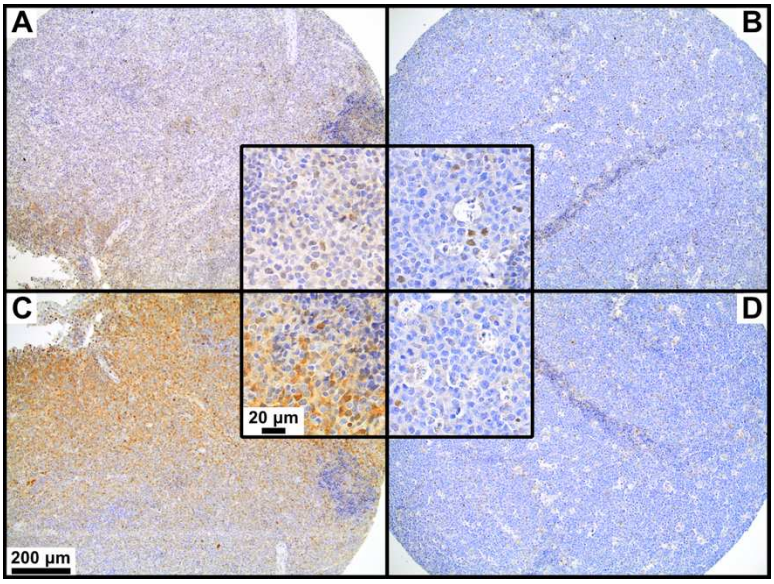

Figure 3.03: Differential expression of pAKT (S473) and p4EBP1 (T46) in FFPE sections of lymph nodes effaced by canine B-cell lymphoma. 100x magnification photomicrographs of TMA sections immunostained for (**A**, **B**) pAKT (S473) and (**C**, **D**) p4EBP1 (T46). (**A**) High expression of pAKT with frequent moderate to strong perinuclear and cytoplasmic pAKT (S473) immunoreactivity. (**B**) Low pAKT expression with rare specific discrete perinuclear pAKT (S473) immunoreactivity. (**C**) High expression of p4EBP1 with abundant strong cytoplasmic and perinuclear p4EBP1 (T46) immunoreactivity throughout many neoplastic lymphocytes, characterized by larger nuclei with open chromatin and frequent prominent nucleoli, while not present in clusters of smaller well differentiated and infiltrating lymphocytes (**inset**). (**D**) Low expression of p4EBP1 with rare discrete specific moderate to strong perinuclear and moderate cytoplasmic p4EBP1 (T46) immunoreactivity. Insets are magnified to 800x to show cellular morphology and staining. DAB chromogen and hematoxylin counterstain. Photomicrographs are corrected for white-balance, using the same preset adjustment for all images.

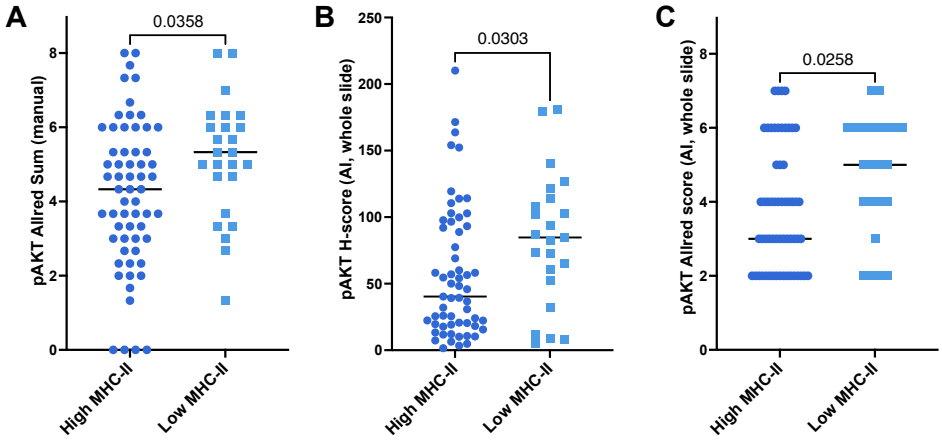

Figure 3.04: pAKT expression correlates to MHC-II expression in canine B-cell lymphoma (BCL). Plots of immunohistochemical scores for pAKT (S473) in canine BCL. Increased pAKT (S473) immunoreactivity in TMA sections of spontaneous canine BCL correlates to MHC-II expression, as a negative prognostic indicator by three scoring methodologies. (**A**) Manually applied pAKT Allred score from three 0.237 mm^2 fields per sample (approximately 3000-4000 cells). (**B**) Whole-slide pAKT H-scores, applied over entire TMA section per case, analyzed by AI software. (**C**) Whole-slide pAKT Allred score, analyzed by AI software. P-values are reported for each plot.

The correlation to MHC-II expression was not significant for p4EBP1 IHC scores. When comparing all samples (unpaired t-test), samples from patients relapsing after CHOP therapy were found to have higher p4EBP1 H-scores (P = 0.0195) and Allred scores than pre-treatment samples, both by manual count (P = 0.0097) and by calculation from AI whole-slide analysis (P = 0.0376) (**Figure 3.05**). When considering only those patients for which there was a paired sample from the same patient for both pre-CHOP and upon post-treatment relapse, the manually scored samples retained statistical significance (P = 0.0152) (**Supplemental Figure S3.04**). However, paired comparison of samples analyzed by AI did not retain statistical significance for H-scores (P = 0.0500) or Allred scores (P = 0.0961) (**Figure 3.05**). There was not a significant correlation between pAKT or p4EBP1 H-scores or Allred scores and progression free interval or survival times. There was also no significant correlation between immunoreactivity and WHO stage/substage or the percentage of infiltrating T cells with specific immunophenotypic markers (CD25, CD4, CD8), by flow cytometry. Summary data and linear regressions of IHC scoring results can be found in **Supplemental Figures S3.05–S3.07**.

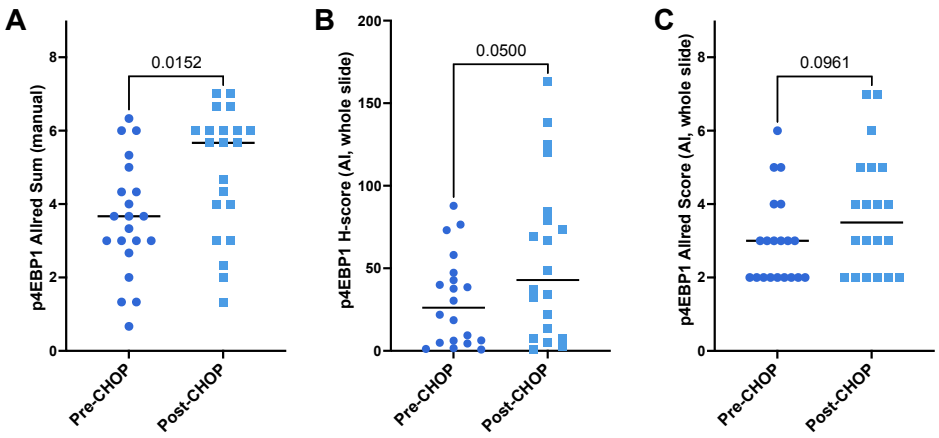

Figure 3.05: p4EBP1 expression correlates to post-treatment relapse in canine B-cell lymphoma (BCL). There is a trend in correlation between higher p4EBP1 expression to relapsed BCL. Plots of immunohistochemical scores for p4EBP1 (T46) in samples paired by patient for pre-treatment (pre-CHOP) and post-relapse (post-CHOP) comparison, with median scores denoted by the black line. (**A**) Manually applied p4EBP1 Allred score from three 0.237 mm^2 fields per sample. (**B**) Whole-slide p4EBP1 H-scores, applied over entire TMA section per case, analyzed by AI software. (**C**) Whole-slide p4EBP1 Allred score, analyzed by AI software. P-values are reported for each plot, demonstrating $P < 0.05$ for manually applied Allred scores, $P = 0.05$ for H-scores, but no statistical significance for AI-applied Allred scores. Unpaired comparison of IHC scores between relapsed patients and all pre-CHOP samples can be found in **Supplemental Figure S3.04**.

VDC597 inhibits cell proliferation and promotes cell death in canine lymphoma and leukemia cells

Sensitivity to VDC597 *in vitro* was assessed in CLL1390, and 1771 cell lines by fluorescent quantification of metabolically active cells following a 72-hour incubation. When comparing to controls, the growth inhibition in the 1771 cell line was significant at VDC597 concentrations of 0.625 μM ($P = 0.0018$), 1.25 μM ($P = 0.0024$), and 2.5 μM ($P < 0.0001$) (**Figure 3.06A**). When comparing to controls, growth inhibition in the CLL1390 cell line was significant at all concentrations tested ($P < 0.0001$) (**Figure 3.06B**). In both cell lines the half maximum inhibitory concentration (IC_{50}) value for VDC597 was within or near a pharmacologically achievable concentration, with IC_{50} values of 1.41 μM for CLL1390 and 2.56 μM for 1771 (**Figure 3.06C**). Growth inhibition curves for both cell lines are shown in **Supplemental Figure S3.08**.

The bioreductive method utilized above cannot discriminate between inhibition of cell proliferation and induction of cell death. Therefore, in addition to growth inhibition, the degree to which *in vitro* cell death was induced with VDC597 administration was examined by using the Incucyte® live cell tracking system with the green fluorescent carbocyanine dimeric cell death indicator dye, oxazole yellow homodimer (YOYO®-1). Cell death for 1771 cells treated with VDC597 increased in a dose-dependent manner. Compared to DMSO vehicle-control treated cells, percent cell death in 1771 cells was significantly greater for cells treated with VDC597 at concentrations of 0.25 μM ($P = 0.0463$); 0.5 μM ($P < 0.0001$); and 1 μM ($P < 0.0001$) (**Figure 3.06D**). Plots of the percent of cell death over 48 hours at varying concentrations of VDC597 are shown in **Supplemental Figure S3.09**.

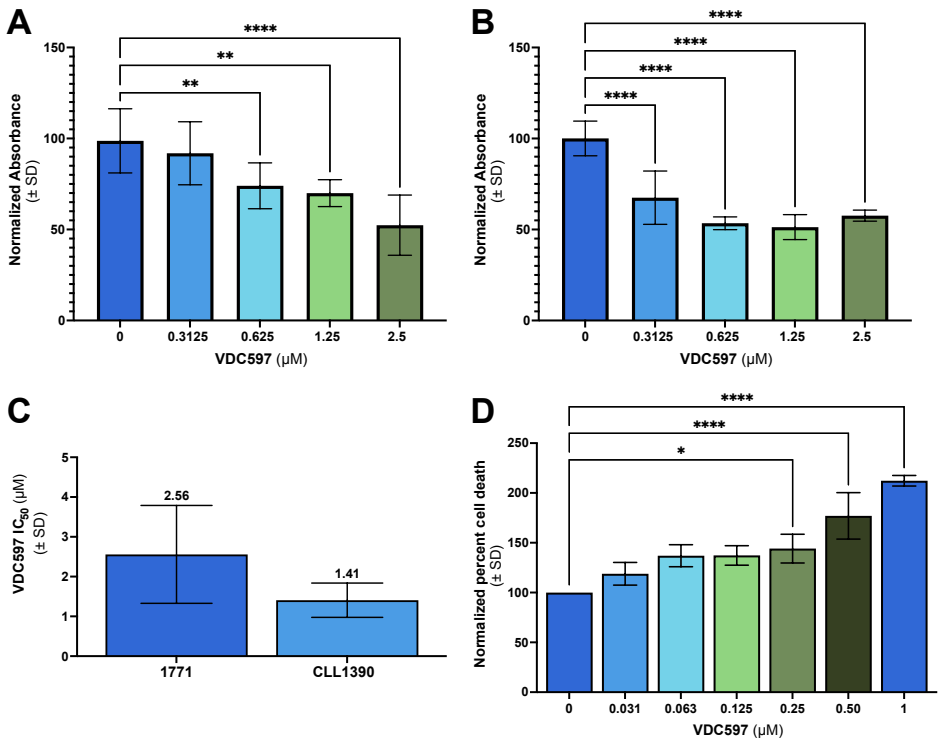

Figure 3.06: in vitro growth inhibition and promotion of cell death by VDC597.
VDC597 induces *in vitro* dose-dependent growth inhibition and promotion of cell death in canine B-cell lymphoma and lymphocytic leukemia cells. (**A** and **B**) Normalized absorbance, representing end-point cell viability from growth inhibition assays following 72-hour incubation with varying concentrations of VDC597 in (**A**) 1771 and (**B**) CLL1390 cells. (**C**) IC_{50} values for 1771 and CLL1390 cell lines, calculated from growth inhibition assays. (**D**) VDC597 increased cell death of 1771 cells *in vitro* such that percent cell death increases in a dose-dependent manner, with significant differences from control values occurring at and above 0.25 μM VDC597. Results are representative of 3 experimental replicates. Error bars represent standard deviation and significance indicators are as follows: * P < 0.05; ** P < 0.005; *** P < 0.0005; **** P < 0.0001.

Combined VDC597 and CHOP chemotherapy drugs inhibit proliferation in canine lymphoma cells

In addition to single-agent analysis, *in vitro* growth inhibition was examined when 1771 cells were treated with a combination of VDC597 and dexamethasone, doxorubicin, or vincristine. The reduction in IC_{50} values and end-point cell viability was greater for all three drugs with the addition of VDC597 (**Supplemental Figure S3.10**). The reduction of the IC_{50} value was less for vincristine than for doxorubicin and dexamethasone. The combination index (CI) values for dexamethasone and VDC597 indicate that the two drugs are synergistic (CI < 1) in their activity, especially at lower concentrations. For doxorubicin and VDC597, the CI values distributed near CI = 1 indicate that the effect of combined treatment additive to mildly synergistic at lower concentrations, except for the highest doses of doxorubicin, which were antagonistic (CI > 1). CI values for vincristine and VDC597 indicate effects were additive to mildly antagonistic (**Figure 3.07**).

VDC597 inhibits angiogenesis in canine lymphoma and leukemia cells

In both cell lines, there was dose-dependent reduction in VEGF production following 24-hour incubation with varying concentrations of VDC597. This effect was significant for 1771 at the 1 μM concentration (P = 0.0003). The effect was more pronounced for CLL1390 at the 0.25 μM (P = 0.0046), 0.5 μM (P = 0.0010), and 1 μM (P = 0.0003) concentrations (**Figure 3.08**).

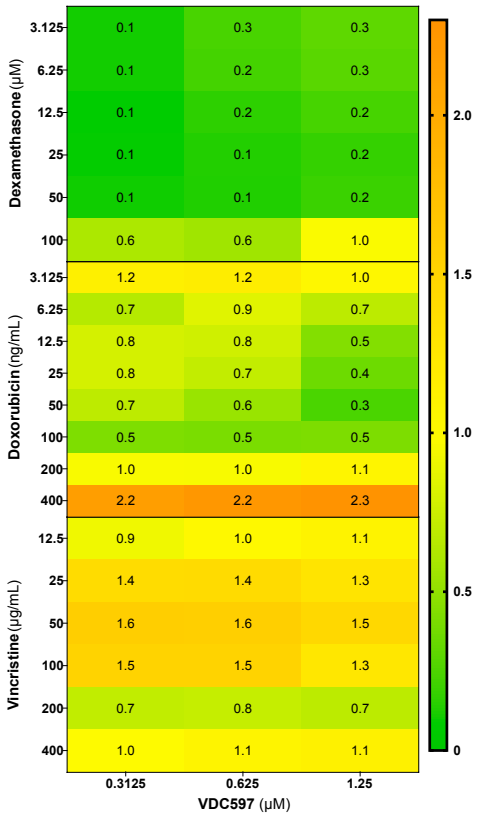

Figure 3.07: The combined *in vitro* growth inhibition effects of VDC597 and CHOP chemotherapy drugs are synergistic to additive, with moderate antagonism at high doses. Mean drug combination indices (CI) for VDC597 with dexamethasone (**top**), doxorubicin (**middle**), or vincristine (**bottom**) in 1771 cells demonstrating *in vitro* synergistic effects (CI < 1) for dexamethasone doxorubicin and additive (CI = 1) to moderately antagonistic (CI > 1) effects for vincristine. There is also strong antagonism at the highest doxorubicin concentration (400 ng/mL). VDC597 concentrations are listed at the bottom. Results are representative of 3 experimental replicates.

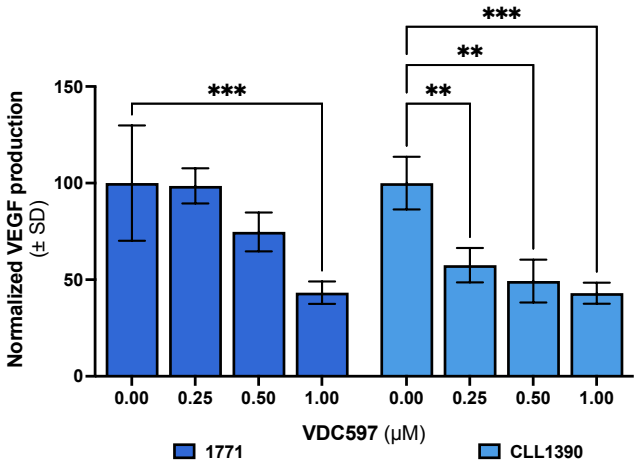

Figure 3.08: in vitro inhibition of VEGF production by VDC597 in canine lymphoma and leukemia cells. VDC597 induces *in vitro* dose-dependent reduction of VEGF production in (**A**) 1771 and (**B**) CLL1390 cell lines, following 24-hour incubation. Results are representative of 3 experimental replicates. Error bars represent standard deviation and significance indicators are as follows: * P < 0.05; ** P < 0.005; *** P < 0.0005; **** P < 0.0001.

Discussion

PI3K-AKT-mTOR signal transduction is frequently dysregulated in multiple canine and human tumor types, and is involved in neoplastic cell proliferation, survival, increased metabolic activity, and promotion of angiogenesis, as well as migration and invasion in solid tumors.[7] For this reason, there is potential promise in multi-nodal inhibition of the pathway. In our previous investigations into the efficacy of the dual-PI3K/mTOR-inhibitor, VDC597, against canine hemangiosarcoma and osteosarcoma, we found that many of these neoplastic processes were inhibited *in vitro* and tumor growth was reduced *in vivo*.[25,45] In canine hematopoietic tumors, mutations and aberrations in expression of components of PI3K-AKT-mTOR pathway activity and regulation have been well reported, and discussed in our review of pathway activity in canine cancer.[7] Interventions that target pathway activity have also proven to be a potentially valuable avenue for treatment of canine LSA both *in vitro* and *in vivo*, especially when used in conjunction with other chemotherapeutic agents.[10,19,22,23] However, in many cases, single-point inhibitors have been found to have antitumor activity for only a period of time or to induce an incomplete response, likely related to the feedback pathways involved in PI3K-AKT-mTOR signaling.[7,46] In the present study, we examine the *in vitro* efficacy of a dual-inhibitor of PI3K and mTORC1/2, VDC597, against canine LSA and CLL cells.

Previous studies have demonstrated the role of PI3K-AKT-mTOR signaling in both lymphoid activation and neoplastic proliferation.[7,47] In the present study we found a dose-dependent *in vitro* inhibition of cell growth for both the LSA and CLL cell lines examined. We also noted IC_{50} values within pharmacologically achievable

concentrations, based on the findings of unpublished pharmacokinetic studies in dogs examining the plasma concentration of VDC597 following oral administration (A. Kousba and D.F. Beyerlein, personal communication). These findings also correlate to a phase-I clinical trial in tumor bearing dogs, finding that oral administration of VDC597 at doses that resulting in plasma concentrations reaching IC_{50} values reported here was well tolerated.[48] These findings indicate that administration of VDC597 may be valuable in inhibiting growth of canine lymphoma and leukemia. We also found that, in addition to a reduction in the number of viable cells, there was also a dose-dependent increase in cell death when 1771 cells were treated with VDC597 *in vitro*, indicating a potential reduction in BCL tumor burden due both to reduced growth and increased cell death.

In human oncology research, the addition of PI3K/AKT/mTOR inhibition to chemotherapy protocols has been shown to promote chemosensitization and/or ameliorate chemoresistance.[22,49-51] While there have not been studies demonstrating similar reduction in cases of canine LSA to the authors' knowledge, there may be value in the addition of targeted pathway inhibitors to chemotherapy protocols for a more complete response to treatment. Our examination of the *in vitro* effects of VDC597 in conjunction with the frequently used CHOP chemotherapy drugs (dexamethasone, doxorubicin, and vincristine) demonstrated a greater growth inhibition when used in combination than when used alone. For dexamethasone and doxorubicin, the effects were synergistic to additive, supporting the hypothesis that it may be advantageous to add PI3K-AKT-mTOR signaling inhibition to conventional chemotherapy protocols.

VEGF is an important component of malignancy for neovascularization and—in conjunction with mTORC2 signaling and matrix metalloproteinase activity—for cellular

migration/invasion in both solid tumors and round cell tumors.[7] The role of PI3Kδ in CLL cellular chemotaxis and stromal interaction has also been examined and inhibited *in vitro*, indicating that the inhibition of PI3K signaling in hematopoietic tumor cells not only affects the cells but also the microenvironmental signals.[52] VEGF has been noted as a biomarker in human LSA, and in both canine LSA and CLL cases higher plasma VEGF concentrations have been found than in dogs without tumors with potential prognostic implications.[53,54] Additionally, immunocytochemical and transcriptomic examinations of spontaneous canine CLL and LSA found higher VEGF expression in neoplastic cells as compared to aspirates from normal lymph nodes.[55,56] The regulation of VEGF production by the PI3K-AKT-mTOR signaling pathway, through 4EBP1 and hypoxia inducible factor 1 subunit alpha, has been well established.[7] On this basis, we sought to examine the *in vitro* effect of VDC597 on VEGF expression in 1771 and CLL1390 cells. The dose-dependent decrease in VEGF production by both cell lines supports the hypothesis that VDC597 inhibits angiogenic downstream effects of pathway activation.

In light of the above findings, it was important to verify that there was a correlated reduction in PI3K-AKT-mTOR signal transduction activity in the neoplastic round cells examined. Our findings demonstrate a dose-dependent reduction in pAKT for both 1771 and CLL1390 cell lines when treated with VDC597 *in vitro*. In a previous study utilizing whole exome sequencing and immunoblotting to correlate mutations in genes involved in mitogen-activated protein kinase (MAPK) and PI3K-AKT signaling to activated pMAPK1/3 and pAKT, both 1771 and CLL1390 cell lines were noted to constitutively express pAKT both in the presence and absence of serum. This study also found that both cell lines had mutations in genes related to the PI3K-AKT-mTOR

pathway. In the 1771 cell line, there were mutations reported in *MTOR*, *PTPRO*, and *NRAS*.[9] These findings broadly align with the response to treatment with VDC597 in both cell lines observed in our present study. While both cell lines were reported to constitutively express pAKT in the previous study, we found a lower pAKT signal by western blot, as well as less pAKT immunoreactivity by IHC, in the 1771 cell line as compared to the CLL1390 cell line. Our western and IHC findings correlate to the more pronounced growth inhibition, lower IC_{50} value, and greater reduction in VEGF expression for CLL1390 cells when treated with VDC597, as compared to 1771 cells. As BCL is the more commonly diagnosed neoplasm, we also examined the duration of effect on PI3K-AKT-mTOR signaling by VDC597 on the 1771 cell line following a single dose of VDC597, using pAKT and p4EBP1 as indicators of pathway inhibition. Results demonstrated a rapid onset of inhibition with maintenance of pAKT and p4EBP1 expression near half that of the control cells over 24 hours, indicating the potential utility of daily oral administration of VDC597 in cases of canine LSA.

The above findings that there was a differential response between cells that express proteins indicating a high degree of PI3K-AKT-mTOR pathway activation (CLL1390) and cells that have a lower baseline constitutive expression (1771) support the hypothesis that treatment with targeted pathway inhibitors offers the greatest benefit in cases for which there is extant high signal transduction activity. The role of PI3K in B-cell differentiation, activation, survival, metabolic activity, and the development of malignancy has been well documented in human immunology and oncology research, and is reviewed elsewhere.[57,58]

Additionally, genetic mutations and aberrations in protein expression of multiple components of the PI3K-AKT-mTOR signaling pathway are reported in canine lymphoid neoplasms.[7] As one might expect, prognosis in canine lymphoma cases has been shown to be worse for stage V and/or substage b neoplasms than for stage I-IV and/or substage a tumors.[28] Higher CD25 expression in infiltrating T cells and lower MHC-II expression in canine BCL has also been shown to be associated with a poorer prognosis.[27,32] Given the association of PI3K-AKT-mTOR pathway activation with features of malignancy in multiple tumors and the role of pathway signaling in canine BCL, we hypothesized that higher pAKT (S473) and p4EBP1 (T46) immunoreactivity would be associated with shorter PFI and poorer prognostic indicators in spontaneous canine BCL.

To evaluate the pathway activity in cases of spontaneous canine BCL, we manually applied Allred scoring and used AI analysis to apply H-scoring and Allred scoring to TMA's constructed from FFPE samples of lymph nodes from dogs with confirmed BCL immunostained for pAKT (S473) and p4EBP1 (T46). We found that the scoring systems correlated well, and that there were the expected associations between lower MHC-II expression and higher pAKT (S473) IHC scores, as an indicator of pathway activation. While not directly mechanistically related, this correlation provides reasoning for further examination of pAKT expression in cases of canine BCL with low MHC-II expression. Interestingly, we also observed higher p4EBP1 IHC scores in the samples from patients relapsed following CHOP therapy. We hypothesized that there would be a concurrent increase in pAKT immunoreactivity in the post-CHOP relapse samples as well. However, that was not observed. There are several potential

explanations for one or both of these findings. While selection pressures for LSA cells with mutations in genes for PI3K is a consideration, it does not explain the disparity between phosphorylation of 4EBP1 and AKT. It is worth noting that phosphorylation of p4EBP1 occurs in a sequential fashion with T46 being the second residue phosphorylated and crucial for altering activation.[59,60] Canonical AKT phosphorylation, on the other hand, occurs non-sequentially primarily at two sites by two proteins: S473 by mTORC2 and T308 by 3-phosphoinositide-dependent protein kinase 1 (PDPK1).[7] For the catalytic role of AKT to be fully activated, both sites must be phosphorylated.[61] However, it is still possible for AKT to engage in diminished signaling activity that still results in mTORC1 activation leading to 4EBP1 phosphorylation.[62] Researchers demonstrated that, in human non-small cell lung cancer, AKT phosphorylation at S473 was less directly correlated than T308 for subsequent inactivating phosphorylation of TSC2 by pAKT, though in this study S473 phosphorylation was present throughout.[63] It is still possible for AKT to engage in signaling activity leading to the activation of mTORC1 through TSC2, with only the T308 residue phosphorylated.[61] Thus, it is possible that AKT partially phosphorylated at only the T308 residue was simply not detected in the sections examined, but still resulted in 4EBP1 phosphorylation through mTORC1. Additionally, when considering the possibility of alternative mechanisms for 4EBP1 phosphorylation, such as RAS/MAPK signaling or serine/threonine-protein kinase pim-2 (PIM2), it is not necessarily surprising that p4EBP1 immunoreactivity could be increased without concurrent increase in pAKT.[64,65] Another potential explanation involves the mechanisms of phosphorylation of these proteins. Mutations in the genes responsible for PI3K isoforms are reported in canine and human LSA, but not as great

as the frequency for which AKT phosphorylation is reported.[7,66,67] As one might expect, given the complexity and interactions with other pathways involved in PI3K-AKT-mTOR signaling, the greater degree of AKT phosphorylation without apparent mutations in PI3K indicate that pathway activity may still be playing a significant role in the progression of LSA and it is reasonable to expect that there might be aberrant expression of p4EBP1, as a component of this or other pathways.[66] Regardless of the specific explanation for immunoreactivity differences between p4EBP1 (T46) and pAKT (S473) in the post-CHOP relapse sections examined, further investigation into the finding of increased p4EBP1 (T46) immunolabeling in this type of case is warranted.

While the above findings are interesting, there was not a significant association with IHC scoring and WHO stage/substage, PFI, patient survival time, or immunophenotypic markers measured by flow cytometry. In summation, the results from the IHC analysis of pAKT (S473) and p4EBP1 (T46) in patient derived spontaneous canine BCL neoplasms indicate that there is not a correlation between the IHC scores and outcome data or prognostic indicators beyond that of the two correlations discussed above. Though it may be tempting to read significance into these limited findings, the lack of correlation in other variables indicates that caution should be taken to avoid overinterpretation. Given that mutations and activation in the PI3K-AKT-mTOR signaling cascade are well documented in spontaneous canine TCL and cell lines, there may be utility in examining pAKT and p4EBP1 IHC scores in canine TCL for correlation to outcome data and prognostic indicators in that specific neoplasm.[7,9,68]

There are significant limitations to the scope of this study and further investigation is warranted to expand upon the initial findings documented herein. We

made no report of PI3K-AKT-mTOR signal transduction activity or efficacy of VDC597 in canine TCL lines. Given the aforementioned documentation of pathway activity in canine TCL, this would be a fruitful avenue for investigation. Investigation into the degree of PI3K-AKT-mTOR signaling dysregulation in canine acute lymphoblastic leukemia is also warranted. It is important to note that only *in vitro* activity of VDC597 against CLL and BCL lines was examined in this study. For this potential therapeutic agent in LSA and CLL to be thoroughly evaluated, *in vivo* efficacy and safety should be examined in mouse models and further investigated in larger clinical trials. While our *in vitro* findings did report the time to onset and duration of pAKT inhibition in the BCL line examined, we did not employ washout experiments to evaluate the persistence of inhibition following withdrawal of the drug. This would be useful information for refinement of oral administration protocols in the treatment of canine BCL. A limitation to the IHC assessment of both cell lines and in the TMA sections examined exists in our analysis of phosphorylation of AKT at the S473, but not T308 residue. As previously mentioned, full activation of AKT requires phosphorylation at both sites, but mTORC1 activation and or other mechanisms 4EBP1 phosphorylation may have still occurred and the role of pAKT (T308) remained unknown. While concurrent IHC detection of pAKT (T308) would have been preferable, the antibodies and protocols tested in our experimentation yielded poor to no immunolabeling in FFPE tissues. Unlike our *in vitro* experiments, the samples from which TMA sections were made came from patients who were not treated with mTOR or PI3K inhibitors, and the specific mechanism for greater p4EBP1 immunoreactivity without concurrent increase in pAKT (S473) immunoreactivity in these cases is presently left to postulation.

The IHC scoring systems and methods used also possessed their own limitations. Allred scoring is a relatively coarse scoring system for producing semi-quantitative results, which was originally instituted for IHC assessment of hormone receptors in human breast cancer specimens.[36,37] Of course, any manual application of IHC scoring is susceptible to bias. While we found fairly good correlation between the manually applied Allred scores and those applied by AI, the coarseness of this scoring system can result in false elevations in correlation between manual and AI Allred scoring. H-scoring offers finer granularity for differentiation of degrees of immunoreactivity.[69] However, any IHC scoring system applied through supervised AI analysis is dependent both on effective training of the AI engine and on the ability of AI to accurately apply scoring to brightfield photomicrographs. The former is variable in supervised AI training methodologies, and dependent on both the AI engine and the human ability and expertise in appropriately adjusting parameters used by the AI.[70] The latter is a well-known shortcoming of AI image analysis in its current development. Unlike immunofluorescent images, which have separate color channels that are comparatively easy for AI image analysis, brightfield require the AI software to be able to read through the combinatorial effects of multiple colors within any given pixel being analyzed for scoring, which is dependent upon not only training but also staining quality and variation.[71,72] For these reasons, it is worthwhile to compare H-scoring of these and other similar IHC samples in the same manner that was reported here for Allred scoring.

Conclusions

There is hyperactivation of the PI3K-AKT-mTOR signaling cascade in canine BCL (1771) and CLL (CLL1390), as detected by western and IHC examination of phosphoprotein expression. VDC597 inhibits PI3K-AKT-mTOR signal transduction as detected by IHC and western blot, inhibits proliferation, promotes cell death, and inhibits VEGF in canine BCL and CLL cell lines *in vitro*. Sections of spontaneous canine BCL demonstrate variably dysregulated expression of phosphoproteins involved in PI3K-AKT-mTOR signaling, and further investigation into the applicability of pathway activity in cases of canine BCL is warranted for the potentially effective use of targeted inhibitors, like VDC597.

Supplementary Materials

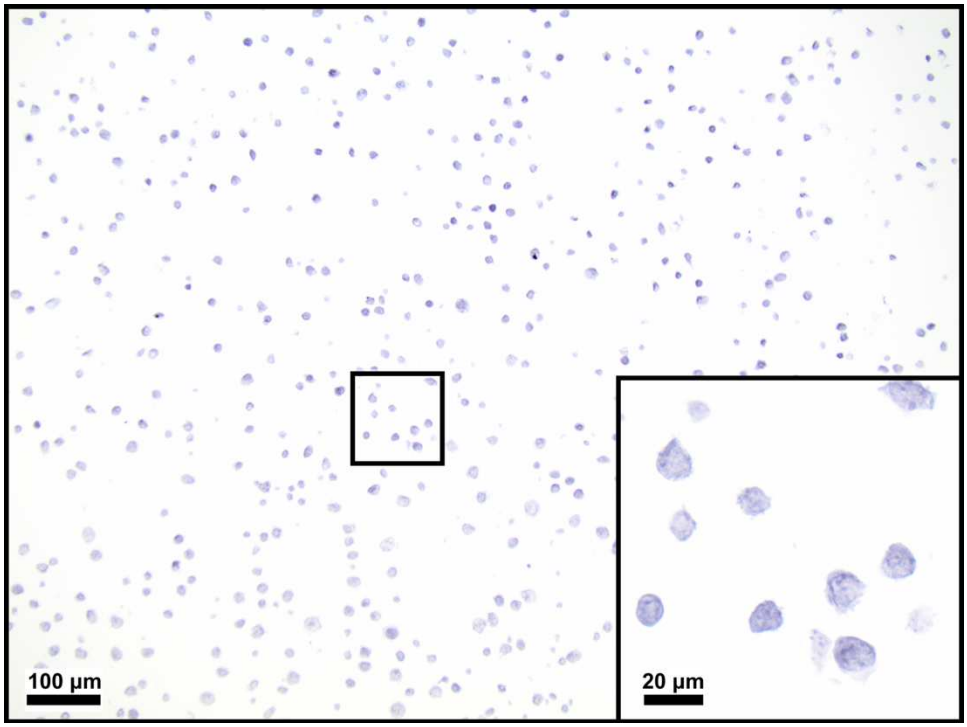

Supplemental Figure S3.01: Cell suspension IHC isotype control; 200x magnification; CLL1390 cell line cultured under control conditions. Sections were incubated in rabbit IgG isotype-control at equivalent dilution (1:200) as the test antibody (p4EBP1). Inset acquired at 400x magnification and enlarged to 800x to show cellular morphology and staining. Images are corrected for white-balance, using the same preset adjustment for all images used in **Figure 3.02**. DAB chromogen and hematoxylin counterstain.

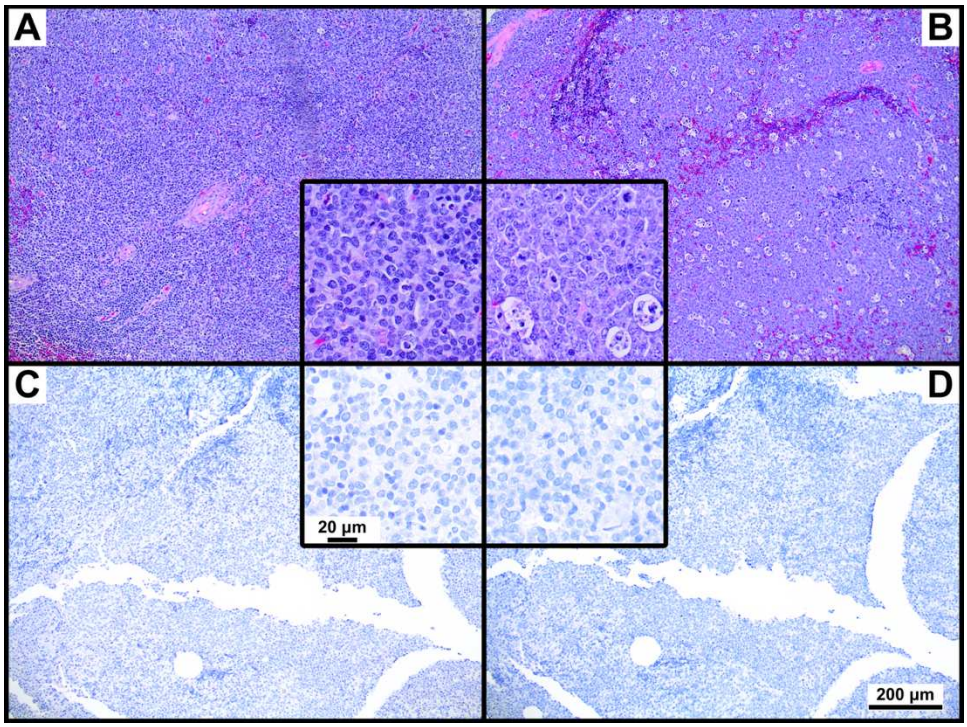

Supplemental Figure S3.02: Tissue microarray H&E and IHC control sections. 100x magnification photomicrographs of hematoxylin and eosin-stained (H&E) tissue microarray (TMA) sections (**A** and **B**) corresponding to the sections displayed in **Figure 3.03**. 100x magnification photomicrographs of TMA sections for (**C**) no primary antibody and (**D**) isotype IHC controls. 400x magnification insets show cellular morphology. Photomicrographs of IHC controls are corrected for white-balance, using the same preset adjustment for all images in **Figure 3.03**. DAB chromogen and hematoxylin counterstain.

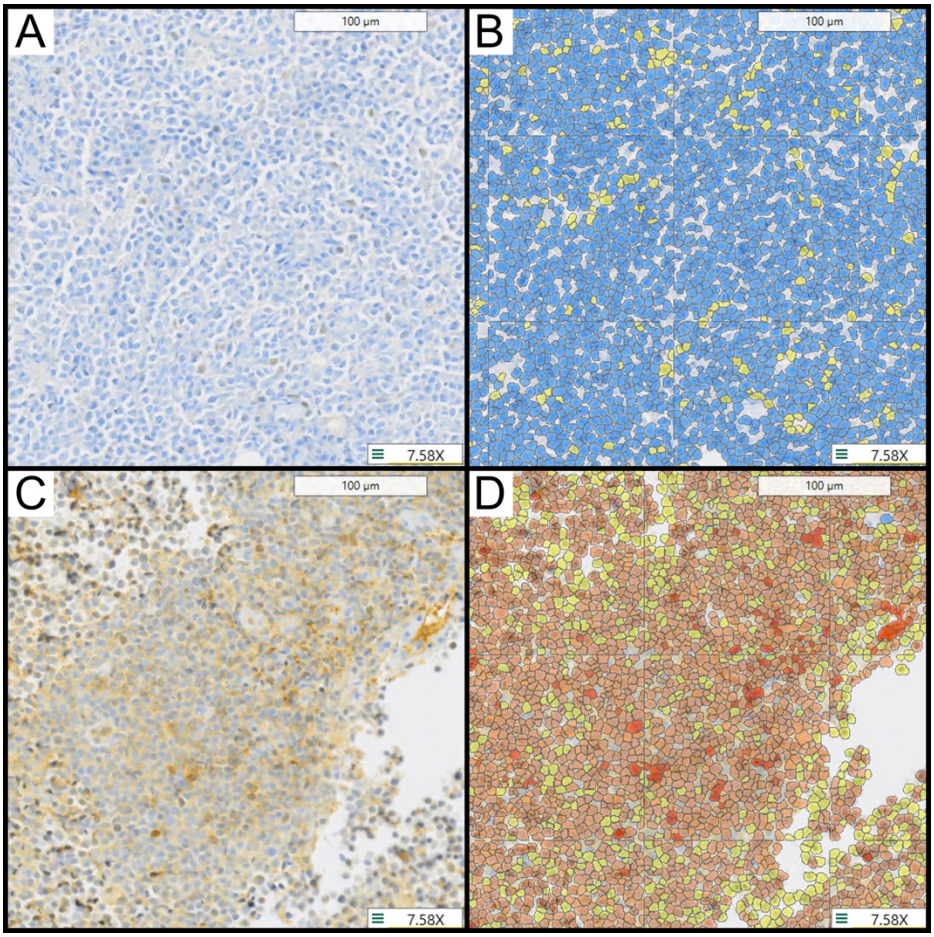

Supplemental Figure S3.03: Sample images of TMA photomicrographs immunolabeled for pAKT, and analyzed by Visiopharm AI software. (**A** and **B**) Photomicrographs of low pAKT expression. (**C** and **D**) Photomicrographs of high pAKT expression. (**A** and **C**) Images of TMA sections. (**B** and **D**) Images of the same sections, with colorized notation applied by the Visiopharm AI algorithm for cellular identification and IHC staining intensity labeled by IHC scoring (blue = 0; yellow = 1; orange = 2; red = 3). DAB chromogen and hematoxylin counterstain.

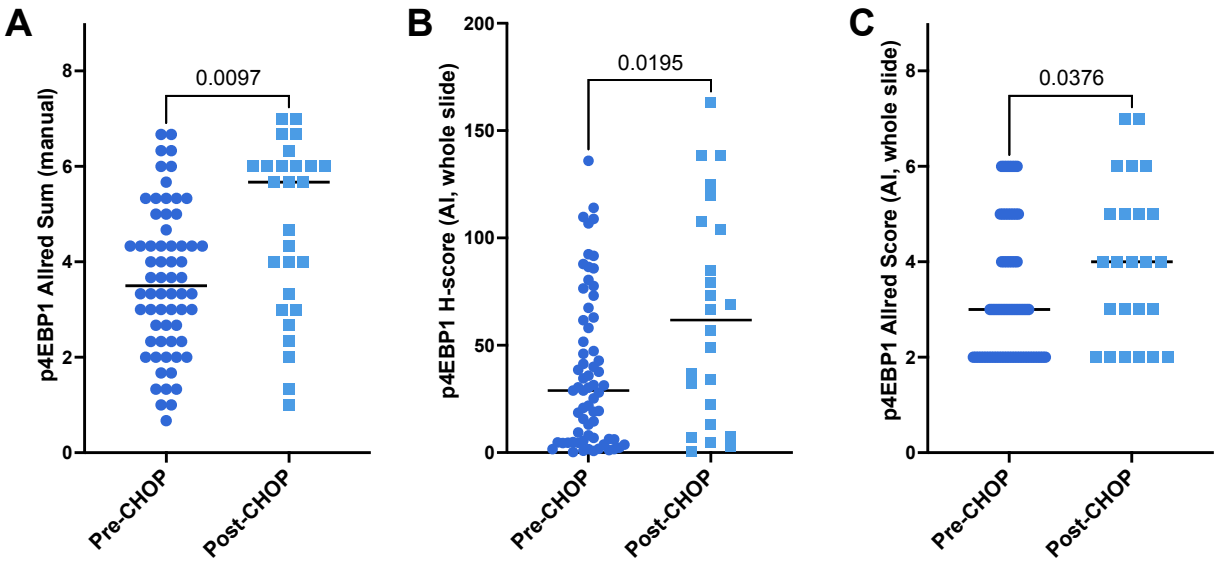

Supplemental Figure S3.04: Correlation between higher p4EBP1 expression to relapsed B-cell lymphoma. Plots of immunohistochemical scores for p4EBP1 (T46) in unpaired comparison between samples from pre-treatment (pre-CHOP) patients and post-relapse (post-CHOP) patients, with median scores denoted by the black line. (**A**) Manually applied p4EBP1 Allred score from three 0.237 mm^2 fields per sample. (**B**) Whole-slide p4EBP1 H-scores, applied over entire TMA section per case, analyzed by AI software. (**C**) Whole-slide p4EBP1 Allred score, analyzed by AI software. P-values are reported for each plot.

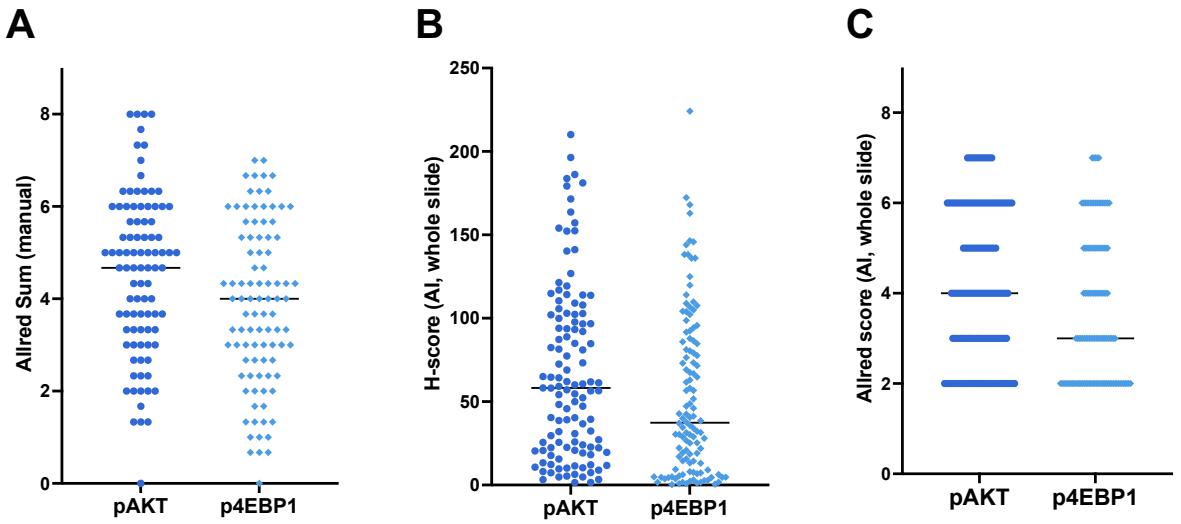

Supplemental Figure S3.05: Overall IHC scoring distributions of (**A**) manually applied Allred scores, (**B**) H-scores, and (**C**) AI analyzed Allred scores for all BCL samples analyzed in TMAs (bar = median). There is similar overall distribution across all three scoring methods. It is noteworthy that there are greater numbers of lower AI analyzed scores for both H-scores Allred scores than for manually applied Allred scores. The authors also hypothesize that the differences in distribution between manual and AI analyzed scores could be related to a combination of differences between randomly selected fields and whole-slide analysis, the insensitivity of AI analysis for brightfield IHC, and/or subconscious selection bias in fields analyzed for Allred scoring. This raises interesting questions about the accuracy and efficacy of manual vs automated IHC scoring methodologies. Black lines represent median values.

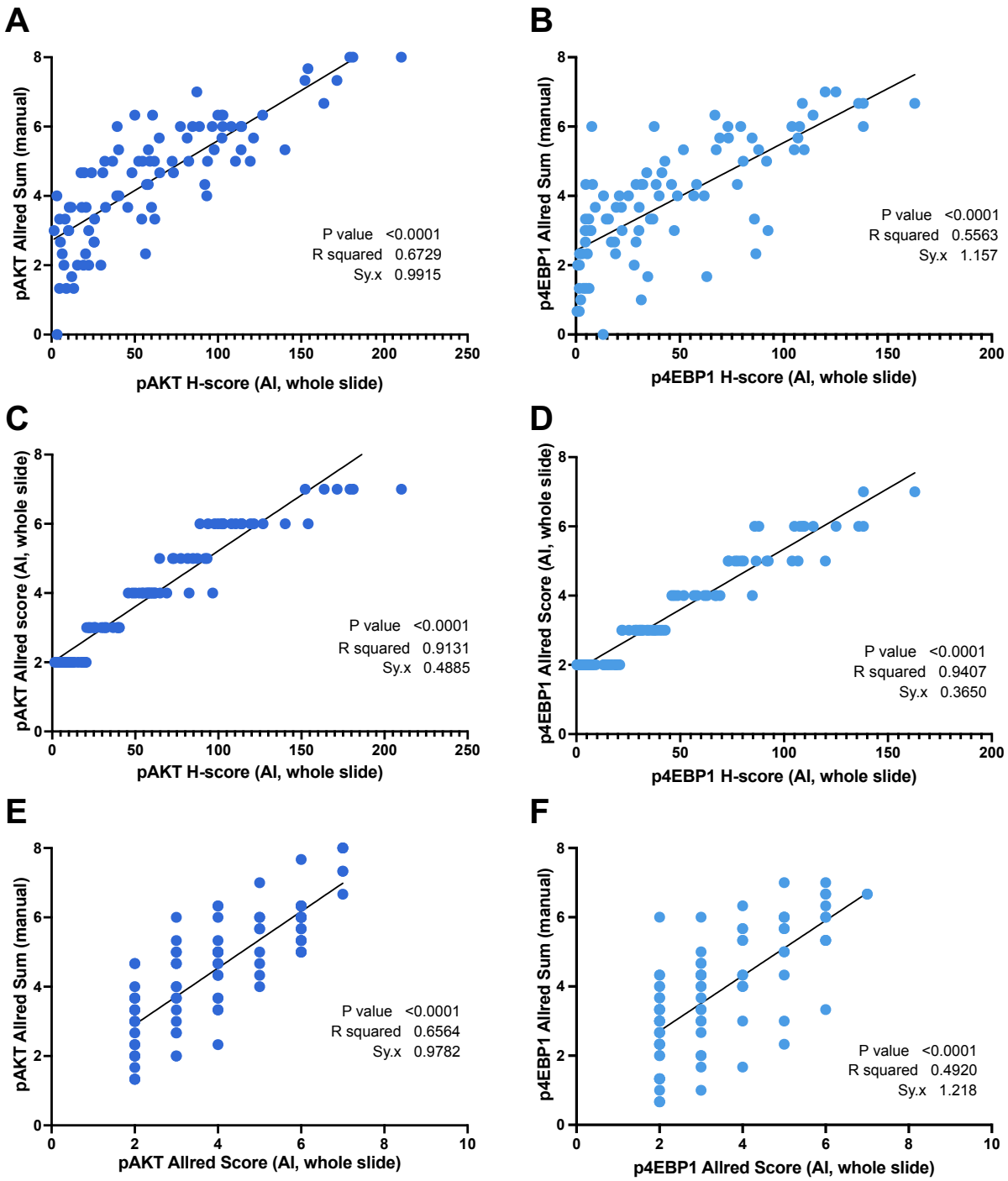

Supplemental Figure S3.06: X-Y scatter plots of correlation of (**A**) pAKT H-score to manually applied pAKT Allred score, (**B**) p4EBP1 H-score to manually applied p4EBP1 Allred score, (**C**) pAKT H-score to AI calculated pAKT Allred score, (**D**) p4EBP1 H-score to AI calculated p4EBP1 Allred score, (**E**) AI calculated pAKT Allred score to manual pAKT Allred score, (**F**) AI calculated p4EBP1 Allred score to manual p4EBP1 Allred score. P-values, R-squared, and standard deviation values (Sy.x) from linear regression analysis are reported on each plot.

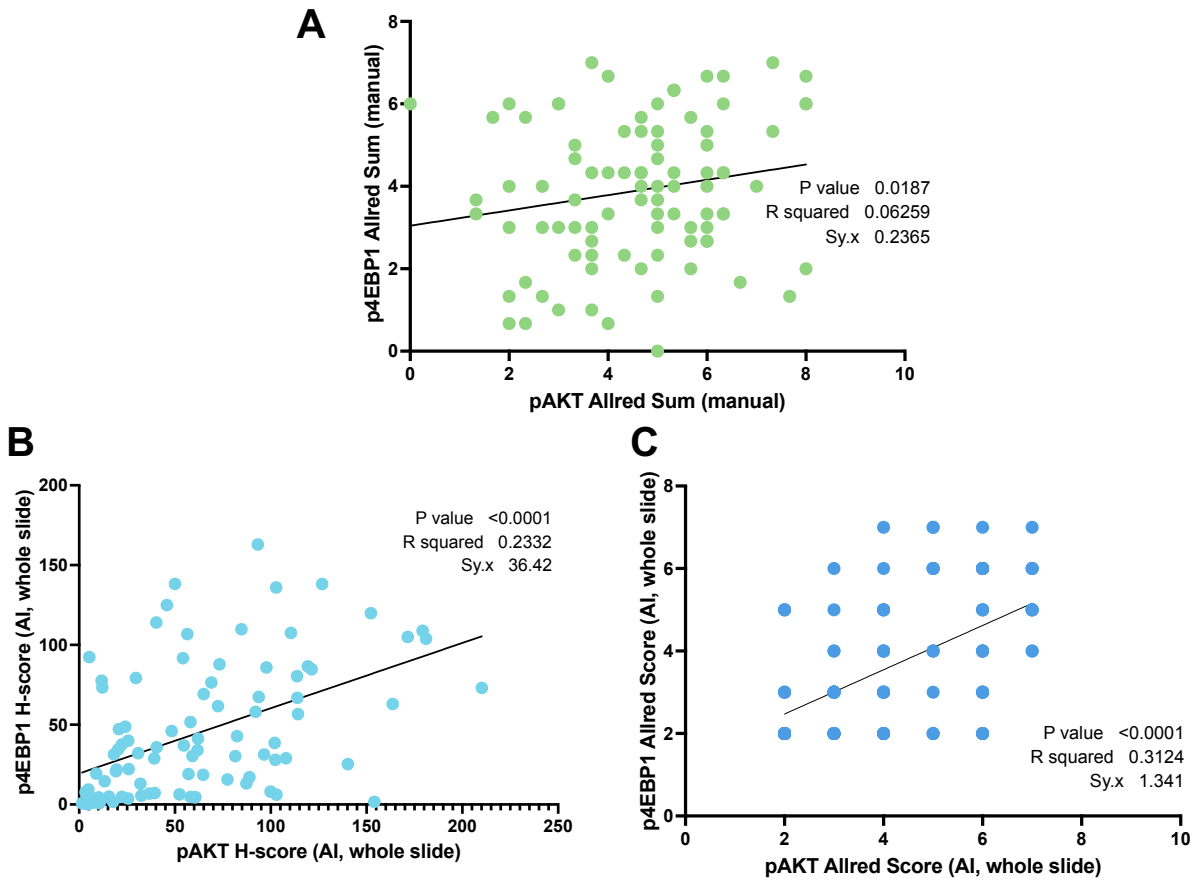

Supplemental Figure S3.07: X-Y scatter plots of correlation for (**A**) manual pAKT Allred score to manual p4EBP1 Allred score, (**B**) AI applied pAKT H-score to p4EBP1 H-score, (**C**) AI calculated pAKT Allred score to AI calculated p4EBP1 Allred score. P-values, R-squared, and standard deviation values (Sy.x) from linear regression analysis are reported on each plot.

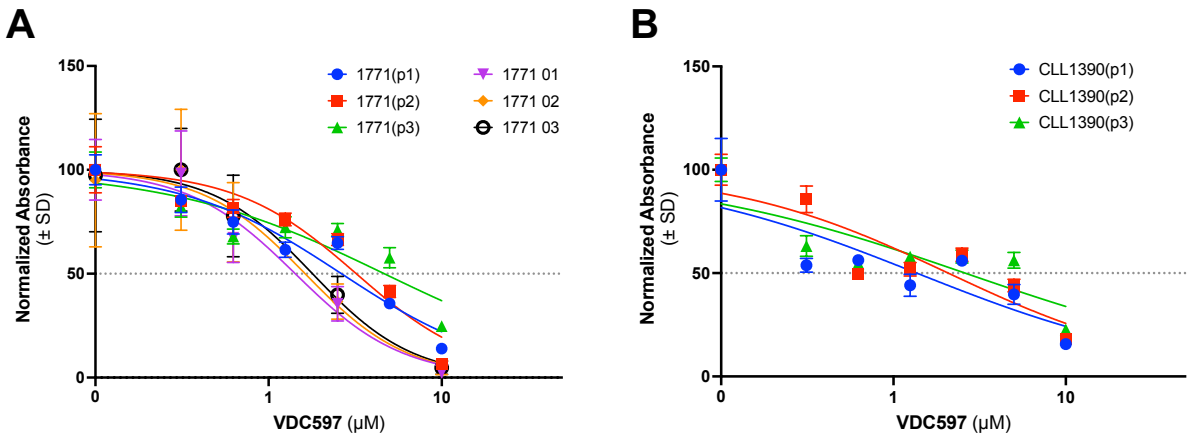

Supplemental Figure S3.08: Normalized growth inhibition curves for (**A**) 1771 cells and (**B**) CLL1390 cells, demonstrating reduction cell viability following 72-hour incubation with varying concentrations of VDC597; colored points and curves represent individual experimental replicates, denoted by the passage number following cell line name. Error bars represent standard deviation.

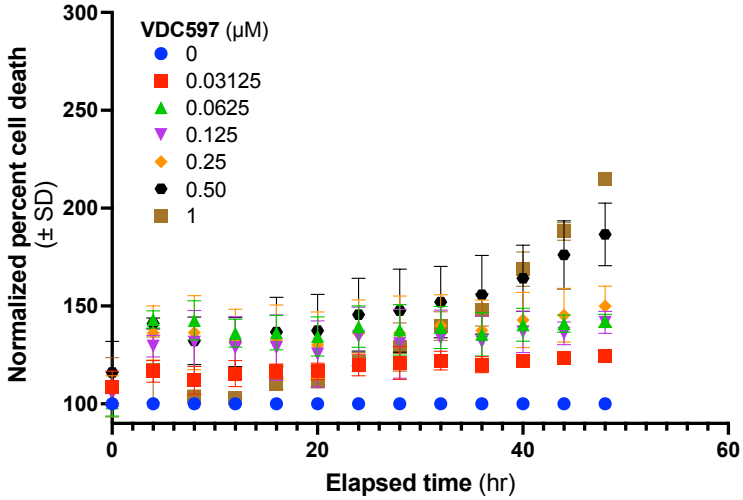

Supplemental Figure S3.09: *in vitro* cell death in the 1771 cell line measured as a percentage of living cells over 48 hours with varying concentrations of VDC597; the control group is set to a baseline value at 100, and values for other treatment conditions are expressed as relative to the control baseline for each time-point. Results are representative of 3 experimental replicates. Error bars represent standard deviation.

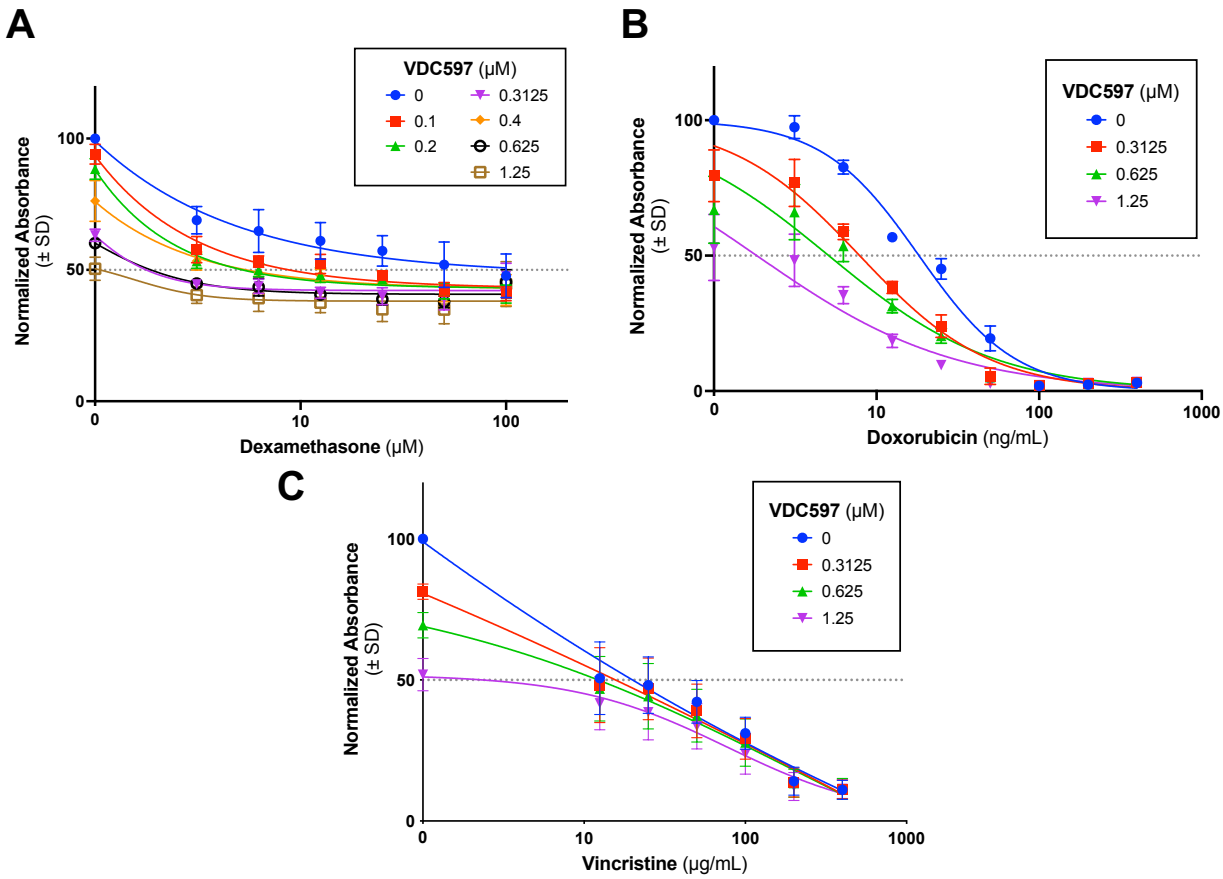

Supplemental Figure S3.10: Normalized growth inhibition curves for 1771 cells, demonstrating reduction cell viability following 72-hour incubation with varying concentrations of VDC597 and (**A**) dexamethasone, (**B**) doxorubicin, or (**C**) vincristine; in comparison to these chemotherapy drugs alone the reduction in cell viability with the addition of VDC597 is especially pronounced at lower concentrations chemotherapy agents. Results are representative of 3 experimental replicates. Error bars represent standard deviation.

References

1. Vail DM, Pinkerton ME, Young KM. Hematopoietic Tumors. In: Withrow SJ, Vail DM, Page RL, eds. *Withrow and MacEwen's Small Animal Clinical Oncology*. 5th ed. St. Louis, MO; Elsevier/Saunders; 2013:608–678. https://doi.org/10.1016/B978-1-4377-2362-5.00032-3

2. Valli VE, Kass PH, San Myint M, Scott F. Canine lymphomas: association of classification type, disease stage, tumor subtype, mitotic rate, and treatment with survival. *Vet Pathol*. 2013;50(5):738–48. https://doi.org/10.1177/0300985813478210

3. Valli VE, Bienzle D, Meuten DJ. Tumors of the Hemolymphatic System. In: Meuten DJ, ed. *Tumors in Domestic Animals*. 5th edition ed. Ames, Iowa; John Wiley & Sons, Inc.; 2017:203–321. https://doi.org/10.1002/9781119181200.ch7

4. Avery AC. The genetic and molecular basis for canine models of human leukemia and lymphoma. *Front Oncol*. 2020;10:23–23. https://doi.org/10.3389/fonc.2020.00023

5. Benjamin SE, Sorenmo KU, Krick EL, et al. Response-based modification of CHOP chemotherapy for canine B-cell lymphoma. *Vet Comp Oncol*. 2021;19(3):541–550. https://doi.org/10.1111/vco.12693

6. Montaner-Angoiti E, Marín-García PJ, Llobat L. Epigenetic Alterations in Canine Malignant Lymphoma: Future and Clinical Outcomes. *Animals (Basel)*. 2023;13(3)https://doi.org/10.3390/ani13030468

7. Meuten TK, Dean GA, Thamm DH. Review: The PI3K-AKT-mTOR signal transduction pathway in canine cancer. *Vet Pathol*. 2023;6(3)(3):339–356. https://doi.org/10.1177/03009858231207021

8. Zamani-Ahmadmahmudi M, Najafi A, Nassiri SM. Reconstruction of canine diffuse large B-cell lymphoma gene regulatory network: detection of functional modules and hub genes. *J Comp Pathol*. 2015;152(2-3):119–130. https://doi.org/10.1016/j.jcpa.2014.11.008

9. Das S, Idate R, Cronise KE, Gustafson DL, Duval DL. Identifying candidate druggable targets in canine cancer cell lines using whole-exome sequencing. *Mol Cancer Ther*. 2019;18(8):1460–1471. https://doi.org/10.1158/1535-7163.Mct-18-1346

10. Aresu L, Ferraresso S, Marconato L, et al. New molecular and therapeutic insights into canine diffuse large B-cell lymphoma elucidates the role of the dog as a model for human disease. *Haematologica*. 2019;104(6):e256–e259. https://doi.org/10.3324/haematol.2018.207027

11. Ferraresso S, Aricò A, Sanavia T, et al. DNA methylation profiling reveals common signatures of tumorigenesis and defines epigenetic prognostic subtypes of canine Diffuse Large B-cell Lymphoma. *Sci Rep*. 2017;7(1):11591. https://doi.org/10.1038/s41598-017-11724-w

12. Aricò A, Ferraresso S, Bresolin S, et al. Array-based comparative genomic hybridization analysis reveals chromosomal copy number aberrations associated with clinical outcome in canine diffuse large B-cell lymphoma. *PLoS One*. 2014;9(11):e111817. https://doi.org/10.1371/journal.pone.0111817

13. Alsaihati BA, Ho K-L, Watson J, et al. Canine tumor mutational burden is correlated with TP53 mutation across tumor types and breeds. *Nat Commun*. 2021;12(1):4670–4670. https://doi.org/10.1038/s41467-021-24836-9

14. Tsuji S, Yabe R, Usui T, Mizuno T, Ohama T, Sato K. Anti-tumor effects of perphenazine on canine lymphoma. *J Vet Med Sci*. 2016;78(8):1293–1298. https://doi.org/10.1292/jvms.15-0707

15. Saba CF, Thamm DH, Vail DM. Combination chemotherapy with L-asparaginase, lomustine, and prednisone for relapsed or refractory canine lymphoma. *J Vet Intern Med*. 2007;21(1):127–32. https://doi.org/10.1892/0891-6640(2007)21[127:ccwlla]2.0.co;2

16. Suenaga M, Tomiyasu H, Watanabe M, et al. Comprehensive analysis of gene expression profiles reveals novel candidates of chemotherapy resistant factors in canine lymphoma. *Vet J*. 2017;228:18–21. https://doi.org/10.1016/j.tvjl.2017.10.002

17. Mee MW, Faulkner S, Wood GA, Woods JP, Bienzle D, Coomber BL. Longitudinal Study of Transcriptomic Changes Occurring over Six Weeks of CHOP Treatment in Canine Lymphoma Identifies Prognostic Subtypes. *Vet Sci*. 2024;11(11)https://doi.org/10.3390/vetsci11110540

18. Klinghoffer RA, Bahrami SB, Hatton BA, et al. A technology platform to assess multiple cancer agents simultaneously within a patient's tumor. *Sci Transl Med*. 2015;7(284):284ra58. https://doi.org/10.1126/scitranslmed.aaa7489

19. Tomiyasu H, Goto-Koshino Y, Fujino Y, Ohno K, Tsujimoto H. Antitumour effect and modulation of expression of the ABCB1 gene by perifosine in canine lymphoid tumour cell lines. *Vet J*. 2014;201(1):83–90. https://doi.org/10.1016/j.tvjl.2014.04.002

20. Beaufils F, Cmiljanovic N, Cmiljanovic V, et al. 5-(4,6-Dimorpholino-1,3,5-triazin-2-yl)-4-(trifluoromethyl)pyridin-2-amine (PQR309), a Potent, Brain-Penetrant, Orally Bioavailable, Pan-Class I PI3K/mTOR Inhibitor as Clinical Candidate in Oncology. *J Med Chem*. 2017;60(17):7524–7538. https://doi.org/10.1021/acs.jmedchem.7b00930

21. Shao Y, Xie S, Zhu H, Du X, Xu RA. Development of a novel and quick UPLC-MS/MS method for the pharmacokinetic analysis of duvelisib in beagle dogs. *J Pharm Biomed Anal*. 2020;187:113355. https://doi.org/10.1016/j.jpba.2020.113355

22. Shin N, Li YL, Mei S, et al. INCB040093 Is a Novel PI3Kδ Inhibitor for the Treatment of B Cell Lymphoid Malignancies. *J Pharmacol Exp Ther*. 2018;364(1):120–130. https://doi.org/10.1124/jpet.117.244947

23. Lainscsek X, Kong W, Rütgen BC, et al. Transcriptomic profiling in canine B-cell lymphoma supports a synergistic effect of BTK and PI3K inhibitors. *Front Vet Sci*. 2025;12:1577028. https://doi.org/10.3389/fvets.2025.1577028

24. Gardner HL, Rippy SB, Bear MD, et al. Phase I/II evaluation of RV1001, a novel PI3Kδ inhibitor, in spontaneous canine lymphoma. *PLoS One*. 2018;13(4):e0195357–e0195357. https://doi.org/10.1371/journal.pone.0195357

25. Meuten T, Farrell KB, Rose BJ, et al. Phosphatidylinositol 3-kinase and mechanistic target of rapamycin dualinhibitor, VDC597, as a therapeutic agent for canine osteosarcoma. *J Pharmacol Exp Ther*. 2025;392(10):103715. https://doi.org/10.1016/j.jpet.2025.103715

26. Frantz AM, Sarver AL, Ito D, et al. Molecular profiling reveals prognostically significant subtypes of canine lymphoma. *Vet Pathol*. 2013;50(4):693–703. https://doi.org/10.1177/0300985812465325

27. Rao S, Lana S, Eickhoff J, et al. Class II major histocompatibility complex expression and cell size independently predict survival in canine B-cell lymphoma. *J Vet Intern Med*. 2011;25(5):1097–105. https://doi.org/10.1111/j.1939-1676.2011.0767.x

28. Jagielski D, Lechowski R, Hoffmann-Jagielska M, Winiarczyk S. A retrospective study of the incidence and prognostic factors of multicentric lymphoma in dogs (1998-

2000). *J Vet Med A Physiol Pathol Clin Med*. 2002;49(8):419–24. https://doi.org/10.1046/j.1439-0442.2002.00458.x

29. Fowles JS, Dailey DD, Gustafson DL, Thamm DH, Duval DL. The Flint Animal Cancer Center (FACC) Canine Tumour Cell Line Panel: a resource for veterinary drug discovery, comparative oncology and translational medicine. *Vet Comp Oncol*. 2017;15(2):481–492. https://doi.org/https://doi.org/10.1111/vco.12192

30. Bio-Rad. Image Lab Software (Version 6.1.0, build 7) [computer software]. 2020.

31. GraphPad Software LLC. GraphPad Prism (Version 10.4.1 (532)) [computer software]. 2024. https://www.graphpad.com/

32. Wolf-Ringwall A, Lopez L, Elmslie R, et al. Prospective evaluation of flow cytometric characteristics, histopathologic diagnosis and clinical outcome in dogs with naïve B-cell lymphoma treated with a 19-week CHOP protocol. *Vet Comp Oncol*. 2020;18(3):342–352. https://doi.org/10.1111/vco.12553

33. Olympus Corporation. cellSens (Version 1.17) [computer software]. Evident Scientific; 2017. www.olympus-lifescience.com.

34. Visiopharm A/S. Visiopharm Software (Version 2023.09.7.16662 x64) [computer software]. 2023. www.visiopharm.com

35. Shousha S. Oestrogen receptor status of breast carcinoma: Allred/H score conversion table. *Histopathology*. 2008;53(3):346–7. https://doi.org/10.1111/j.1365-2559.2008.03075.x

36. Harvey JM, Clark GM, Osborne CK, Allred DC. Estrogen receptor status by immunohistochemistry is superior to the ligand-binding assay for predicting response to adjuvant endocrine therapy in breast cancer. *J Clin Oncol*. 1999;17(5):1474–81. https://doi.org/10.1200/jco.1999.17.5.1474

37. Allred DC, Harvey JM, Berardo M, Clark GM. Prognostic and predictive factors in breast cancer by immunohistochemical analysis. *Mod Pathol*. 1998;11(2):155–68.

38. Teske E, van Heerde P, Rutteman GR, Kurzman ID, Moore PF, MacEwen EG. Prognostic factors for treatment of malignant lymphoma in dogs. *J Am Vet Med Assoc*. 1994;205(12):1722–8.

39. BioTek Instruments. Gen5 (Version 3.11.19) [computer software]. Agilent BioTek; 2019. https://www.agilent.com/

40. Chou T-C, Martin N. CompuSyn For Drug Combinations User's Guide. A computer program for quantitation of synergism and Antagonism in drug combinations, and the determination of IC50 and ED50 values. Paramus, NJ: ComboSyn, Inc.; 2004. p. 1–65.

41. Chou TC, Talalay P. Quantitative analysis of dose-effect relationships: the combined effects of multiple drugs or enzyme inhibitors. *Adv Enzyme Regul*. 1984;22:27–55. https://doi.org/10.1016/0065-2571(84)90007-4

42. Chou TC, Martin N. CompuSyn (Version 1.0) [computer software]. ComboSyn Inc.; 2014. https://www.combosyn.com/

43. Sartorius BioAnalytical Instruments Inc. Incucyte SX5 Controller and GUI (Version 2023A Rev2) [computer software]. 2023. https://www.sartorius.com/

44. Sartorius BioAnalytical Instruments Inc. Incucyte ZOOM Controller and GUI (Version 2015A Rev1) [computer software]. 2015. https://www.sartorius.com/

45. Pyuen AA, Meuten T, Rose BJ, Thamm DH. In vitro effects of PI3K/mTOR inhibition in canine hemangiosarcoma. *PLoS One*. 2018;13(7):e0200634–e0200634. https://doi.org/10.1371/journal.pone.0200634

46. Li H, Wen X, Ren Y, et al. Targeting PI3K family with small-molecule inhibitors in cancer therapy: current clinical status and future directions. *Mol Cancer*. 2024;23(1):164. https://doi.org/10.1186/s12943-024-02072-1

47. Patel RK, Mohan C. PI3K/AKT signaling and systemic autoimmunity. *Immunol Res*. 2005;31(1):47–55. https://doi.org/10.1385/ir:31:1:47

48. Thamm DH, Weishaar K, Meuten TK, Gustafson DL. Phase-I clinical trial of the dual PI3K/mTOR inhibitor VDC-597 in dogs with spontaneous neoplasia. 2018:

49. Li J, Wang X, Ma C, et al. Dual PI3K/mTOR inhibitor NVP-BEZ235 decreases the proliferation of doxorubicin-resistant K562 cells. *Mol Med Rep*. 2021;23:301. https://doi.org/10.3892/mmr.2021.11940

50. Safaroghli-Azar A, Bashash D, Sadreazami P, Momeny M, Ghaffari SH. PI3K-δ inhibition using CAL-101 exerts apoptotic effects and increases doxorubicin-induced cell death in pre-B-acute lymphoblastic leukemia cells. *Anticancer Drugs*. 2017;28(4):436–445. https://doi.org/10.1097/cad.0000000000000477

51. Liu D, Liu L, Li H, Huang Z, Wang Y. Sphingosine kinase 1 counteracts chemosensitivity and immune evasion in diffuse large B cell lymphoma cells via the PI3K/AKT/PD-L1 axis. *Int Immunopharmacol*. 2024;143(Pt 2):113361. https://doi.org/10.1016/j.intimp.2024.113361

52. Hoellenriegel J, Meadows SA, Sivina M, et al. The phosphoinositide 3'-kinase delta inhibitor, CAL-101, inhibits B-cell receptor signaling and chemokine networks in chronic lymphocytic leukemia. *Blood*. 2011;118(13):3603–12. https://doi.org/10.1182/blood-2011-05-352492

53. Gentilini F, Calzolari C, Turba ME, et al. Prognostic value of serum vascular endothelial growth factor (VEGF) and plasma activity of matrix metalloproteinase (MMP) 2 and 9 in lymphoma-affected dogs. *Leuk Res*. 2005;29(11):1263–9. https://doi.org/10.1016/j.leukres.2005.04.005

54. Aresu L, Aricò A, Comazzi S, et al. VEGF and MMP-9: biomarkers for canine lymphoma. *Vet Comp Oncol*. 2014;12(1):29–36. https://doi.org/10.1111/j.1476-5829.2012.00328.x

55. Aricò A, Giantin M, Gelain M, et al. Matrix metalloproteinases and vascular endothelial growth factor expression in canine leukaemias. *Vet J*. 2013;196(2):260–2. https://doi.org/10.1016/j.tvjl.2012.10.004

56. Aricò A, Giantin M, Gelain ME, et al. The role of vascular endothelial growth factor and matrix metalloproteinases in canine lymphoma: in vivo and in vitro study. *BMC Vet Res*. 2013;9:94. https://doi.org/10.1186/1746-6148-9-94

57. Pauls SD, Lafarge ST, Landego I, Zhang T, Marshall AJ. The phosphoinositide 3-kinase signaling pathway in normal and malignant B cells: activation mechanisms, regulation and impact on cellular functions. *Front Immunol*. 2012;3:224. https://doi.org/10.3389/fimmu.2012.00224

58. Jellusova J, Rickert RC. The PI3K pathway in B cell metabolism. *Crit Rev Biochem Mol Biol*. 2016;51(5):359–378. https://doi.org/10.1080/10409238.2016.1215288

59. Gingras AC, Gygi SP, Raught B, et al. Regulation of 4E-BP1 phosphorylation: a novel two-step mechanism. *Genes Dev*. 1999;13(11):1422–37. https://doi.org/10.1101/gad.13.11.1422

60. Gingras AC, Kennedy SG, O'Leary MA, Sonenberg N, Hay N. 4E-BP1, a repressor of mRNA translation, is phosphorylated and inactivated by the Akt(PKB) signaling pathway. *Genes Dev*. 1998;12(4):502–513. https://doi.org/10.1101/gad.12.4.502

61. Szwed A, Kim E, Jacinto E. Regulation and metabolic functions of mTORC1 and mTORC2. *Physiol Rev*. 2021;101(3):1371–1426. https://doi.org/10.1152/physrev.00026.2020

62. Manning BD, Toker A. AKT/PKB Signaling: Navigating the Network. *Cell*. 2017;169(3):381–405. https://doi.org/10.1016/j.cell.2017.04.001

63. Vincent EE, Elder DJ, Thomas EC, et al. Akt phosphorylation on Thr308 but not on Ser473 correlates with Akt protein kinase activity in human non-small cell lung cancer. *Br J Cancer*. 2011;104(11):1755–61. https://doi.org/10.1038/bjc.2011.132

64. Wang Y, Xiu J, Ren C, Yu Z. Protein kinase PIM2: A simple PIM family kinase with complex functions in cancer metabolism and therapeutics. Review. *Journal of Cancer*. 2021;12(9):2570–2581. https://doi.org/10.7150/jca.53134

65. She QB, Halilovic E, Ye Q, et al. 4E-BP1 is a key effector of the oncogenic activation of the AKT and ERK signaling pathways that integrates their function in tumors. *Cancer Cell*. 2010;18(1):39–51. https://doi.org/10.1016/j.ccr.2010.05.023

66. Baohua Y, Xiaoyan Z, Tiecheng Z, Tao Q, Daren S. Mutations of the PIK3CA gene in diffuse large B cell lymphoma. *Diagn Mol Pathol*. 2008;17(3):159–65. https://doi.org/10.1097/PDM.0b013e31815d0588

67. Uddin S, Hussain AR, Al-Hussein KA, et al. Inhibition of phosphatidylinositol 3'-kinase/AKT signaling promotes apoptosis of primary effusion lymphoma cells. *Clin Cancer Res*. 2005;11(8):3102–3108. https://doi.org/10.1158/1078-0432.ccr-04-1857

68. Comazzi S, Riondato F. Flow Cytometry in the Diagnosis of Canine T-Cell Lymphoma. *Front Vet Sci*. 2021;8:600963. https://doi.org/10.3389/fvets.2021.600963

69. Ahmadi Bidakhvidi N, Gevaert T, De Schepper M, et al. Comparison of PSMA immunohistochemistry scoring systems to parametric [(18)F]PSMA-1007 PET/MRI in primary prostate cancer. *Eur J Nucl Med Mol Imaging*. 2025;52(2):766–778. https://doi.org/10.1007/s00259-024-06903-7

70. Tizhoosh HR, Diamandis P, Campbell CJV, et al. Searching Images for Consensus: Can AI Remove Observer Variability in Pathology? *Am J Pathol*. 2021;191(10):1702–1708. https://doi.org/10.1016/j.ajpath.2021.01.015

71. Janowczyk A, Madabhushi A. Deep learning for digital pathology image analysis: A comprehensive tutorial with selected use cases. *J Pathol Inform*. 2016;7:29. https://doi.org/10.4103/2153-3539.186902

72. Fassler DJ, Abousamra S, Gupta R, et al. Deep learning-based image analysis methods for brightfield-acquired multiplex immunohistochemistry images. *Diagn Pathol*. 2020;15(1):100. https://doi.org/10.1186/s13000-020-01003-0

CHAPTER 4: CONCLUSIONS AND FUTURE DIRECTIONS

Conclusions

The studies documented and reviewed within this dissertation review and further characterize the activation of PI3K-AKT-mTOR signal transduction in canine osteosarcoma and lymphoid tumors, as well as examine the efficacy of multi-nodal inhibition against these tumor types. As reviewed in Chapter 1, the PI3K-AKT-mTOR pathway has been long studied in immunology and cancer biology. Dysregulation and constitutive activation are reported in a wide range of both canine and human tumors. The specific mutations and mechanisms responsible for signal transduction dysregulation are less well understood in veterinary oncology than in human tumors, but knowledge has expanded with the development and availability of better tools for genetic, transcriptomic, and proteomic investigation in veterinary medicine. Various single-point, isoform-specific, and multi-nodal pathway inhibitors have been examined with variable results in human medicine, and to a much lesser extent in veterinary medicine. The ubiquity of this highly conserved signaling pathway throughout multiple tissues and organs has presented challenges for both efficacy and tolerance of pathway inhibitors. The complex feedback mechanisms and interactions with other oncogenic signal transduction pathways present challenges for resistance to targeted inhibitors.

Chapters 2 and 3 document increased PI3K-AKT-mTOR pathway activation in canine osteosarcoma, lymphoma, and leukemia cell lines and biopsy samples from spontaneous patient-derived tumors. Our *in vitro* experiments demonstrated hyperactivation of the signaling cascade in cell lines of these tumor types, which further

contributes to the body of research documenting signaling dysregulation in canine neoplasms. The findings in these aggressive tumor types comport with expectations, given the integral role of the PI3K-AKT-mTOR pathway in neoplastic cell proliferation, survival, angiogenesis, and migration and invasion.

Chapter 2 reports that VDC597 inhibited phosphorylation of signal transduction proteins within the pathway, inhibited cellular proliferation, viability, migration, invasion, and VEGF production in canine osteosarcoma cells *in vitro*. These effects were additive to mildly synergistic with other chemotherapy drugs, which varied with dose and to a lesser degree between cell lines. In a xenograft mouse model, osteosarcoma tumor growth was inhibited, survival times were increased, and there was reduced pathway activation detected by immunohistochemistry in xenograft tumors when mice were treated with VDC597 alone and in conjunction with carboplatin. We also sought to examine pathway expression and correlation to outcome and prognostic indicators in patient-derived spontaneous osteosarcoma samples. However, evaluation of decalcified, formalin fixed, paraffin embedded biopsy sections for expression of phosphoproteins in the pathway proved to be unfeasible and a downstream target was used as a proxy indicator, based on our findings in the xenograft tumor sections. The hypothesized correlations were only present in two prognostic indicators and there was no correlation to outcome data, indicating a potentially interesting avenue for future investigation.

Chapter 3 reports that canine lymphoma and leukemia cells exhibited hyperactivation of the PI3K-AKT-mTOR pathway that was inhibited by VDC597 *in vitro*. Treatment lymphoma and leukemia cells also resulted in inhibition of proliferation and

cell viability with induction of cell death and reduced VEGF production, alone and in combination with other chemotherapy drugs in an additive to mildly synergistic fashion. Our evaluation of formalin fixed paraffin embedded canine lymphoma biopsy samples for pathway activation demonstrated a variability in phosphorylation of signaling proteins between patients and did not consistently correlate to other prognostic indicators often cited in canine lymphoma. This is consistent with the variation in mutation status and mechanisms of signaling activation reported in human B-cell neoplasms and may indicate utility in examining the status of pathway activation in the canine patient to better tailor treatment regimens involving targeted inhibitors. While there has been previous research into the use of targeted PI3K/AKT/mTOR inhibitors as a component of canine cancer treatment, study has largely focused on isoform-specific and single-point inhibitors.

Building on the body of literature in human and canine studies, we sought to evaluate the efficacy of the PI3K/mTOR dual-inhibitor, VDC597, against these tumors. In the cell lines examined there was robust *in vitro* inhibition of pathway activation that was correlated to increased cell death with decreases in proliferation, production of angiogenic factors, migration, and invasion, which were predominantly additive to synergistic when combined with other chemotherapeutic drugs. In the xenograft mouse model evaluated, there was reduced tumor growth and longer survival times with the use of dual-pathway inhibition alone and in conjunction with chemotherapy. These findings indicate that the evaluation of pathway activity and the use of dual-inhibition of PI3K/mTOR signaling may be beneficial in canine osteosarcoma and hematopoietic neoplasms.

Future Directions

The body of knowledge and research reported herein remains incomplete, and there is opportunity for more thorough investigation of PI3K-AKT-mTOR dysregulation and inhibition in canine osteosarcoma and lymphoid tumors. There is value in evaluating the degree of pathway activation and response to inhibition in a wider array of hematopoietic and solid tumors both *in vitro* and *in vivo*. In the literature and in preliminary findings during our investigation, there is indication for the potential benefit of PI3K/mTOR dual-inhibition in canine T-cell neoplasms, as well as melanoma and a subset of carcinomas. There would also be value in expansion of the study design to include a greater number of cell lines from the tumor types we examined to ensure that cell lines with more widely varying levels of constitutive pathway activation and evaluating response to targeted inhibition in a sample of greater heterogeneity.

In the process of our evaluation of *in vivo* PI3K/mTOR inhibition, there were failed attempts to develop xenograft mouse models that better recapitulated the natural disease than those reported here. For use in the clinical setting, safety and efficacy of VDC597 should be assessed in a mouse model for the lymphocytic tumors examined as well as other canine lymphoma subtypes. Similarly, while our experiments demonstrated efficacy against subcutaneously xenografted osteosarcoma growth, we did not address metastatic disease, which is the leading cause of death in osteosarcoma cases. Intravenous or intramedullary injection of luciferase-expressing osteosarcoma cells can be used to simulate pulmonary osteosarcoma metastasis, followed by antemortem serial evaluation of pulmonary tumor burden to observe disease progression, evaluate response to pathway inhibition, and correlate to signaling

activity from postmortem samples. The superior option would be the use of an orthotopic xenograft mouse model with luciferase-expressing cells, which could recapitulate the heterogeneity and biologic behavior of the natural disease as well as treatment of metastatic disease following amputation. Likewise, orthotopic xenograft mouse models have previously been successful with human and canine cell lines and the use of this model with additional canine cell lines for study with this compound would be similarly advantageous.

The reader may note that the theme in the experiments suggested above is in the aim to capture the heterogeneity of spontaneous tumors. In the osteosarcoma biopsy specimens, examining activation of signaling proteins within the pathway was not possible. The findings from our IHC evaluation of a downstream target (FOXO1) likely exemplified the complexity of tumor heterogeneity, as well as interactions and cross-talk in signal transduction, and warrants further investigation. To address this, a larger and more thorough survey of patient-derived tumor samples, correlating proteomic, transcriptomic, and genetic aberrations in the PI3K-AKT-mTOR signaling cascade would allow for both a greater understanding of variation in expression and mutation status. Along with the establishment of additional representative cell lines, this may help to better guide future decisions regarding the use of targeted inhibitors by answering questions like “Is there greater efficacy in PI3K/mTOR inhibition in canine tumors with a mutation within the pathway as compared to those with mutations in upstream receptors that may initiate activation or with post-transcriptional alteration?” Based on our experiments demonstrating greater efficacy when VDC597 is combined with

chemotherapy drugs, these combinations should be considered in all of the above suggested routes of investigation.

Of course, the goal is to move beyond mouse models to clinical trials for VDC597, alone and in combination with standard-of-care chemotherapy drugs. With additional mouse model experiments that recapitulate the natural disease process, there is opportunity to more thoroughly evaluate safety and efficacy of VDC597, alone and in combination with standard-of-care chemotherapy drugs. In combination with previously reported pharmacokinetic studies and phase 1 clinical trial results for VDC597, this may allow for study designs in future clinical trials that can move more efficiently past phase 1 with a more refined dosing schedule for VDC597 in conjunction with standard-of-care drugs. During our initial mouse model experiments we found that the combination of VDC597 and carboplatin administered at regular doses and intervals was well tolerated, but the inhibition of tumor growth was so marked that it resulted in apparent complete remission of the xenograft tumors. While this result is certainly not expected in clinically detectable spontaneous tumors, it may indicate that there is some utility in investigating how chemotherapy dosing and/or intervals may be adjusted in patients that do not tolerate standard-of care cytotoxic chemotherapy drugs. There may be significant benefit to the ability to tailor chemotherapy protocols to the patient with the incorporation of targeted signal transduction inhibitors, especially when employed with the benefit of diagnostic tests demonstrating the degree of pathway activation and/or mutation status in a patient.

APPENDIX

Table A1: Antibodies and reagents used in this study. Superscripts in the first column indicate the entry is either a target protein (a) or a reagent (b)
Abbreviations: 4EBP1 (eukaryotic translation initiation factor 4E-binding protein 1); p4EBP1 (phosphorylated eukaryotic translation initiation factor 4E-binding protein 1); aa (amino acid); AKT (AKT serine/threonine kinase); pAKT (phosphorylated AKT serine/threonine kinase); C-terminal (carboxy-terminal); conj. (conjugated); CST (Cell Signaling Technology, Danvers, MA); equiv. (equivalent dilution to the test antibody); GAPDH (glyceraldehyde-3-phosphate dehydrogenase); H+L (heavy chain + light chain); HRP (horseradish peroxidase conjugate); IgG (immunoglobulin G); IHC (immunohistochemistry); mAb (monoclonal antibody); N/A (not applicable); pAb (polyclonal antibody); S (serine); T (threonine); TFS (Thermo Fisher Scientific);

Target [a]/Reagent [b] (residue/epitope)	**Source (Isotype, clonality)**	**Manufacturer (Product #)**	**Stock Concentration**	**Western dilution**	**IHC dilution**
Total AKT [a] (C-terminal)	Rabbit (IgG, pAb)	CST (#9272)	31 µg/mL	1:1000	1:200
pAKT [a] (S473)	Rabbit (IgG, mAb)	CST (#4060)	91 µg/mL	1:1000	1:50
4EBP1 [a] (T46)	Rabbit (IgG, mAb)	CST (#4923)	184 µg/mL	1:400	1:250
p4EBP1 [a] (T37/46)	Rabbit (IgG, mAb)	CST (#2855)	60 µg/mL	1:500	1:200
GAPDH [a] (aa 50-150)	Rabbit (IgG, pAb)	Abcam (#ab37168)	1 mg/mL	1:1000	–
Isotype control [b] (N/A)	Rabbit (IgG)	Invitrogen (#02-6102)	5 mg/mL	–	equiv.
Rabbit IgG [a] (H+L)	Goat (IgG, pAb), HRP	TFS (#31460)	0.533 mg/mL	3:40k	1:100
Rabbit/mouse IgG [a] (H+L)	Goat (IgG, pAb), Dual Link HRP	Agilent Dako (#K4063)	–	–	N/A

LIST OF ABBREVIATIONS

4EBP1 (p4EBP1): eukaryotic translation initiation factor 4E-binding protein 1 (phosphorylated eukaryotic translation initiation factor 4E-binding protein 1)
5S rRNA: ribosomal RNA with sedimentation rate of 5 Svedberg units
ABC: activated B cell
AI: artificial intelligence
aka: also known as
AKT (pAKT): AKT serine/threonine kinase (phosphorylated AKT serine/threonine kinase); also/previouusly known as protein kinase B (PKB)
ALP: alkaline phosphatase
ANOVA: analysis of variance
AS: angiosarcoma
AUC: area under the curve
BAD: BCL2 associated agonist of cell death
BCA: bicinchoninic acid
BCL2: BCL2 apoptosis regulator (formerly B-cell CLL/lymphoma 2)
BCL2L1: BCL2-like 1
BCR: B-cell receptor
BNIP3: BCL2 interacting protein 3
BSA: bovine serum albumin
BRAF: B-Raf proto-oncogene, serine/threonine kinase
BTK: Bruton's tyrosine kinase
°C: degrees Celsius
C10: complete media
CD: cluster of differentiation marker (e.g. CD25, CD45)
CDK4: cyclin dependent kinase 4
CDKI: cyclin dependent kinase inhibitor
CDKN1A: cyclin dependent kinase inhibitor 1A (aka p21)
CDKN1B: cyclin dependent kinase inhibitor 1A (aka p27)
CHOP: chemotherapy protocol using cyclophosphamide (C), doxorubicin (H), vincristine (O), and prednisone (P)
CI: combination indices (or combination index)
CLL: chronic lymphocytic leukemia
CO_2: carbon dioxide
COX: cyclooxygenase
CREB1: cAMP responsive element binding protein 1
CSF1: colony stimulating factor 1
CSU: Colorado State University
DAB: 3,3'-diaminobenzidine
DAG: diacylglycerol

DFI: disease free interval
DLBCL: diffuse large B-cell lymphoma
DMEM: Dulbecco's modified Eagle culture medium
DMSO: dimethylsulfoxide
ECM: extracellular matrix
EGF: epidermal growth factor
EGFR: epidermal growth factor receptor
EIF4E: eukaryotic translation initiation factor 4E
ELISA: enzyme-linked immunosorbent assay
ERBB2: erb-b2 receptor tyrosine kinase 2 (aka HER2; human epidermal growth factor 2)
ERBB4: erb-b2 receptor tyrosine kinase 4 (aka HER4)
FASLG: Fas ligand
FBS: fetal bovine serum
FFPE: formalin fixed paraffin embedded
FGF2: fibroblast growth factor 2 (formerly basic fibroblast growth factor; bFGF)
FGFR: fibroblast growth factor receptor
FK506: tacrolimus
FKBP: FK506-binding protein
FPR1: formyl peptide receptor 1
FRS2: fibroblast growth factor receptor substrate 2
FOXO: forkhead box O transcription factor (e.g. FOXO1, FOXO3)
G: relative centrifugal force, expressed as a multiple of earth’s gravitational force (e.g. 400xG)
GAB1/2: GRB2-associated-binding protein 1 and/or 2
GAP: GTPase-activating protein
GAPDH: glyceraldehyde-3-phosphate dehydrogenase
GBC: germinal center B cell
GF: growth factor
GOC: green object count
GPCR: G-protein-coupled receptor
GSK3: glycogen synthase kinase 3
H-score: histochemical score
H&E: hematoxylin and eosin
HGF: hepatocyte growth factor
HGFR: hepatocyte growth factor receptor (aka MET; mesenchymal-epithelial transition factor; c-MET)
HIF1: hypoxia inducible factor 1
HIF1α: hypoxia inducible factor 1 subunit alpha
hr: hour

HRP: horseradish peroxidase
HSA: hemangiosarcoma
HSP90: heat shock protein 90
IACUC: Institutional Animal Care and Use Committee
IC_{50}: half maximum inhibitory concentration
IGF1R: insulin-like growth factor 1 receptor
IHC: immunohistochemistry
IκB: inhibitor of nuclear factor kappa-light-chain-enhancer of activated B cells
IKK: IκB kinase
IKKε: IκB kinase subunit epsilon
IL: interleukin (e.g. IL-1, IL-6)
INPP4B: inositol polyphosphate-4-phosphatase type II B
INPP5D: inositol polyphosphate-5-phosphatase D (formerly SH2 domain-containing inositol 5'-phosphatase 1; SHIP1)
INPPL1: inositol polyphosphate phosphatase like 1 (formerly SH2 domain-containing inositol 5'-phosphatase 2; SHIP2)
IP_3: inositol-1,4,5-trisphosphate (fermerly Ins(1,4,5)P3),
IR: Insulin receptor
IRS1/2: insulin receptor substrate 1 or 2
IP: intraperitoneal
JNK: c-Jun N-terminal kinase (now abbreviated as MAPK8)
Ki67: marker of proliferation Kiel 67
KIT: KIT proto-oncogene receptor tyrosine kinase (aka c-KIT; mast/stem cell growth factor receptor Kit)
LOX: lipoxygenase
LSA: lymphoma
M: methionine amino acid
MAPK: mitogen-activated protein kinase (e.g. MAPK1, MAPK8)
MAP3K: mitogen-activated protein kinase kinase kinase (e,g, MAP3K5, MAP3K8)
MAPK8IP1: mitogen-activated protein kinase 8 interacting protein 1
mLST8: mTOR associated protein mLST8 (formerly mammalian ortholog of lethal with SEC13 protein 8)
MCT: mast cell tumor
MEK: MAPK/ERK signal transduction pathway (e.g. “MEK inhibitor”)
Mel: melanoma
MGT: mammary gland tumor
MHC-II: major histocompatibility complex class two
µg: microgram
µL: microliter
µm: micrometer

μM: micromolar
mL: milliliter
mm: millimeter
mM: millimolar
MMP: matrix metalloproteinase
MST: median survival time
MTA1: metastasis associated protein 1
mTOR (mTORC1; mTORC2): mechanistic target of rapamycin (mechanistic target of rapamycin complex 1; mechanistic target of rapamycin complex 2)
MYC: MYC proto-oncogene, basic helix loop helix transcription factor
NBF: neutral buffered formalin
nm: nanometer
NFκB: nuclear factor kappa-light-chain-enhancer of activated B cells
NOS: nitric oxide synthase (e.g. NOS2, NOS3)
NOTCH1: notch receptor 1
NRAS: NRAS GTPase
ODC: ornithine decarboxylase
OSA: osteosarcoma
PBMC: peripheral blood mononuclear cells
PBS: phosphate buffered saline
PCR: polymerase chain reaction
PDPK1: 3-phosphoinositide-dependent kinase 1 (also often abbreviated as PDK1)
PFI: progression free interval
PFKFB3: 6-phosphofructo-2-kinase/fructose-2,6-biphosphatase 3
PFKM: phosphofructokinase, muscle
PH: Pleckstrin homology (e.g. Pleckstrin homology domain)
PHLPP: PH domain and leucine rich repeat protein phosphatase
PI: phosphatidylinositol
PI3K: phosphatidylinositol-3 kinase (aka phosphatidylinositol-4,5-bisphosphate 3-kinase), where isoforms are abbreviated PI3Kα, PI3Kβ, PI3Kγ
p38:
p85: phosphatidylinositol-3 kinase, regulatory subunit
p110: phosphatidylinositol-3 kinase catalytic subunit alpha
PIK3CA: phosphatidylinositol 3-kinase catalytic subunit alpha (p110α) gene
PIK3CB: phosphatidylinositol 3-kinase catalytic subunit beta (p110β) gene
PIK3CG: phosphatidylinositol 3-kinase catalytic subunit gamma (p110γ) gene
PIK3R1: phosphoinositide-3-kinase regulatory subunit 1 gene
PLCB4: phospholipase C beta 4 gene
PI3P: phosphatidylinositol 3-phosphate
PIM2: serine/threonine-protein kinase pim-2

PIP: phosphatidylinositol-phosphate (term for the family of molecules including PIP_3)
PIP_2: phosphatidylinositol (4,5)-bisphosphate (formerly PtdIns(4,5)P2 or PI(4,5)P2)
PIP_3: phosphatidylinositol (3,4,5)-trisphosphate (formerly PtdIns(3,4,5)P3 or PI(3,4,5)P3)
PKC: protein kinase C
PKCδ: protein kinase C delta
PKN2: protein kinase N2
PLC: phospholipase C
PLCB4: phospholipase C beta 4 gene
PO: *per os*
PP2A: protein phosphatase 2A
PTCL: peripheral T-cell lymphoma
PTEN: phosphatase and tensin homolog
PTPRD: protein tyrosine phosphatase receptor type D
PTPRO: protein tyrosine phosphatase receptor type O
PVDF: polyvinylidene difluoride
R: arginine amino acid
RAF1: RAF proto-oncogene, serine/threonine kinase
RAPTOR: Regulatory-associated protein of TOR
RB1: RB transcriptional corepressor 1 (formerly retinoblastoma 1)
RECQL4: RecQ like helicase 4
RHEB: Ras homolog, mTORC1 binding (formerly Ras homolog enriched in brain)
RICTOR: rapamycin-insensitive companion of TOR
RNA: ribonucleic acid
ROC: red object count
ROI: region of interest
RPMI: Roswell Park Memorial Institute cell culture medium
RPS6: ribosomal protein S6
rRNA: ribosomal ribonucleic acid
RTK: receptor tyrosine kinase
RT-PCR: reverse transcription polymerase chain reaction
RXXS: abbreviation for the biochemical signaling protein sequence of arginine (R)–any amino acid (X)–any amino acid (X)–serine (S)
S: serine amino acid
S473: serine 473 amino acid residue
S6K1: ribosomal protein S6 kinase beta 1 (now abbreviated RPS6Kβ1; formerly p70S6K)
SLC2A: solute carrier family 2 member 1 (formerly GLUT1)
SLC2A4: solute carrier family 2 member 4 (formerly GLUT4)

SHIP1/2: SH2 domain-containing inositol 5'-phosphatase 1 or 2 (now abbreviated as INPP5D or INPPL1, respectively)
T: threonine amino acid
T20: Tween 20
T46: threonine 46 amino acid residue
T308: threonine 308 amino acid residue
TANK: TRAF family member associated NFκB activator
TBC1D4: TBC1 domain family member 4
TBK1: TANK-binding kinase 1
TBS: tris-buffered saline
TBST: tris-buffered saline with 0.5% Tween 20
TMA: tissue microarray
TNF: tumor necrosis factor
TP53: tumor protein 53
TRAF: TNF receptor associated factor
TRAIL: tumor necrosis factor-related apoptosis-inducing ligand
TRIM24: tripartite motif containing 24
tRNA: transfer ribonucleic acid
TSC1/2: TSC complex subunit 1 or subunit 2 (formerly tuberous sclerosis 1/2)
USP: United States Pharmacopeia
UV: ultraviolet
v.: software version
v/v: volume per volume (concentration)
V659E: oncogenic mutation in the transmembrane domain of the ERBB2 protein
VDC597: PI3K/mTOR dual-inhibitor with molecular formula $C_{26}H_{30}F_2N_8O_4S$
VEGF: vascular endothelial growth factor
VEGFR: vascular endothelial growth factor receptor (e.g. VEGFR1, VEGFR2)
WHO: World Health Organization
XIAP: X-linked inhibitor of apoptosis
XPO1: exportin 1
YB1: Y-box binding protein 1
YOYO™-1: trademarked green-fluorescent (491/509) cell-impermeant nucleic acid stain
YXXM (e.g. YXXM motif): abbreviation for the biochemical signaling protein sequence of tyrosine (Y)–any amino acid (X)–any amino acid (X)–methionine (M)